

**GEOMATERIAL GRADATION INFLUENCES ON
INTERFACE SHEAR BEHAVIOR**

A Dissertation
Presented to
The Academic Faculty

by

Andrew Richard Fuggle

In Partial Fulfillment
of the Requirements for the Degree
Doctor of Philosophy in the
School of Civil and Environmental Engineering

Georgia Institute of Technology
May 2011

**GEOMATERIAL GRADATION INFLUENCES ON
INTERFACE SHEAR BEHAVIOR**

Approved by:

Dr. J. David Frost, Advisor
School of Civil & Environmental
Engineering
Georgia Institute of Technology

Dr. Susan E. Burns
School of Civil & Environmental
Engineering
Georgia Institute of Technology

Dr. Arun M. Gokhale
School of Materials Science and
Engineering
Georgia Institute of Technology

Dr. James S. Lai
School of Civil & Environmental
Engineering
Georgia Institute of Technology

Dr. J. Carlos Santamarina
School of Civil & Environmental
Engineering
Georgia Institute of Technology

Date Approved: 3 February, 2011

To the Lord Jesus Christ,
through whom and for whom all things have been created

and

In loving memory of
Ethan John

ACKNOWLEDGEMENTS

This research would not have been accomplished, were it not for the support and encouragement of many people.

I would like to express my sincere thanks to my academic advisor, Dr. David Frost, for his support and guidance throughout my years at Georgia Tech. I am very grateful for the opportunity that he afforded me, to not only conduct this research, but to freely explore those ideas that were of the most interest. His insightful observations, probing questions, willingness to challenge convention, and his overall approach to solving problems and finding meaning in data, have advanced not only this research, but my thinking on issues beyond the scope of this thesis. It has been a pleasure to work with him and I appreciate his friendship, sure word and gracious heart.

I would like to thank the other members of my thesis committee, Dr. Susan Burns, Dr. Arun Gokhale, Dr. James Lai and Dr. Carlos Santamarina. Your questions, comments and assistance have helped clarify and improve many parts of this research. Dr. Santamarina's undimmed and enthusiastic interest in all things remotely geo-related serve as an example and inspiration. I would also like to thank Dr. Paul Mayne, Dr. Glenn Rix and Dr. Leonid Germanovich for their contributions and assistance over the years.

My time at Georgia Tech would not have been nearly as rich if I had not had the pleasure of working with so many wonderful students from all parts of the world. I would like to thank Alfredo Fernandez, Pierre Ramondenc, Mehmet Iscimen, Alec McGillivray, Catherine McGillivray, Greg Hebler, T. Matt Evans, Xuan Yang, Duhwan Kim, Ye Lu, Mesut Turel, Tanay Karademir, Guillermo Zavala, Laura Spencer, Joan Larrahondo, Bate

Bate and Robert Hurt, as well as all the other students, both past and present, for your friendship, assistance with research and great lunch time conversations.

My time in Atlanta has been all the more meaningful thanks to my church family. Your faith buttressed mine when I was shaken, your hope in things not yet seen has encouraged and inspired, and your love has nourished my soul – thank you.

The seeds for this research were, in some way, planted when I was a child. I would like to thank my parents, Richard and Wendy, for their love, selfless devotion to ensuring the best upbringing for my sister and I, their support of academic pursuits, encouragement to ask questions and find answers, and for the many family vacations and occasional sabbaticals that we took to places near and far. Never a day went by without learning something. Thank you for your fine example. Thank you also to my sister, Heather, with whom I shared many of these learning experiences and life lessons.

Lastly, I would like to express my most heartfelt love and thanks to my beautiful wife, Cheryl. Her unwavering encouragement and unconditional support have given me the strength to complete this research. I am deeply grateful and appreciative of her unequivocal belief in me and for her many sacrifices through the years, some of which I am aware of, and no doubt, some of which I am unaware of. I love you, MVSP! It is an amazing experience to be a new parent and we are very thankful for our precious daughter, Nicole. You are a joy and a delight, the one who with a single smile can melt this heart. Thank you for the wonder and hope that you bring.

TABLE OF CONTENTS

ACKNOWLEDGEMENTS	IV
LIST OF TABLES	IX
LIST OF FIGURES	XI
SUMMARY	XV
1. INTRODUCTION	1
1.1. Context for this research	1
1.2. Outline and organization of dissertation	3
2. CURRENT UNDERSTANDING OF GEOMATERIAL GRADATION EFFECTS AND INTERFACE SHEAR BEHAVIOR	5
2.1. Introduction.....	5
2.2. Particle Mixtures.....	6
2.2.1. Packings of Particles	9
2.2.2. Mixtures of Particles of Different Sizes.....	11
2.2.3. Intergranular void ratios.....	13
2.2.4. Strength tests on mixtures.....	16
2.3. Behavior at Interfaces	18
2.3.1. Friction at Interfaces	18
2.3.2. Particulate Materials at Interfaces.....	19
2.3.3. Interface Shear in Soil Mechanics	21
2.3.4. Wear of Counterface Surfaces	26
2.3.5. Measures of Relative Roughness	27
3. METHODS AND MATERIALS.....	30
3.1. Introduction.....	30
3.2. Materials Tested.....	30
3.2.1. Particulate Materials	30
3.2.2. Counterface Materials.....	37
3.2.2.1. Geomembrane	37
3.2.2.2. Smooth Steel	37
3.2.2.3. Artificial Rough Counterfaces	38
3.2.2.4. Pipe Surfaces.....	38
3.3. Experimental Apparatus and Procedures	38
3.3.1. Limiting Void Ratio Tests	38
3.3.2. Direct Shear Tests	41
3.3.3. Stylus Profilometry	42
3.3.4. Interface Shear Tests.....	45

3.3.4.1.	Device Description.....	45
3.3.4.2.	Tests on smooth geomembranes	48
3.3.4.3.	Tests on rough counterface surfaces	48
4.	PROPERTIES OF BINARY PARTICLE MIXTURES	50
4.1.	Introduction.....	50
4.2.	Limiting Void Ratios	52
4.2.1.	General discussion on limiting void ratios.....	52
4.2.2.	General factors affecting limiting void ratios	54
4.2.3.	Limiting void ratios of binary mixtures	54
4.2.4.	Visualization of Binary Mixtures.....	57
4.2.5.	Selection of particle size ratios for this study	58
4.2.6.	Results of limiting void ratio tests	59
4.2.6.1.	Minimum Void Ratio.....	59
4.2.6.2.	Maximum Void Ratio	61
4.2.6.3.	Same data – improved presentation	62
4.2.6.4.	Correlating e_{\min} to e_{\max}	70
4.2.6.5.	Comparison with source sands.....	72
4.2.7.	Segregation Tests	73
4.3.	Shear Strength.....	76
4.3.1.	Introduction.....	76
4.3.2.	General discussion on direct shear testing	76
4.3.3.	Results.....	77
4.4.	Conclusions.....	96
5.	INTERFACE SHEAR BEHAVIOR OF BINARY PARTICLE MIXTURES WITH SMOOTH COUNTERFACES	100
5.1.	Introduction.....	100
5.2.	Interface Shear Tests with Smooth HDPE.....	101
5.2.1.	Interface Shear Results of Uniform Sands	101
5.2.2.	Interface Shear Behavior of Particle Mixtures.....	110
5.3.	Surface Profilometry of Smooth HDPE.....	121
5.3.1.	Pre-Shear Profiles	121
5.3.2.	Post-Shear Profiles.....	123
5.3.2.1.	Post-Shearing Profiles: Uniform Sands	124
5.3.2.2.	Post-Shearing Profiles: Particle Mixtures.....	131
5.4.	Contact Mechanics and Friction	137
5.4.1.	Single Particle Contact Behavior (Hertzian Contact)	138
5.4.1.1.	Adhesion Component of Friction.....	141
5.4.1.2.	Plowing Component of Friction.....	144
5.4.2.	Multiple Uniform Particles in Contact.....	150
5.4.2.1.	Adhesion Component of Friction for Multiple Uniform Particles..	151
5.4.2.2.	Plowing Component of Friction for Multiple Uniform Particles....	153
5.4.3.	Binary Mixtures in Contact.....	159

6. INTERFACE SHEAR BEHAVIOR OF BINARY PARTICLE MIXTURES WITH ROUGH COUNTERFACES	164
6.1. Relative Roughness.....	164
6.2. Choosing a representative particle size for binary mixtures.....	175
6.2.1. Weighted-Average Approach	176
6.2.2. Sectional Approach.....	178
6.3. Interface Shear Results	183
6.3.1. Changing surface roughness – uniform sands	183
6.3.2. Changing the mixture proportions	185
6.3.3. Changing mixture proportions while maintaining the same weighted-average D_{50}	187
6.4. Aggregate Analysis of Results.....	189
6.4.1. Peak Interface Shear Strength – Uniform Sands.....	189
6.4.2. Post Peak Interface Shear Strength – Uniform Sands.....	192
6.4.3. Peak Interface Shear Strength – Mixed Sands	194
6.4.4. Post Peak Interface Shear Strength – Mixed Sands	198
6.5. Shear Zone Thickness	201
6.5.1. Shear Zone Thickness of Uniform Sands	206
6.5.2. Shear Zone thickness of Binary Mixtures.....	207
7. CONCLUSIONS AND RECOMMENDATIONS	210
7.1. Introduction.....	210
7.2. Conclusions.....	211
7.2.1. Binary Particle Mixtures	211
7.2.1.1. Packing of Mixtures	211
7.2.1.2. Mixture Shear Strength.....	212
7.2.2. Interface Shear with Smooth HDPE Counterface.....	213
7.2.2.1. Uniform Sands	213
7.2.2.2. Particle Mixtures	213
7.2.2.3. Induced Roughness	214
7.2.2.4. Contact Mechanics Based Interface Friction Model.....	214
7.2.3. Interface Shear with Rough Counterface	215
7.2.3.1. Relative Roughness.....	215
7.2.3.2. Interface Shear Strength.....	215
7.2.3.3. Shear Zone Thickness	216
7.3. Recommendations for future research	217
APPENDIX A.....	219
REFERENCES	220

LIST OF TABLES

Table 2.1 Examples of Uniform Sands	9
Table 2.2 Properties of Regular Packings, data from (Deresiewicz 1958).....	10
Table 3.1 Properties of Source Sands	31
Table 3.2 Properties of Scalped Sands.....	32
Table 3.3 Shape Descriptors of Studied Particles.....	35
Table 3.4 Properties of smooth HDPE geomembrane	37
Table 3.5 Properties of Mild Steel Plate	37
Table 3.6 Repeatability measurements along same path	43
Table 3.7 Repeatability measurements on different coupons	44
Table 4.1 Comparison with source sands	72
Table 4.2 Direct Shear Test Data for P.S.R. 2.1	77
Table 4.3 Direct Shear Test Data for P.S.R. 2.8	78
Table 4.4 Direct Shear Test Data for P.S.R. 6.1	79
Table 4.5 Peak friction angles at different normal stress levels	83
Table 4.6 Dilation Angles for P.S.R. 6.1	95
Table 5.1 Interface Shear Test Data for P.S.R. 2.1	116
Table 5.2 Interface Shear Test Data for P.S.R. 2.8.....	117
Table 5.3 Interface Shear Test Data for P.S.R. 6.1	117
Table 5.4 Model Parameters	154
Table 6.1 Weighted Average Particle Size for Binary Particle Mixtures	177
Table 6.2 Different Combinations of Particles with the same Weighted Average Particle Size.....	178
Table 6.3 Representative Particle Size using Two Section Approach.....	181
Table 6.4 Representative Particle Size using Three Section Approach.....	182

Table 6.5 Interface Shear Test Data for Rough Counterfaces with Uniform Particles...	183
Table 6.6 Interface Shear Test Data for Rough Counterfaces	195
Table 6.7 Interface Shear Test Data for Rough Counterfaces	201
Table 6.8 Shear Zone Thickness for Uniform Sands	206
Table 6.9 Shear Zone Thickness for Binary Mixtures	208

LIST OF FIGURES

Figure 2.1 Bilinear Roughness-Friction Relationship (Uesugi and Kishida, 1986)	24
Figure 3.1 Grain Size Distribution.....	32
Figure 3.2 Sands used in this study, from the top: 20/25, 50/60 and 100/140.....	33
Figure 3.3 Particle Shape Reference Charts, clockwise from top left: Krumbein and Sloss, 1963; Powers, 1953; Ozol, 1978 (after Santamarina, 2001).....	34
Figure 3.4 Grain Size Distribution Plots of Binary Mixtures	36
Figure 3.5 Photograph of Modular Interface Shear Device.....	47
Figure 3.6 Repeatability Test for Rough Counterface Testing (Mixture of 10% 100/140 and 90% 50/60).....	49
Figure 4.1 Changes in fabric in a binary particle mixture (Vallejo, 2001).....	55
Figure 4.2 Visualization of Binary Mixtures	57
Figure 4.3 Maximum observed packing of binary mixtures (McGeary, 1961)	58
Figure 4.4 Minimum void ratios	60
Figure 4.5 Maximum void ratios	62
Figure 4.6 VRR data for particle size ratio 6.1	65
Figure 4.7 VRR data for particle size ratio 2.8	66
Figure 4.8 VRR data for particle size ratio 2.1	67
Figure 4.9 VRR data for e_{\max} and e_{\min}	69
Figure 4.10 Correlations between e_{\max} and e_{\min}	71
Figure 4.11 Literature correlations between e_{\max} and e_{\min} (Thomas, 1997)	72
Figure 4.12 Segregation Testing.....	74
Figure 4.13 Typical direct shear data.....	80
Figure 4.14 Direct shear friction angle calculation.....	82

Figure 4.15 Peak Strength Envelope.....	84
Figure 4.16 Large Displacement Strength Envelope	85
Figure 4.17 Peak Effective Stress Ratio	87
Figure 4.18 Peak shear strength of a binary mixture (Vallejo, 2001).....	89
Figure 4.19 Large Displacement Effective Stress Ratio.....	90
Figure 4.20 Large Displacement Friction Angles (50 and 100 kPa)	92
Figure 4.21 Large Displacement Friction Angles (300 and 500 kPa)	93
Figure 4.22 Dilation Angle for PSR 6.1	96
Figure 5.1 Interface Shear Behavior for Smooth HDPE.....	102
Figure 5.2 Peak Friction Coefficient for Uniform Soils	105
Figure 5.3 Post-Peak Friction Coefficient for Uniform Soils.....	105
Figure 5.4 Average Friction Coefficients for Uniform Soils.....	107
Figure 5.5 Particle Size Effect on Interface Shear Behavior	109
Figure 5.6 Interface Shear Tests for PSR 2.1 (100/140 and 50/60).....	111
Figure 5.7 Interface Shear Tests for PSR 2.8 (50/60 and 20/25).....	112
Figure 5.8 Interface Shear Tests for PSR 6.1 (100/140 and 20/25).....	113
Figure 5.9 Peak Friction Coefficient for Particle Mixtures	114
Figure 5.10 Post-Peak Friction Coefficient for Particle Mixtures	115
Figure 5.11 Peak Friction Coefficients (Dove, 1999).....	119
Figure 5.12 Pre-Shear Surface Profile at Various Scales	122
Figure 5.13 Post-Shear Surface Profiles for 20/25 Sand	125
Figure 5.14 Post-Shear Surface Profiles for 50/60 Sand	126
Figure 5.15 Post-Shear Surface Profiles for 100/140 Sand	127
Figure 5.16 Average Roughness after Shearing for Uniform Sands	128
Figure 5.17 Dominant wavelength in surface profile (post-shear, uniform sands)	130

Figure 5.18 Post-Shear Surface Profiles for P.S.R. 2.1 at 500kPa	132
Figure 5.19 Post-Shear Surface Profiles for P.S.R. 2.8 at 500kPa	133
Figure 5.20 Post-Shear Surface Profiles for P.S.R. 6.1 at 500kPa	134
Figure 5.21 Average Roughness after Shearing for P.S.R. 2.1 Mixture.....	135
Figure 5.22 Average Roughness after Shearing for P.S.R. 2.8 Mixture.....	135
Figure 5.23 Average Roughness after Shearing for P.S.R. 6.1 Mixture.....	136
Figure 5.24 Illustration of particle radius, R, and contact radius, a.....	139
Figure 5.25 Components of Friction: Adhesion and Plowing (Dove, 1999).....	141
Figure 5.26 Calculation of pressure coefficient, α	143
Figure 5.27 Calculation of τ_0	144
Figure 5.28 Plowing Component of Friction	146
Figure 5.29 Friction Coefficient due to Plowing	147
Figure 5.30 Friction Coefficient due to Plowing	148
Figure 5.31 Limiting Stable Packing Arrangements.....	150
Figure 5.32 Effect of Packing Density, β	155
Figure 5.33 Effect of Young's Modulus of the Surface, E_2	156
Figure 5.34 Effect of Young's Modulus of the Surface, E_2	157
Figure 5.35 Effect of Young's Modulus of Particle, E_1	158
Figure 5.36 Comparison with Experimental Data	159
Figure 5.37 Estimation of friction coefficient for binary particle mixture	163
Figure 6.1 Typical Sandpaper Surface Profiles	167
Figure 6.2 Local R_{\max} Histograms	168
Figure 6.3 Comparison of modal and mean normalized roughness parameters - sandpaper	169
Figure 6.4 Comparison of modal and mean normalized roughness parameters - pipes .	171

Figure 6.5 Mean Normalized Roughness - Sandpaper	172
Figure 6.6 Modal Normalized Roughness - Sandpaper	173
Figure 6.7 Mean Normalized Roughness - Pipes.....	174
Figure 6.8 Modal Normalized Roughness - Pipes	174
Figure 6.9 Two Section Approach	179
Figure 6.10 Three Section Approach	180
Figure 6.11 Effect of Surface Roughness on Interface Shear.....	184
Figure 6.12 Effect of changing mix percentage (P.S.R 6.1, SP #100).....	186
Figure 6.13 Different Mixtures with d_{50} of 0.26mm.....	187
Figure 6.14 Different Mixtures with d_{50} of 0.39mm.....	188
Figure 6.15 Different Mixtures with d_{50} of 0.58mm.....	188
Figure 6.16 Normalized Roughness, R_n (using the mean)	190
Figure 6.17 Normalized Roughness, mR_n (using the mode).....	191
Figure 6.18 Post-Peak, Normalized Roughness, R_n (using the mean)	192
Figure 6.19 Post-Peak, Normalized Roughness, mR_n (using the mode).....	193
Figure 6.20 Normalized Roughness, R_n , for mixed sands	196
Figure 6.21 Normalized Roughness, mR_n , for mixed sands	197
Figure 6.22 Post Peak, Normalized Roughness, R_n , for mixed sands.....	199
Figure 6.23 Post Peak, Normalized Roughness, mR_n , for mixed sands.....	200
Figure 6.24 Evidence of Shear Zone adjacent to Interface	203
Figure 6.25 Measurement of Shear Zone Thickness	205
Figure 6.26 Shear Zone Thickness for Uniform Sands.....	207
Figure 6.27 Shear Zone Thickness for Binary Mixtures.....	209

SUMMARY

Particulate materials are ubiquitous in the natural environment and have served throughout human history as one of the basic materials for developing civilizations. In terms of human activity, the handling of particulate materials consumes approximately 10% of all the energy produced on earth. Advances in the study and understanding of particulate materials can thus be expected to have a major impact on society.

Geotechnical engineers have a long history of studying particulate materials since the fundamental building blocks of the profession include sands, silts, clays, gravels and ores, all of which are in one form or another particulates. The interface between particulates and other engineered materials is very important in determining the overall behavior of many geotechnical systems. Laboratory experimental studies into interface shear behavior has until now, been largely confined to systems involving uniformly graded sands comprised of a single particle size.

This study addresses these potential shortcomings by investigating the behavior of binary particle mixtures in contact with surfaces. The binary nature of the mixtures gives rise to a changing fabric state which in turn can affect the shear strength of the mixture. Accordingly, packing limit states and the shear strength of binary mixtures were investigated across a range of mixtures, varying in particle size ratio and the proportion of fine particles to provide a reference.

Binary mixtures in contact with smooth surfaces were investigated from both a global shear response and a contact mechanics perspective. A model was developed that allowed for the prediction of an interface friction coefficient based on fundamental

material properties, particle and mixture parameters. Surface roughness changes as a result of shearing were also examined.

The interface shear behavior with rough interfaces was examined in the context of the relative roughness between particles and surface features. The interpretation of traditional measures of relative roughness suffer from the need for a definitive average particle size, which is ambiguous in the case of non-uniform mixtures. Measures of an applicable average particle size for binary mixtures were evaluated.

1. INTRODUCTION

1.1. Context for this research

Particulate materials occupy a very prominent role in the world. They are ubiquitous in the natural environment and have served throughout human history as one of the basic materials for developing civilizations.

Particles are present in the atmosphere, the oceans and on land. There is a virtually inexhaustible supply of sand particles on our shorelines and in deserts, which comprise more than 10% of the land area of the earth. In terms of human activity, particulates are no less important. The handling of this class of materials consumes approximately 10% of all the energy produced on earth (Duran, 2000). This ranks particulate materials second on a list of human priorities, behind only water. Advances in the study of particulate materials are thus bound to have a major impact on society.

Particulate materials are processed in many diverse industries and are handled in some form in every nation on earth. Some of the industries that are major handlers of particulates include mining (ore), agriculture (food grains, seed, fertilizer), construction (sand, gravel, cement) and the pharmaceutical industry. Low-cost raw materials form a large part of the particulate materials handled by industry. The processes of extracting, crushing, grinding, separating, transporting and storing of these materials are generally carried out using somewhat basic technologies. Since the rise of more specialized industries that also use particulate materials, such as the cosmetic and pharmaceutical industries, the incentive to optimize and control particulate processing has increased and increasingly sophisticated processing technologies are being demanded and developed.

At many stages in the handling of particulates, the particles are placed in contact with a solid surface. These interface interactions between grains and silo walls, ores and conveyor belts, sands and geomembranes, and gravels and concrete piles are often the controlling factor in determining how these systems will behave.

Geotechnical engineers have a long history of studying particulate materials (soils) and the behavior of the interface between a particulate soil and a continuum solid is of fundamental importance to the performance of many geotechnical engineering systems. Examples of such geotechnical systems include: contact surfaces between soil and man-made elements (pile foundations, tunnels, retaining walls), the boundaries between adjacent soil and rock layers, and internal shear zones formed within individual soil masses. In addition, many laboratory and in-situ geotechnical testing techniques are influenced by interface behavior (for example the rigid cell permeameter and the cone penetration test). Despite the prevalence and importance of interfaces in geotechnical engineering, the study of geotechnical interfaces has typically received less attention than the study of internal soil behavior, although this is beginning to change as evidenced by the recent International Symposium on the Characterization and Behavior of Interfaces held in 2008 (Frost, 2010).

This dissertation seeks to extend the work done in this field by investigating binary particle mixtures in contact with both smooth and rough interfaces. The dissertation focuses solely on non-plastic coarse granular soils. Specifically, quartz sands varying in diameter from approximately 0.1mm to 1.0mm were used in the study. Smaller size particles were not studied as surface effects related to the specific surface then become dominant. Both uniform sands and binary mixtures made of these sands were

studied. Various counterface materials were studied, representing some of the common geomaterials found in use today.

1.2. Outline and organization of dissertation

This dissertation presents results and discussion focused on the general topic of geotechnical interface behavior. In addition to this introduction, the thesis is organized into six chapters, the contents of which are outlined below:

Chapter 2

Chapter 2 provides a summary of previous research findings that have important implications for the current study. In particular, similarities to and differences between previous work and the current study are examined. Chapter 2 is divided into two main sections: the first reviews particle mixtures and their behavior, and the second part reviews interface shear behavior.

Chapter 3

Chapter 3 presents the information related to the materials studied and the experimental methods and equipment used to study them. Information related to the particles themselves is presented, along with information related to the counterface surfaces tested. Details of all experimental procedures are also provided.

Chapter 4

Chapter 4 describes the results of tests on binary particle mixtures. Since the limiting case of a binary mixture would be a uniform soil, the study of uniform soils is also included here.

Data and discussion from limiting void ratio and direct shear tests comprise the majority of this chapter.

Chapter 5

Chapter 5 presents the results and analysis of binary mixtures in contact with smooth counterfaces. Again, uniform soils are first examined in order to provide a reference point for the binary mixtures. Interface shear test data is presented showing the stress-strain response of the interface system. Surface profilometry data is also presented which quantifies the changes in the counterface surface due to shearing against uniform and binary particle mixtures.

The observed behavior is then examined from a tribological perspective, seeking to understand the behavior by relating the results to fundamental Hertzian contact mechanics and principles of friction. A model is presented that allows for the interface friction coefficient to be estimated based on the particle and counterface properties. This model is extended to apply to binary mixtures.

Chapter 6

Chapter 6 presents the results and analysis from tests with binary mixtures in contact with hard, rough counterfaces. The concept of relative roughness is re-examined, seeking a relationship between particle size, surface feature size and observed interface shear behavior. The effect of changing surface roughness and mixture proportions is examined.

Chapter 7

Chapter 7 presents the conclusions of the study and provides recommendations for future study on this topic.

References and appendices are presented at the end of the dissertation.

2. CURRENT UNDERSTANDING OF GEOMATERIAL GRADATION EFFECTS AND INTERFACE SHEAR BEHAVIOR

2.1. Introduction

This chapter summarizes previous research findings that have important implications for the current study. In particular, similarities to and differences between previous work and the current study are examined. A central thread running through this study, and thus through this chapter, is that the particle size distribution of an assembly of particles has an important influence on the way in which the particles pack relative to one another, both at the formation of the assembly (inherent microstructure) as well as during any process that causes the particles to move relative to one another (induced microstructure).

The influence of different particle sizes and particle size distributions will be examined through the study of binary particle mixtures, i.e. mixtures comprised of particles of two distinct sizes. This is a simpler and more illustrative and instructive case as compared to more complex ternary (or higher order) mixtures. A review of the behavior of binary particle mixtures will be presented below, drawing largely on literature from fields outside of geotechnical engineering. Various packing arrangements, models for describing void ratio changes and shear strength will all be reviewed in relation to particle mixtures.

Interactions between particle mixtures and surfaces will be examined by reviewing aspects of tribology as well as the growing body of work within the geotechnical engineering field that specifically considers particulate-continuum interfaces and the process of shearing at those interfaces. The growing significance of this area of

research is reflected by the recent international symposium dedicated to this topic (Frost, 2010). A significant contribution of this thesis will be to examine the effect of particle size distribution on interface shear behavior as this is not a topic that has received any meaningful attention in previously published works.

The interplay between particle size and surface roughness has been demonstrated in previous studies. The relative roughness of a surface plays a very important role in determining the interface shear behavior but this has only previously been examined in cases with uniform particle assemblies. These studies will be reviewed in order to provide insight into the case of more complex particle size distributions.

The effect of hard and soft counterfaces on interface shear behavior has long been established and a review of this work follows in order to provide understanding on how particle mixtures may interact with such surfaces. Wear is an aspect of interest with regards to soft counterfaces although this is only fairly recently receiving attention in the geotechnical community.

2.2. Particle Mixtures

There is a tendency in geotechnical engineering to want to classify soils into one of four primary groups, viz. gravel, sand, silt or clay. This tendency highlights the understanding that these different soil types behave in different ways at the particle level, but also masks the fact that most naturally occurring soils cannot be classified so simply. Naturally occurring soils are usually comprised of a mixture of different particle shapes and sizes rather than a single uniform particle shape or size. Soil mixtures, such as silty-sands and clayey-silts, are more frequently encountered in geotechnical engineering projects than uniform gravels, sands, silts or clays. Soil mixtures are commonly found in

geotechnical construction such as engineered fills, embankments and ground improvement projects.

Gap-graded materials, which can be approximated by binary particle mixtures, form an important group of engineered materials. Such materials are often used for flexible pavements and for water retention filters in dams (Peters and Berney, 2010).

Despite the widespread occurrence of soil mixtures, geotechnical research, and laboratory testing in particular, has tended to focus more on uniform soils. There is thus considerably less data available on soil mixtures and an incomplete understanding of the fundamental behavior of soil mixtures. This incomplete understanding can be attributed, at least in part, to the lack of a unifying theoretical framework with which to characterize and model soil mixtures based on their constituent materials. Part of the difficulty in studying soil mixtures is the complexity of the behavior and the lack of index parameters to characterize them.

There is a recognized need for a framework whereby the macro-scale response and state of soil mixtures can be predicted from the properties of the constituent materials. Such a framework, validated by experimental results, would also prove useful in selecting the optimal materials and mix proportions for the design of engineered soils. Other potential applications include optimizing mix designs for embankments, subgrade soils and for soil improvement projects in areas with marginal soils.

Naturally occurring particles all exhibit some degree of variation in particle size, regardless of the soil chosen or the size measurement method or descriptor employed. An accurate description of particle size for a given soil must include information regarding this size variation. In geotechnical engineering this information is usually presented in the

form of a particle size distribution plot showing the relative frequency with which particles within a number of narrow size ranges occur. Various descriptors, such as the coefficient of uniformity, C_u , and the coefficient of curvature, C_c , are employed to describe and characterize the nature of the size distribution.

In general, mixtures behave as a function of the individual component behaviors as well as a function of how the components are mixed. The combined effect of how the mixture as a whole acts may not necessarily be obvious from the component behaviors alone. There is a need to understand how the components act in isolation (for the limiting case or boundaries of the phenomenon), and also how the components interact with each other and what effect this has on the overall behavior.

Individual components and mixture ratios determine the packing density and structure, this in turn effects the strength. Good models exist that predict the density (or void ratio) from the constituents (Dodds, 1980; Yu and Standish, 1991; Finkers and Hoffmann, 1998), but such models are not available for predicting the shear strength or the interface shear strength and void ratio by itself is not a sufficient predictor of strength.

In one sense, every soil encountered is a mixed soil. Even in the most uniform of sand deposits one will find particles of differing size and shape. Soils used for research purposes that are considered to be uniform include Ottawa 20/30, A.F.S. 50/70, F-110, Monterey #16 and Monterey #0. Table 2.1 presents grain size and grain size distribution data for the aforementioned sands.

Table 2.1 Examples of Uniform Sands

Sand	D_{large} (mm)	D_{50} (mm)	D_{small} (mm)	Cu	Relative Range ($D_{large}-D_{small}$)/ D_{50}
Ottawa 20/30	0.85	0.72	0.60	1.2	0.35
A.F.S. 50/70	0.30	0.26	0.21	1.4	0.35
F-110	0.21	0.14	0.08	1.6	0.93
Monterey #0	0.60	0.38	0.13	1.6	1.24
Monterey #16	2.4	1.2	0.80	1.3	1.33

Note: D_{large} = size of largest particle, D_{small} = size of smallest particle

As can be seen in the table, there is not a well defined range of relative particle sizes that define a uniform soil. By the term “mixed soil” we mean a soil with at least two distinct and readily discernable (based on size) components of the solid phase. For the purposes of this study, binary particle mixtures will be studied. The review will thus focus largely on binary particle mixtures. Binary particle mixtures are studied in disciplines as diverse as ceramics, mining, chemical engineering, and food and pharmaceutical handling. This is reflected in the diverse range of publications covering this topic.

2.2.1. Packings of Particles

Volumes and surface areas of regular geometrical solids are readily determined, and, as such, the majority of research on particle packings has been carried out considering perfectly spherical particles. A review of packing arrangements and characteristics of rigid mono-sized spheres provides an excellent starting point for this review.

Regular packings of rigid mono-sized spheres have been extensively studied with some of the earliest work investigating the flow of water through a soil mass (Slichter

1899). Five distinct stable configurations are identified: simple cubic, cubic-tetrahedral, tetragonal sphenoidal, face-centered cubic and tetrahedral packings (Graton and Fraser, 1935). Table 2.2 shows various properties of these regular packings. These values of porosity are completely independent of the size of the particles and it can be observed how the co-ordination number increases as the void ratio decreases.

Table 2.2 Properties of Regular Packings, data from (Deresiewicz 1958)

Arrangement	Porosity (n)	Void Ratio (e)	Packing Density (1-n)	Co-ordination Number (cn)
Simple Cubic	0.476	0.908	0.524	6
Cubic- Tetrahedral	0.395	0.652	0.605	8
Tetragonal Sphenoidal	0.302	0.432	0.698	10
Face-Centered Cubic	0.260	0.351	0.740	12
Tetrahedral	0.260	0.351	0.740	12

Packings of spherical particles in random arrangements has also been extensively studied. A good summary of early research can be found in (Brown and Richards 1970). Results of tests from many researchers are described and include various types of materials, including poppy seeds, lead shot and glass beads. Particle sizes varied from 0.04mm to 4.8mm and the results were shown to be substantially independent of the particle size. The packing densities are found to range from approximately 0.60 to 0.64, indicating an intermediate density, but tending towards the looser packings. (Santamarina 2001)) indicates that random packings of mono-sized spheres will typically achieve packing densities of between 0.56 and 0.67 and that average co-ordination numbers can

vary from approximately 6 for loose packings to approximately 9.5 for dense packings. A similar range of co-ordination numbers is reported in (Brown and Richards 1970) where values of average coordination number range from 6.2 to 9.5, as determined experimentally.

Lu (2010) recently identified a new measure of soil fabric, called the “packing signature”. This is a meso-scale measure of void ratio throughout a three-dimensional arrangement of particles. It is interesting to note that this packing signature shows definite periodicity, with the size of the particles largely determining the wavelength of the measurement signal.

The minimum and maximum void ratios for real soil particles will differ from those of spherical particles. In general, for more angular particles, there is greater opportunity to build a loose arrangement of particles, resulting in a lower minimum density (greater void ratio). A comprehensive review of the factors affecting the void ratio of soils can be found in (Youd 1973). The most significant findings of that study were that the primary factors controlling the limiting void ratios for clean sands are particle shape and the range of particle sizes present. It was also found, contrary to previous studies, that particle size per se has no significant influence on the limiting void ratios. This would seem to be in agreement with the findings for mono-sized spherical particles which also showed no dependence on the actual particle size.

2.2.2. Mixtures of Particles of Different Sizes

An assembly of mono-sized particles will leave void space between the particles. These voids can be filled with smaller particles which would result in a denser arrangement. In turn, these smaller particles leave voids which can be filled in by even

smaller particles, resulting in an even denser packing. It is thus apparent that the relative size and proportions of particles present will play a very significant role in the packing structure of the entire arrangement. The case of binary mixtures (two components) will be considered as it is a simpler case than ternary (or higher order packings) and allows for the primary aspects to be illustrated clearly without unnecessary complication.

In the earliest related work, (Furnas 1931) was interested in determining mathematical expressions for intermittent and continuous gradations that would achieve the maximum density. The parameter, K , was designated as the ratio of the smallest to the largest particle present and was found to be a very important parameter. This parameter (or its inverse) is named differently by different authors and in the current study will generally be termed “particle size ratio”.

Particle mixtures were further studied by (McGeary 1961) who showed that as the ratio between particle sizes increased (for binary mixtures) a denser arrangement was achieved. An approximately sevenfold difference between particle diameters was found to produce the most efficient packing and this was related to the triangular pore size created by the large particles through which the smaller particles had to migrate. It was also shown that the percentage of small particles present when the packing reached a maximum density was between 20% and 40%.

Many researchers have attempted to develop mathematical models that relate the particle size distribution to the porosity of the mixture. These models can be broadly classified into two main groups: geometrical models and analytical models (Yu and Standish 1991). All of the geometrical and analytical models have been shown to be able to predict the porosity of particle mixtures with various degrees of success. It is however

noted by many researchers (Stovall, De Larrard et al. 1986); (Ouchiyama and Tanaka 1989) that comparisons between models are very difficult since different assumptions or geometries are used. A brief overview of the development of the primary models will be presented next.

The first analytical model was proposed by Westman and Hugill (1930) and is called the linear packing model. This model has since been extended to multi-component mixtures and continuous distributions (Bierwagen and Saunders 1974). A more recent version of the linear packing model was developed (Stovall, De Larrard et al. 1986) to address some short comings in the previous models. Taking a slightly different approach and basing the new analytical model on the experimental theory of mixtures (Yu and Standish 1988) developed a mixture packing model.

The geometrical models are based on assuming a certain particle geometry. (Dodds 1980) developed a simple statistical geometrical model which assumed that all particles were touching their neighbors. While clearly this is an invalid assumption, the model, which uses tetrahedral sub-units for calculating the porosity, shows results very similar to more complex models. Other geometrical models have been proposed (Suzuki and Oshima 1985); (Ouchiyama and Tanaka 1989). These models all assume a certain particle configuration, which while clearly questionable, does have the advantage of allowing other properties, such as coordination number, to be calculated.

2.2.3. Intergranular void ratios

In the geotechnical literature various aspects related to particle mixtures have found expression in research on silty sands. In particular, research on the undrained shear strength related to liquefaction has been studied extensively.

Traditionally, void ratio has been chosen as one of the most important state variables. This is seen in the choice of void ratio as a central parameter in critical state soil mechanics (Roscoe et al, 1958), in the development of the steady-state concept (Poulos, 1981) and in the formulation of the state parameter concept (Been and Jefferies, 1985). The use of void ratio has however led to some uncertainty in the study of such cases as the undrained shear strength of silty-sands (Thevanayagam, 1998). Alternatives to the traditional concept of void ratio have thus been sought.

Thevanayagam (1998) introduced the concept of the intergranular and interfine void ratios. The intergranular void ratio is defined as the void ratio of the original coarse-grain matrix if the finer particles were removed and is considered to be an index of the active contacts of the coarse-grained component. This measure of void ratio is applicable to soils with a low percentages of finer particles present (below a certain threshold). The interfine void ratio is applicable for soils with a high percentage of finer particles (greater than a certain threshold). Under this proposed framework, the finer particles are regarded as voids when the percentage of finer particles is low and are assumed not to participate in resisting load. When the percentage of finer particles is high, the large grains are considered to be voids. In a similar study, Yang et al. (2006) examined the transitional fines content (TFC) which is the point at which one can separate the material as being either sand-dominated or fines-dominated. Their study examined whether the steady state line, limiting void ratios and various cyclic and liquefaction parameters could be used to determine the TFC. They determined that based on all these different approaches that the TFC for the studied sand-non-plastic fines mixture was approximately 30%.

Thevanayagam et al. (2002) introduced an equivalent intergranular void ratio which sought to account for the contributions of the coarse and fine components at high and low percentages of finer particles, respectively. This equivalent intergranular void ratio requires an additional parameter which represents the fraction of finer particles that participate in load transfer through the soil. Predicting this parameter is problematic and has generally been back calculated. Rahman et al. (2008) attempted to address this by developing a semi-empirical relationship between this parameter and the size and percentage of finer particles in the context of binary mixtures.

Gutierrez (2003) developed very similar relationships from the starting point of mixture theory. Good correlations were found between the percentage of finer particles and various other parameters, including the cyclic undrained shear strength and mixture void ratio.

These concepts of intergranular void ratios and transitional fines content all apply to soil mixtures. While the studies undertaken to date generally consider the fine component to be significantly smaller than the coarse component, the current study will investigate whether the same concepts can be applied to mixtures where there is not such a large particle size discrepancy.

Binary particle mixtures have also been studied using numerical simulations. The work by Consiglio et al. (2003) showed how the void ratio of binary particle mixtures at different mixture ratios could be obtained using Monte-Carlo simulations. Results showed a minimum void ratio at approximately a 12% concentration of larger spheres. That study was completed only for particles that had a size ratio of 2 and for a very limited number of mixture ratios. Due to the large (100,000) number of simulations

performed, the expected error in the reported results was estimated to be very low. Results do differ however from other experimental results on spherical particles at similar size ratios.

2.2.4. Strength tests on mixtures

A number of studies have been conducted that have examined the shear strength of cohesionless sand-gravel mixtures (Holtz and Gibbs, 1956; Doddiah et al., 1969; Vasileva et al., 1971; Marsal and Fuentes de la Rosa, 1976; Fragaszy et al., 1992). These studies showed that the maximum shear strength of the mixtures approximated that of the sand (finer component) when the percentage of gravel (coarse component) was less than approximately 50% by mass. The maximum mixture shear strength approximated that of the gravel when the gravel fraction was greater than approximately 70%. At concentrations of gravel between 50% and 70% the maximum shear strength of the mixture was some combination of the strengths of the two components.

Similar results were obtained by using binary mixtures of glass beads with a particle size ratio of 12.5 (Vallejo, 2001). In this case, peak shear strengths from direct shear tests also showed three distinct zones of behavior, with the transition zone occurring at mass concentrations between 35% and 70% of the coarse fraction. In that study however, the validity of the tests performed with predominantly coarse grains is questionable due to the very large size of the particles in relation to the size of the testing apparatus.

Simoni and Houlsby (2006) studied the strength and dilatancy of sand-gravel mixtures in a large direct shear box and specifically investigated how the grain size characteristics affected the shearing resistance. They found that adding even a small

amount (less than 10%) of gravel to a sand increased both the peak and constant volume friction angles. They further found that the minimum void ratio could be used as a normalizing parameter. Empirical relationships were developed to predict the peak shear strength of sand-gravel mixtures up to 50% gravel component.

Vallejo and Mawby (2000) investigated the shear strength of sand-clay mixtures. While these results are not directly applicable to the current study due to the plastic nature and relatively small size of the fines component, the results are nonetheless noteworthy. The authors found that if the coarse component was greater than 75%, then the strength of the mixtures was basically that of the coarse component by itself. If the coarse component was less than 40% (by mass) then the strength was basically that of the clay. For the situation when the coarse fraction was between 40 and 75% the strength of the mixture was partially controlled by each component. The proposed explanation for this behavior is based on the porosity resulting from mixing the components. The point at which maximum density was achieved represented the boundary between where the mixture strength was sand controlled or clay controlled.

The relationship between binary mixture properties and shear banding has also been experimentally studied (Viggiani et al. 2001). Monodisperse and binary mixtures were both studied under plane strain conditions using stereophotogrammetry to capture the onset of localization and shear band characteristics. The results confirmed that the shear band thickness does depend on the mean grain size, but that orientation does not. The authors concluded that grain size distribution has a major effect on shear band characteristics but that simple descriptors of the size distribution cannot be directly related to the shear band characteristics.

The angle of repose of particle mixture has been studied by Chik (2005) using the ASTM C1444-00 Funnel Test. Results indicate that the basal surface upon which the particles are placed is also a very important factor. On a “rough” basal surface the angle of repose was found to decrease by approximately 5 degrees with the addition of finer material. This suggests that the fine particles fill in the spaces found between the surface texturing, thereby reducing the effective roughness. For a “smooth” basal surface the angle of repose increased by approximately 5 degrees with addition of finer material. No quantification of the surface roughness was attempted so any relationship between strength and relative roughness was not established. It is clear, however, that the strength of binary mixtures can vary significantly depending on the mixture ratio and that the interface (in this case the basal surface) does play a significant role in the measured strength (taking the angle of repose to be a measure of strength).

2.3. Behavior at Interfaces

2.3.1. Friction at Interfaces

The basic laws of friction as summarized by Bowden and Tabor (1956) indicated that:

1. Friction is independent of the contact area between surfaces
2. Friction is proportional to the load transferred between surfaces

These statements are a restatement of Amonton’s Laws of Friction first elucidated in the 17th century. Since the frictional force is independent of the gross area of contact, one can express the same relationships in terms of boundary shear stresses and normal stresses as is more commonly done in geotechnical engineering. Amonton’s Laws imply a constant friction coefficient but many materials in fact do not obey this law as their

friction coefficients can vary with normal load. For a detailed analysis of friction, refer to Bowden and Tabor (1956).

In modeling real surfaces Archard (1957) found that contact behavior is a function of the number of asperities touching the surfaces. Elastic conditions at these contact points resulted in a variable friction coefficient while plastic conditions resulted in a constant friction coefficient. Real materials exhibit a behavior somewhere between the two extremes and Archard presented a generalized equation linking the contact area to the applied load. A thorough review of this work can be found in Dove and Frost (1999).

2.3.2. Particulate Materials at Interfaces

When discrete particles are moved relative to the surface they are contacting, they are able to either slide along the surface or roll. This is in contrast to asperities from another contacting surface in that those asperities do not have the option to roll.

The contacting particulate assembly can deform partially or completely in one of two mechanisms: sliding and shearing. Pure sliding is characterized by translation with respect to the counterface with no internal particle rearrangement. Pure sliding of a particulate assembly along a counterface can occur under the following conditions: (1) the surface is smooth relative to the contacting particle size, (2) the normal stress remains below the critical stress level, thereby preventing particles from embedding in the surface, which can lead to surface ploughing, or particle fracturing, and (3) the surface is sufficiently hard so that abrasive wear is negligible during shear. In the case of pure sliding, interface friction is generated solely due to sliding at the particle-counterface contacts and therefore volume change in the adjacent particulate structure is negligible.

Shearing of the particulate structure occurs to varying degrees when one of the conditions for pure sliding is not met. A change in the continuum surface roughness, the confining stress, the continuum hardness, or particulate shape can result in sliding at the particle-counterface contacts no longer being the mechanism with the lowest friction coefficient (i.e. requiring the minimum energy). When internal shearing within the particulate medium provides less resistance to shear than sliding at the interface at least partial shear will occur. For example, for shear against smooth surfaces at low normal stress, sliding at the counterface contacts provides the least resistance, as sliding can occur with essentially no particle rearrangement and therefore no volume change. However, if for example the surface roughness is increased slightly, sliding at the interface results in higher frictional resistance as particles must displace into the contacting particulate structure to overcome surface asperities. This translational movement requires the contacting particulate structure to deform to allow the particles to pass over the asperity. In conditions where both sliding and shearing occur simultaneously, the internal shear deformation of the particulate structure permits sliding at the interface contacts. The case of pure interface shearing is analogous to shearing within a global particulate mass, and occurs when the interface resistance is higher than the internal resistance over the entire contact area, essentially clogging the interface.

These two basic types of particle motion, sliding and rolling, were shown by Fang et al. (1993) in their study of single sand particles placed between two metal surfaces. One surface was displaced relative to the other. It was observed that sliding particles left tracks in the form of a groove while particles that rolled caused serial pitting of the surface. In this same, study the authors attempted to account for the factors that would

cause either rolling or sliding. It was proposed that the main determining factor was the ratio of the vertical to horizontal moment arms of the couples keeping the particle in equilibrium and that sliding would occur only if this ratio exceeded the friction coefficient. Experimental evidence confirms this by showing that particles with ratios greater than the friction coefficient did in fact slide, while particles with lower ratios rolled.

It was further shown that this ratio increases with either an increase in the normal load or with a decrease in particle size, thus making the particle more likely to slide. This is a very interesting result given that it is also known that larger particles are more likely to slide on a given surface than smaller particles (Uesugi and Kishida, 1986; Paikowsky et al., 1995). In these cases, it appears as if the increase in normal load per particle outweighs the effect of increasing particle size. Another observation was that maximum value of the friction coefficient of a rolling particle was greater than that of a sliding particle.

2.3.3. Interface Shear in Soil Mechanics

The placement of particulate material (soil) adjacent to a continuum material (foundation, tunnel, landfill component) creates an interface between two different materials. This particulate-continuum interface governs the behavior of many geotechnical systems, including deep foundations, geosynthetic liners, earth retaining structures and trenchless technology projects. A fundamental understanding of the mechanisms governing the behavior of these geomaterial interfaces is essential if the design of these systems is to be improved.

Numerous factors that affect measured geomaterial interface behavior have been identified and can broadly be categorized into three groups: particulate properties, continuum (counterface) properties, and test conditions.

Particulate properties that affect interface shear behavior are particle shape (at various scales, including overall shape, angularity, and surface roughness), density, particle size (this will be more extensively reviewed in later sections) and particle size distribution. Continuum or counterface properties that are of interest are the roughness of the surface and the hardness. Testing conditions that affect the measured interface response include the normal stress applied across the interface, the strain rate and the method of testing employed (type of device used).

All of these factors play some role in affecting the observed interface behavior, although to varying degrees of significance and to varying degrees of relevance to this study. The following sections will focus on the most relevant factors.

Early contributions in the study of interface shear strength mechanisms were made by (Potyondy 1961)) and (Brumund and Leonards 1973). Conclusions from these initial efforts showed that continuum surface roughness was a factor contributing significantly to the interface shear strength, as were normal load, moisture content and the properties of the sand particles. The particulate properties identified were size, angularity and surface texture. It was observed that as the surface roughness of the counterface was increased, the interface friction angle increased. This occurred until the interface friction angle was equal to the internal friction angle of the soil, leading to failure occurring within the soil mass and not at the interface.

Skinner (1969) investigated glass balls in contact with a glass plate and found that the presence of water had a very significant effect on the shear resistance. This was attributed to the change from sliding to rolling when water was present. However, the effect of water was limited to the interface since tests with glass balls in a direct shear device did not show the same increase in strength when water was present.

Yoshimi and Kishida (1981) conducted tests on dry sands at different densities in contact with steel surfaces of varying roughness. The conclusion from these ring torsional shear tests was that the coefficient of friction was mainly dependent on the continuum surface roughness and to a far lesser extent on the density of the dry sands. Further tests carried out on sand-steel interfaces by Uesugi and Kishida (1986) using a simple interface shear device showed that the continuum surface roughness, mean particle diameter, sand density and mineralogy were factors that did significantly influence the interface shear strength. They showed that there was a strong connection between mean particle size and surface roughness. This led to both the very important realization that surface roughness should be considered as a measure relative to the mean particle size and to their proposal of a modified roughness parameter, R_n , which captured this interaction.

Uesugi and Kishida (1986) found further that below a “critical roughness” the particles simply slid along the steel surface while if the surface roughness was greater than this “critical roughness” then the failure moved from occurring at the interface to occurring within the soil mass. This can be seen in Figure 2.1 below. They also found that the testing apparatus, coefficient of uniformity and applied normal stress did not play as meaningful a role in controlling the interface shear strength.

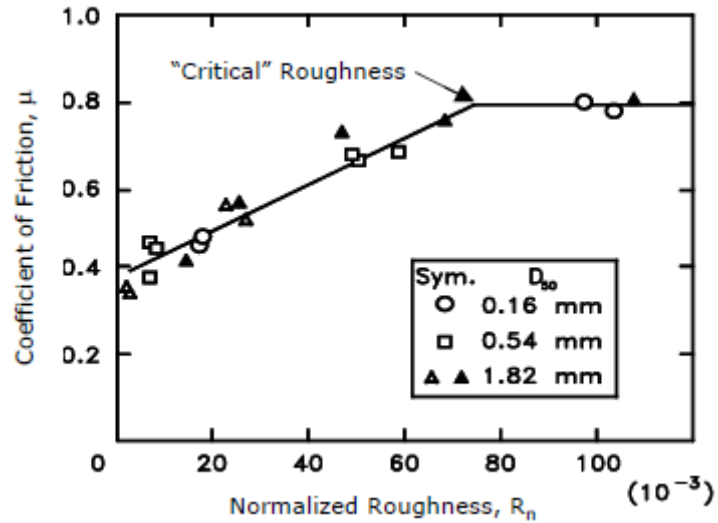


Figure 2.1 Bilinear Roughness-Friction Relationship (Uesugi and Kishida, 1986)

Williams and Houlihan (1987) studied a range of soil-geomembrane interfaces and, similarly to research with steel interfaces, it was found that the interface friction depended upon surface roughness, particle size, type and composition and the water content of the soil. Similarly to previous research, it was observed that as the roughness of the counterface increased, the failure plane moved from the interface and into the soil mass. In contrast to some of the research with steel interfaces, it was found that the normal stress and soil density did play a role, as did the tensile strength and modulus of the geomembrane.

O'Rourke et al. (1990) conducted interface shear tests on sand-polymer interfaces and focused their investigation on the effect of the surface hardness of the polymer. Both high-density polyethylene (HDPE) and polyvinyl chloride (PVC) smooth geomembranes were tested to give a range of hardness values. They observed that the interface strength decreased as the hardness of the counterface increased. Relatively hard materials (HDPE) induced sliding at the interface while relatively soft materials (PVC) induced rolling of the particles.

Using a dual interface shear apparatus Paikowsky et al. (1995) identified three distinct zones of roughness, as measured with R_n . For “smooth” surfaces ($R_n < 0.02$) the failure occurred at the soil-continuum interface while for “rough” surfaces ($R_n > 0.5$) the failure occurred within the soil mass since the internal friction of the soil was fully mobilized during shearing.

Dove (1996) completed experimental and theoretical analyses showing that the shear mechanisms for smooth geomembrane-granular material interfaces are elastic-plastic sliding and plowing. It was also found that surface roughness has a first order effect on granular material-geomembrane interface strength but there is a limit to the beneficial effect with increasing degrees of surface texturing.

Dove and Frost (1999) have shown that for Ottawa 20/30 sand in contact with a smooth HDPE geomembrane, the interface friction will initially decrease with an increase in normal stress. This will occur up until a critical stress is reached, after which the interface friction will increase as normal stress increases. At stress levels below this critical stress level, which is dependent on the material, the contact stress per particle decreases with increasing global normal stress due to an increase in the number of particles contacting the surface. The interface friction is thus decreased due to the reduced contact stresses even though the global stress level is increasing. At the critical stress, the number of particles per unit area in contact with the surface reaches a maximum and any increase in the global normal stress is reflected not in an increase in the number of contacting particles but rather in an increase in the contact stress per particle. This results in the particles plowing into the surface of the geomembrane and leads to a greater force needed to translate the soil relative to the geomembrane. There is

thus an increase in the interface friction. The critical stress was found to be approximately 60 kPa for the geomaterials tested. Plowing is especially evident for softer geomaterials, such as geomembranes, but not significant for harder materials, such as steel. Particles plowing into the geomembrane cause the geomembrane surface to change and the extent of this change can be quantified (Zettler *et al.*, 2000).

Studies have shown (Lings and Dietz 2005), that two thresholds exist in terms of interface shear behavior and surface roughness. Below a certain relative roughness the interface behavior is non-dilatative. Above this threshold, but beneath the upper limit of relative roughness, the interface behavior is that typical of sand stress-dilatancy behavior. At relative roughness values greater than the upper limit, the shear zone moves fully into the soil mass and the strength characteristics from direct shear tests are seen.

As has been summarized above, surface roughness plays a critical role in determining overall interface strength. It has also been noted that for smooth HDPE geomembranes, the displacement of sand particles relative to the geomembrane results in wear of the surface and changes in the surface roughness even at very modest normal stress levels. It is thus of great importance to further explore the mechanisms causing the changes in surface roughness and to quantify these changes.

2.3.4. Wear of Counterface Surfaces

Wear can be defined as the progressive damage, involving material loss, which occurs on the surface of a component as a result of its motion relative to adjacent working parts. It is evident that this definition can be applied to a soil-geomembrane interface. For interface shear behavior the volume of wear debris generated is not of direct interest but rather the change in surface roughness due to wear is. For the purposes of subsequent

discussion, the definition of wear will mean the change in surface roughness as measured by surface profiles taken perpendicular to the shearing direction.

Vaid and Rinne (1995) noted that grooves were formed in smooth HDPE geomembranes after shearing in a ring shear apparatus. For angular sands the groove depth did not exceed 10% of the mean particle size and the maximum amount of scarring was observed at the initiation of the residual shear stress.

Zettler *et al.* (2000) specifically investigated the wear of smooth HDPE geomembranes in contact with both sands and glass beads and showed that changes in the surface topography were a function of shear displacement, normal stress and particle shape. Results showed that angular sands resulted in the highest peak interface strengths as well as the greatest amount of surface wear while the glass beads resulted in the lowest interface strengths and least amount of wear. This is due to the propensity for the angular sands to plow into the geomembrane as a result of the higher contact stresses induced by the angular features of the particles. At low normal stresses, the angular sands did not behave significantly differently than the other sands due to the fact that, in common with the other sands, the particles slid along the surface rather than plowed into it. The transition from a sliding to plowing mode occurred at a lower global normal stress for the angular particles. Angularity was identified as an important parameter, as was normal stress. For plowing, and thus wear, to occur the normal stress must be sufficiently high so that the yield stress of the geomembrane is exceeded.

2.3.5. Measures of Relative Roughness

There are many ways of determining the roughness of a surface and many researchers have developed new ways of calculating the roughness (for a comprehensive

review see Sozer, 2005). The first study to recognize and quantify the relative aspect of surface roughness in the context of interface shear was by Uesugi and Kishida (1986). Analysis of their results showed a strong interaction between average particle size and surface roughness which indicated the importance of relating the surface roughness to the particle size. They proposed a normalized roughness parameter, R_n , which is calculated by measuring the vertical relief between the highest peak and the lowest valley over a length of profile equal to the average particle diameter and then dividing that through by the average particle diameter. This realization led to the classic bilinear plot shown earlier in Figure 2.1.

More recently research by DeJong (2001) and Sozer (2005) has moved further in this direction by developing techniques that link the particle size and characteristics to surface profiles. Kinematic measures of roughness consider a particle rolling over a surface and thus take into account the interaction between the surface and the particle. Examples of such kinematic measures are the E-system, motif system and the centroid trace method. Additional details on the E-system and motif system are provided in Sozer (2005).

The significance of “relative size” is evident in the centroid trace (CT) experiments performed by DeJong et al. (2001). CT experiments reveal that a 1.0mm and a 20.0mm diameter particle experience the same surface profile in different ways. The relative dimensions of the particle and the surface profile comprising of peaks and valleys is captured by the CT method. Complete details on the centroid trace method are presented in DeJong (2001).

Disadvantages of the aforementioned systems are that particle shapes need to be assumed a-priori and this shape is assumed to be spherical (or circular in two dimensions). This is clearly a reasonable first approximation although the affect of this assumption has not been demonstrated. The centroid trace method is essentially the same as applying a series of filters to the profile and in itself does not produce a value of relative roughness but a new profile that approximates the path that a circular particle would have taken.

3. METHODS AND MATERIALS

3.1. Introduction

This chapter describes the test program carried out in order to investigate the effect of geomaterial gradation on interface shear. The particulate and continuum materials used in this study are described and analyzed. The experimental apparatus used and procedures carried out are also presented along with analysis thereof.

3.2. Materials Tested

3.2.1. Particulate Materials

The particles used as components of the particle mixtures were obtained by scalping specific size fractions from commercially available sands, termed the “source” sands. This enabled strict control over the particle size and resulted in a very narrow range of particle sizes for each component that was then to be mixed. The three source sands used were:

- ASTM 20/30, poorly graded medium sand
- A.F.S. 50/70, poorly graded fine sand
- F-110, poorly graded fine sand

All are quartz sands with a specific gravity of approximately 2.65 (U.S. Silica data sheets). These source sands were chosen because of their appropriately different sizes and because they were all comprised of particles of the same mineralogy, specific gravity and particle shape. Bolton (1986) has shown that mineralogy plays an important role in the internal friction of sands and thus it was desired to use sands of the same

mineralogy. The sands were supplied by the U.S. Silica Company. Additional properties of these three source sands is given below in Table 3.1.

Table 3.1 Properties of Source Sands

Sand	D ₁₀ (mm)	D ₅₀ (mm)	Cu ^a	Cc ^b	e _{min} ^c	e _{max} ^d
Ottawa 20/30	0.65	0.72	1.15	1.02	0.502	0.741
A.F.S. 50/70	0.24	0.26	1.43	0.96	0.612	0.861
F-110	0.081	0.14	1.62	0.99	0.535	0.848

Note: ^aC_u=D₆₀/D₁₀; ^bC_c=D₃₀²/(D₆₀xD₁₀); ^cASTM D4253 method 1A; ^dASTM D4254 method B

The three sands obtained by scalping are designated by the sieve sizes used to scalp out the desired size fraction. The scalped components are thus termed 20/25, 50/60 and 100/140 and were scalped from the ASTM 20/30, A.F.S. 50/70 and F-110, respectively. The amount of sand obtained from scalping was as follows:

- Yield of 20/25 from source: 67%
- Yield of 50/60 from source: 81%
- Yield of 100/140 from source: 53%

These percentages show that sieving was an efficient way in which to scalp out the desired size fractions from the “heart” of the source sands while leaving behind the “head” and “tail”. While sieving does have disadvantages, one notably being that particle shape plays a role in determining which particles pass through the mesh, the advantages are significant. Principally, sieving provides a means of simultaneously characterizing and separating by size. Other methods for grain size characterization (for example by light scattering or optical methods) do not actually separate the components, which was necessary in this case.

While scalping out the desired size fractions, it was important to limit the amount of material placed into the nest of sieves. The source sands themselves were poorly

graded and thus contained a very high percentage of material that would be retained on a single sieve. This had the effect of clogging up that single sieve if too much material was sieved at a time. An amount of approximately 300g was sieved at a time to ensure that the particles did not clog any single sieve, allowing for an accurate sorting of the grains. Sieving was done for 10 minutes on a mechanical shaker as recommended by Lambe (1951).

Grain size distribution curves for the source sands as well as for the scalped sands are shown below in Figure 3.1. Additional properties of the scalped sands are given in Table 3.2 and representative microscope images are shown in Figure 3.2.

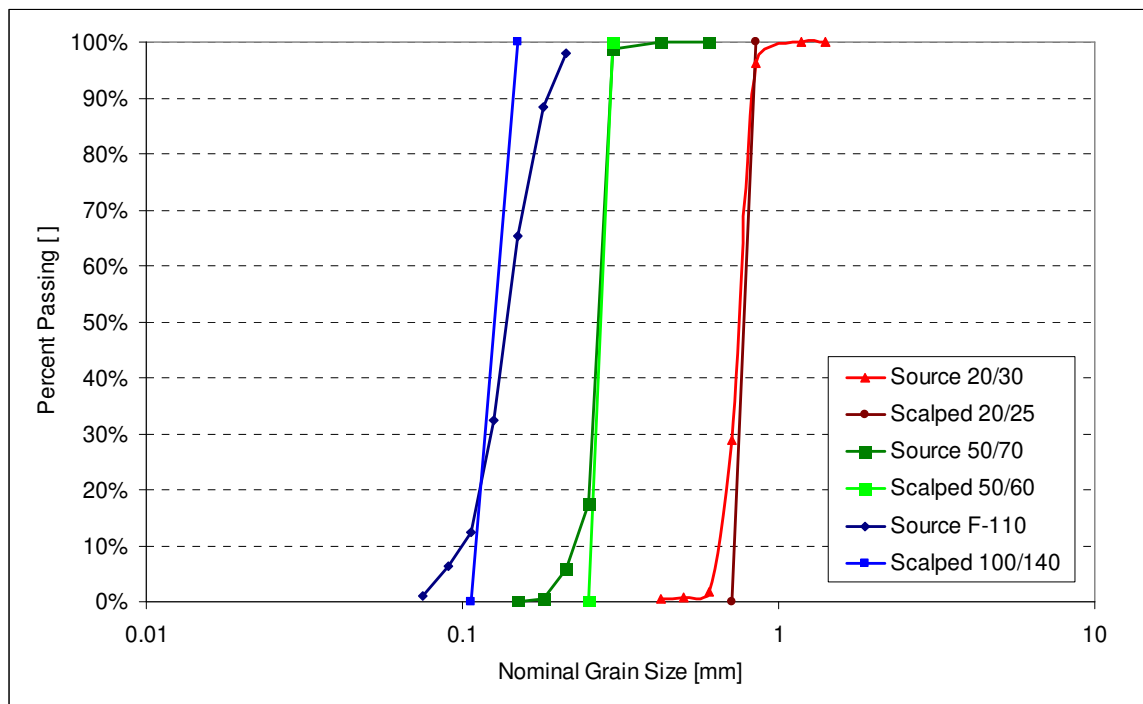


Figure 3.1 Grain Size Distribution

Table 3.2 Properties of Scalped Sands

Sand	D_{50} (mm)	e_{min}^a	e_{max}^b
20/25	0.78	0.529	0.767
50/60	0.28	0.604	0.857
100/140	0.13	0.636	0.899

Note: ^aASTM D4253 method 1A; ^bASTM D4254 method B

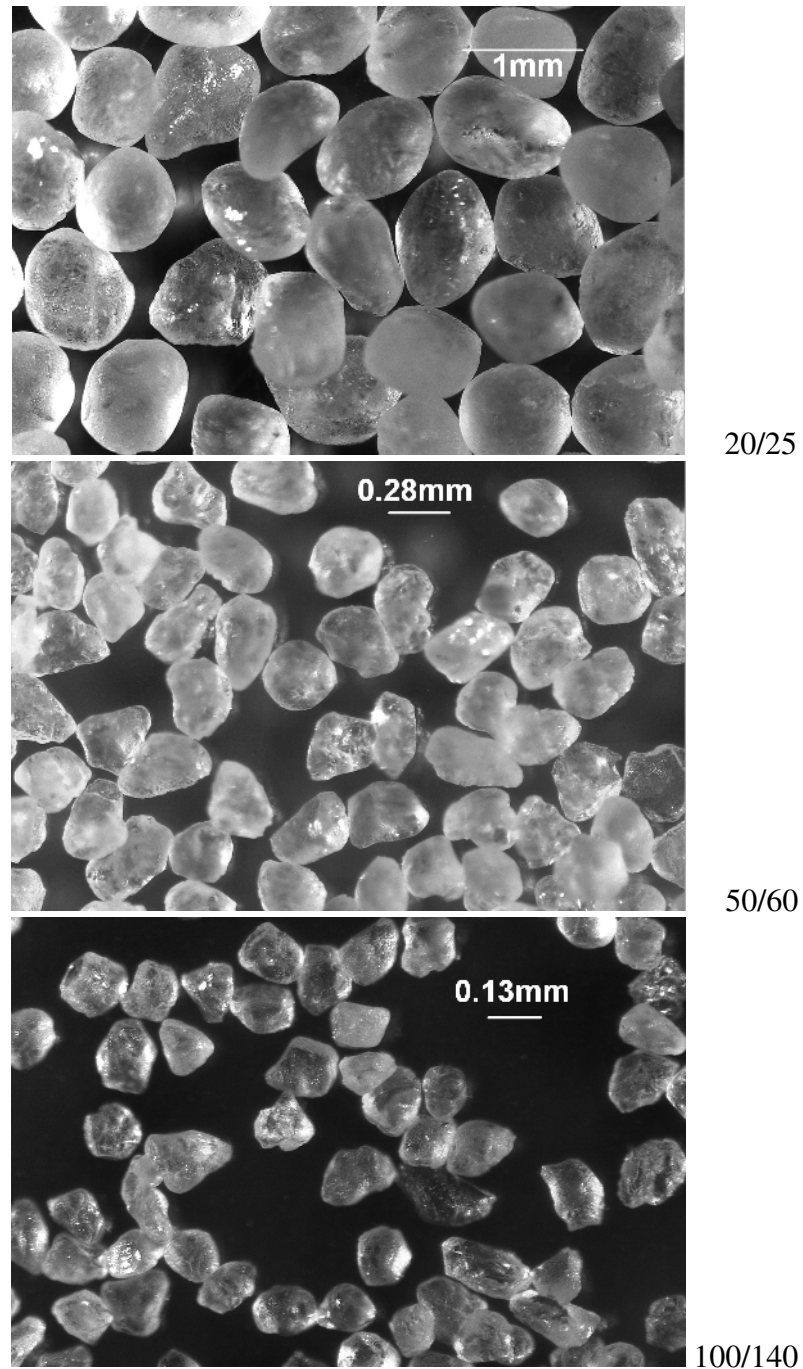


Figure 3.2 Sands used in this study, from the top: 20/25, 50/60 and 100/140

Particle shape is an inherently difficult parameter to quantify. Numerous researchers have developed different methods to quantify particle shape but no method has become accepted as standard. For this study, where particle shape is considered to be a secondary influence, a comparison of the particles to long-standing but simple shape

descriptors is made through the use of reference charts, such as the ones shown in Figure 3.3.

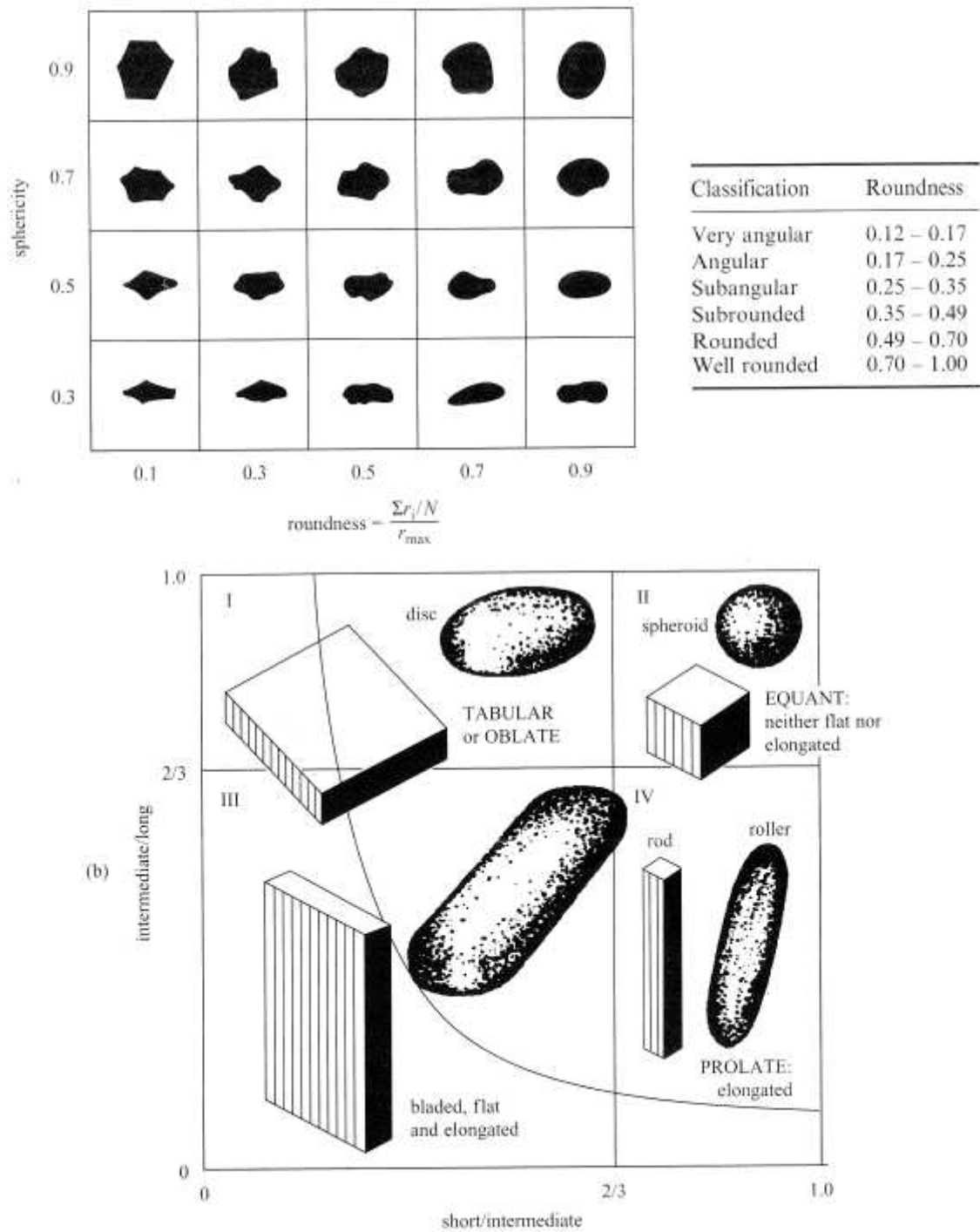


Figure 3.3 Particle Shape Reference Charts, clockwise from top left: Krumbein and Sloss, 1963; Powers, 1953; Ozol, 1978 (after Santamarina, 2001).

In relation to these reference charts, the shapes of the sands used can be described, as is summarized in Table 3.3.

Table 3.3 Shape Descriptors of Studied Particles

Particle	Shape (Ozol, 1978)	Sphericity (Krumbein and Sloss, 1963)	Roundness (Krumbein and Sloss, 1963)	Description (Powers, 1953)
20/25	Spheroid	0.7	0.9	Well rounded
50/60	Spheroid	0.7	0.7	Rounded
100/140	Spheroid	0.7	0.4	Subrounded

The shape of the sands will, to some extent, effect the observed behavior. This study is deliberately focused on the role that the size ratio and mixture proportions have.

The three sands resulting from the scalping were then combined in different ratios by mass to produce the sand mixtures that were tested. Particle size ratios of 6.1, 2.8 and 2.1 were produced by mixing 100/140 and 20/25, 50/60 and 20/25, and 100/140 and 50/60 respectively. The various mix proportions are expressed as a mass percentage of the finer particles. For example, a mixture named as “P.S.R. 2.8 60%” would be comprised of 60% 50/60 and 40% 20/25. It is important to note that the mixtures have been combined based on the weight of the components and not on the number of particles or specific surface or any other measure. This was done for practical reasons (it is simpler to accurately determine mass rather than number of particles or specific surface) and it is consistent with the other studies that have been completed on soil mixtures.

Grain size distribution plots for mixtures with different particle size ratios and percentage of smaller particles are shown below in Figure 3.4.

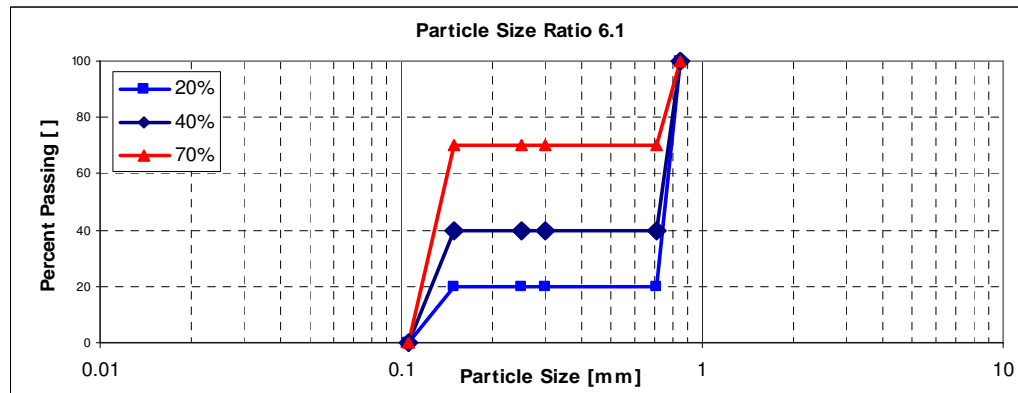
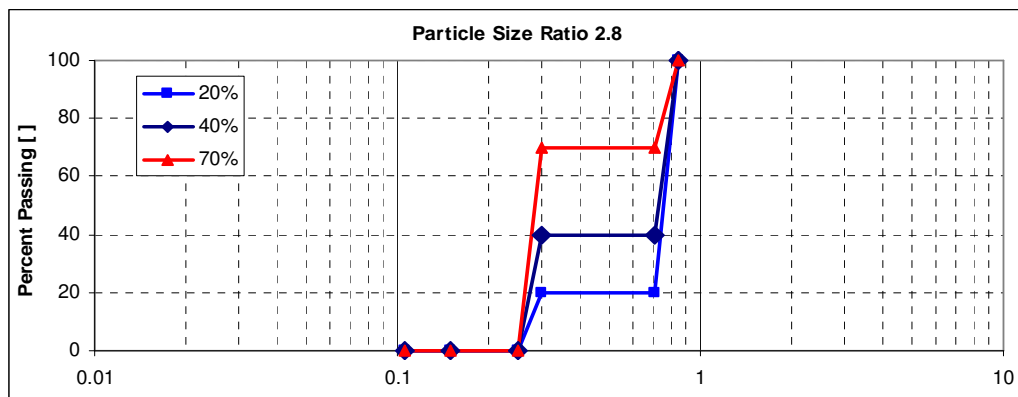
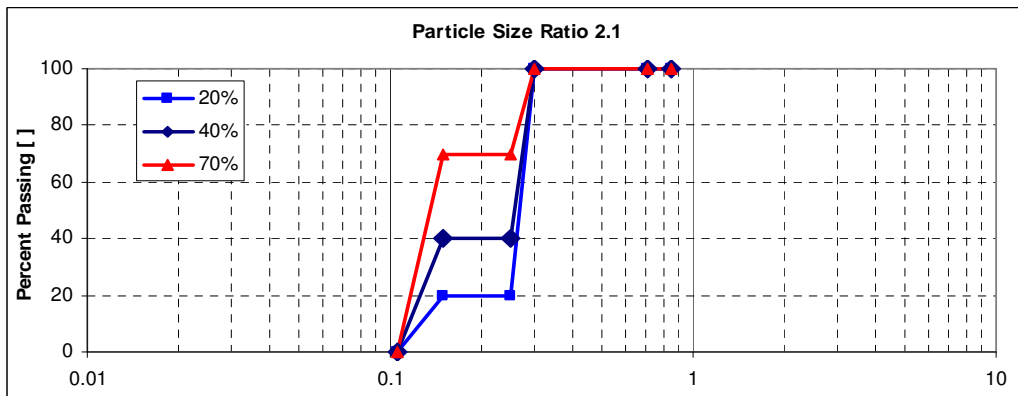
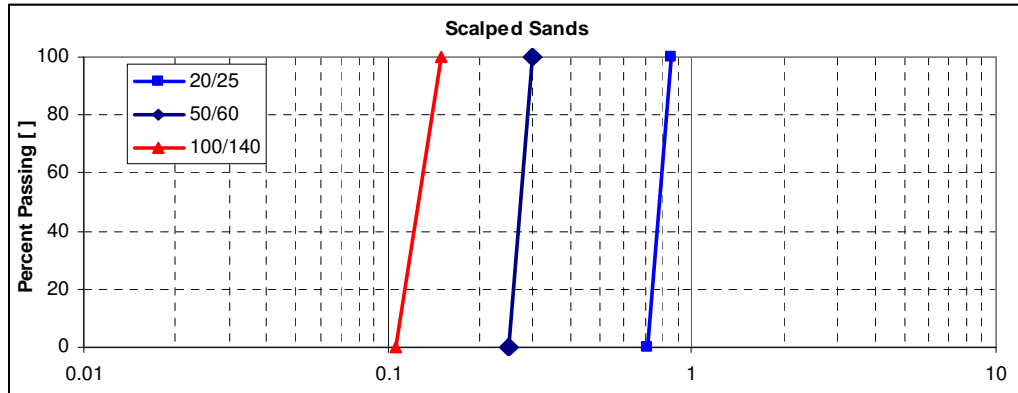


Figure 3.4 Grain Size Distribution Plots of Binary Mixtures

3.2.2. Counterface Materials

3.2.2.1. Geomembrane

The geomembrane used in this study was a smooth high-density polyethylene (HDPE) Dura Seal HI geomembrane supplied by the National Seal Company. HDPE is currently the most widely used geomembrane material due to its high tensile properties at low strain levels. Other commonly used geomembrane materials include very flexible polyethylene (VFPE) and polyvinyl chloride (PVC).

The selected geomembrane is produced from formulated polyethylene resin and contains 97.5% polyethylene and 2.5% carbon black. Selected engineering properties are listed below in Table 3.4.

Table 3.4 Properties of smooth HDPE geomembrane

Thickness (mm)	Density (g/cm ³)	Tensile Properties			
		σ_y (Pa)	σ_b (Pa)	ϵ_y (%)	ϵ_b (%)
1.0	0.94	15.4	26.6	13	700

Note: y designates yield, b designates break

3.2.2.2. Smooth Steel

The steel plates used in this study were gauge 26 mild steel. The assumed properties of the steel are listed below in Table 3.5.

Table 3.5 Properties of Mild Steel Plate

Property	Value
Elastic Modulus	200 GPa
Poisson's Ratio	0.3

3.2.2.3. Artificial Rough Counterfaces

The rough counterface surfaces were created by securing commercially available sandpaper sheets to an acrylic base using epoxy. The sandpapers were supplied by Norton Abrasives and the following grit sizes were used: 36, 60, 80, 100, 120, 150, 320 and 600. These range from a very coarse to an extra fine texture.

Care was taken when securing the sandpaper to the base to ensure that no folds, air bubbles or any other disturbances were present when the surfaces had been bonded together. A light roller, not heavy enough to damage the sandpaper surface, was used to smooth out the surface. Results from the testing of these surfaces are presented in Chapter 6.

3.2.2.4. Pipe Surfaces

The pipe surfaces tested as a part of this study were supplied from contacts in the pipe jacking industry. Short sections of pipe were provided (usually two or three feet long) which were then cut into coupons to be tested. Tested sections included pipes made from fiber-reinforced polymer (HobasTM), polycrrete, steel, vitrified clay and concrete (both a wet-cast and a pre-cast (PackerheadTM)).

3.3. Experimental Apparatus and Procedures

3.3.1. Limiting Void Ratio Tests

The maximum and minimum void ratios were determined by following the procedures specified in ASTM D4254-00 (Method B) and D4253-00 (Method 1A) respectively.

For each of the three particle size ratios, tests to determine the limiting void ratios were conducted at 10% intervals of finer component by mass. This resulted in 30

different samples being tested. For the minimum void ratio (maximum density), three trials per sample were performed, for a total of 90 trials. Due to potential particle breakage during the minimum void ratio tests, the sands were sieved between tests to ensure continually uniform particle sizes for each size fraction. It should be noted that the grain size distribution curves before and after testing were indistinguishable, indicating that particle crushing or breakage was not occurring during testing. This is due to the sands being comprised of quartz. If sands of a different mineralogy were tested (for example a calcium carbonate sand) then this may have been very important.

For the maximum void ratio (minimum density), 10 trials per test were performed, for a total of 300 trials. The difference between the number of trials for the minimum and maximum void ratio tests is due to the short duration of the maximum void ratio test and the desire to obtain some relevant statistics related to this test. The pipe pullout method was adopted as this method produced the minimum densities. This method is however somewhat influenced by the manner in which the particles are initially placed into the pipe. This is because the particles in the centre of the pipe (in a vertical column) do not move very much when the pipe is removed. The particles closer to the pipe flow and move to fill up the mold, but a substantial portion of the particles do not.

Pouring the sand into the pipe did result in some segregation of the particles based on size, this was more pronounced for the higher PSR mixtures and for higher pouring heights. For these reasons the lowest possible pouring height was used and the flow of particles into the pipe was disturbed using a long metal spoon in order to prevent this segregation from occurring.

The pipe used for the limiting void ratio tests was made from PVC and the static electricity build up due to friction with the sand particles was noticeable. The charges were large enough to influence the behavior of the 100/140 sand particles, but the other particles were unaffected due to their larger mass. This effect was mitigated by wiping down the pipe with an antistatic cloth before each test.

A further variable in these tests is the rate at which the pipe is removed from the mold. This has an effect on the way in which the particles move to fill the mold. If the pipe is removed at a very rapid rate then the sand mass inside the pipe can be lifted up and dropped back into the mold, increasing the energy input into the formation of the specimen. If the pipe is removed too slowly then a stop/start or slick/slip type of motion occurs. Based on the experience of performing many tests, the correct manner in which to perform these tests was at the slowest possible speed that would allow for a continuous flow of particles from the base and sides of the pipe as it was removed. This was quite easily achieved with some practice and is thus not considered to have had any significant effect on the measured results.

With multiple trials being performed for each test there are a number of different ways in which the test result can be reported. A simple arithmetic mean could be reported as the average result but since the test is designed to find the limiting condition it is plausible to choose the limiting (or most extreme) result and to report that as the limiting void ratio. The approach adopted in this study was to choose the limiting value provided that it was not considered to be an outlier. Outlier data points that clearly seemed to be unrepresentative of the material behavior but a reflection of some other influence (be it a procedural error or something else) were not used. The process used to obtain the results

does thus contain a subjective element. In practice, however, the limiting values used and the mean average approach were seldom very different due to the simple nature and repeatability of the test. This was an additional reason to conduct so many trials, since the more trials that one performed the more confidence one would have in the data. Results from the limiting void ratio tests are presented in Chapter 4. The complete record of all limiting void ratio tests performed is presented in Appendix A.

An additional series of maximum void ratio tests was performed in order to assess the propensity of the particle mixtures to segregate during testing. Mixtures comprising 40% finer particles and with a particle size ratio of 6.1 were used for these tests. This particle size ratio is the most susceptible to segregation due to the large difference in particle size.

The samples were built and tested in exactly the same way as was done previously. At the completion of the test the particles were carefully removed in four layers of equal mass. The particles from each layer were then independently sieved to determine the percentage of each component for each layer. Results from the segregation tests are presented in Chapter 4.

3.3.2. Direct Shear Tests

Direct shear tests were conducted in order to obtain the strength parameters of the various soil mixtures. The peak and post-peak strengths were obtained, and thus a measure of the dilatancy could be determined. Tests were conducted for each particle size ratio on particle mixtures of 20%, 40%, 60% and 80% of finer particles at stress levels of 50, 100, 300 and 500 kPa (the same stress levels that were used for the interface shear tests). The uniform sands were also tested, giving a total of 60 tests.

A GeoComp ShearTrac direct shear device was used to conduct the direct shear tests on the particle mixtures. The device contained a 63.5mm circular shear box. All testing parameters were controlled and monitored through a connected computer utilizing GeoComp test control and data acquisition software. The maximum displacement was approximately 8mm. The shearing rate was set at 1mm/min (the same as for the interface shear tests) and measurement readings were taken every second. The vertical and horizontal force applied and the vertical and horizontal displacements were all continuously monitored. Rough porous stones were placed in the base of the shear box and between the top of the sample and the loading cap.

Dry samples were prepared in the shear box to relative densities of approximately 80% +/- 5%. These densities could be consistently obtained across the range of particle mixtures using a dry tamping method and building the sample in three layers with the predefined shear plane passing through the center of the middle layer. Results from the direct shear tests are presented in Chapter 4.

3.3.3. Stylus Profilometry

Surface profiles of each counterface surface tested in interface shear were recorded using a Taylor-Hobson Form Talysurf Series 2 stylus profilometer. The stylus tip was set to move at a speed of 1mm/second. The gauge range for the relief was set at 2.1 mm and the data was acquired with a resolution of 32 nm in the vertical direction. Data points were recorded at micron intervals in the travel direction.

Many roughness parameters can be calculated from a surface profile, each one having generally been developed with a specific purpose or application in mind (see Sozer, 2005 for a thorough treatment). For the purposes of this study and to facilitate

comparison with previous work, the average roughness parameter, R_a , was used. This widely used and accepted parameter provides the average vertical deviation of the surface profile from the mean line.

Profiles were recorded over a length of 40mm and were taken both before and after shearing. This enabled a reliable baseline to be established. In addition, repeat measurements were taken across various spatial scales to verify the precision and repeatability of the profilometer results. One set of surface roughness measurements was taken by passing the stylus over the same path multiple times. This was achieved by securely clamping the geomembrane to the testing platform and ensuring that the correct travel limits were set on the profilometer. Ten passes were made over what was, within the accuracy of the setup, the same travel path. The results of these ten passes, together with some measures of variation in the data are shown below in Table 3.6.

Table 3.6 Repeatability measurements along same path

Pass	R_a (10^{-4}mm)
1	1.473
2	1.642
3	1.586
4	1.682
5	1.506
6	1.517
7	1.643
8	1.668
9	1.501
10	1.617
Arithmetic Mean	1.583
Standard Deviation	0.074
Coefficient of Variation	0.047

As can be seen in Table 3.6 the coefficient of variation for this set of measurements is 4.7%. This indicates a narrow spread in the data and good repeatability

of the R_a measurement. The minor variations seen in the data are most likely due to the stylus not tracing the exact same path across the surface. The tip of the stylus may fall on either side or on top of peaks in the surface resulting in slightly different measurements.

A second set of repeatability measurements was made to compare the average roughness measurements across different locations on a single coupon cut from a large roll of geomembrane. Ten profile measurements were made on each of three coupons. The results are presented in Table 3.7 below.

Table 3.7 Repeatability measurements on different coupons

Pass	Coupon A	Coupon B	Coupon C
1	1.4921	1.6751	1.5602
2	1.5075	1.6388	1.3341
3	1.2737	1.5915	1.5577
4	1.3154	1.6345	1.4488
5	1.5296	1.7715	1.2839
6	1.6655	1.1750	1.6472
7	1.7065	1.2966	1.2874
8	1.8474	1.3839	1.2397
9	1.8329	1.2354	1.4671
10	1.7245	1.3824	1.6561
Arithmetic Mean	1.59	1.48	1.45
Standard Deviation	0.189	0.197	0.147
Coefficient of Variation	0.119	0.134	0.102

Note: All measurements: R_a (10^{-4} mm)

This set of data indicates that within each coupon there is a coefficient of variation of approximately 11.8%. This is greater than the variability seen for multiple measurements of a single profile so the increase is due to the different locations of the profiles within the coupon. This is entirely expected but still indicates that there is not a significant variation in roughness across an individual coupon. There is also not a

significant variation across the three different coupons, indicating that regardless of where the material was cut from within the large roll the average surface roughness is approximately the same. The overall average roughness for the smooth HDPE geomembrane in its virgin state is thus taken as 1.51×10^{-4} mm, the average across the coupons tested.

Profiles recorded post-shearing were taken at the midpoint of the path traveled by the particulate specimen as this location had been found to be the point at which maximum surface wear occurred (Zettler et al., 2000). Since the roughness induced by the shearing was of specific interest, a Gaussian filter was used to omit some frequency components. Wavelengths greater than 2.5mm and less than 8 μ m were omitted from the roughness calculations. This enabled comparisons with data sets from previous researchers who had used these standard filters.

3.3.4. Interface Shear Tests

3.3.4.1. Device Description

The interface shear tests were performed using a custom built modular shear device. The base device has been through a number of design changes since it was first constructed and these changes were summarized by Zettler (1999). The device uses a ball screw-jack driven by a 120 volt DC motor to displace the shear box relative to the counterface. Gear reducers are used to achieve the slow strain rates required for testing and the drive system is controlled electronically through a DART speed control system. Limit switches are used to prevent the device from running beyond allowable physical limits. Vertical load is applied through a pneumatic cylinder which is mounted directly

beneath the sample and can move to stay in the same position relative to the sample. A photograph of the device can be seen in Figure 3.5.

The sensing devices consist of two load cells, monitoring vertical and horizontal force, and an LVDT measuring the horizontal displacement. The signals transmitted from the load cells and LVDT were collected by a data acquisition system consisting of three parts: a data acquisition/switch unit, a 16-channel multiplexer module, and a USB/GRIB Interface. The multiplexer module had a maximum scanning rate of 250 channels per second and has a 22 bit resolution. External wiring was minimized in order to reduce the amount of noise entering the system. The data could be monitored in real time using HP BenchLink software installed at the switch unit.

There are a number of issues related to testing using these types of interface shear devices. Particles can slide underneath the shear box that is moving over the top of the counterface. Smaller particles, greater surface texturing and high normal stresses will accentuate this issue. Particles can become lodged between the box and the surface, potentially increasing the shear stress. Lodged particles may also plough into softer counterface materials. As particles are lost out the rear of the box the measurements of vertical displacement become uncertain. Since there is not an established way to account for these effects by post-processing of the data it is best to minimize this effect through careful design.

Shear stresses can also develop along the inside walls of the shear box. By constructing the shear box out of hard, smooth, low-friction surfaces these effects can be minimized. The normal stress applied may also be non-uniformly distributed across the surface. Ensuring an adequately rigid load-transfer plate and centralized point of load

application will minimize these effects. During testing it was observed that the applied normal stress was varying by approximately 5% from the expected value, with a generally decreasing trend as the test progressed. This was most likely due to the leak-off of air from the pneumatic system. Since the variation was small this issue was not directly addressed during testing. The data reported from the affected tests is also shown in normalized format which reduces the impact of this minor variation.

Inherent to particulate materials is the formation of force chains to transfer load. This cannot be controlled experimentally. Shearing at the interface is also progressive in nature, generally starting at the rear of the specimen and propagating forward (in the direction of travel). This can cause peak shear stress measurements to be dependent on the size of the shear box. Residual shear stress measurements will not be similarly affected.

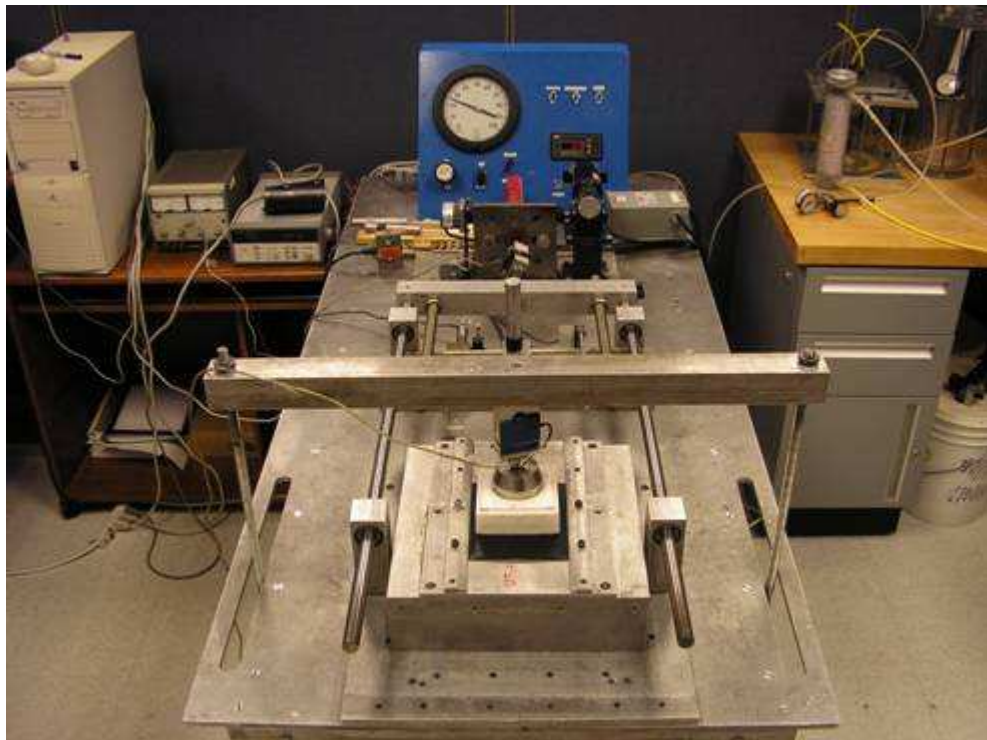


Figure 3.5 Photograph of Modular Interface Shear Device

3.3.4.2. Tests on smooth geomembranes

For these tests the direct interface shear module was used in conjunction with a circular 63.5mm diameter Teflon shear box. The specimen height was 38.1mm and specimens were prepared to a relative density of 80 (± 5)% using a dry tamping method and preparing the sample in 5 layers of equal mass. The lower layers were under-tamped to account for the additional tamping that was to come as subsequent layers were placed.

Geomembrane specimens were cut from a larger roll and clamped securely to the testing platform. The orientation of the geomembrane with respect to machine direction and shearing direction was consistent across all tests but was not considered to have any effect on the results. This is due to the uniformity of the smooth geomembranes used. Tests were performed at applied normal stresses of 50, 100, 300 and 500 kPa at a constant displacement rate of 1mm/minute, these parameters are the same as those used for the direct shear tests. Tests were performed to a maximum of 40mm total displacement. During testing, the vertical load, horizontal load and horizontal displacement were each recorded at a frequency of 1 Hertz using the digital data acquisition system.

3.3.4.3. Tests on rough counterface surfaces

The same suite of tests as was conducted on the smooth counterface was conducted on the rough sandpaper surfaces. The only difference was that a newly designed shear box was used in place of the circular shear box.

A new shear box was designed and built specifically for the current study. The shear box attaches to the drive train of the device in the same way as the circular shear

box described before. The purpose of the new shear box is to allow direct visual observation of the particles in contact with the counterface.

The new shear box, known as the “VisionBox”, is rectangular and made of smooth aluminum. One side is made of polycarbonate, which is optically clear and rigid. The maximum mid-span deflection in this panel is estimated to be less than 0.1mm. Machine tolerances were approximately 0.05mm.

Figure 3.6 below shows the repeatability of this shear box when sheared against a rough counterface. Minor variation is noticed in the displacement to peak friction coefficient but otherwise the graphs are virtually identical.

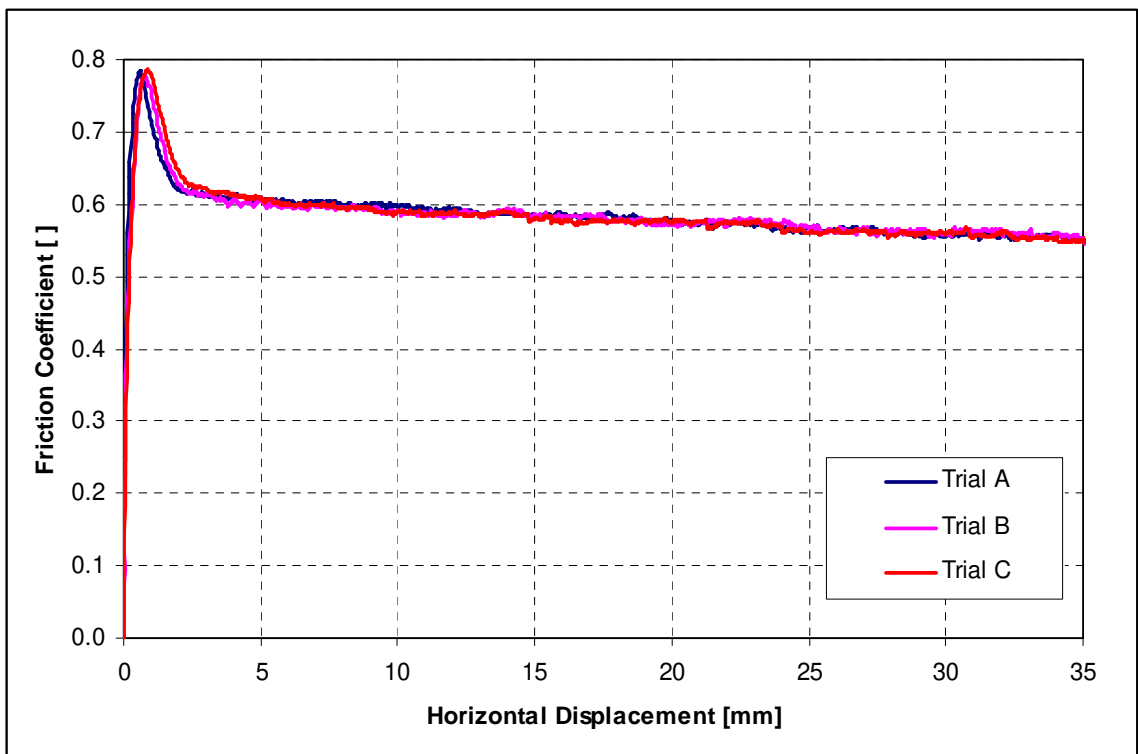


Figure 3.6 Repeatability Test for Rough Counterface Testing (Mixture of 10% 100/140 and 90% 50/60)

4. PROPERTIES OF BINARY PARTICLE MIXTURES

4.1. Introduction

In a general sense, mixtures are often created with the purpose of combining the properties of the separate components in order to achieve a mixture that has more desirable properties than either of the separate components acting alone. An example of this would be a retirement portfolio that holds a combination of stocks and bonds. The combination of these two asset classes produces a superior risk-adjusted return than either of the two asset classes would by themselves.

A mixture between two components can also result in a fundamental change in the materials. For example, the mixture of two liquids in a chemistry laboratory may give rise to a liquid and a gas. An engineering example would be a fiber-reinforced composite, where the combination of glass fibers and a polymer matrix gives rise to a material with properties very different from either of the components.

In contrast, mixing two different granular soils together does not fundamentally alter the nature of the material. The resulting mixture is still a granular material comprised of discrete particles that can be described by the same mechanics and set of parameters. As such, the mixtures can be readily compared with the separate components in order to understand how the particle size ratio and percentage of finer material affects the behavior and properties. While the mixtures are fundamentally similar to the components, there are interactions possible in a mixture that are not possible in either of the components alone, and these interactions may give rise to behaviors that were not obvious from examination of the components alone. One such behavior that is not

possible for an individual component is that of segregation. The separation of different particles based on size is a concern only for mixtures with different sized particles. The segregation phenomenon is a fundamental property of the granular state (Duran, 2000) and is often referred to as the “Brazil nut” phenomenon because of the observation that when transporting a mixture of nuts in the back of pickup trucks in South America, the Brazil nuts (the largest) invariably ended up on top of the pile. Segregation is an entire topic of discussion by itself and a detailed examination of it will not be attempted here. A brief look at segregation is, however, required since the effect of segregation poses a question when one is considering how to prepare a homogenous sample of a mixture that has a tendency to separate out.

A mixture of two granular soils, each of which may actually possess similar characteristics (such as strength or permeability), may not always be feasible in order to balance strengths and weaknesses (as was the case for the retirement portfolio). In this study the materials that have been mixed are relatively similar, differing mainly in their size. A unique material was created when the components were mixed but the objective was not to create a new material to study, rather the purpose was two-fold: (i) to approximate a gap-graded soil; and (ii) to create a set of soils that could be tested which varied within a well defined and measurable framework (the percentage of finer to course material and the size ratio between the particles).

The choice to study binary mixtures, as opposed to ternary or other higher order mixtures, was made in order to limit the potential number of mixtures that had to be tested in order to test materials occupying the entire experimental space. Binary mixtures

can readily be characterized by the particle size ratio and the percentage of finer material. These are the two aspects that fundamentally characterize the mixtures in this study.

This chapter will focus first on the way that particles in a binary mixture pack together. The void ratios at the states of maximum and minimum density will be examined and a model developed that will allow for the prediction of the mixture void ratio as a function of the void ratios of the components, the particle size ratio and the percentage of finer material in the mixture.

The shear strength of mixtures will be examined in the second part of the chapter by utilizing a unique data set obtained from direct shear testing. The peak and residual shear strengths are examined in relation to the mixture properties. The effects of normal stress and dilation will also be examined. This section of the study will also serve as a reference point for the interface shear strength studies that will be presented in Chapters 5 and 6.

4.2. Limiting Void Ratios

4.2.1. General discussion on limiting void ratios

The void ratio describes the relative amount of void volume to solid volume in a given sample. A given soil can exist through a range of void ratios, so the void ratio given for a particular soil describes the current state of the soil. It is oftentimes more helpful to describe the state of a soil in relation to some reference or limiting state. Two reference states exist, the maximum and minimum void ratios. These correspond to the arrangement of particles that give the minimum and maximum densities, respectively.

Narsilio and Santamarina (2008) suggest that there exists a terminal void ratio (or terminal density) corresponding to each soil and the process used to achieve that terminal

void ratio. They also propose that there exist two limiting states: a state of certain dilation (a geometric limit) and a state of certain contraction (a stability limit). All possible terminal void ratios would fall between these two limits. Based on this approach it would appear to be more appropriate to consider that the limiting void ratios found experimentally be considered not to be the ultimate limiting states, but rather, to be the terminal void ratios of the particular process used to achieve that state. To claim that the limiting void ratios found experimentally are in fact the ultimate limiting void ratios (or true limits) implies that the process followed was indeed that single process that resulted in the true limiting state being found. Since it would be a never ending process to determine what that exact process was, it implies that the true limit can never actually be attained experimentally (or numerically for that matter).

The procedures set forth in the relevant ASTM standards are however expected to give values very close (perhaps even indistinguishable from) the true limiting values. It must also be noted that the standards do allow for different methods to be used to determine the maximum void ratio, and the method that results in the maximum values should be used. This is a tacit acknowledgement that different soils will achieve limiting states via different processes. While the limiting void ratio found in this study may not be the true limits, there is not expected to be any significant difference between the limiting void ratio values presented and the true (theoretical) limiting values.

A very helpful concept in the study of limiting void ratios is the notion of relative density. This parameter expresses the void ratio as a percentage between 0% and 100% where 0% corresponds to the maximum void ratio and 100% corresponds to the minimum void ratio. The expression for relative density is:

$$D_r = \frac{e_{\max} - e}{e_{\max} - e_{\min}} \quad \text{Equation 4.1}$$

where: e_{\max} = maximum void ratio

e_{\min} = minimum void ratio

e = current void ratio

4.2.2. General factors affecting limiting void ratios

Limiting void ratios have been extensively studied in the past. An excellent summary of information can be found in Selig and Ladd (1973). It is shown that both maximum and minimum void ratios decrease with an increase in mean particle size (for clean sands). The effect is not strong and is not expected based on theoretical considerations which indicate that the void ratio should be independent of mean particle size. It is also shown that both the maximum and minimum void ratios decrease with increasing particle roundness. This effect is most pronounced for particles characterized as very angular and angular and is somewhat weak for particles described as rounded and subrounded. The particles used in the current study are classified between being well rounded and subrounded (Chapter 3) and therefore the effect of particle shape is not expected to be a strong factor. The particle size distribution as measured by C_u is also shown to influence the limiting void ratios. An increasing C_u corresponds to a decreasing void ratio. This effect is stronger for the maximum void ratio than for the minimum void ratio.

4.2.3. Limiting void ratios of binary mixtures

Consider a stable assembly of identical spheres: the void space can be filled with smaller spheres resulting in an assembly with a lower void ratio. This process can in turn

be repeated ad infinitum with ever decreasing size particles. A number of general observations can be made:

- Mixing particles of different sizes results in a denser mixture
- The greater the difference in particle size the denser the mixture
- A maximum density must be reached once some fraction of smaller particles has been added

Consider the changes in the fabric of the binary particle mixture shown below:

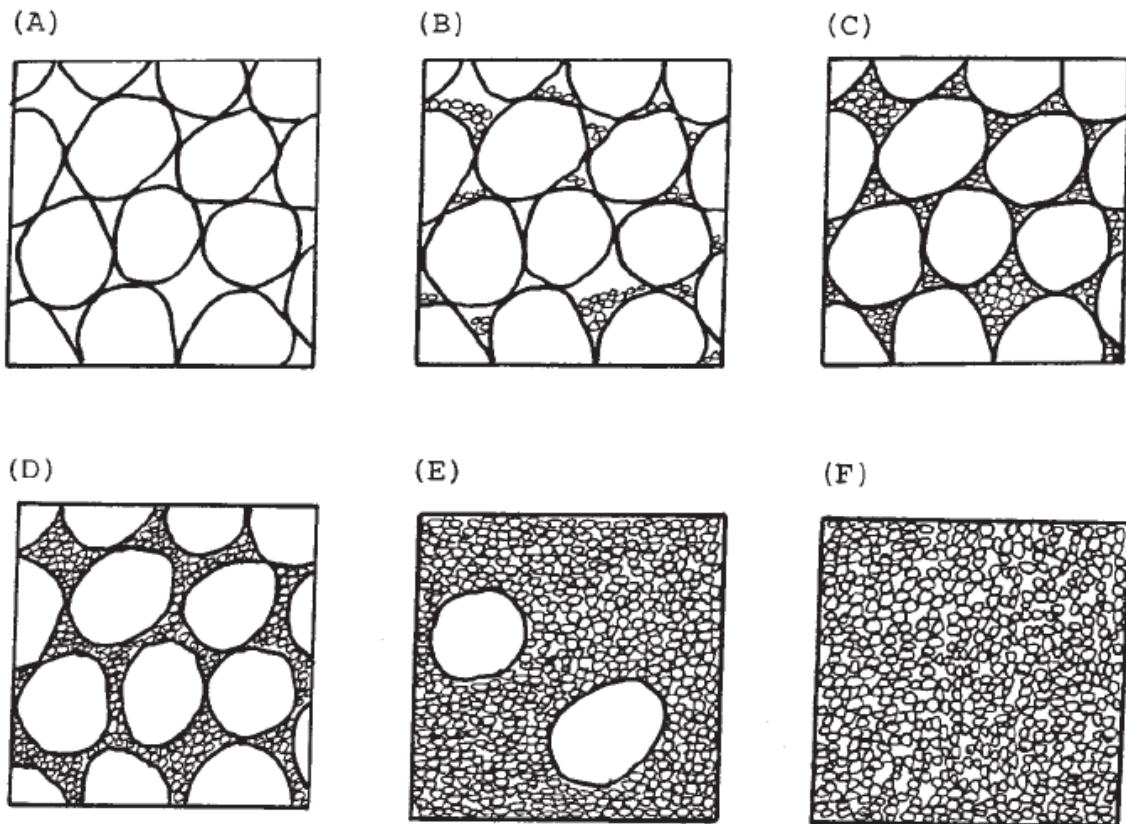


Figure 4.1 Changes in fabric in a binary particle mixture (Vallejo, 2001)

Case A shows a coarse grain matrix without finer particles. Case B shows a case when some small amount of finer particles have been added to the coarse matrix. Case B will have a lower void ratio than case A. The smaller particles may serve as wedges

which will constrain rotation and relative movement between particles, thus leading to an increase in the shear strength. The smaller particles will not however participate in force chains and the load will be carried predominantly by the large particles. There are not sufficient small particles to provide lateral support to the force-carrying large particles. There will be an increase in the average coordination number as well.

Continuing to add finer particles will result in case C, where all of the available void space between the coarse particles is filled with finer particles. Case C thus corresponds to the state of minimum void ratio. In this case the smaller particles are present in sufficient numbers to provide lateral support to the force chains. The smaller particles provide many contact points with the larger particles leading to a large increase in the average coordination number and allowing the stress being carried to be more evenly distributed throughout the assembly. The smaller particles also serve to prevent rotation and relative displacement between particles. One may expect a soil at this state to reflect the highest shear strength.

If additional finer particles are added they will start to take the place of the coarser grains. The coarser grains will no longer be in contact and will float within a sea of smaller particles, as is shown in cases D and E. The properties (friction, surface roughness, mineralogy) of the smaller particles is thus now primary. The large particles are surrounded by smaller particles and as such the average coordination number for the large particles is very high. The average coordination number for the smaller particles is lower, and is basically that of an assembly of all smaller particles.

Case F is the opposite of case A, the entire assembly is made of finer particles. Note that the only difference from case A to F is that of scale, one can expect the two

assemblies to have the same void ratio (assuming particle characteristics, except for size, remain constant).

4.2.4. Visualization of Binary Mixtures

The previous section illustrated in general terms how the addition of a second component creates a binary mixture and the associated fabric with varying amounts of finer and larger particles. For the mixtures used in this study, namely of P.S.R. 2.1, 2.8 and 6.1, the diagrams (in two dimensions) for the percentage of finer material of 0%, 40% and 100% are shown below in Figure 4.2.

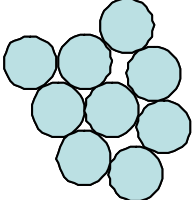
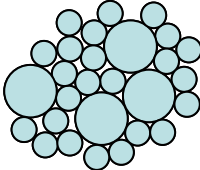
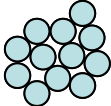
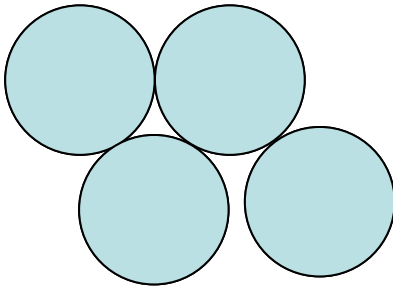
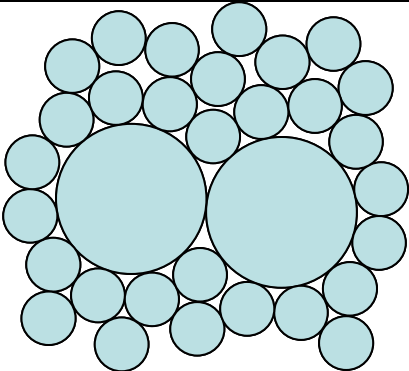
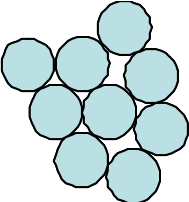
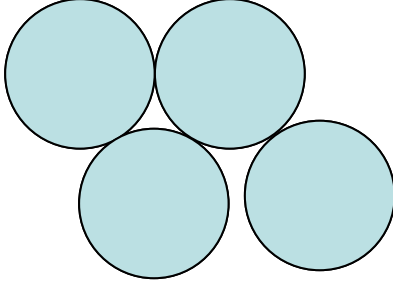
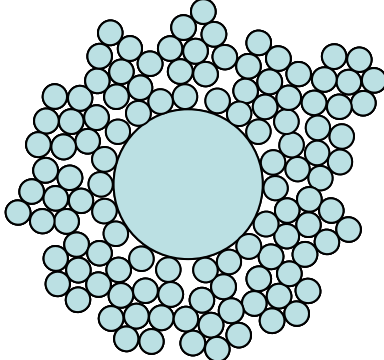
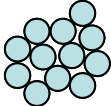
PSR	Percentage Finer Material		
	0%	40%	100%
2.1			
2.8			
6.1			

Figure 4.2 Visualization of Binary Mixtures

4.2.5. Selection of particle size ratios for this study

The particulate materials were introduced in Chapter 3 but it is now time for a more detailed examination of why the particular size ratios were chosen for this study. To recall, the particle size ratio is defined as the ratio of the largest to the smallest particle and the particle size ratios chosen were: 6.1, 2.8 and 2.1.

The figure below demonstrates the rationale clearly:

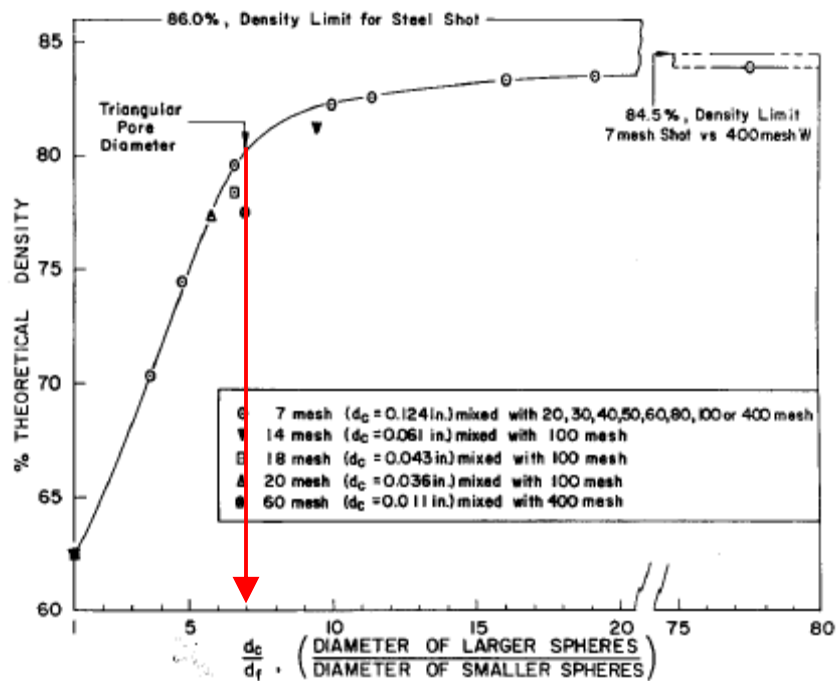


Figure 4.3 Maximum observed packing of binary mixtures (McGeary, 1961)

Beyond a size ratio of approximately 7 (indicated by the red arrow at the “knee” of the curve) the density (or void ratio) is not expected to change significantly as the size ratio changes. The expected void ratio for mixtures with a size ratio of 20 is not that different from a mixture with a size ratio of seven. On the other hand, for mixtures with size ratios between 1 and 7, there is a significant change in the expected void ratio. A “mixture” with a size ratio of one is not a mixture, but just a uniform soil. Choosing size

ratios of 2.1, 2.8 and 6.1 covered the region where the expected void ratio changes with size ratio would be the greatest.

Another consideration in choosing the size ratios was when segregation due to vibration was considered. The minimum void ratio test is a situation where such a situation exists. In vibratory situations there is a critical diameter ratio which will allow for continuous rise of the larger particles due to vault effects. This is when we consider the stability of a larger intruder particle rising through a continuum of vault configurations such that the intruder particle is stable when it rests on two particles below its center of gravity (Duran, 2001). The critical diameter ratio is found analytically to be 2.78 which agrees with values found from numerical simulations.

Based on the above observations the size ratios chosen cover values above and below this critical ratio as well as covering the region of behavior where the greatest changes in void ratio as a function of particle size ratio are likely to take place.

4.2.6. Results of limiting void ratio tests

4.2.6.1. Minimum Void Ratio

The vast majority of previous studies have examined the case of minimum void ratio (or maximum density). Results from the current study are presented below.

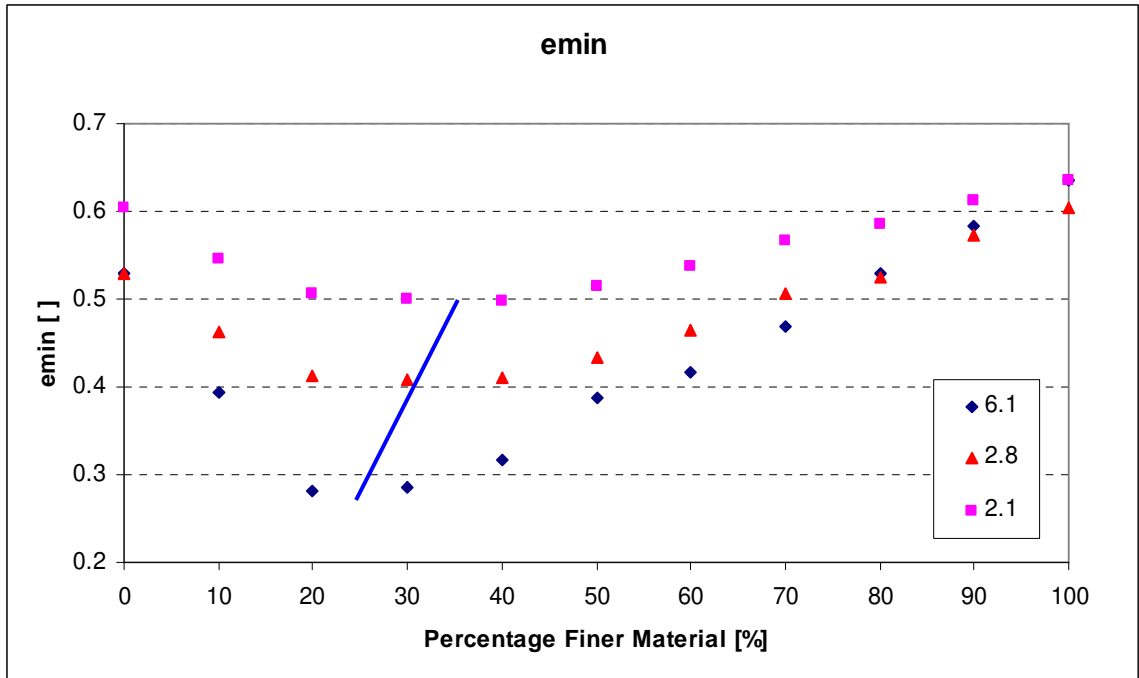


Figure 4.4 Minimum void ratios

Figure 4.4 shows how for all the size ratios considered the minimum void ratio varies as the percentage of finer material ranges from 0% to 100%. A number of observations can be made:

- All the data show a similar trend; an initial decrease in the void ratio as finer material is added, a gradual bottoming out, and a subsequent increase in the void ratio until only the finer material is present.
- The decrease in void ratio becomes more exaggerated with an increase in the particle size ratio.
- As the particle size ratio increases, the percentage of finer material required to reach a minimum void ratio decreases (as indicated by the blue line).

- The percentage of finer material at the minimum void ratio varies from approximately 25% for the 6.1 size ratio, to 30% for 2.8 and to 35% for the case with a size ratio of 2.1.
- At 0% finer particles the difference between 20/25 and 50/60 is explained by the minor difference in particle shape. The 20/25 is a more rounded shape than the 50/60 and thus the 0% point for particle size ratios of 6.1 and 2.8 are less than the void ratio for the 0% point for a particle size ratio of 2.1.
- At 100% finer particles a similar observation can be made. The 100/140 particles are more angular than the 50/60 particles, resulting in a higher void ratio.

4.2.6.2. Maximum Void Ratio

The data for the maximum void ratio is shown below:

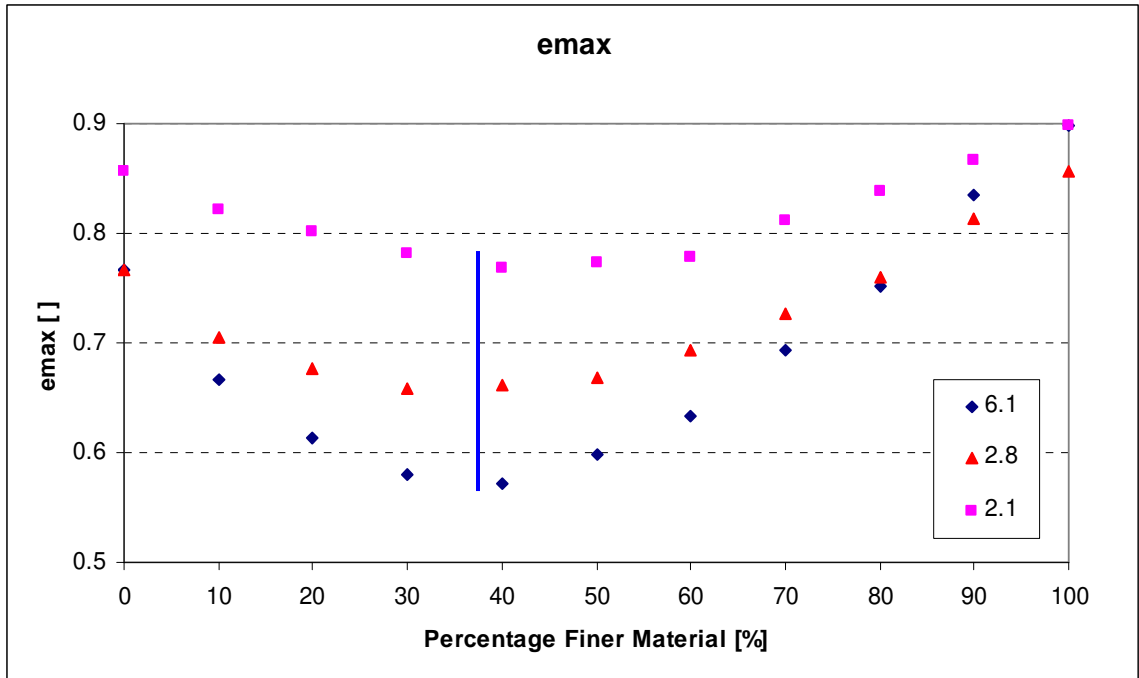


Figure 4.5 Maximum void ratios

Figure 4.5 shows how for all the size ratios considered the maximum void ratio varies as the percentage of finer material ranges from 0% to 100%. A number of observations can be made:

- All of the curves show a similar shape to each other as well as to the minimum void ratio curves.
- The lowest values for these cases are almost the same (blue line), indicating that the percentage of finer material required to achieve the lowest maximum density is approximately constant regardless of the particle size ratio and is approximately 38% for all the particle size ratios.

4.2.6.3. Same data – improved presentation

The general trends and some general observation can be made from the above void ratio plots but the data is somewhat obscured by the fact that the initial and final

points (0% and 100% percentage finer material) are at different levels. This is inevitable when using real particles as the limiting void ratio depends on a number of factors, as previously discussed.

The differing start and end points makes direct comparisons less clear and also does not facilitate modeling the data. An improved method of examining the data was thus developed. This will allow more clear comparisons, and thus a better interpretation of the data, as well as allow for a simpler approach when developing predictive equations.

The new approach for examining the data seeks to isolate the effect of mixing the two components while minimizing any other effects. The method developed determines the ratio between two volumes. One volume is the sum of the volumes of the two components when each component is not mixed. The other volume is the volume of the mixture resulting from mixing the same two components. Visually, it can be thought of as the ratio between the volume of a layered system versus the volume of a homogenous mixture, for the same mass of material.

The volume reduction is expressed as a ratio between these two volumes and can be calculated as a function of the percentage finer material, the porosity of the mixture and the porosity of each of the individual components. The method applies equally well to either the minimum or maximum void ratio cases. The volume reduction ratio can be expressed as:

$$VRR = \left[\frac{(1 - n_{mix})(p_{small})}{(1 - n_{small})} + \frac{(1 - n_{mix})(1 - p_{small})}{(1 - n_{large})} \right]^{-1} \quad \text{Equation 4.2}$$

Alternatively, the n_{mix} can be expressed as:

$$n_{mix} = \frac{\frac{(p_{large})}{(n_{large} - 1)} + \frac{(p_{small})}{(n_{small} - 1)} + \frac{1}{VRR}}{\frac{(p_{large})}{(n_{large} - 1)} + \frac{(p_{small})}{(n_{small} - 1)}} \quad \text{Equation 4.3}$$

where:

n_{mix} = porosity of the mixture

n_{small} = porosity of the small particles alone

n_{large} = porosity of the large particle alone

p_{small} = percentage of small particles

$p_{large} = (1 - p_{small})$ = percentage of large particles

VRR = volume reduction ratio

The benefits of remapping the data are clear below:

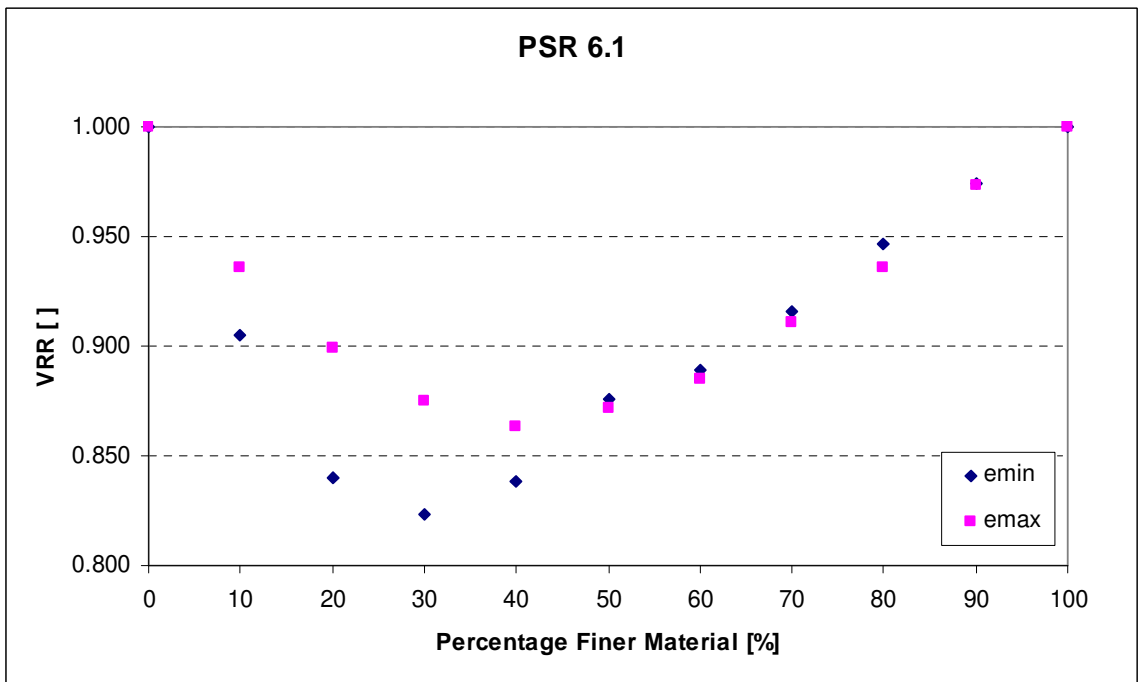
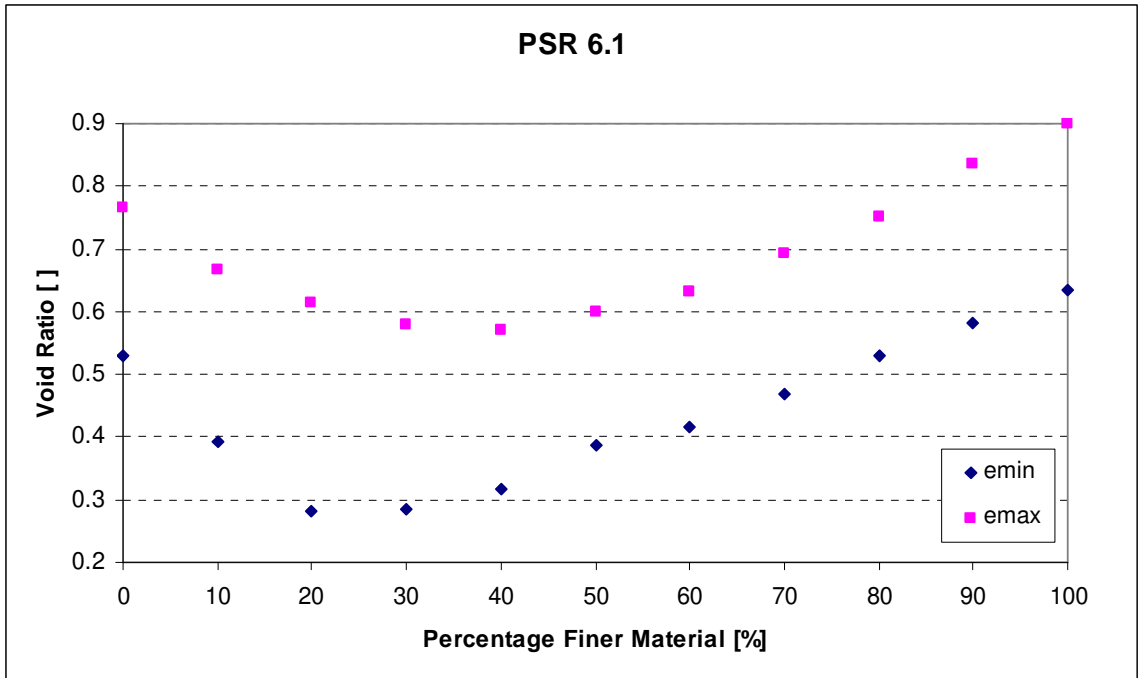


Figure 4.6 VRR data for particle size ratio 6.1

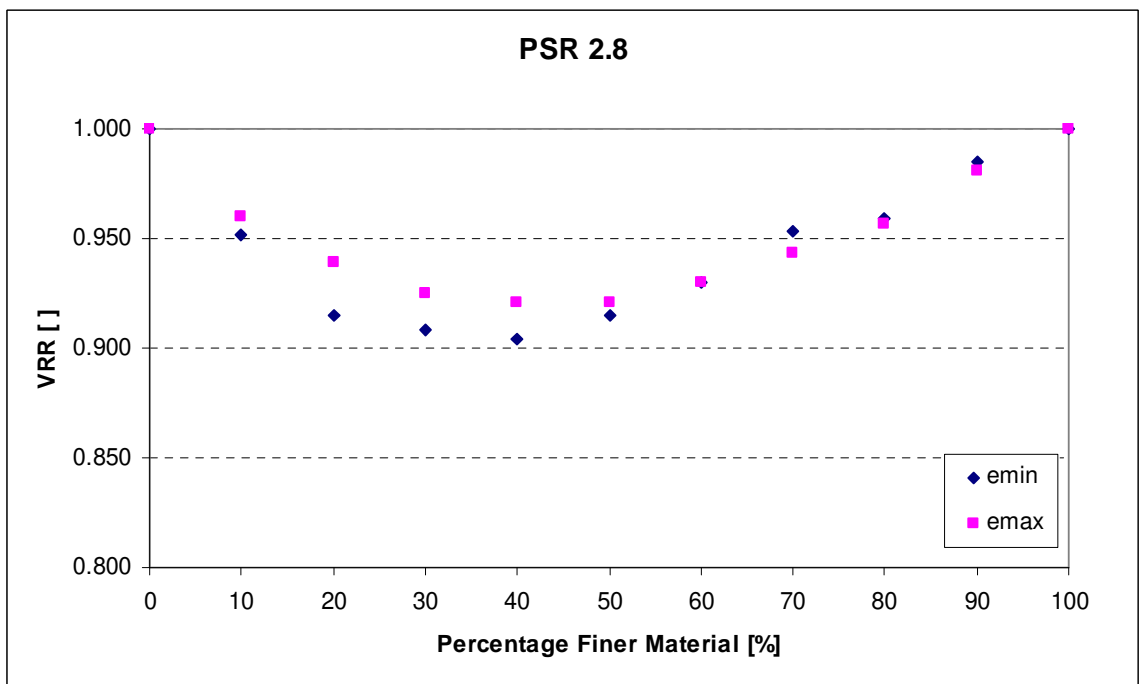
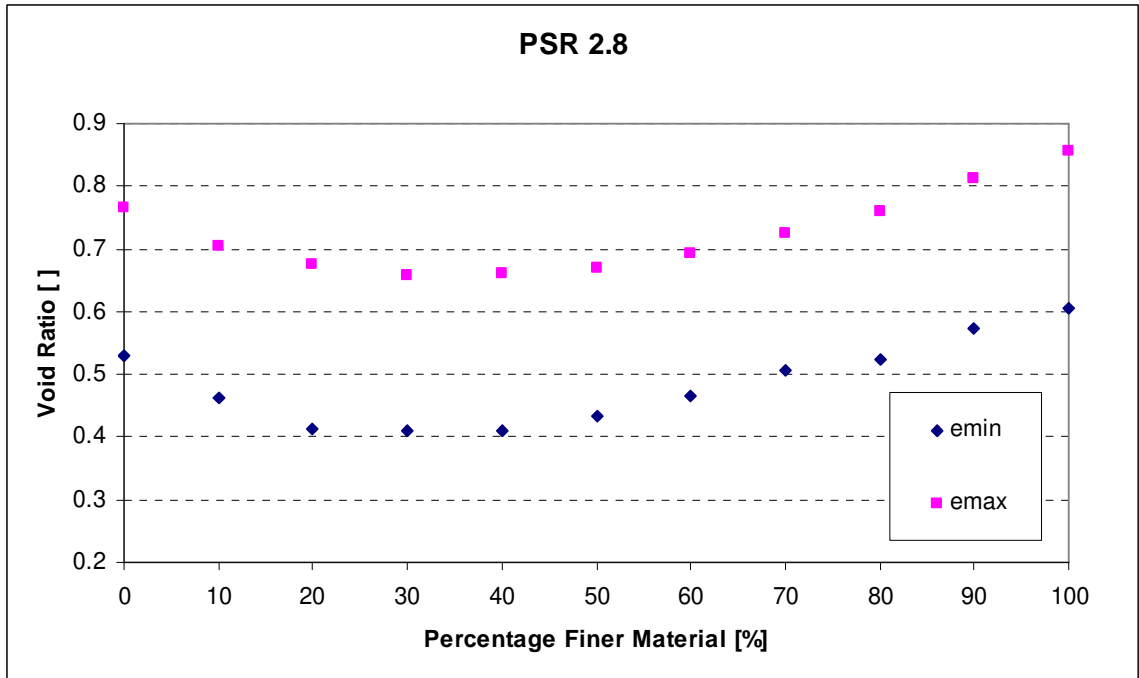


Figure 4.7 VRR data for particle size ratio 2.8

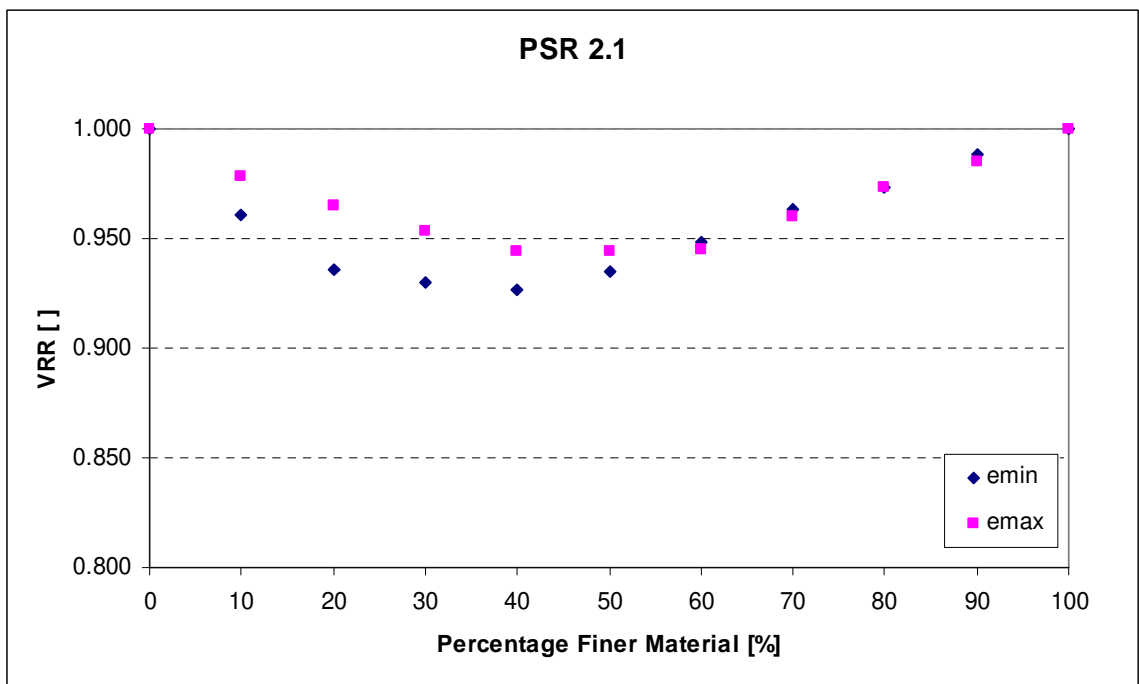
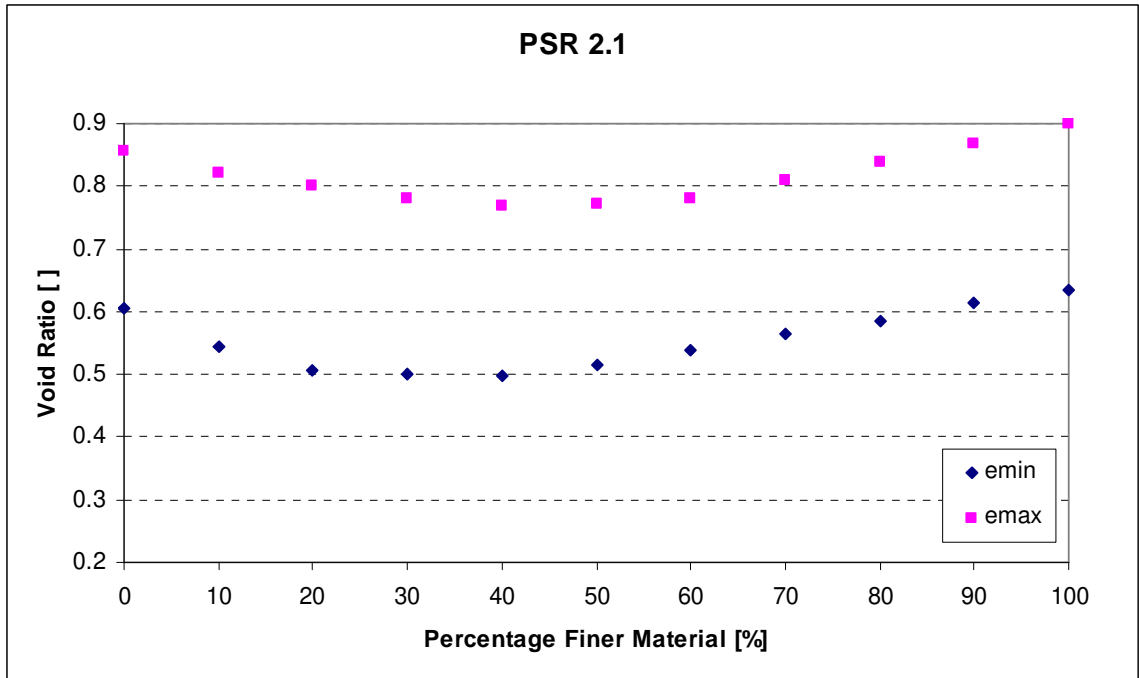


Figure 4.8 VRR data for particle size ratio 2.1

In each case with the data plotted as straight void ratio any comparison between the behavior of the e_{max} and e_{min} are very difficult due to the gap between the data and the differing start and end points. In the VRR charts a comparison is far simpler. One can

readily see that due to mixing the void ratios decrease (as we saw before) but the relative nature of change is now clear.

It is apparent that the minimums are more sharply defined in the VRR plots and it is clear that at a level of approximately 60% smaller particles there is a change in the behavior of the materials. At amounts of smaller particles greater than 60% the volume reduction due to mixing is virtually identical for both the e_{\min} and e_{\max} cases. For all other amounts of smaller particles the volume reduction is significantly greater for the e_{\min} case. The difference appears greatest at approximately 20% smaller particles.

Utilizing this new approach we can reexamine the data across the range of particle size ratios:

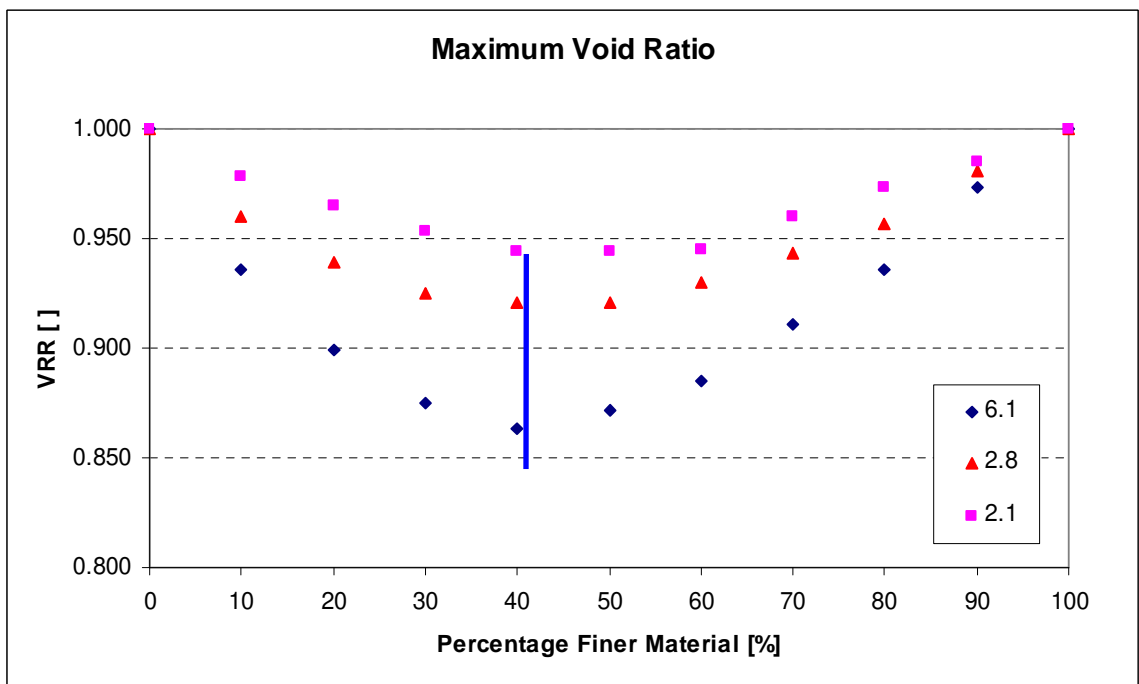
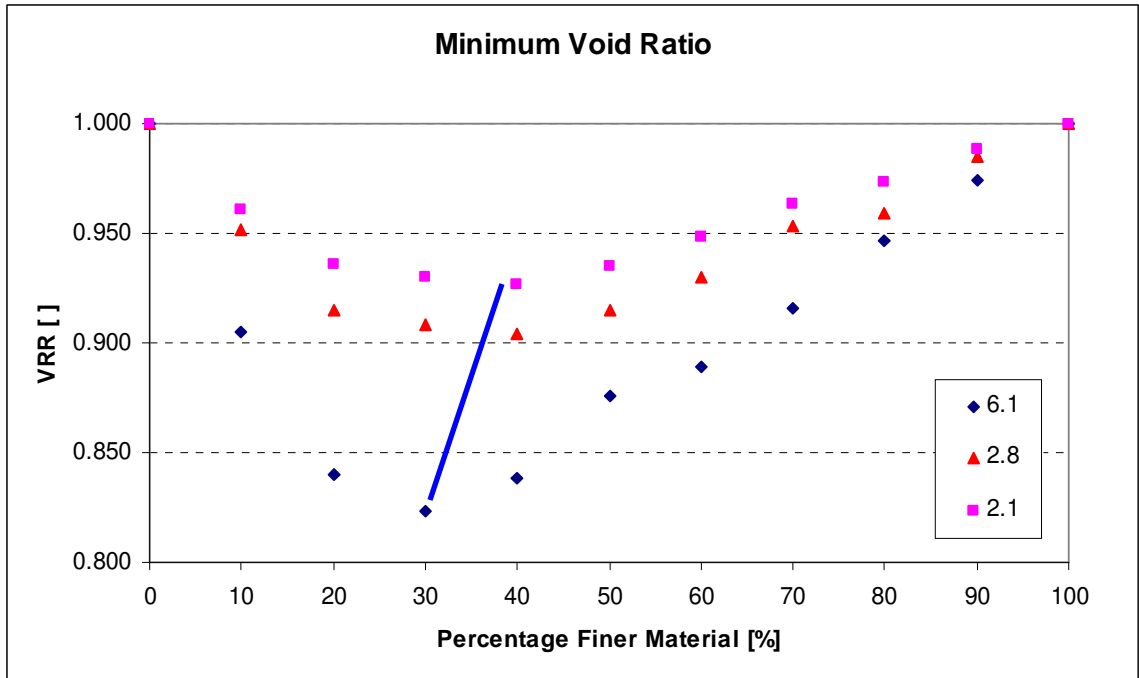


Figure 4.9 VRR data for e_{\max} and e_{\min}

Plotting this data in this framework and on the same scaled axes allows a number of additional observations:

- The intermediate size ratio, which is closer to the case with size ratio 2.1, now tracks more closely with the 2.1 case. This is more reflective of the true material behavior.
- The lowest values for the e_{\min} case is further left and more angled than for the e_{\max} case.
- The minimum void ratio case (maximum density) is arguably more sensitive to mixing as the size ratio increases.

4.2.6.4. Correlating e_{\min} to e_{\max}

The limiting void ratios are sometimes expressed as ratios of one another. This is usually done to fit a correlation, and presumably to determine both limits by only performing a single test.

The relationship between e_{\min} and e_{\max} for all of the mixtures tested is shown below:

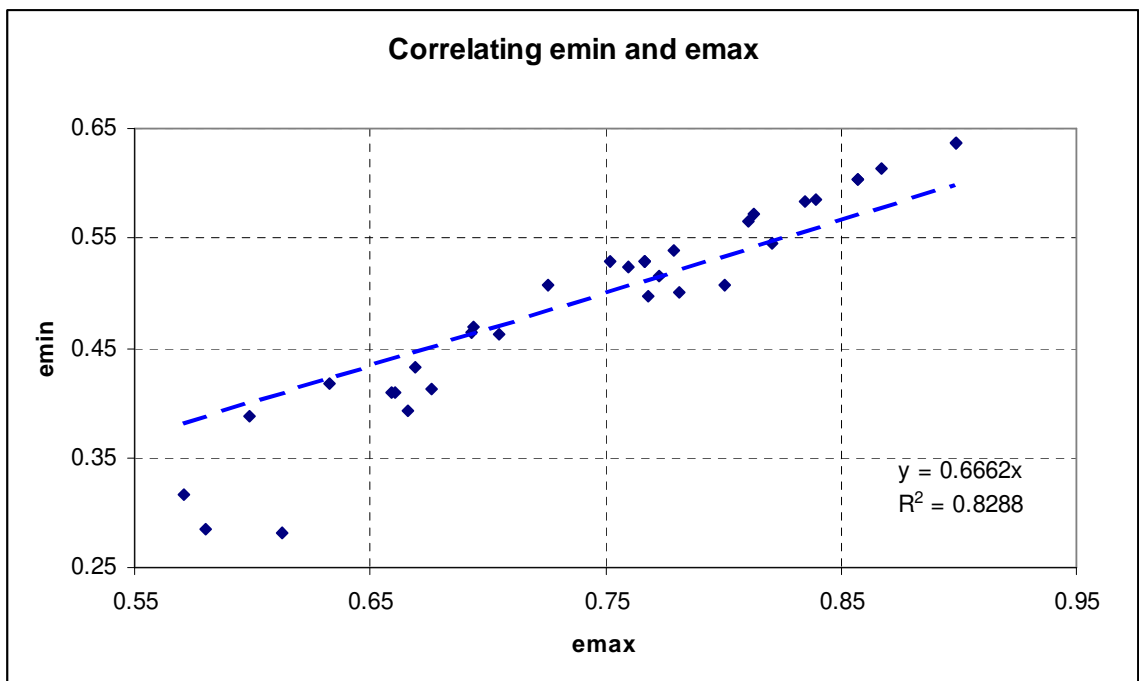
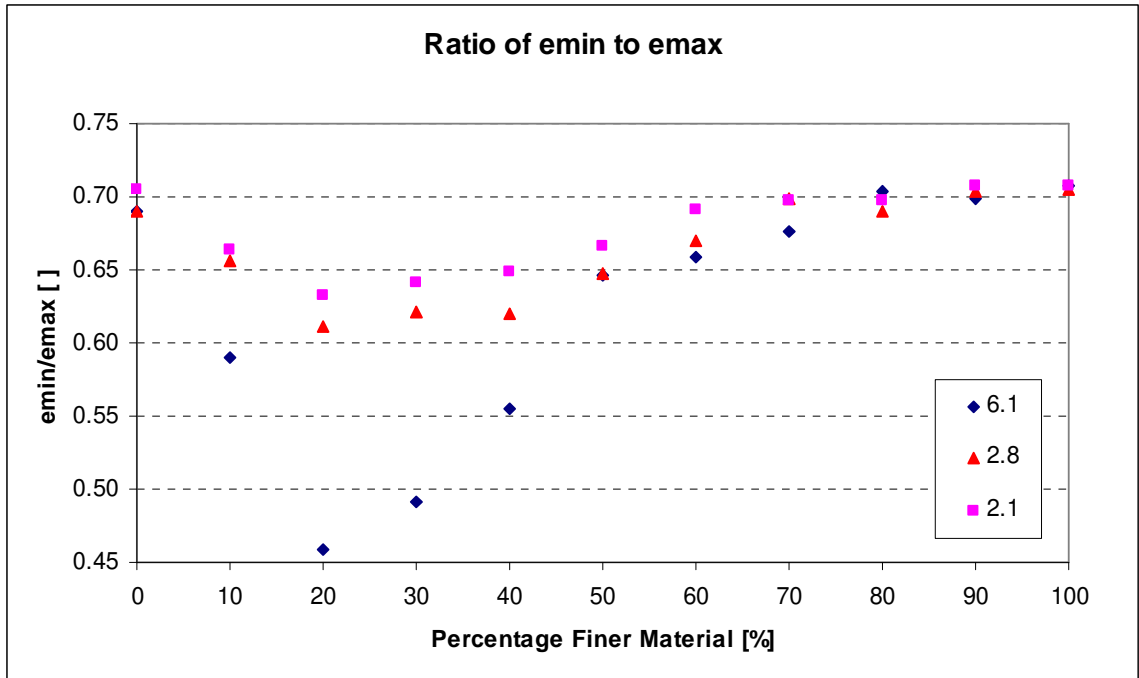


Figure 4.10 Correlations between e_{max} and e_{min}

As can be seen in Figure 4.10, $e_{min} = 0.6662e_{max}$ (correlation fitted assuming the origin to be a point). This correlation is very comparable to other published data sets as summarized by Thomas (1997) and shown in Figure 4.11 below. The dashed blue line in

Figure 4.11 is the best-fit line from Figure 4.10. While the fit is reasonable for the data in aggregate the upper part of Figure 4.10 indicates that there is a definite pattern to the variation in this ratio. The ratio between the respective void ratios can differ by as much as 67% from the mean.

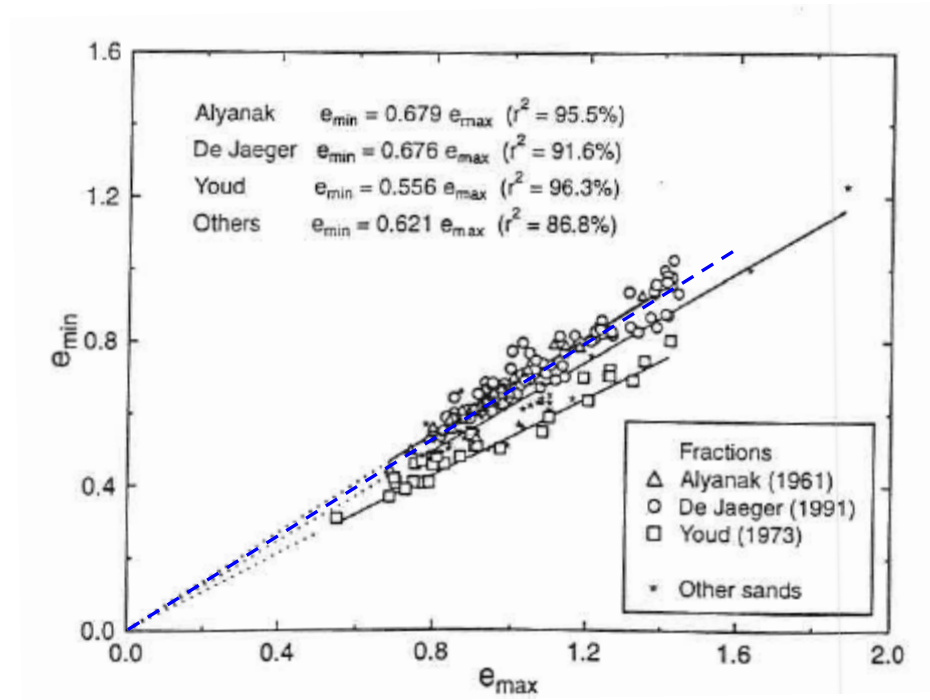


Figure 4.11 Literature correlations between e_{max} and e_{min} (Thomas, 1997)

4.2.6.5. Comparison with source sands

The sands tested were scalped from different source sands so it will be beneficial to examine how the scalped portions compare to the source sands. The scalped sands by design have a narrower range of particle sizes present and this should be reflected in the limiting void ratio data.

Table 4.1 Comparison with source sands

	Ottawa 20/30	20/25	A.F.S. 50/70	50/60	F-110	100/140
e_{min}	0.502	0.529	0.612	0.604	0.535	0.636
e_{max}	0.741	0.767	0.861	0.857	0.848	0.899

Table 4.1 indicates how the minimum and maximum void ratios have changed as a result of the scalping. For the cases of the Ottawa 20/30 and the F-110 sands, when the scalped fractions were tested both the limiting void ratios showed increases, quite noticeable was the large increase in the minimum void ratio for F-110. This general behavior was expected due to the decrease in the available particle sizes (and hence a decrease in C_u). In contrast, A.F.S. 50/70, when scalped, showed very slight decreases.

4.2.7. Segregation Tests

The results of the segregation testing are shown below in Figure 4.12. Three trials were conducted and each is shown in a different color in the figure. The mass percentage of finer particles is shown for each of the excavated layers. For reference, the dashed blue line indicates where the data points would plot for a mixture with a perfectly uniform spatial distribution of each component.

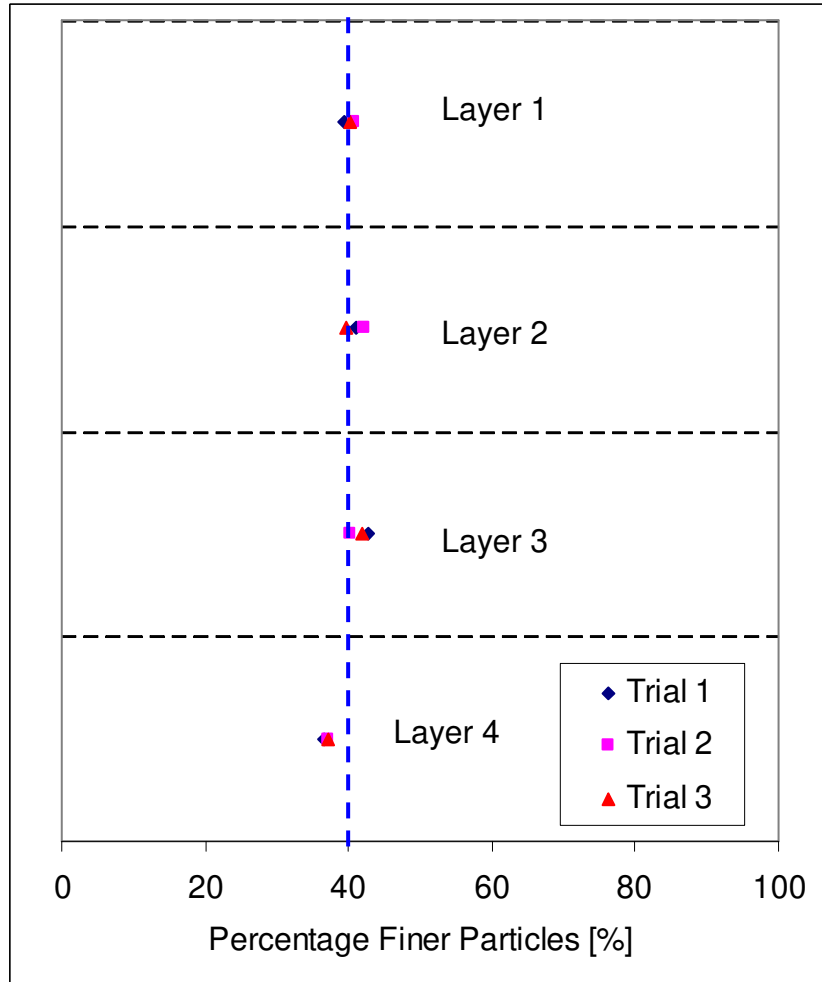


Figure 4.12 Segregation Testing

Figure 4.12 shows that Layer 4, the bottom layer, contains a lower average percentage (37%) of finer particles than would be expected. Layer 3, immediately above layer 4, shows a slightly higher average percentage (42%) of finer particles than would be expected. The upper two layers, layers 1 and 2, shows percentages of finer particles of 40% and 41%, respectively.

These numbers indicate that segregation is not a significant factor during the limiting void ratio tests. The deviation from the reference of 40% is at most 3% (layer 4). This is, however, a repeatable deviation, as is evidenced by the cluster of data points in

layer 4. The reason for the decrease in the percentage of finer particles in this lowest layer is due to the method by which the particles are initially placed in the pipe (the pipe-pullout method was used for the maximum void ratio testing). The mixture of particles was poured from a container into the pipe, with a drop height approximately equal to the height of the pipe used. As the particles move against the sides of the container and out of it, the small and large particles partially separate, with the larger particles rising to the surface and being the first to exit the container and fall into the pipe. This leads to the larger percentage of larger particles in the lowest layer. This effect was mitigated by disturbing the flow of particles, just before they exited the container.

Segregation for the mixtures with P.S.R. 2.1 and 2.8 is not expected to be as significant an effect as it is for the P.S.R. 6.1 mixture, which itself has been shown to be of negligible effect. These findings, however, do indicate that there may be a very minor overestimate of VRR, since the assumption of homogeneity is not strictly valid.

4.3. Shear Strength

4.3.1. Introduction

When one considers the shear strength of a particulate material at the particle level, one identifies a number of factors that all concurrently, and to varying degrees, contribute to the overall strength. These factors are, amongst others; interparticle friction, dilatancy, particle geometry and rolling frustration (Santamarina, 2001). Which of these factors are being affected most significantly by the binary nature of the mixtures is an important consideration. Due to the choice of particles used in this study the influence of interparticle friction and particle geometry have been minimized. In this next part of the study, the focus will be on how the particle size ratio and percentage of finer material influences the peak and large displacement strengths as well as the dilatancy.

As well as being of interest in and of itself, the results of the direct shear experiments will be very helpful in understanding the results from the interface shear tests.

4.3.2. General discussion on direct shear testing

The direct shear test is arguably the oldest and simplest test for measuring the shear strength of soils – this has both advantages and disadvantages. For detailed reviews of the history and current state of the art of direct shear testing please refer to Lings and Dietz (2004).

The primary reason for selecting the direct shear test was because it is most directly relatable to the interface shear tests conducted as part of this study. It is of vital importance that the results from the two different tests be compared and contrasted and this was most easily achieved by using the direct shear test.

4.3.3. Results

The data from the direct shear tests is presented in the tables below:

Table 4.2 Direct Shear Test Data for P.S.R. 2.1

P.S.R. 2.1	20/25	50/60	100/140	Test Reference	Normal Stress [kPa]	Relative Density [%]	Peak Friction Coeff.	Large Disp. Friction Coeff.
	0	100	0	50/60_50	50	84	0.819	0.586
				50/60_100	100	81	0.732	0.604
				50/60_300	300	80	0.632	0.582
				50/60_500	500	81	0.648	0.573
	0	80	20	21_20_50	50	83	0.743	0.586
				21_20_100	100	84	0.733	0.573
				21_20_300	300	82	0.633	0.550
				21_20_500	500	85	0.598	0.514
	0	60	40	21_40_50	50	83	0.715	0.533
21_40_100				100	81	0.715	0.579	
21_40_300				300	82	0.645	0.549	
21_40_500				500	84	0.606	0.525	
0	40	60	21_60_50	50	81	0.771	0.593	
			21_60_100	100	85	0.716	0.582	
			21_60_300	300	85	0.663	0.582	
			21_60_500	500	84	0.614	0.551	
0	20	80	21_80_50	50	80	0.693	0.566	
			21_80_100	100	82	0.625	0.581	
			21_80_300	300	81	0.616	0.592	
			21_80_500	500	83	0.612	0.549	
0	0	100	100/140_50	50	80	0.721	0.624	
			100/140_100	100	83	0.651	0.609	
			100/140_300	300	84	0.637	0.627	
			100/140_500	500	82	0.631	0.627	

Table 4.3 Direct Shear Test Data for P.S.R. 2.8

P.S.R. 2.8	20/25	50/60	100/140	Test Reference	Normal Stress [kPa]	Relative Density [%]	Peak Friction Coeff.	Large Disp. Friction Coeff.
	100	0	0	20/25_50	50	81	0.662	0.530
				20/25_100	100	85	0.680	0.503
				20/25_300	300	82	0.607	0.533
				20/25_500	500	82	0.618	0.495
	80	20	0	28_20_50	50	81	0.720	0.508
				28_20_100	100	85	0.700	0.502
				28_20_300	300	84	0.696	0.520
				28_20_500	500	80	0.688	0.526
	60	40	0	28_40_50	50	82	0.796	0.610
28_40_100				100	85	0.754	0.589	
28_40_300				300	83	0.716	0.573	
28_40_500				500	85	0.625	0.548	
40	60	0	28_60_50	50	82	0.812	0.586	
			28_60_100	100	84	0.730	0.579	
			28_60_300	300	83	0.701	0.595	
			28_60_500	500	85	0.666	0.611	
20	80	0	28_80_50	50	80	0.803	0.620	
			28_80_100	100	85	0.754	0.624	
			28_80_300	300	80	0.661	0.628	
			28_80_500	500	83	0.646	0.640	
0	100	0	50/60_50	50	84	0.819	0.586	
			50/60_100	100	81	0.732	0.604	
			50/60_300	300	80	0.632	0.582	
			50/60_500	500	81	0.648	0.573	

Table 4.4 Direct Shear Test Data for P.S.R. 6.1

P.S.R. 6.1	20/25	50/60	100/140	Test Reference	Normal Stress [kPa]	Relative Density [%]	Peak Friction Coeff.	Large Disp. Friction Coeff.
	100	0	0	20/25_50	50	81	0.662	0.530
				20/25_100	100	85	0.680	0.503
				20/25_300	300	82	0.607	0.533
				20/25_500	500	82	0.618	0.495
	80	0	20	61_20_50	50	85	0.844	0.603
				61_20_100	100	84	0.786	0.544
				61_20_300	300	84	0.715	0.522
				61_20_500	500	84	0.695	0.534
60	0	40	61_40_50	50	83	0.875	0.640	
			61_40_100	100	85	0.767	0.619	
			61_40_300	300	85	0.699	0.575	
			61_40_500	500	80	0.695	0.600	
40	0	60	61_60_50	50	84	0.714	0.549	
			61_60_100	100	83	0.722	0.605	
			61_60_300	300	81	0.644	0.583	
			61_60_500	500	81	0.571	0.523	
20	0	80	61_80_50	50	85	0.630	0.519	
			61_80_100	100	81	0.631	0.548	
			61_80_300	300	85	0.601	0.539	
			61_80_500	500	80	0.593	0.543	
0	0	100	100/140_50	50	80	0.721	0.624	
			100/140_100	100	83	0.651	0.609	
			100/140_300	300	84	0.637	0.627	
			100/140_500	500	82	0.631	0.627	

Typical data from the direct shear tests is shown below:

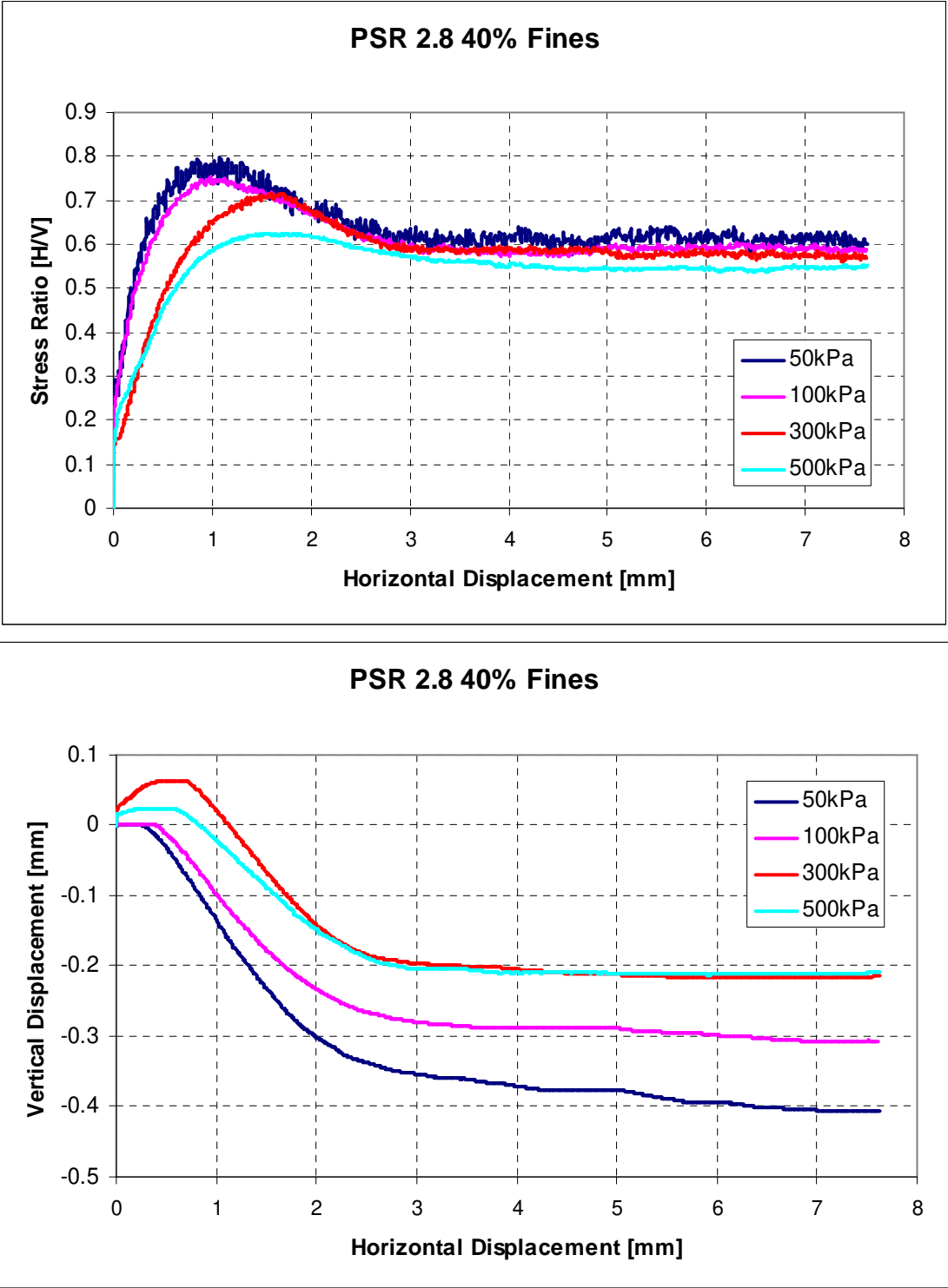


Figure 4.13 Typical direct shear data

A number of observations are made with respect to the stress-strain plot:

- Peak strength is dependent on the normal stress. As the normal stress increases the peak strength decreases. The normal stress was varied from 50 kPa to 500 kPa and in this case the peak angle of friction is observed to vary from 32 degrees to 38.5 degrees.
- The strength at large displacement is very weakly, if at all, dependent on the normal stress level. This indicates that the large displacement strength does not reflect the normal stress level, but only the particle characteristics.
- The strain to peak strength increases with increasing normal stress.
- The shape of the stress-strain curve changes with normal stress. The flattening of the peak occurs with the increase in normal stress, reflecting the suppression of the dilative tendency of these medium to dense sand specimens.

One can also make a number of observations from the plot of vertical displacement:

- At low normal stresses (50 and 100 kPa) the samples did not contract, but did subsequently dilate (reflecting the medium to dense packing of the soil specimens).
- At higher normal stresses (300 and 500 kPa) the samples initially contracted, and then dilated.
- In all cases, after some strain the samples sheared at a nearly constant volume (or constant void ratio) reflecting the formation of a fully mobilized zone of shear failure in the center of the sample.

- An increase in the normal stress resulted in a suppression of the dilation.

Using the type of data shown above the relationship between peak shear stress and normal stress can be plotted in order to calculate an overall friction angle for the specimen.

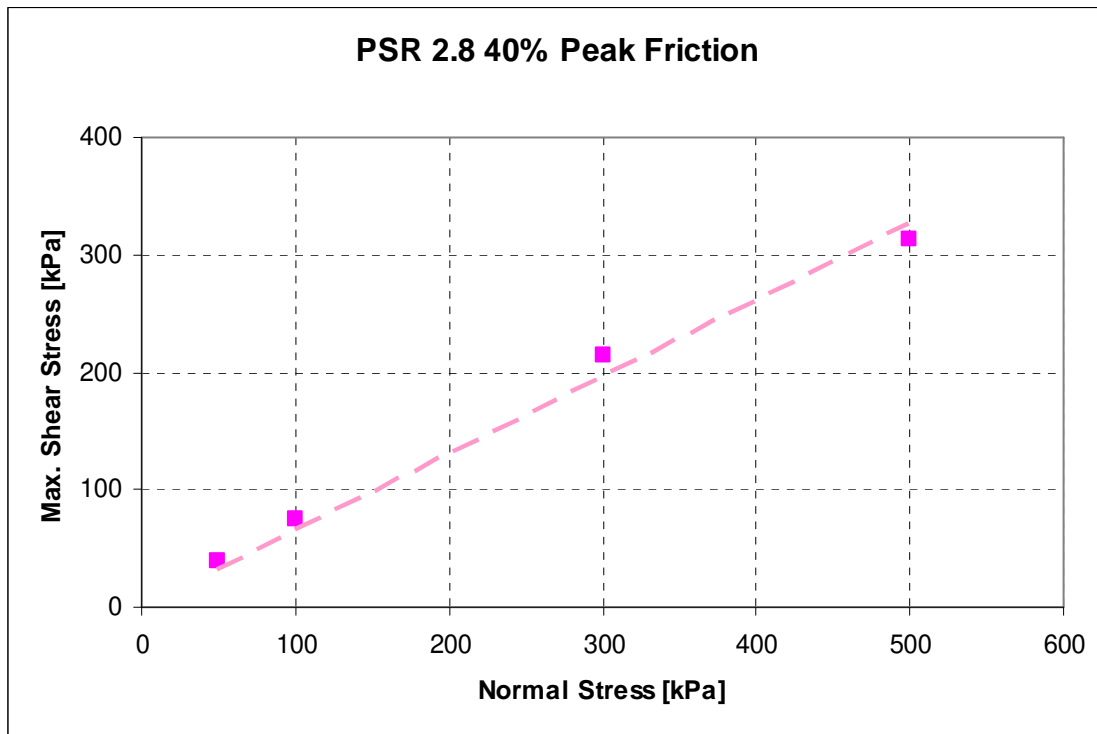


Figure 4.14 Direct shear friction angle calculation

In the figure above, a straight line has been fitted through the data points and the origin. One can confidently use the origin as a point on this line since the frictional basis for the shear strength of soils implies that at zero normal stress the shear strength will be zero. Note that this may not be the case for sands that are cemented or have some fluid present. The slope of this line defines the peak angle of friction, which is 33.1 degrees.

A measure of the goodness of the fit of this model can be provided by the coefficient of determination, R^2 . In this case $R^2 = 0.9851$, indicating a good fit to the data. Although the high R^2 value in this case is somewhat misleading, given the fact that we

have already observed that the strength is stress dependent. If one calculates the peak friction angle for each of the four normal stresses, the following are the results:

Table 4.5 Peak friction angles at different normal stress levels

Normal Stress (kPa)	Peak Shear Stress (kPa)	Peak Friction Angle
50	39.8	38.5
100	75.4	37.0
300	214.9	35.6
500	312.4	32.0
Linear Regression		33.1

One can immediately observe that the overall or average peak friction angle determined from the linear regression does not accurately reflect the soil behavior, despite the high R^2 value. This is due to the low number of data points and the fact that the data point for the 500 kPa normal stress has a disproportionately large effect on the slope of the regression line due to it being the furthest from the origin (which acts as a kind of pivot point).

The data from the direct shear tests is presented from here on in summary form. The peak effective shear stress ratios were calculated based on the recorded horizontal and vertical load data and the large displacement values were obtained from an average over the region of the curve where shearing continued at a constant volume and at a constant shear stress.

The plot below shows the boundaries of the peak strength envelope for all soil mixtures tested, excluding the uniform soils. The uniform soils are plotted as orange points on the same plot. The upper blue line represents a peak friction angle of 35.2 degrees while the red lower bound represents a peak friction angle of 30.1 degrees.

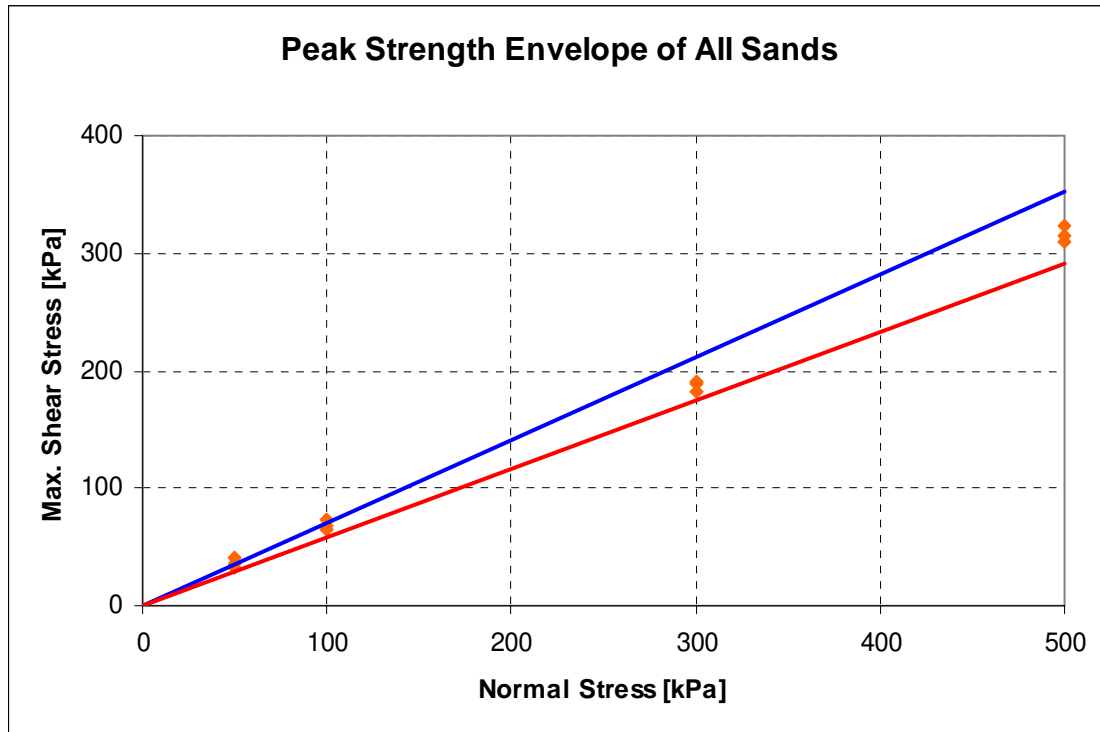


Figure 4.15 Peak Strength Envelope

From the plot it can be seen that at low normal stresses the uniform soils plot slightly above or very close to the upper boundary. Indicating that compared to the soil mixtures, the uniform soils have relatively higher peak friction angles. At high normal stresses the uniform soils plot towards the middle to lower bound, indicating relatively lower peak friction angles.

From this overview of the data it may be inferred that uniform soils are more sensitive to the effect of normal stress on peak strength than mixed soils.

A similar plot can be drawn for the large displacement strength, as is shown below:

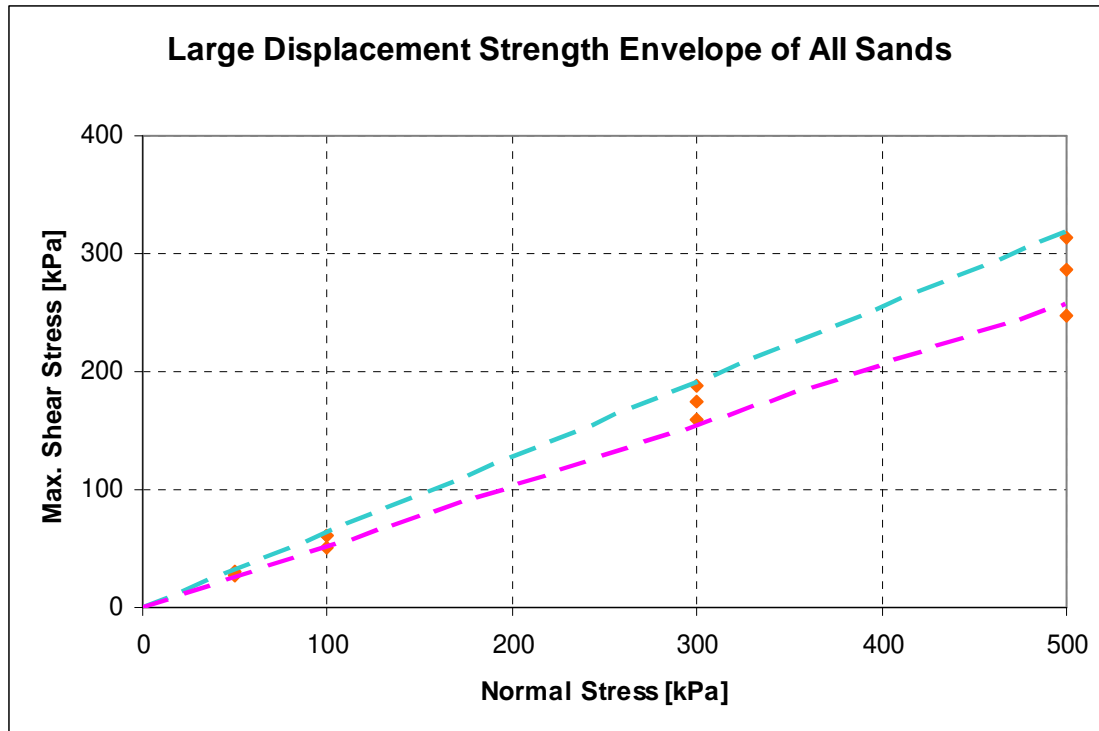


Figure 4.16 Large Displacement Strength Envelope

It can be seen in the plot above that for the large displacement strengths, two of the uniform soils bracket the envelope, while the third lies in the center of the envelope. The upper bound is mirrored by the 100/140 soil while the lower bound by the 20/25 soil. This indicates a size and/or shape effect on the large displacement strengths.

The most rounded of the particles is the 20/25 and this corresponds to the lowest large displacement friction angles. The most angular of the particles, though still only mildly sub-angular, is the 100/140 which shows the largest large displacement friction angles.

Uniform soils are thus seen to bound the large displacement friction angles which is not the case for the peak friction angles.

The upper bound corresponds to a friction angle of 32.5 degrees and the lower bound to 27.3 degrees. These angles are clearly lower than the peak friction angles, with

both bounds shifting by the same amount of 2.7 degrees. The internal range of each of the envelopes is thus also the same, at 5.2 degrees.

This leads to an important observation: the effect of the particle mixing on the peak friction angles is greater than the effect of dilatancy (the portion of strength greater than the critical state). This is true by a factor of almost two.

To summarize, the effect of mixing is indicated by the internal range of the peak strength envelope. This range is approximately 5.2 degrees. The dilatancy effect (difference between the peak and large displacement values) is approximately 2.7 degrees. This indicates that the mixing characteristics have the potential to be almost twice as significant as the effect of dilatancy for the binary mixtures studied between 50 and 500 kPa.

A further examination of the peak effective stress ratio is shown below:

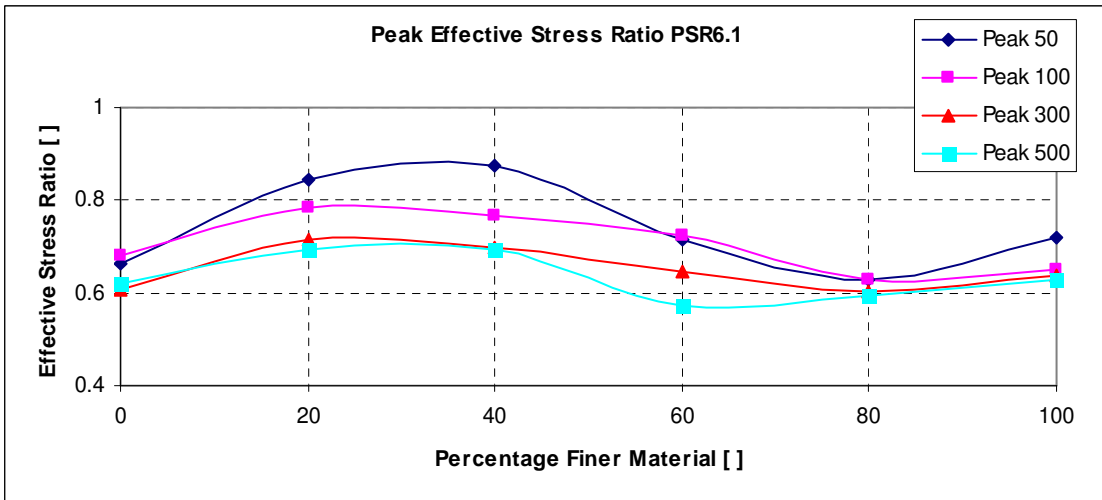
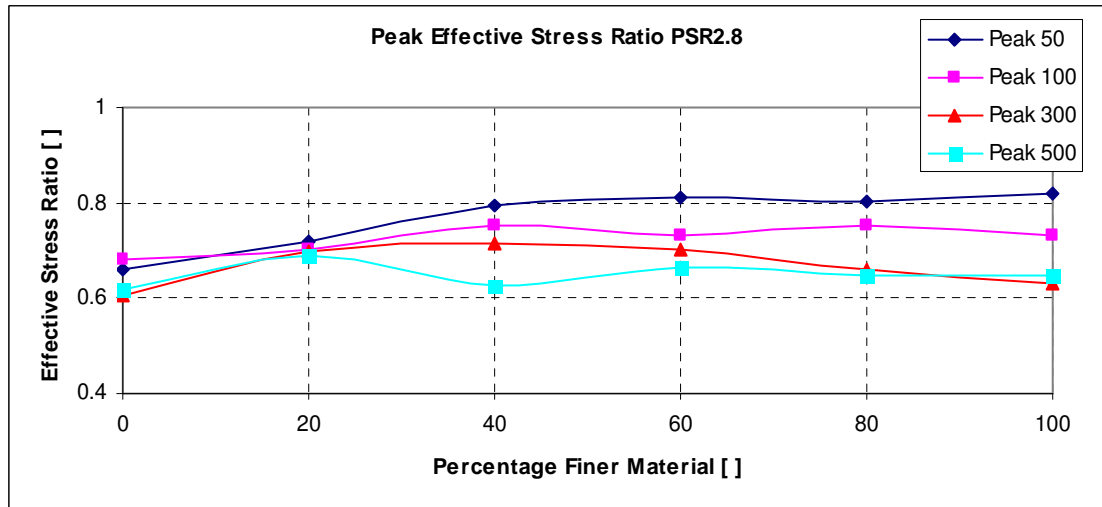
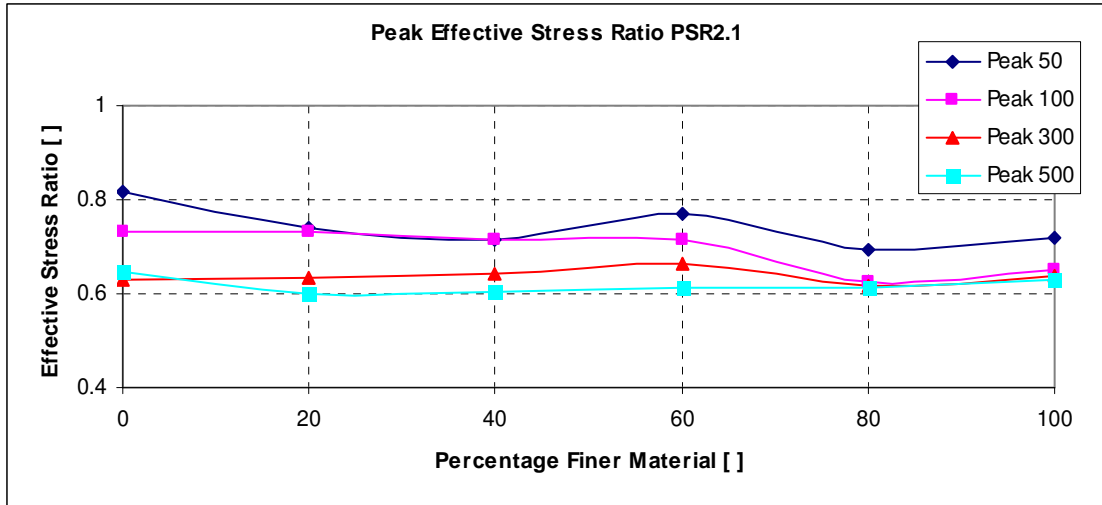


Figure 4.17 Peak Effective Stress Ratio

The plots above show the peak effective stress ratio for each particle size ratio and mixture percentage for all four normal stresses. The following observations can be made:

- Lower normal stresses lead to consistently greater peak stress ratios
- In the case of the PSR's of 2.1 and 2.8 the range of values for the peak ratio is very much in line with the bounding values at 0 and 100%. The values are not perfectly linearly varying, but there are no particularly strong trends in the data.
- In the case of PSR 6.1 there is a very clear pattern in the data.
 - Note that the starting and ending ratios (at 0 and 100%) are approximately the same.
 - The intermediate values (at some ratio of finer to coarse material) the peak ratio is generally higher than at the boundaries.
 - Peak ratios are found at approximately 30% to 40% of finer material
 - Peak ratios decrease to approximately 80% finer content.
 - Stress ratio at 20% finer particles is always greater than at 0% finer particles.
 - The trend is more pronounced for lower normal stress values.

Note that this pattern is also reflected in the data from Vallejo (2001) in Figure 4.18, albeit to a greater extent. The data from Vallejo (2001) is however based on measurements performed where the size of the device containing the particles is only 12.7 times larger than the diameter of the largest particles. The large difference between the 0% and 100% cases in this data cannot readily be

explained since glass beads were used for this study deliberately to reduce the influence of particle shape and mineralogy. The box-size effect appears to have been ignored in the study but it is thought to play a significant role.

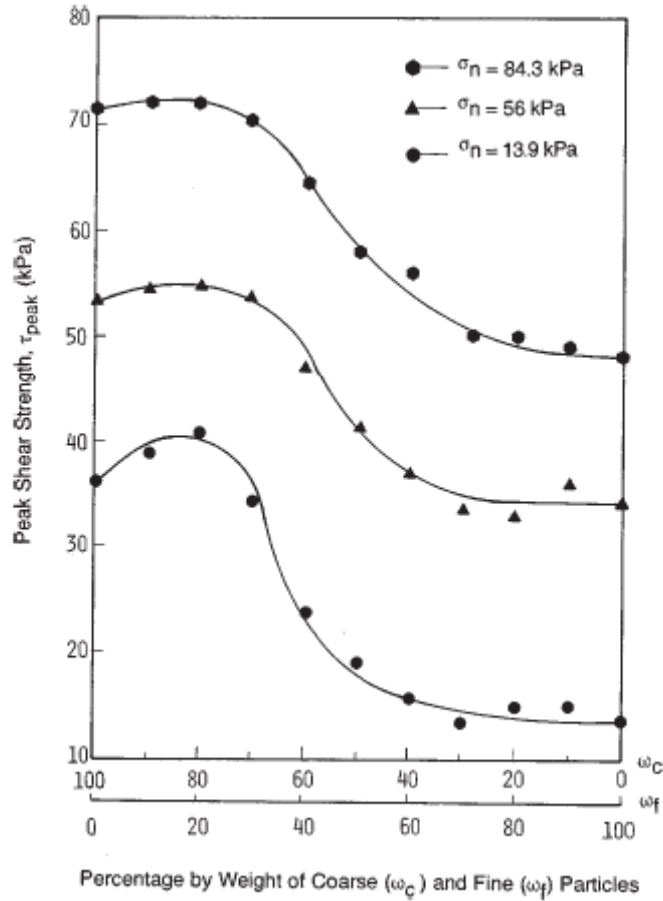


Figure 4.18 Peak shear strength of a binary mixture (Vallejo, 2001)

It is important to note that the large displacement friction angle is not strictly the same as the critical state value. Lings and Dietz (2004) have shown that the critical state friction angle and the large displacement friction angle as measured in direct shear are related by the expression:

$$\tan \sigma_{ld} = \sin \sigma_{crit}$$

The large-displacement effective stress ratios are graphed in Figure 4.19 below for each particle size ratio.

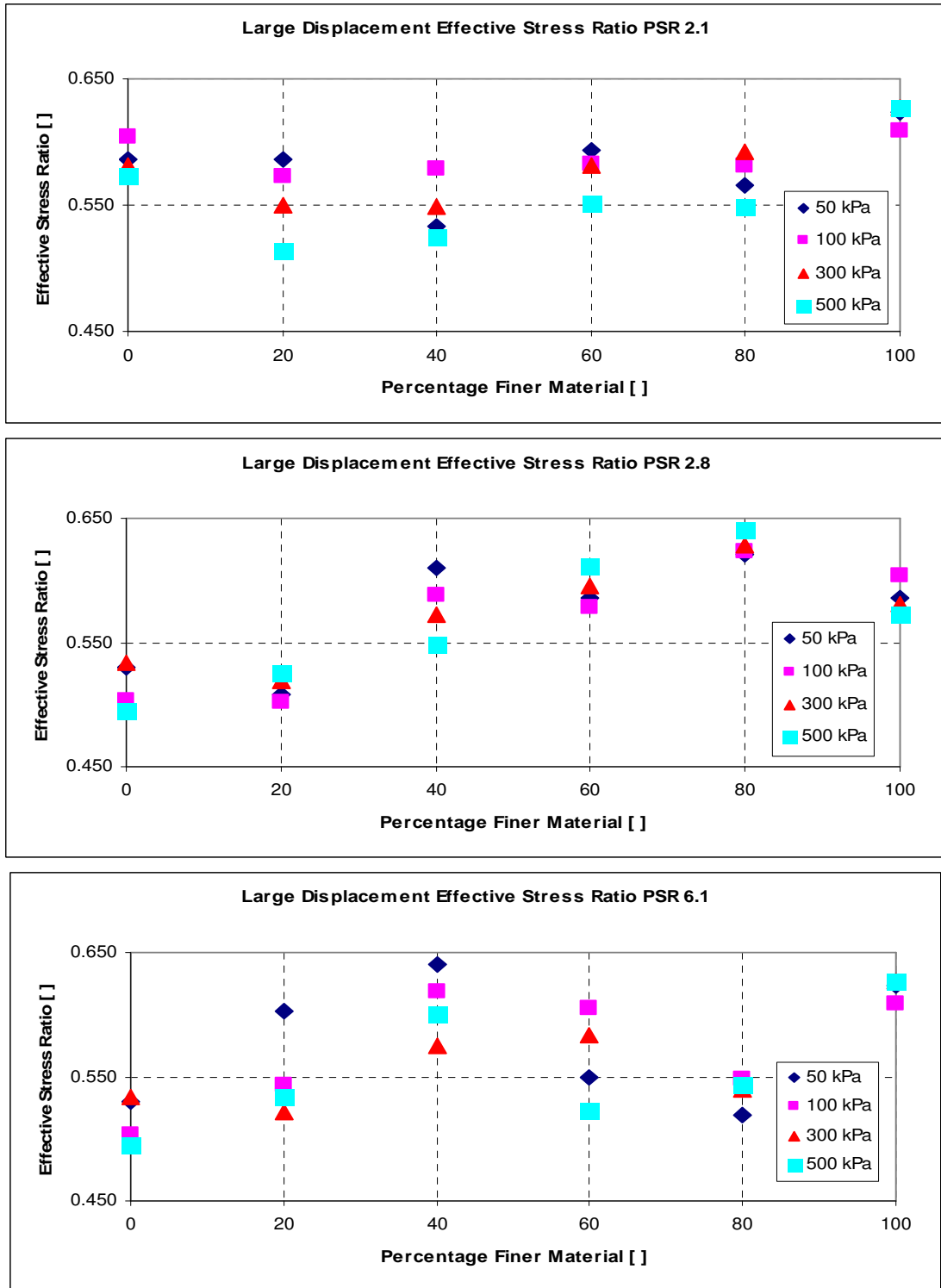


Figure 4.19 Large Displacement Effective Stress Ratio

Figure 4.19 shows no clear trend across all of the materials tested. For the P.S.R. 2.1 material the large displacement stress ratio appears to remain relatively constant across the range of mixture proportions and normal stresses tested. In this case, the stress ratio is slightly increased at the 0 and 100% cases, indicating that uniform sands have a greater large displacement strength.

For the P.S.R. 2.8 case a more clear trend is evident. The trend is one of increasing large displacement stress ratio with an increasing percentage of finer material in the mixture.

For the P.S.R. 6.1 case, a peak is evident in the plot at the 40% mark, indicating that the large displacement stress ratio is the greatest when 40% of the total mixture is made up of the smaller particles. This trend is not however present in the other two cases examined.

An alternative way to examine this data is to present it as a friction angle plotted against the percentage of finer material. In the following graphs, Figure 4.20 and Figure 4.21, the data is grouped into four charts by normal stress.

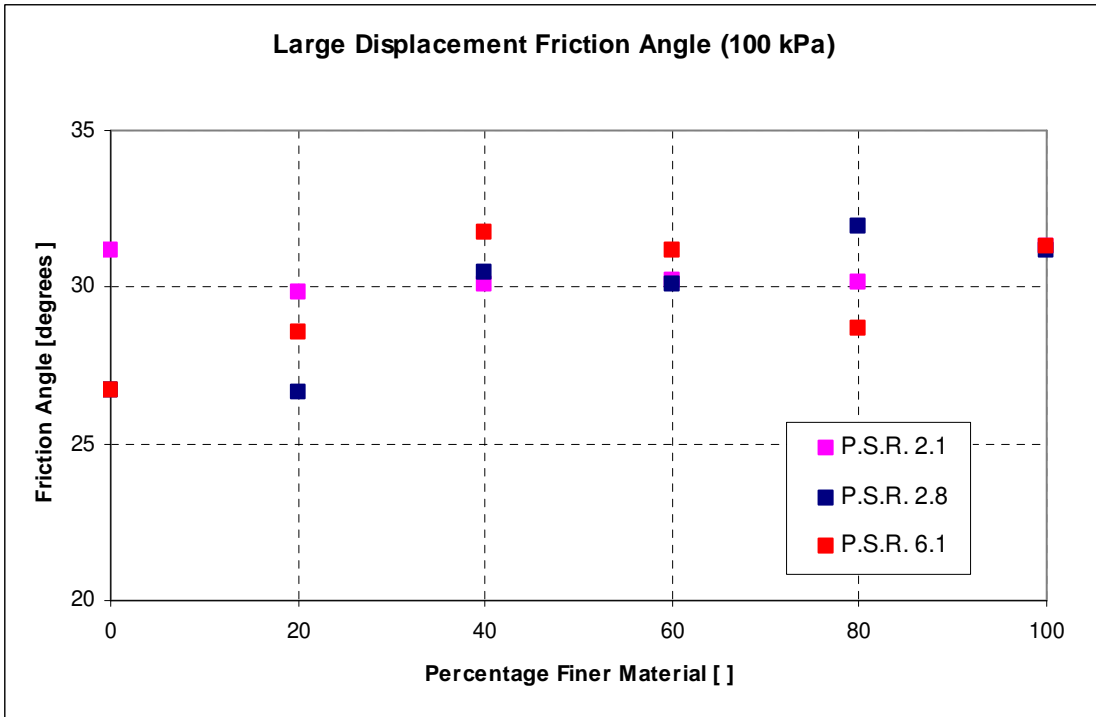
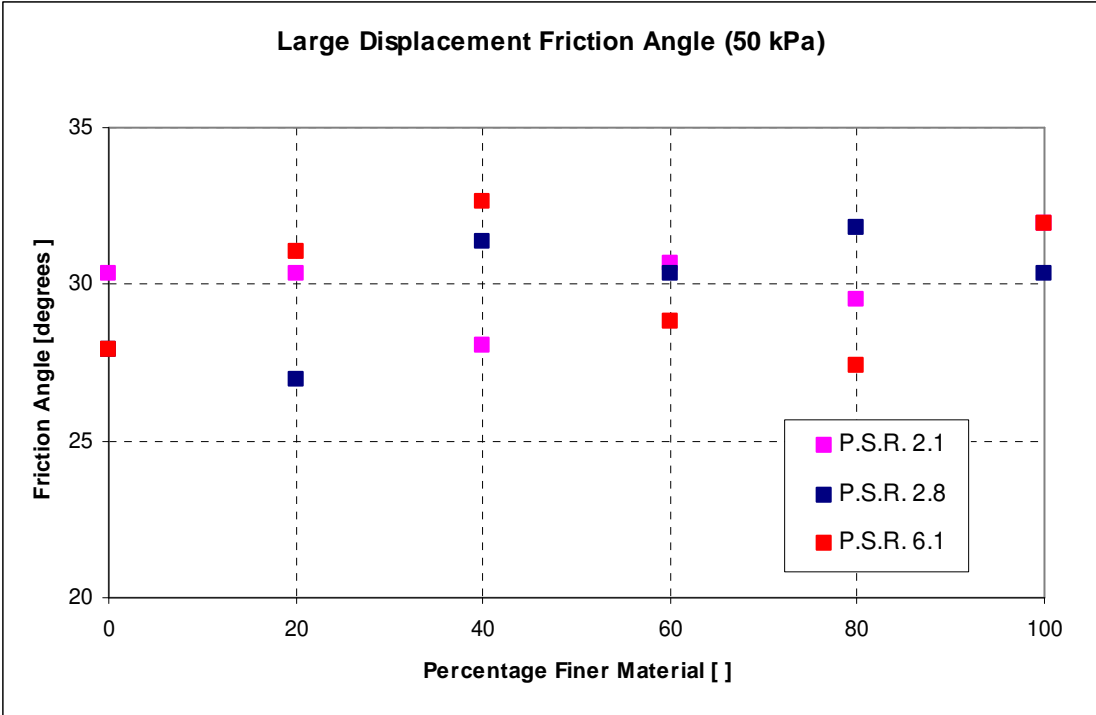


Figure 4.20 Large Displacement Friction Angles (50 and 100 kPa)

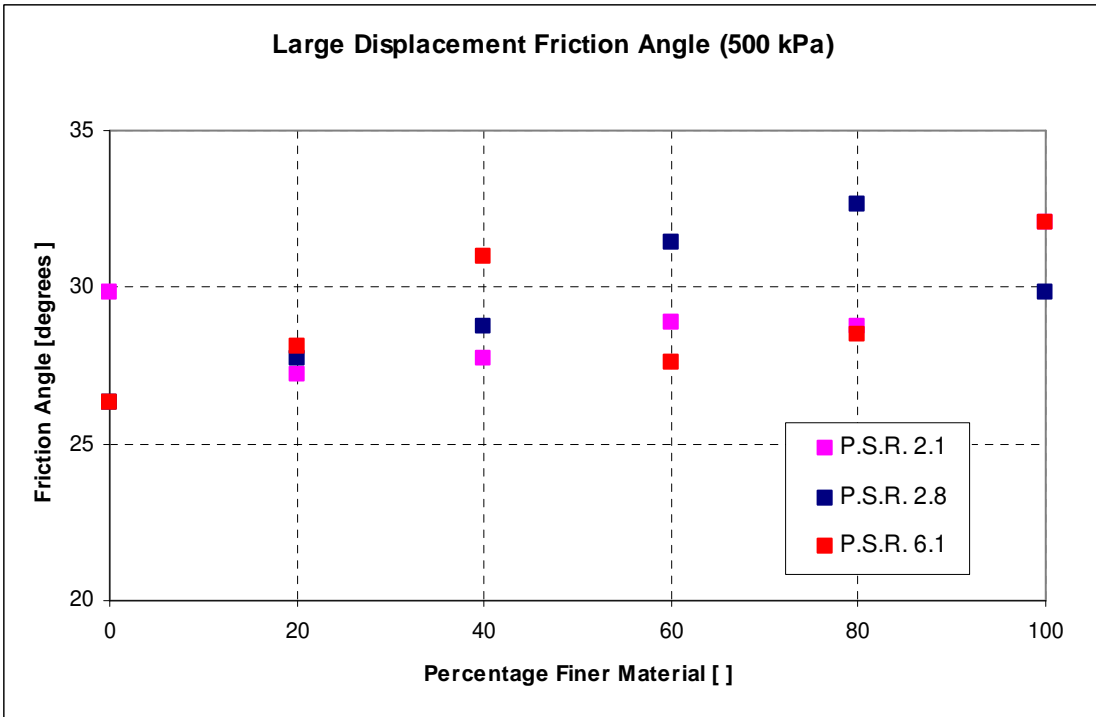
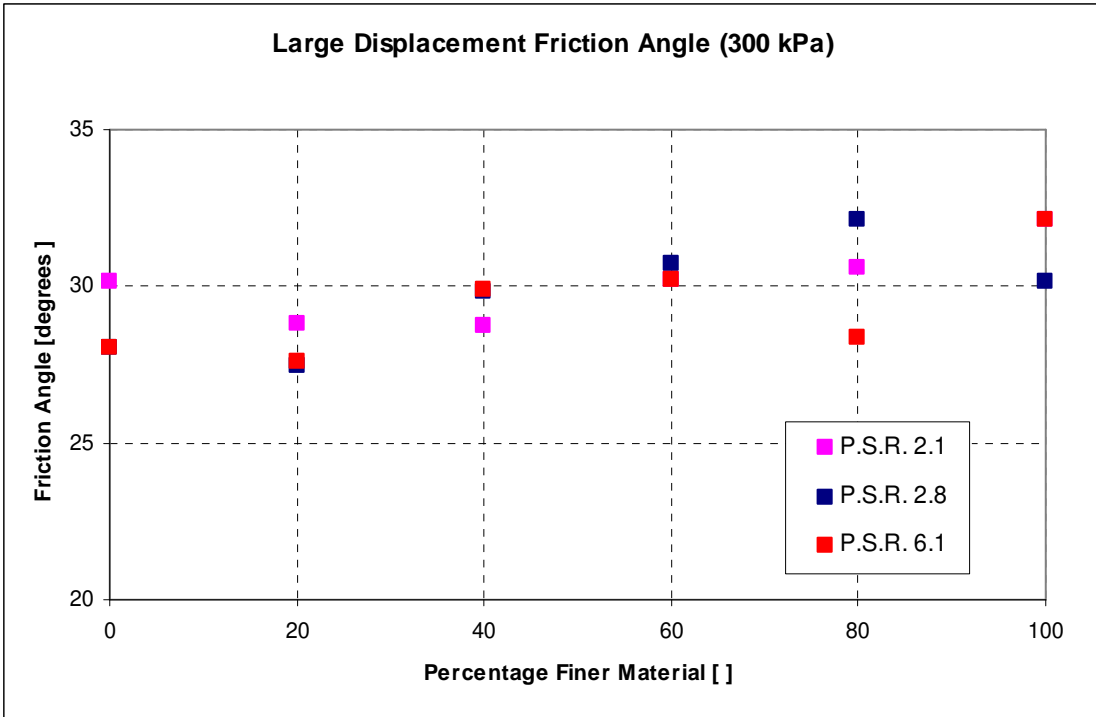


Figure 4.21 Large Displacement Friction Angles (300 and 500 kPa)

Viewing the same data in this manner it is observed that across all materials and normal stresses tested the total range of the data is from approximately 26.5 degrees to 32.5 degrees, a range of 6 degrees. No obvious trends emerge from the data, however.

Since the large displacement friction angle is assumed to be relatively independent of the normal stress applied, the variation in the large displacement friction angle is due to a combination of the changing of the material (particle size ratio and mixture percentages) and inherent variability in experimental soil testing.

The dilation of the samples is indicated by the difference between the peak and large displacement values. Taylor's flow rule (Taylor, 1948) has been adopted since it was originally developed for direct shear testing. Other flow rules have also been proposed for sands, notable by Rowe (1962) and Bolton (1986), but these were both formulated using plane strain parameters. Jewell (1989) reports that the differences between these different flow rules is only relevant at large dilation angles.

Taylor's relationship is expressed as:

$$\tan \sigma_p = \tan \sigma_{ld} + \tan \psi_p$$

where: σ_p = peak friction angle

σ_{ld} = friction angle measured at large displacement

ψ_p = peak dilation angle

The dilatancy effect can thus be explored as a function of the normal stress and mixture characteristics (particle size ratio and percentage of finer material).

As was seen above, only the PSR 6.1 mixture showed a strong trend in relation to the percentage of finer material.

Tabulating the dilation angle data using Taylor’s relationship gives the following results for the P.S.R. 6.1 mixture, as shown in Table 4.6. For a given mixture percentage, the column on the far right gives the range in the measured dilation angles across the full range of normal stress tested (50 to 500 kPa). For a given normal stress, the bottom-most row gives the range in the measured dilation angle across all the mixtures tested.

Table 4.6 Dilation Angles for P.S.R. 6.1

% Finer Material	50 kPa	100 kPa	300 kPa	500 kPa	Range across σ_n
0	7.5	10.0	4.2	7.0	5.82
20	13.6	13.6	10.9	9.2	4.44
40	13.2	8.4	7.1	5.4	7.82
60	9.3	6.7	3.5	2.8	6.59
80	6.4	4.7	3.5	2.8	3.52
100	5.5	2.4	0.5	0.2	5.31
Range across % finer	8.03	11.17	10.39	8.93	

From Table 4.6 it can be observed that for a particular mixture ratio the maximum range for the dilation angle is 7.8 degrees (for 40% finer content) across the full range of normal stresses tested. It is noteworthy that for any particular normal stress, the range of dilation angle across the range of mixture ratios is always greater than 7.8 degrees, with a maximum of 11.2 degrees.

For the materials and normal stress conditions tested, the mixture ratio plays a larger role in determining the dilation angle than the normal stress, which varied by one order of magnitude.. This is a clear indication of the role that the mixture characteristics can have on the strength of binary mixtures.

Figure 4.22 shows graphically how the dilation angle varies with the percentage of finer material. Data is plotted in a different color for each normal stress tested.

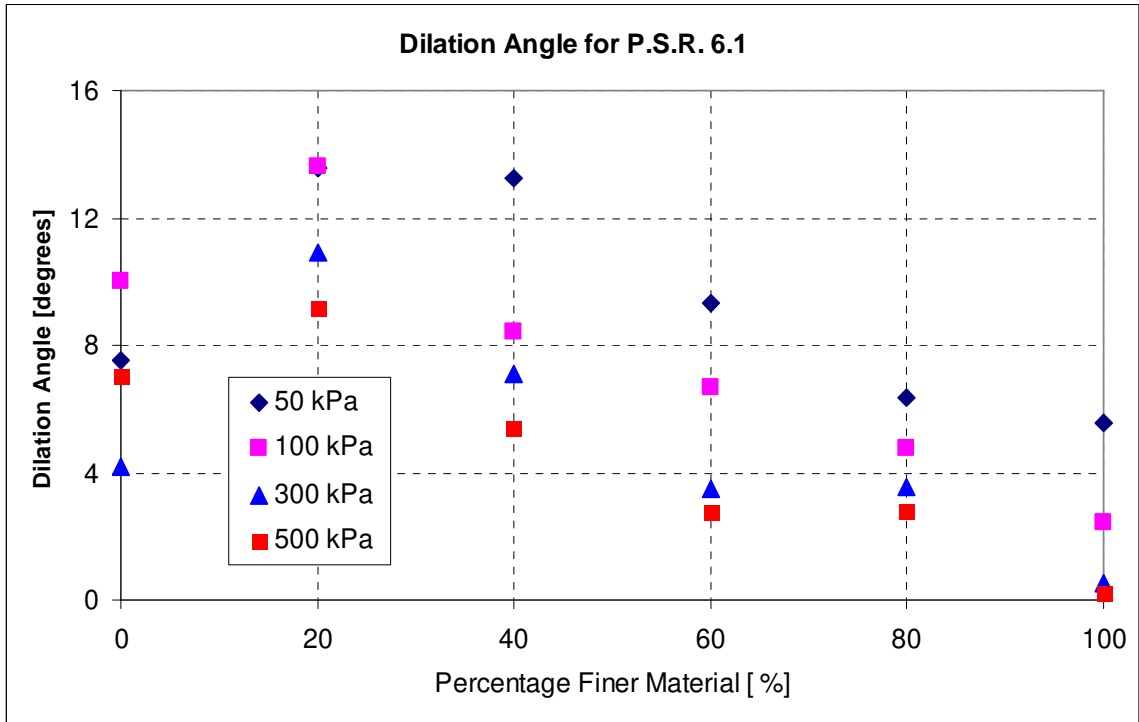


Figure 4.22 Dilation Angle for PSR 6.1

As can be seen in Figure 4.22, the dilation angle shows a significant decrease with an increasing percentage of finer material from 20% through to 100%. There is an increase in the dilation angle from 0% to 20% finer particles. This trend is pronounced for all stress levels.

It is interesting to note that the dilation angle peaks, for all cases, when the mixture percentage of finer particles is 20%.

4.4. Conclusions

- The minimum void ratio for a particle mixture occurs at a mixture ratio of between 25% and 35% finer particles by mass.

- The greater the particle size ratio the lower the amount of finer material is required to obtain the minimum void ratio.
- The lowest value for the maximum void ratio occurs at a mixture ratio of approximately 38%.
- This value does not vary as the particle size ratio varies and is also greater than observed for the minimum void ratio case.
- A new parameter, VRR, was developed to isolate the effect of mixing on the packing of particle mixtures.
- Using VRR, it is clear that for the minimum void ratio case the largest reduction in void ratio due to mixing occurs for ratios of finer material between 30% and 40%. The data shows that for larger particle size ratios the amount of finer material to have an equivalent effect is lower.
- For the maximum void ratio case, the amount of finer material required to exhibit the largest decrease in void ratio due to mixing is independent of particle size ratio and occurs at approximately 40% of finer material by mass.
- Divergence in the VRR between the minimum and maximum void ratio cases occurs for all particle size ratios at approximately 60% finer particles by mass.
- Mixing two particles together in ratios of greater than approximately 60% finer particles does not alter the way in which the particles pack together. At any ratio greater than 60% the packing structure remains essentially the same. Note that coordination number and void ratio do change, but the

presence of the larger particles does not alter the way in which the smaller particles are arranged.

- At mixture ratios less than approximately 60% there is not an interaction effect between the different sized particles.
- The relationship between e_{min} and e_{max} is not constant, but varies as a function of both the particle size ratio and mixture ratio. This e_{min}/e_{max} relationship is particularly sensitive at low concentrations of finer particles and higher particle size ratios.
- The e_{min}/e_{max} ratio becomes substantially less influenced by particle size ratio when the amount of finer material reaches 50%.
- Segregation between the two different components during limiting void ratio tests was minimal. Some minor segregation occurred in the lowest layers of particles as a result of the manner in which the particles were initially placed inside the pipe. The minor degree of segregation is not expected to influence the results in a meaningful way.
- The large displacement strength of mixtures is bounded by the large displacement strength of the uniform soils.
- Peak strengths of mixtures are not similarly bounded by uniform soils. In this case, the strengths of uniform soils form an upper bound at low normal stresses while at higher normal stresses they tend towards the bottom of the peak strength envelope.
- Large displacement friction angles vary from approximately 26.5 to 32.5 degrees across the entire range of materials and normal stresses tested.

This range reflects the changes in the materials, in terms of particle size ratio and mixture proportions, as well as inherent variability in experimental soil testing. No significant trends emerged from the data set.

- The dilatancy angle is significantly affected by the mixture ratio. A change from 20% to 100% finer particles shows a decrease in the dilation angle. The dilation angle increases from 0% to 20% of finer material.
- The peak dilation angle is found at a 20% mixture percentage.
- For the materials tested, the mixture percentage plays a more dominant role than the applied normal stressing determining the dilation angle.

5. INTERFACE SHEAR BEHAVIOR OF BINARY PARTICLE MIXTURES WITH SMOOTH COUNTERFACES

5.1. Introduction

In this chapter the interaction between particulates and smooth counterface surfaces will be investigated. The shear mechanisms and interface shear behavior of soils in contact with smooth counterfaces are of interest to geotechnical engineers as these types of materials are commonly found in geotechnical systems and structures. In particular, the use of smooth geosynthetic membranes is widespread in containment applications. Smooth high-density polyethylene (HDPE) was selected for study as it is widely used in such field applications and previously published data is available for comparison. The interface shear strength for this material in contact with a range of different soils will be examined. In particular, the interface shear strength of binary particle mixtures will be evaluated in contrast to that of the individual constituent materials.

This chapter is comprised of several sections. The first section presents the results of the experimental study into the interface shear strength of particles in contact with a smooth HDPE surface. Both uniform sands and particle mixtures will be considered. The second section presents the results of a surface profilometry evaluation of the HDPE surfaces before and after shearing.

In order to fully explore and understand the results presented in the first two sections, an interpretation of the results on the scale of the particle contacts is required. Since the measurements presented in the first section were global values measured on the boundaries of the soil specimens it is necessary to relate these global measurements to

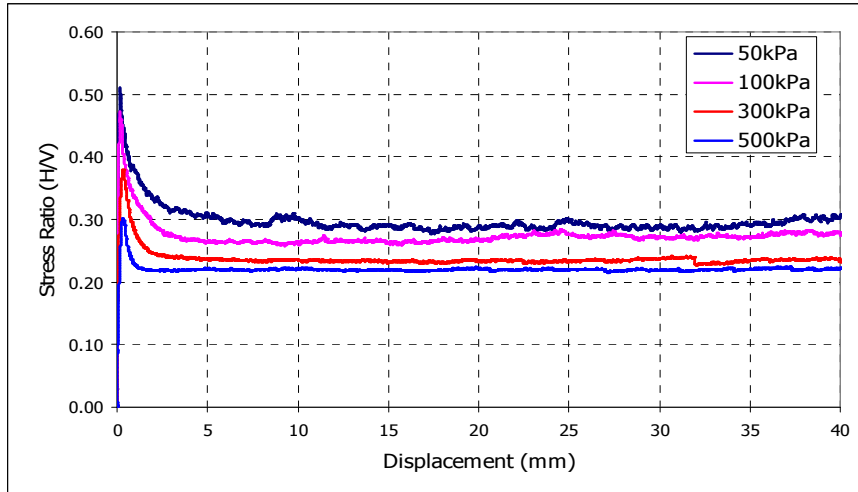
phenomena occurring on the scale of the particle contact. The surface profilometry results give micro-scale insight into the particle-membrane interactions. Particle scale analysis will be presented in the third main section of the chapter where analytical models describing the contact conditions will be used. A brief review of key concepts relating to contact mechanics and friction introduces this third section. The development of models to predict the friction coefficient for both uniform sands and binary mixtures will then be presented.

5.2. Interface Shear Tests with Smooth HDPE

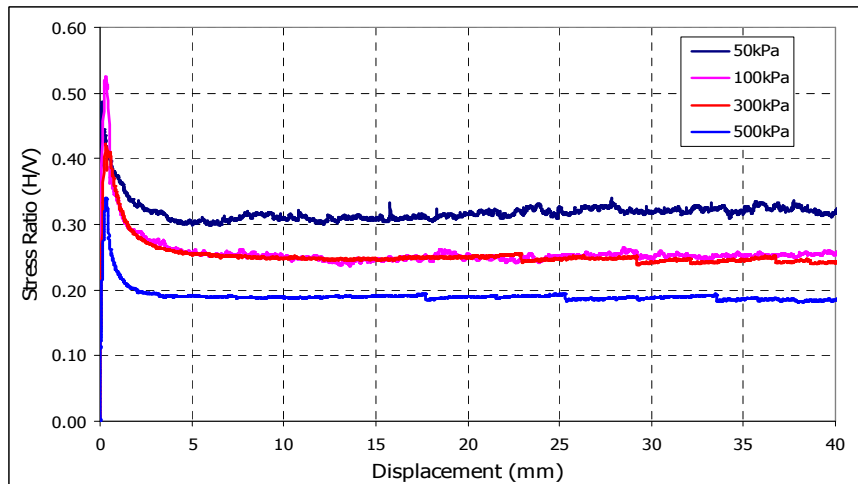
As outlined in Chapter 3, a series of interface shear tests were performed using smooth HDPE as the counterface material and a range of different particulate materials. Results are presented and discussed in subsequent sections.

5.2.1. Interface Shear Results of Uniform Sands

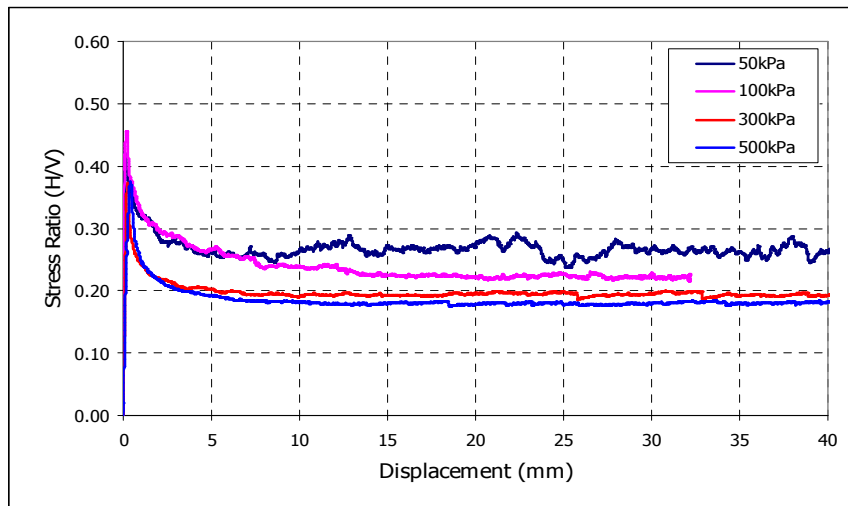
Figure 5.1 shows the stress ratio - displacement response of various uniform sands sheared against a smooth HDPE counterface as measured using the modular interface shear device. The graphs show how the stress ratio (also termed the “friction coefficient”) varies with shear displacement. The particles in each of the three graphs differ principally in size. Each series of tests presented on a single graph covers the same range of normal stresses, from 50 kPa to 500 kPa. The particles range in diameter from 0.78mm (20/25) to 0.13mm (100/140) with the intermediate diameter being 0.28mm (50/60).



(a) 100/140 Particles (0.13mm)



(b) 50/60 Particles (0.28mm)



(c) 20/25 Particles (0.78mm)

Figure 5.1 Interface Shear Behavior for Smooth HDPE

It can be seen in Figure 5.1 how the friction coefficient initially increases rapidly to a peak value before decreasing post-peak to a relatively constant value. This constant value is referred to as the post-peak strength. As can be seen in Figure 5.1, an increase in the normal stress causes a decrease in both the peak and post-peak interface shear strengths. This is further shown in the summary plots below (Figure 5.2 and Figure 5.3). Minor variations in trends are attributed to minor variations in specimen density.

The increased variability evident in the 50 kPa plots in Figure 5.1 is due to the slight variation in the applied normal stress which, relatively speaking, manifests as a larger variability for the lower normal stresses. In Figure 5.1 (b) the plots for 100 kPa and 300 kPa are almost coincidental with one another. This is most likely due to minor variations in the relative density of the prepared specimens. In this particular case, the relative density of the 300 kPa specimen was greater than that of the 100 kPa specimen, thereby yielding plots that exhibit similar coefficient of frictions. The 100 kPa plot in Figure 5.1 (c) is truncated due to an incorrect setting on the contact switch determining the length of the test. This error does not affect any other part of the test and occurs at a point in the test where significant additional variation in the friction coefficient is not expected.

The generally decreasing trend of the peak friction coefficient can be seen in Figure 5.2 where the peak interface friction coefficients decrease from approximately 0.47 at 50 kPa to 0.34 at 500 kPa. These values correspond to interface friction angles of approximately 19 to 25 degrees. As expected, these values are somewhat lower than the values one would expect for these same soils tested under direct shear conditions since the internal friction angle of the soil is the upper limit to what would be measured in an

interface shear device. The smooth HDPE counterface does not mobilize the full internal friction of the soil and thus the measured interface shear strength in this case is less than the internal shear strength of the soil. The values for the post-peak interface friction coefficient, as presented in Figure 5.3, range from approximately 0.30 at 50 kPa to 0.19 at 500 kPa. These values correspond to interface friction angles of between approximately 10 and 17 degrees.

It is interesting to note that the difference between the average peak and post-peak friction angles is approximately 9.6 degrees at 50 kPa and 8.5 degrees at 500 kPa. From a traditional soil mechanics perspective this is not a surprising result since the difference between the peak and post-peak strengths would generally be expected to decrease with an increase in the normal stress. This is due to the phenomenon of dilation (for a dense specimen) and the fact that at increasing normal stresses the dilation can be suppressed. The mechanisms in this case are, however, different and an explanation should not purely be made based on the traditional soil mechanics interpretation.

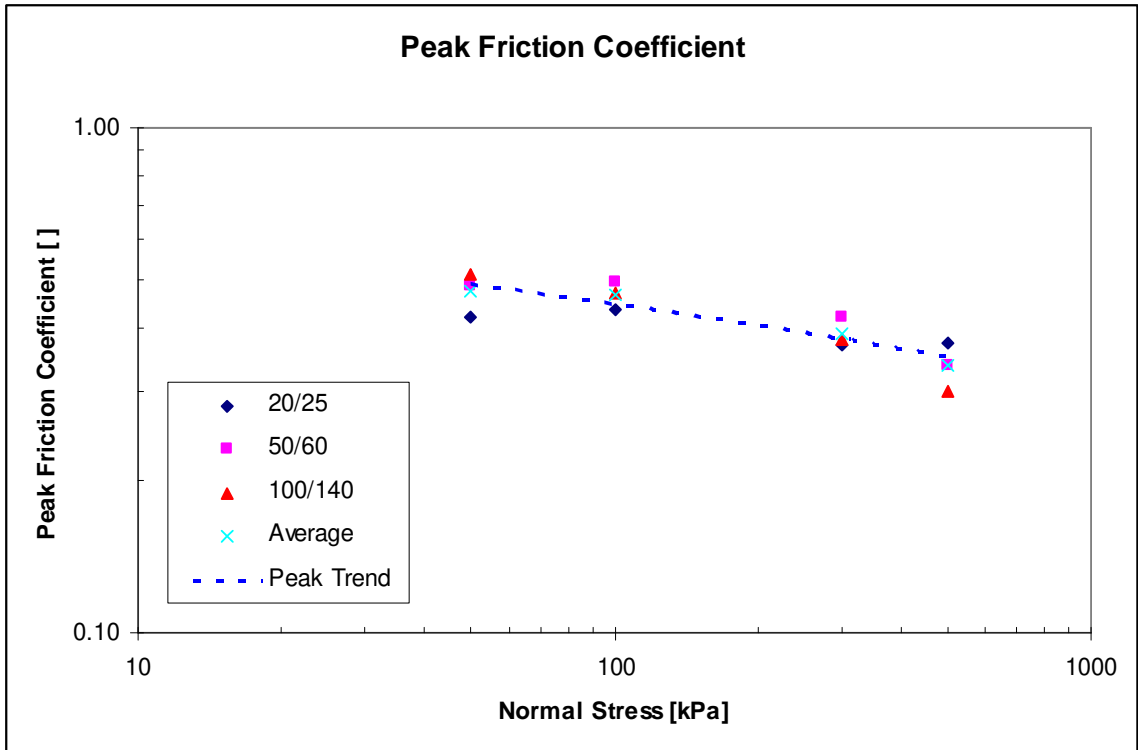


Figure 5.2 Peak Friction Coefficient for Uniform Soils

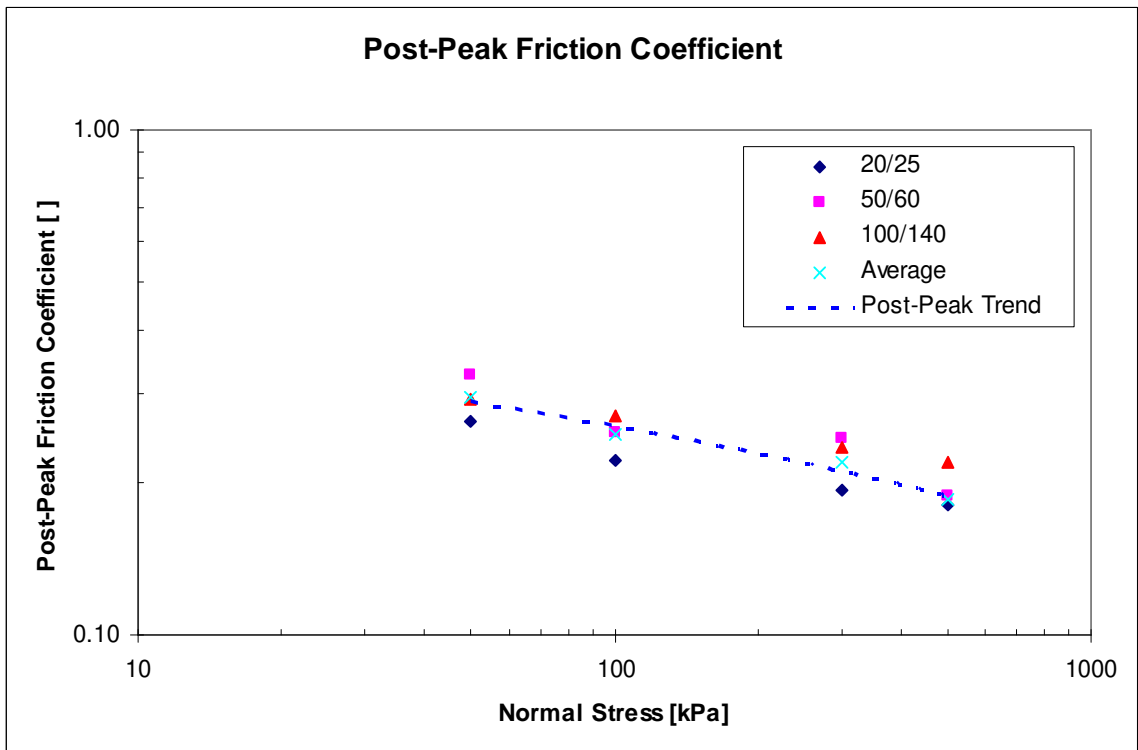


Figure 5.3 Post-Peak Friction Coefficient for Uniform Soils

The decrease in the friction coefficient seen in Figure 5.2 and Figure 5.3 indicates that the true contact area between the particles and the surface (the seat of shear resistance) is increasing at a rate less than the normal stress. The ratio between the horizontal and vertical stresses thus decreases with an increasing normal stress. This decrease is consistent across the entire range of normal stress tested. This type of behavior is consistent with expectations and has also been noted by Archard (1957), Dove (1999) and Iscimen (2004), amongst others.

In Figure 5.2 and Figure 5.3 it can also be observed that the particle size does not have a primary role in controlling the friction coefficient. This is evidenced by the relatively close clusters of data points at each normal stress value. Some of the particles differ in size by more than a factor of 6 and yet it is clearly seen that the level of normal stress is the controlling factor, not the absolute particle size. This is a very important observation and will be related to the contact mechanics of the situation later in the chapter. Since the absolute particle size does not have a controlling effect on the friction coefficients an average friction coefficient can be taken at each stress level with a degree of confidence.

Given that the particles do differ in size by a factor of 6 and that the same shear box is used for all of the tests, the issue of box size relative to particle size arises. However, this is not considered to be a significant factor since even for the largest particle size the smallest dimension of the rectangular shear box is more than 80 times greater than the particle diameter. As a point of reference, ASTM D3080-03 (Standard Test Method for Direct Shear Test of Soils under Constant Drained Conditions)

prescribes that the minimum width of the shear box be only at least 10 times greater than the largest particle diameter.

The comparison between the peak and post-peak friction coefficients is shown in Figure 5.4 below.

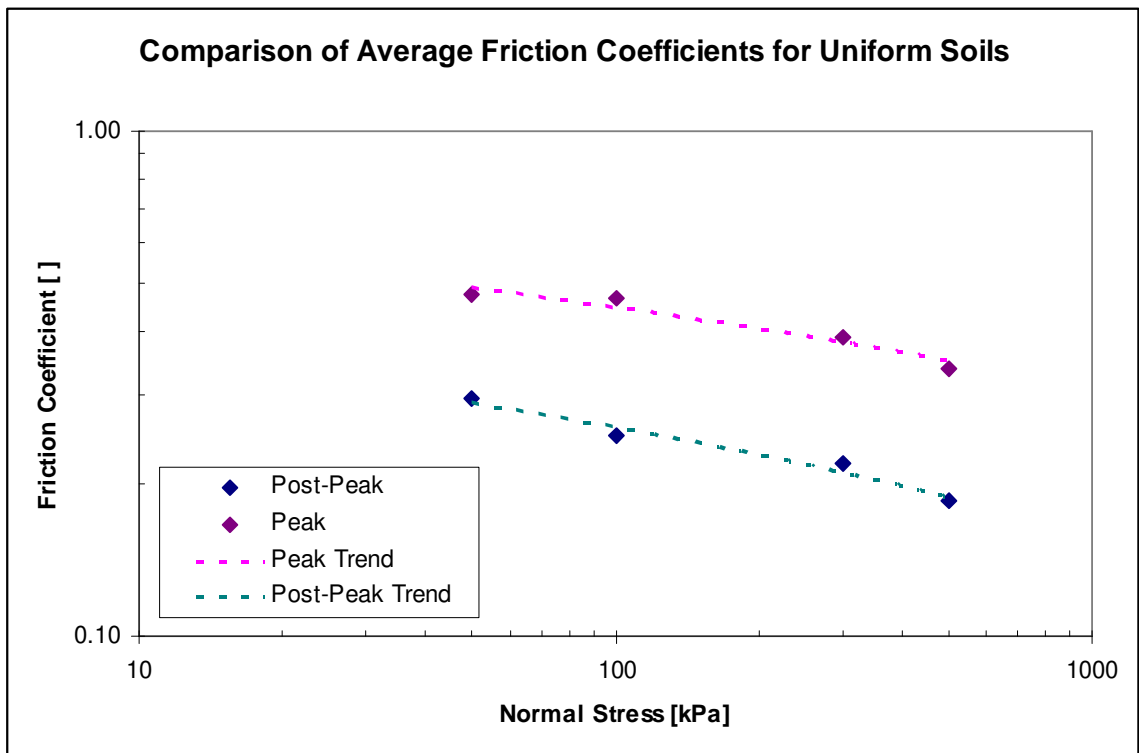


Figure 5.4 Average Friction Coefficients for Uniform Soils

The effect of particle size on the interface shear behavior can be investigated further by using the same data set but presenting the data in alternative formats.

Figure 5.5 presents four graphs, one for each level of normal stress tested. On each graph the response of the three different sized particles can be compared. All of the data is for uniform sands.

It can be seen in Figure 5.5 that the particle size does not have a large effect on the coefficient of friction. However, a closer examination of the peak and post-peak values show some interesting trends.

At the lowest normal stress level of 50 kPa, the smallest particles showed the highest peak strength with the largest particles showing the lowest peak strength. The largest particles also showed the lowest post-peak strength.

In contrast, at the highest normal stress level tested of 500 kPa, the largest particles showed the highest peak strength with the smallest particles showing the lowest peak strength. In all cases, however, the largest particles (20/25) showed the lowest post-peak friction coefficients. This suggests that the mechanisms responsible for the friction coefficient are different at the peak state and at the post-peak state.

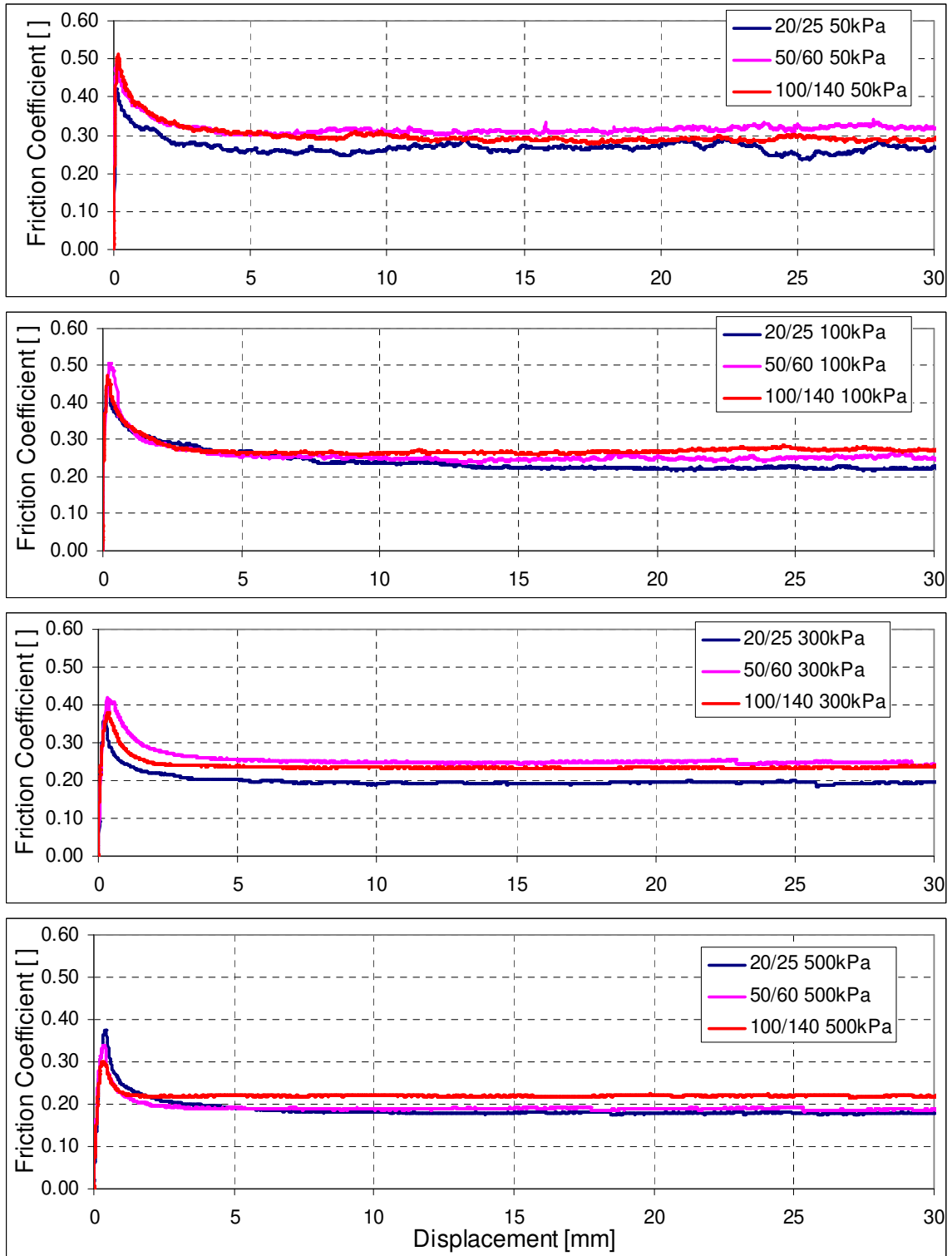


Figure 5.5 Particle Size Effect on Interface Shear Behavior

It is hereby postulated, based on these observations and knowledge of the particle shape and sizes, that the post-peak strength is predominantly controlled by the particle shape. The largest particles, in all cases, exhibited the lowest strength which corresponds well to them being the roundest of all the particles.

The peak strength is likely controlled by the friction conditions that exist just prior to shearing, and will depend on the true contact area between the particles and the surface.

5.2.2. Interface Shear Behavior of Particle Mixtures

Interface shear tests, as have been presented above, were also carried out with particle mixtures with 20%, 40% and 70% of smaller particles. The tests were performed in an identical manner to the tests performed with the monosized particles. Tests were performed at normal stresses of 50, 100, 300 and 500 kPa and each of the three particle size ratios was tested at each of the mixture proportions.

The results of the tests are shown below in Figure 5.6, Figure 5.7 and Figure 5.8. Each figure shows the friction coefficient varying with shear displacement for four different normal stresses and at five different mixture proportion ratios (0, 20, 40, 70 and 100% of smaller particles).

The variation of the peak friction coefficient with normal stress is shown in Figure 5.9 and the post-peak friction coefficients are shown in Figure 5.10. The figures present data for the three different particle size ratios and provides a comparison to the average peak friction coefficient for uniform soils. The dashed blue line is the trend line through the data for the uniform soils (data points not shown). The dashed red line is a trend line through the shown data points (for the binary mixtures).

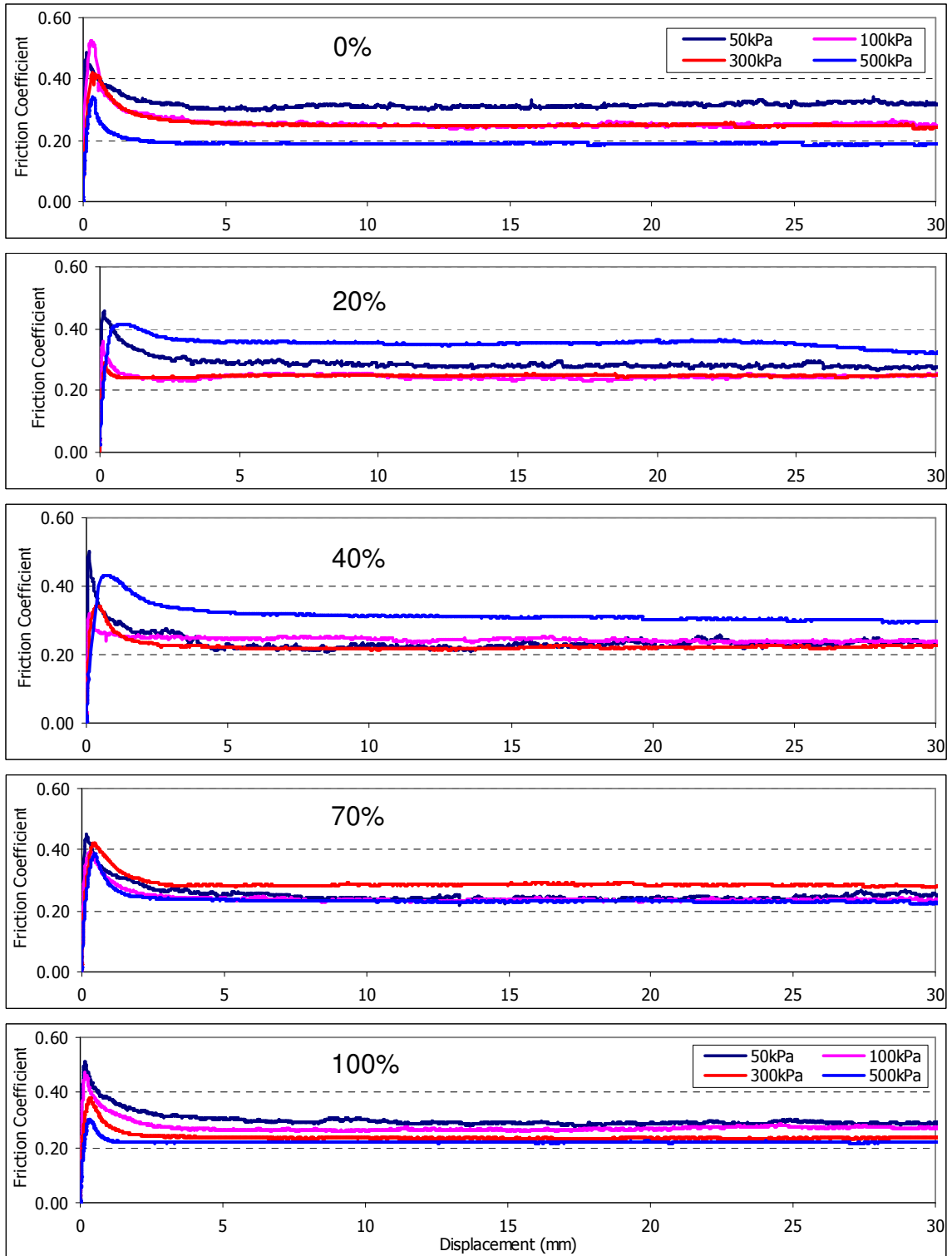


Figure 5.6 Interface Shear Tests for PSR 2.1 (100/140 and 50/60)

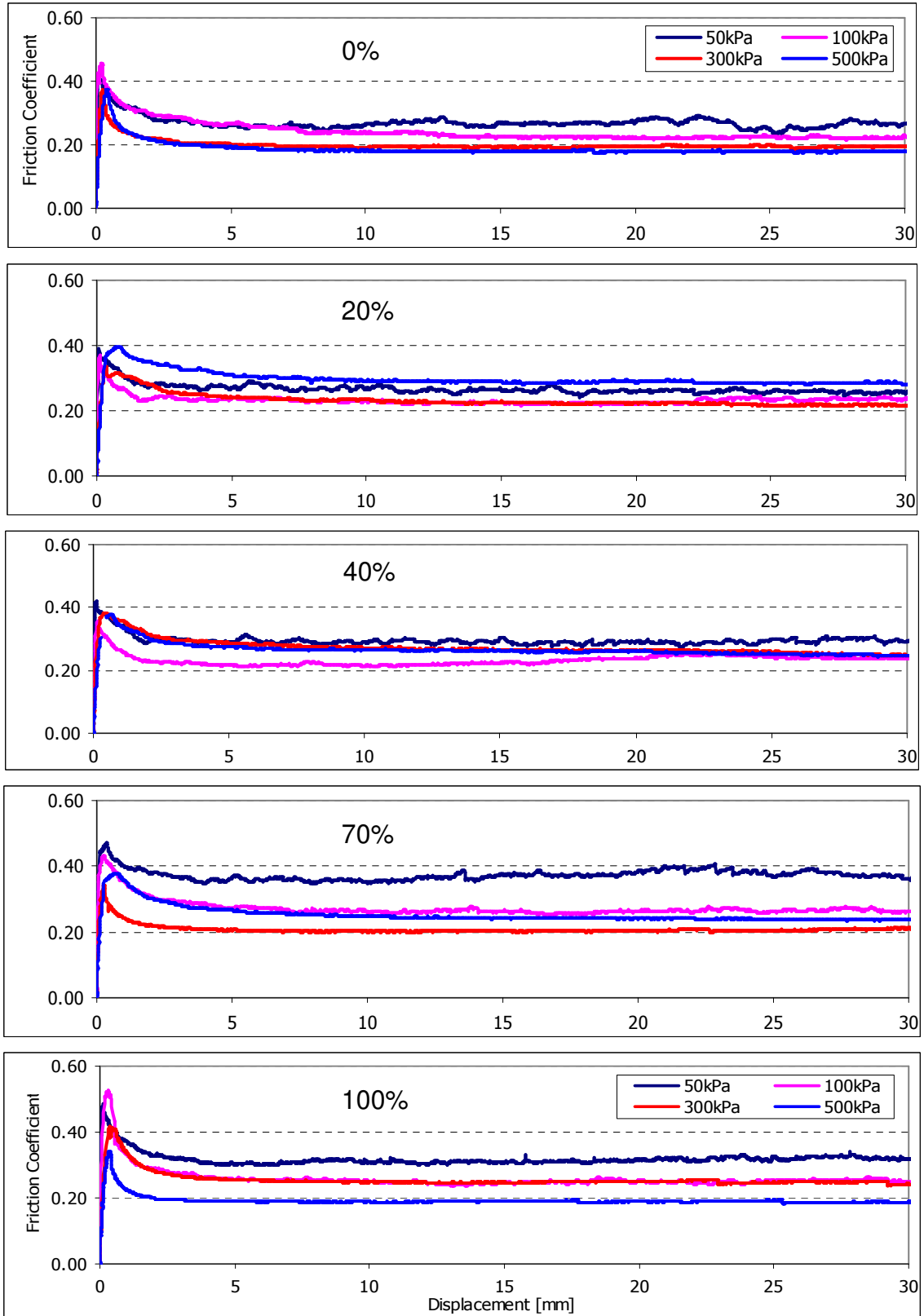


Figure 5.7 Interface Shear Tests for PSR 2.8 (50/60 and 20/25)

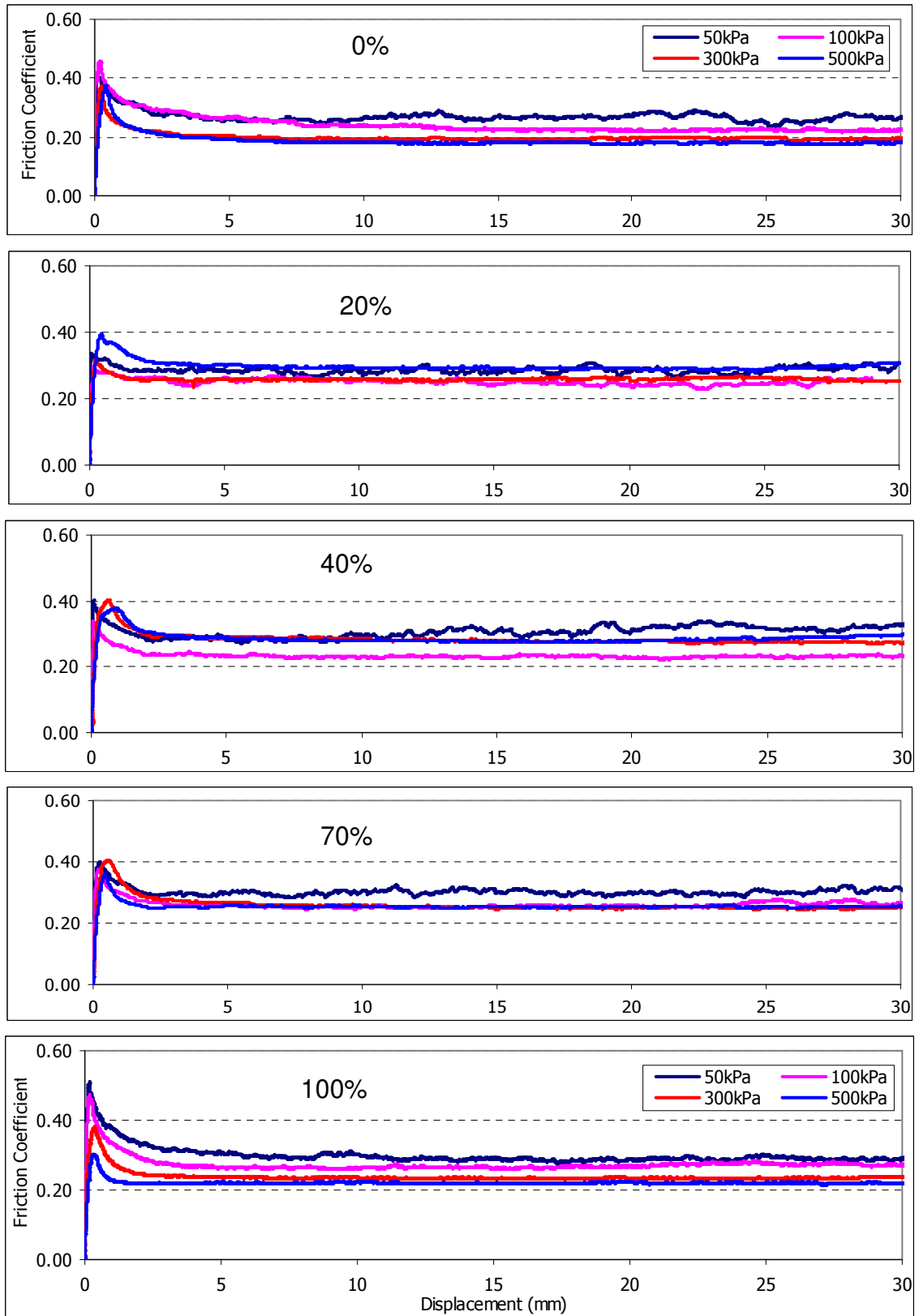


Figure 5.8 Interface Shear Tests for PSR 6.1 (100/140 and 20/25)

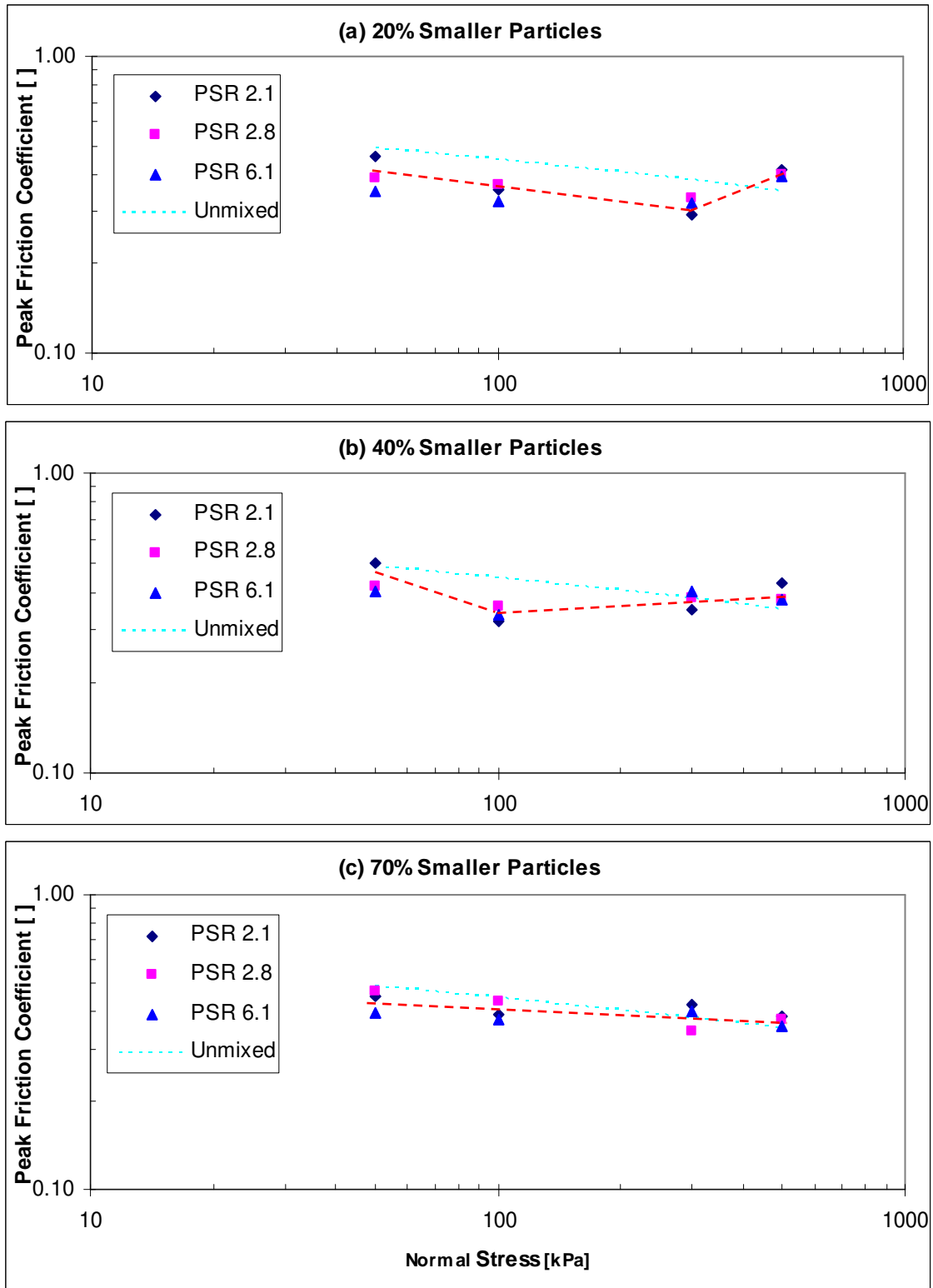


Figure 5.9 Peak Friction Coefficient for Particle Mixtures

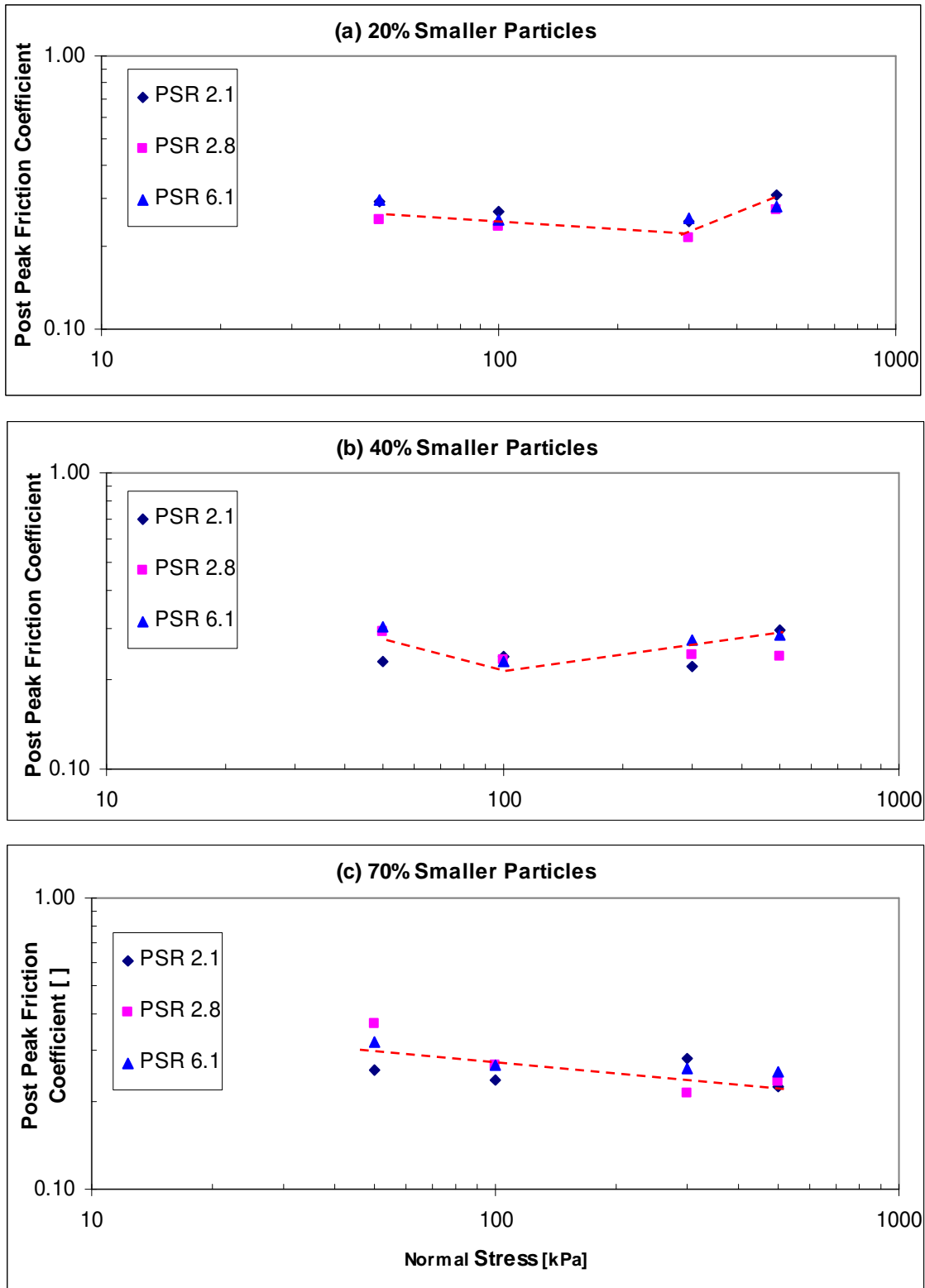


Figure 5.10 Post-Peak Friction Coefficient for Particle Mixtures

The complete data set for both the uniform sands and the particle mixtures in contact with smooth geomembrane is shown in the tables below:

Table 5.1 Interface Shear Test Data for P.S.R. 2.1

				Test Reference	Normal Stress [kPa]	Relative Density [%]	Peak Friction Coeff.	Large Disp. Friction Coeff.
	20/25	50/60	100/140					
P.S.R. 2.1	0	100	0	GM50/60_50	50	80	0.487	0.327
				GM50/60_100	100	82	0.4956	0.252
				GM50/60_300	300	82	0.420	0.245
				GM50/60_500	500	85	0.339	0.189
	0	80	20	GM_2.1_20_50	50	83	0.458	0.292
				GM_2.1_20_100	100	81	0.357	0.271
				GM_2.1_20_300	300	83	0.292	0.249
				GM_2.1_20_500	500	84	0.414	0.311
	0	60	40	GM_2.1_40_50	50	83	0.334	0.232
				GM_2.1_40_100	100	84	0.319	0.24
				GM_2.1_40_300	300	83	0.349	0.223
				GM_2.1_40_500	500	81	0.432	0.296
	0	30	70	GM_2.1_70_50	50	83	0.450	0.256
				GM_2.1_70_100	100	82	0.391	0.236
				GM_2.1_70_300	300	82	0.422	0.282
				GM_2.1_70_500	500	84	0.386	0.225
	0	0	100	GM100/140_50	50	80	0.511	0.292
				GM100/140_100	100	84	0.472	0.272
				GM100/140_300	300	85	0.380	0.235
				GM100/140_500	500	81	0.302	0.220

Table 5.2 Interface Shear Test Data for P.S.R. 2.8

P.S.R. 2.8	20/25	50/60	100/140	Test Reference	Normal Stress [kPa]	Relative Density [%]	Peak Friction Coeff.	Large Disp. Friction Coeff.
	100	0	0	GM20/25_50	50	81	0.422	0.264
GM20/25_100				100	81	0.435	0.222	
GM20/25_300				300	83	0.373	0.193	
GM20/25_500				500	84	0.375	0.181	
80	20	0	GM_2.8_20_50	50	84	0.388	0.25	
			GM_2.8_20_100	100	80	0.369	0.237	
			GM_2.8_20_300	300	84	0.420	0.279	
			GM_2.8_20_500	500	84	0.397	0.273	
60	40	0	GM_2.8_40_50	50	85	0.419	0.291	
			GM_2.8_40_100	100	81	0.358	0.235	
			GM_2.8_40_300	300	85	0.383	0.243	
			GM_2.8_40_500	500	85	0.377	0.241	
30	70	0	GM_2.8_70_50	50	80	0.470	0.372	
			GM_2.8_70_100	100	84	0.434	0.268	
			GM_2.8_70_300	300	83	0.343	0.213	
			GM_2.8_70_500	500	80	0.378	0.233	
0	100	0	GM50/60_50	50	80	0.487	0.327	
			GM50/60_100	100	82	0.4956	0.252	
			GM50/60_300	300	82	0.420	0.245	
			GM50/60_500	500	85	0.339	0.189	

Table 5.3 Interface Shear Test Data for P.S.R. 6.1

P.S.R. 6.1	20/25	50/60	100/140	Test Reference	Normal Stress [kPa]	Relative Density [%]	Peak Friction Coeff.	Large Disp. Friction Coeff.
	100	0	0	GM20/25_50	50	81	0.422	0.264
GM20/25_100				100	81	0.435	0.222	
GM20/25_300				300	83	0.373	0.193	
GM20/25_500				500	84	0.375	0.181	
80	0	20	GM_6.1_20_50	50	80	0.351	0.296	
			GM_6.1_20_100	100	81	0.326	0.250	
			GM_6.1_20_300	300	82	0.318	0.256	
			GM_6.1_20_500	500	80	0.393	0.282	
60	0	40	GM_6.1_40_50	50	81	0.404	0.302	
			GM_6.1_40_100	100	80	0.339	0.232	
			GM_6.1_40_300	300	82	0.405	0.271	
			GM_6.1_40_500	500	82	0.379	0.284	
30	0	70	GM_6.1_70_50	50	85	0.399	0.321	
			GM_6.1_70_100	100	83	0.378	0.266	
			GM_6.1_70_300	300	83	0.404	0.260	
			GM_6.1_70_500	500	81	0.360	0.252	
0	0	100	GM100/140_50	50	80	0.511	0.292	
			GM100/140_100	100	84	0.472	0.272	
			GM100/140_300	300	85	0.380	0.235	
			GM100/140_500	500	81	0.302	0.220	

In Figure 5.9 (c) it can be seen that for a mixture with 70% smaller particles, regardless of the particle size ratio, the mixture acts in a similar way to a uniform soil. That is, the friction coefficient shows a consistent decrease with an increase in the normal stress. For this case, the friction coefficient ranges from approximately 0.44 at 50 kPa to 0.38 at 500 kPa, equivalent to a change in friction angle of approximately 3.5 degrees. This can be compared to the values shown in Figure 5.2 where for a uniform soil the friction coefficient varies from approximately 0.47 to 0.34 (equivalent to a change of approximately 7.5 degrees) over the same normal stress range.

The slight difference in the magnitude of the observed behavior between the uniform and 70% mixtures is not believed to indicate a fundamental difference in how these two different materials behave. The 70% mixture behaves in essentially the same manner as the uniform soil, within the scatter found in the data.

Referring again to Figure 5.9, it is observed that the intermediate cases of 20% and 40% smaller particles exhibit a different type of behavior, with the peak coefficient of friction reaching a minimum at some intermediate normal stress value before increasing as the normal stress increases. The “elbow” in the curves occurs at approximately 300 kPa for the 20% mixtures and at approximately 100 kPa for the 40% mixtures.

Figure 5.10 shows the results for the post-peak friction coefficient, and while the values are less than the peak values, the graphs show substantially similar trends to Figure 5.9. For soil with 70% finer material, the behavior is very similar to that of a uniform sand. For the mixtures with 20% and 40% finer material present, an elbow

occurs, as in Figure 5.9, with the elbow occurring at a lower normal stress in the 40% case.

It is clear from the figures above that the particle mixture proportions have an effect on the friction coefficients while the absolute particle size and particle size ratio have only a secondary influence.

A similar finding was made for uniformly sized particles by Dove (1999) who carried out similar experiments using smooth HDPE surfaces and Ottawa 20/30 sand (D_{50} of 0.72mm) which is very similar to the 20/25 sand used in the current study. A summary of those results are shown below:

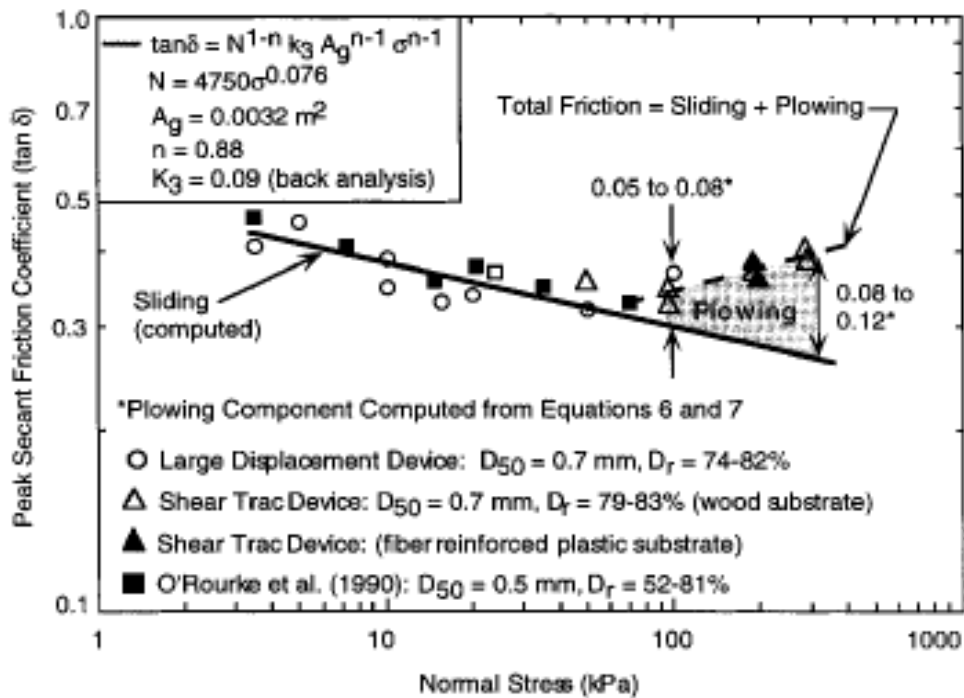


Figure 5.11 Peak Friction Coefficients (Dove, 1999)

The “elbow” in these results can clearly be seen at a normal stress of approximately 60 kPa, slightly less than that observed for the 40% mixtures and significantly less than that observed for the 20% mixtures.

Dove (1999) attributes the elbow to the existence of two different regimes with one dominating on either side of the elbow. At normal stresses less than approximately 60 kPa it is postulated that the predominant mode of shearing is sliding and that adhesion between the surface and real particle contact area is responsible for the resistance to movement. At higher normal stresses it is postulated that the load on the individual grains becomes greater than the yield stress of the surface. This results in plastic indentation of the surface by the particles which in turn leads to a plowing mode of shear when relative displacement occurs.

The experiments reported were for uniform particles ranging in size from 0.5 to 0.7mm and for relative densities ranging from 52% to 83%. It was further reported that the particle size (within the relatively narrow range tested) and the relative density (across a fairly wide range) showed no effect on the behavior.

It can be observed in Figure 5.2 and Figure 5.3 that the absolute particle size does not play a large role in determining the behavior in the current study either. The data shows the same consistent trend even though the particles used vary in size from 0.13mm to 0.78mm, a more than six-fold increase in size.

From Figure 5.9, however, it can be seen how the behavior is affected by the mixture ratio. The cause of this is not the fact that different size particles are present (as this would have manifest in the experiments reported in Figure 5.1) but rather it is the way that the applied normal stress changes the number and type of particles in contact with the surface as well as the load distribution between the contacting particles.

The mixture of 70% finer particles shows similar behavior as the uniform particulate material, indicating that at that ratio, the larger particles are not playing a large

role in the interface shearing behavior, but rather are surrounded by a matrix of smaller particles and in a sense shielded from playing a role.

5.3. Surface Profilometry of Smooth HDPE

Stylus profilometry was used to determine the post-shear surface profiles as well as the reference baseline for the surfaces prior to shearing. This allows for the change to the surface as a result of the shearing action of the particles to be quantified. The amount of wear on the surfaces can then be related to the particle characteristics, surface properties and test conditions. All profiles were recorded perpendicular to the shearing direction and in accordance with the directions stated in Chapter 3.

5.3.1. Pre-Shear Profiles

The significant vertical exaggeration associated with the plotting of surface profile plots can lead to a distorted perspective on the roughness (or smoothness) of a surface. Figure 5.12 shows the same surface profile (or portions thereof) to illustrate this and provide a sense of perspective on the surface roughness relative to the particle size.

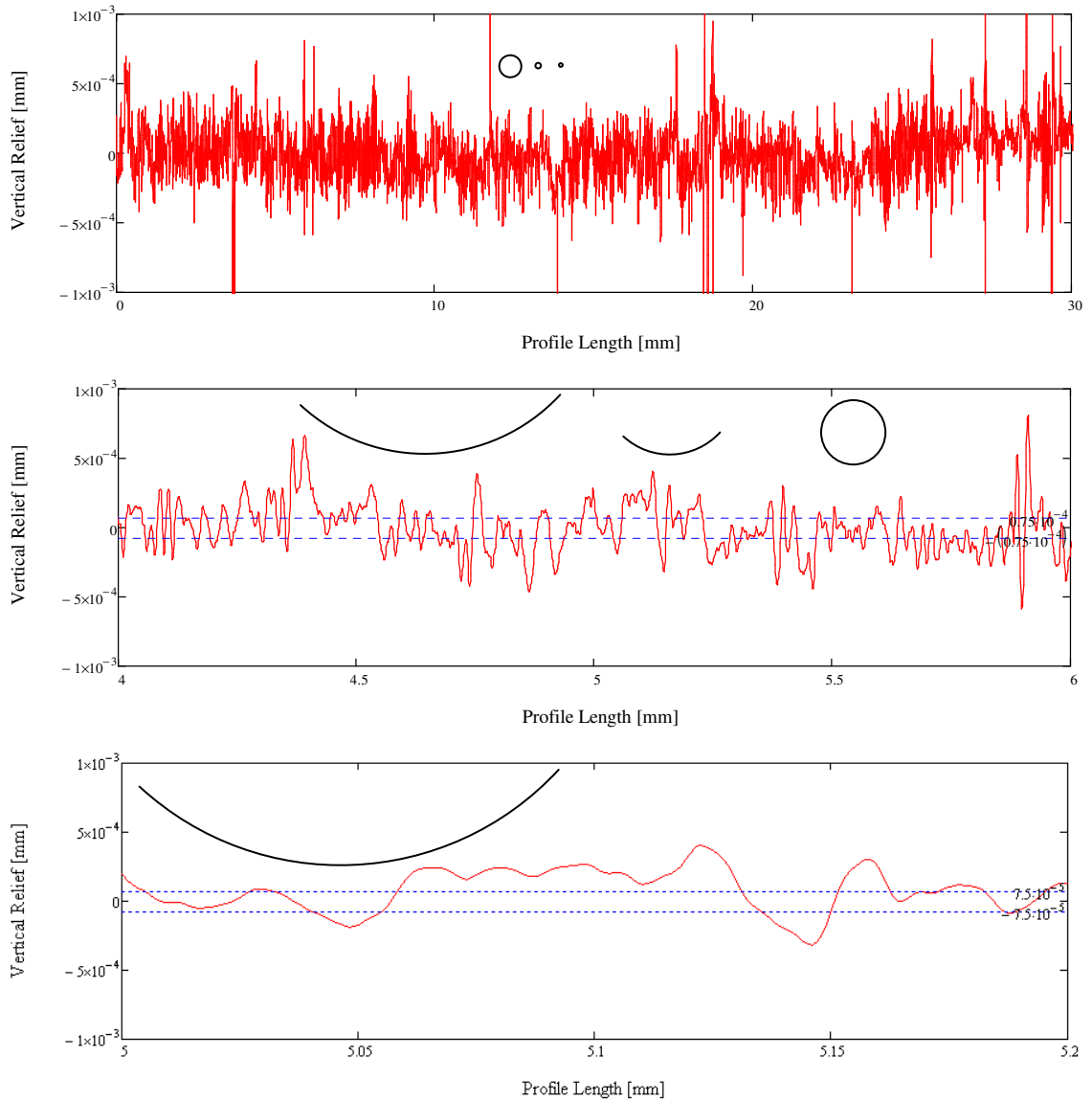


Figure 5.12 Pre-Shear Surface Profile at Various Scales

In Figure 5.12 (a) the entire profile length is shown and all three particle sizes are illustrated alongside, scaled in proportion to the horizontal axis. In part (b) the same particles are shown and in part (c) only the smallest of the particles ($D_{50} = 0.13\text{mm}$) is illustrated.

The blue horizontal markers in parts (b) and (c) indicate the average roughness, R_a , as measured for this surface, which is 1.5×10^{-4} mm. The markers indicate half of the average roughness distance on each side of the horizontal axis.

Another observation is that the sampling interval of $1\mu\text{m}$ enables all the features of the surface to be accurately captured. For scale, the profile in Figure 5.12 (c) is made of 200 data points.

5.3.2. Post-Shear Profiles

Once shearing has taken place the coupons were removed from the shear test setup, brushed lightly with a soft-bristled paint brush and re-profiled using the stylus profilometer. A number of observations can be made:

- No particles adhered to or were otherwise “stuck” in the HDPE surface. Some particles remained on the surface after turning the coupon upside down, but none remained after a very light brushing.
- The area where shearing had taken place on the surface was clearly visible. In some cases (larger normal stresses) tracks and grooves were clearly seen with the naked eye and in other cases (low normal stresses) there appeared to be a slight change in the way light reflected off the surface. It was thus easy to determine where to take the post-shear profiles.
- For these smooth HDPE surface there was a negligible number of particles that escaped out of the rear of the shear box during testing, if any. This can be a concern with rough surfaces but was not an influence in these tests.

- No small particles or flakes of HDPE were observed to be mixed in with the particles or laying on the surface of the coupon. This is a significant observation as it indicates that no third party particles are created as a result of the particles plowing into the surface. The surface material appears to thus be plowed into grooves, but not separated into smaller pieces. No smaller particles of HDPE thus have to be incorporated into modeling of the surface shearing process.

5.3.2.1. Post-Shearing Profiles: Uniform Sands

Figure 5.13, Figure 5.14 and Figure 5.15 show the post-shear surface profiles for smooth HDPE surfaces after having been sheared with uniform sands of mean particle size 0.78, 0.28 and 0.13mm respectively. Profiles are shown for each normal stress tested.

The vertical scale for each figure is the same to allow for comparisons between normal stresses to be made. In each figure the same pre-shear baseline plot has been used for comparison.

Figure 5.16 shows how the average roughness varies with applied normal stress and particle size for uniform sands.

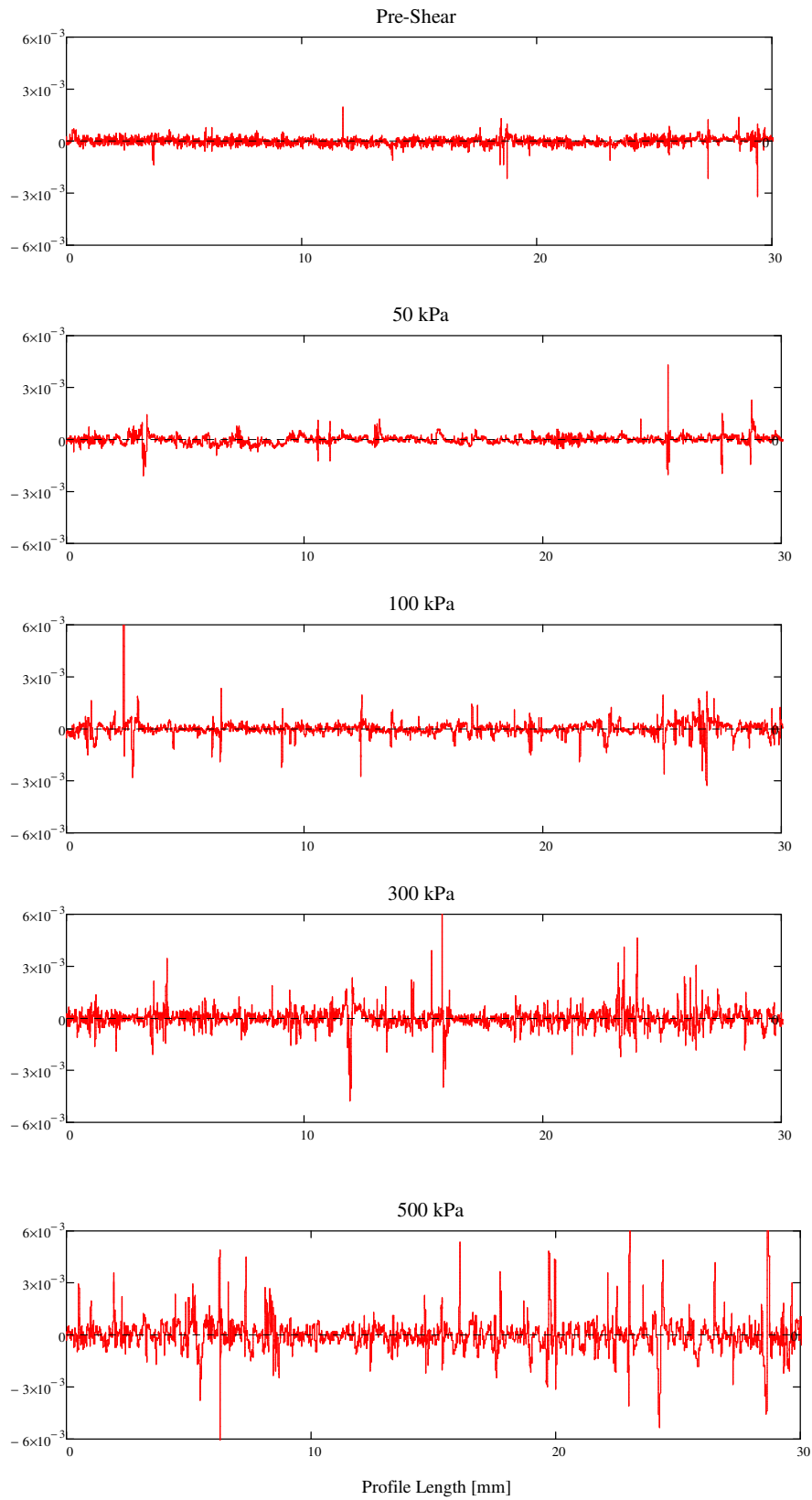


Figure 5.13 Post-Shear Surface Profiles for 20/25 Sand

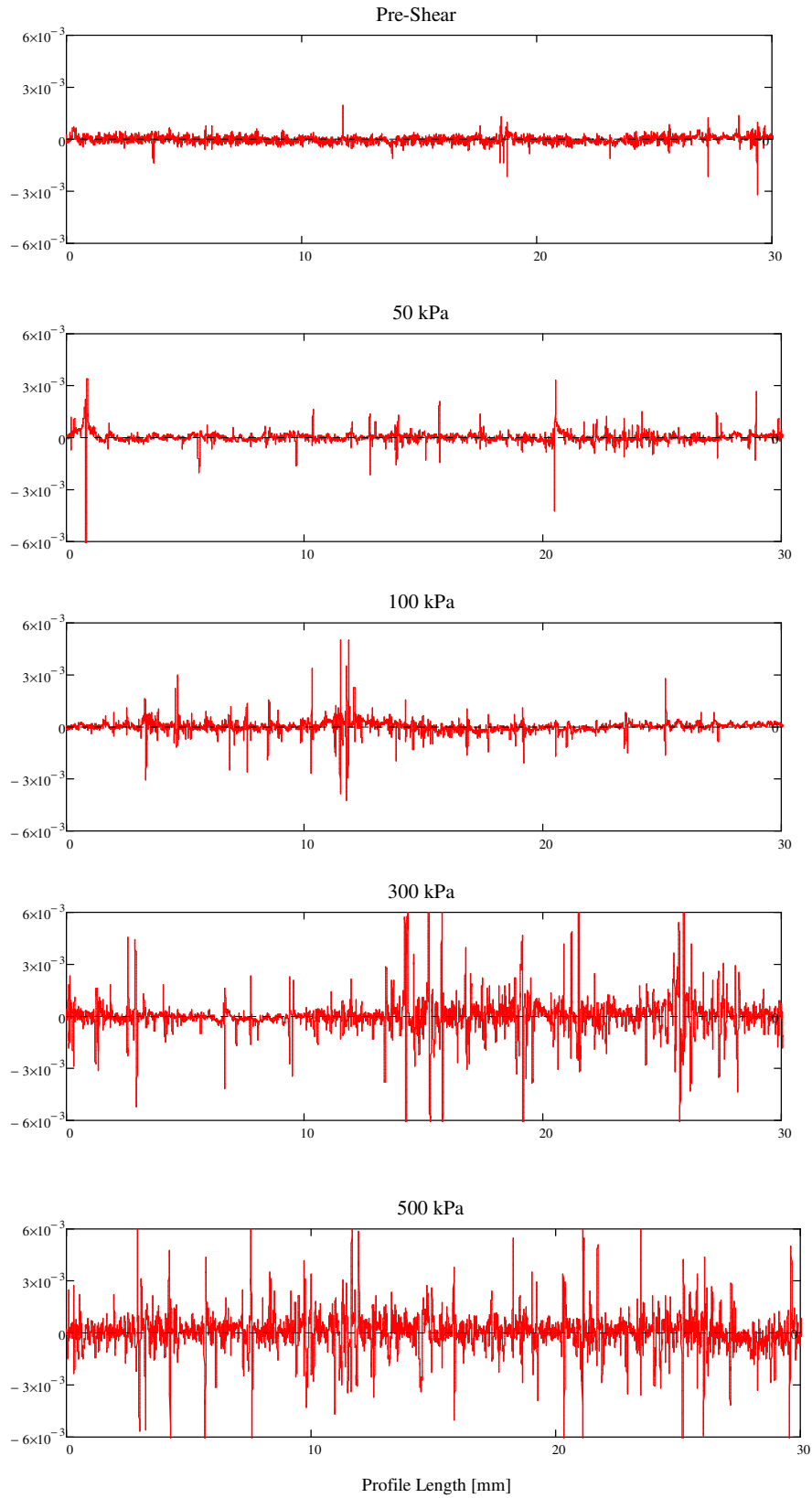


Figure 5.14 Post-Shear Surface Profiles for 50/60 Sand

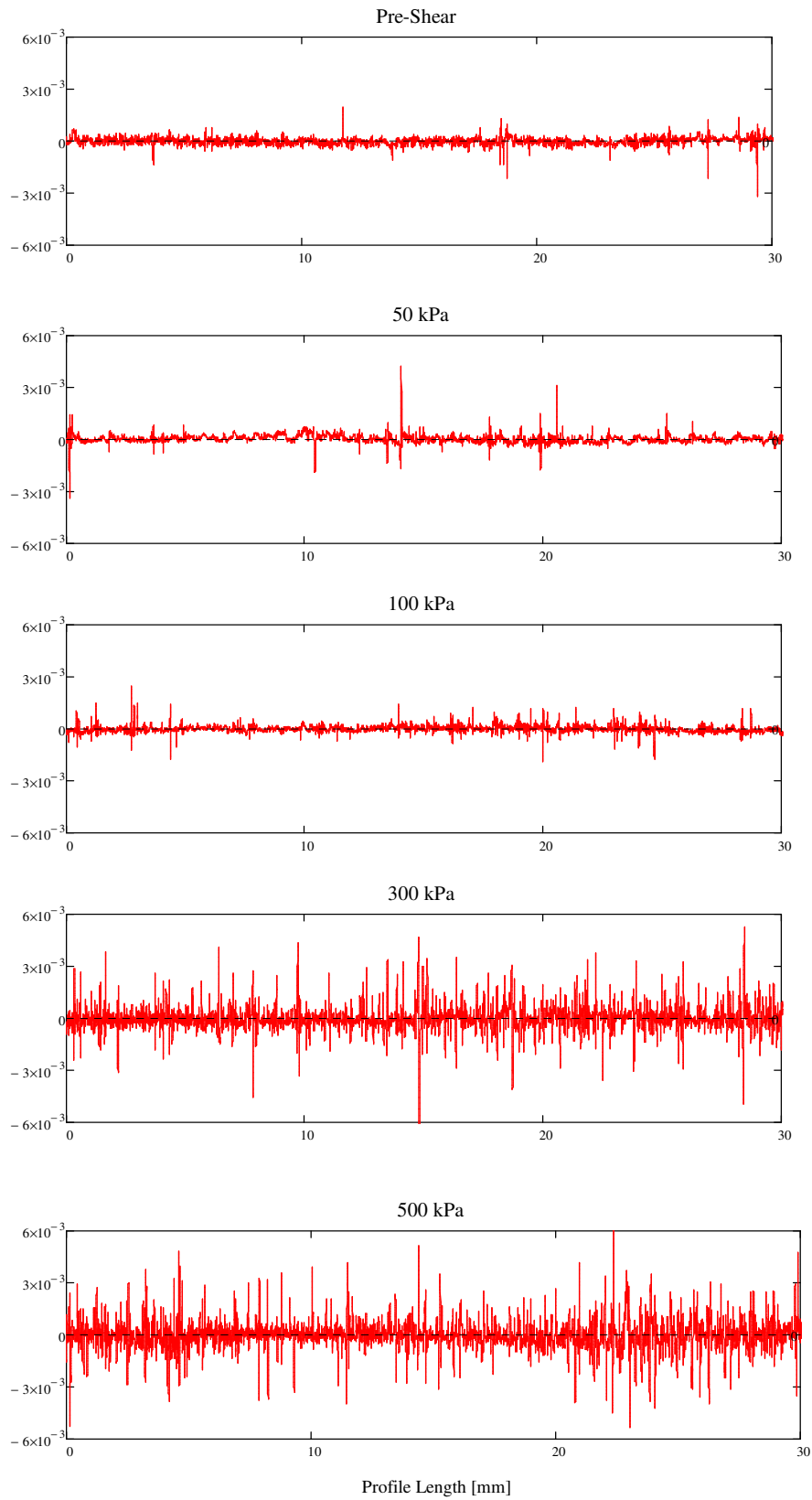


Figure 5.15 Post-Shear Surface Profiles for 100/140 Sand

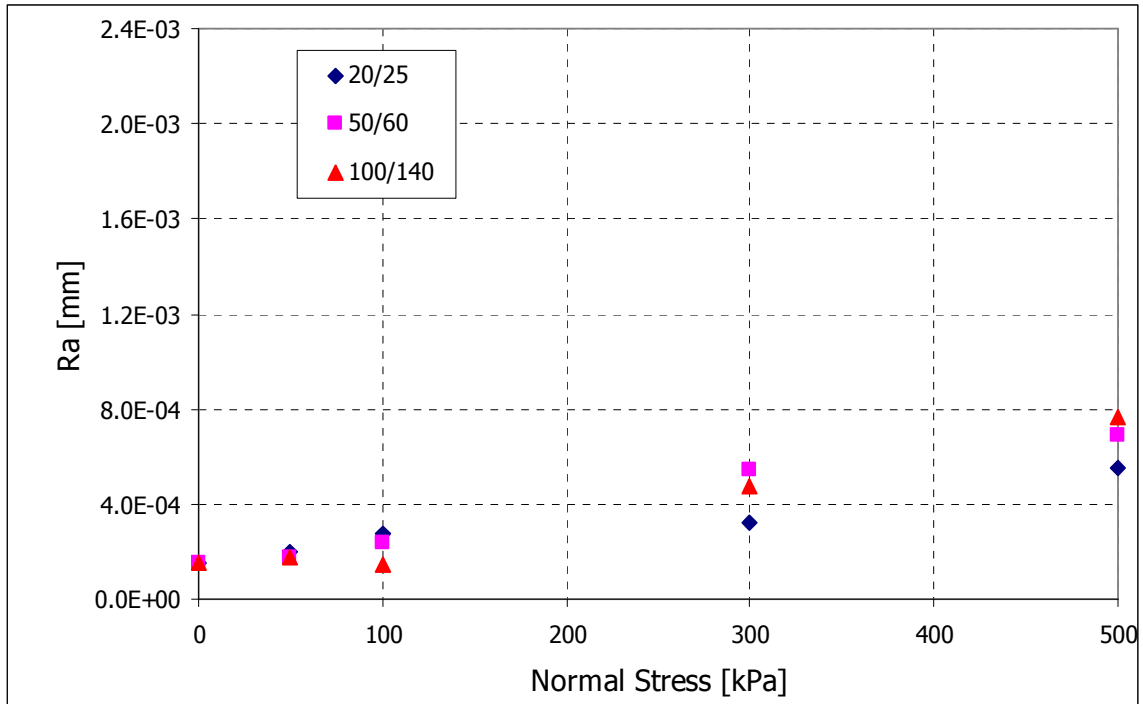


Figure 5.16 Average Roughness after Shearing for Uniform Sands

As can be seen in Figure 5.13, Figure 5.14 and Figure 5.15 there is a clear increase in induced surface roughness as normal stress increases. This is due to the contacting particles being subject to an increasing normal force which indents the particles further into the surface. Upon shearing, the particles carve out more pronounced grooves in the surface, which is reflected in the profiles.

Based on a visual assessment of the surface roughness for the largest uniform sand (Figure 5.13) it is seen that there is a seemingly consistent increase in roughness with normal stress. For the smaller particles, and in particular for the smallest of the three particles tested, the increase in surface roughness is accelerated at a normal stress of 300 kPa and larger. This is especially noticeable in Figure 5.15 where there is a very large change in surface roughness from 100 kPa to 300 kPa. Figure 5.16 shows how, for uniform particles, the average roughness of the surface profiles increases as the normal

stress increases. There is an insignificant change in roughness from the pre-shear state to a normal stress of 50 kPa. The roughness is observed to increase when the normal stress reaches 100 kPa, with the increase sustained throughout the range of normal stress tested. The increase in induced roughness is observed to increase approximately linearly with normal stress up to 500 kPa.

Figure 5.16 shows that the average roughness induced due to shearing of uniform particles reaches a maximum value of approximately 7.5×10^{-4} mm. This is approximately 5 times greater than the average roughness of the virgin material. The increase in average roughness is linearly proportional to the applied normal stress over the range of stress level and material properties tested.

The variation between the three different sized sands is not as great as the effect of the applied normal stress. The difference between the particles may also be attributed to the particle shape since the largest particles are the most rounded while the smallest of the particles are the least rounded. The results for uniform sands suggest that particle shape is a more useful predictor of induced roughness than absolute particle size.

It is also noted that the smallest particle induces the greatest roughness change and the largest particle the smallest amount of roughness change. This likely reflects the different number of particles present at the interface. The increased number of smaller particles increase the average deviation from the mean line of the profile, resulting in an increasing Ra value. To gain further insight into the profile, the dominant wavelength (as found by Fourier analysis of the profile), is presented in Figure 5.17 below plotted as a function of the applied normal stress.

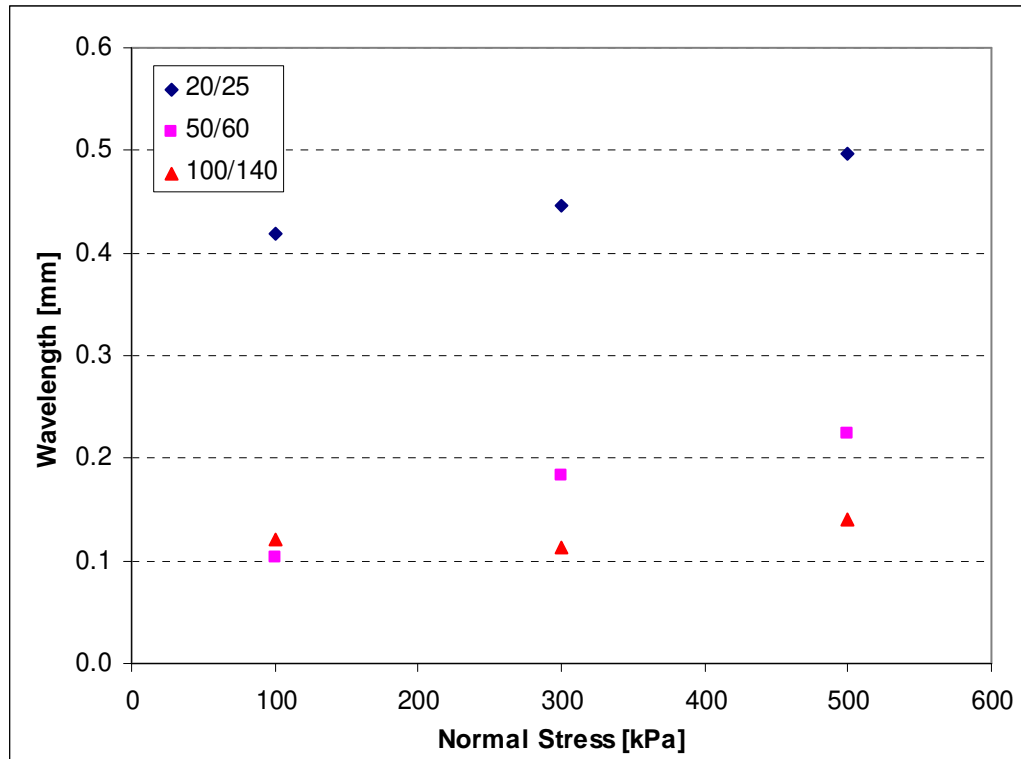


Figure 5.17 Dominant wavelength in surface profile (post-shear, uniform sands)

It can be seen in the above figure how the dominant wavelength is directly influenced by the particle size. The other primary observation is that the dominant wavelength increases as the normal stress increases. The 20/25 sand ($D_{50} = 0.78\text{mm}$) shows a dominant wavelength of 0.42 at 100 kPa and that increases to 0.50 at 500 kPa. The 50/60 sand ($D_{50} = 0.28\text{mm}$) shows an increase from 0.10 to 0.22 over the same normal stress range and the 100/140 sand ($D_{50} = 0.13\text{mm}$) shows a very slight increase from 0.12 to 0.14.

The shorter wavelength of the profiles created by shearing against the smaller particles is clearly a result of the smaller particle size. The increased Ra for the smaller particles is thus a reflection of the increased number of particles in contact with the surface.

The increase with normal stress is a result of the particles becoming further embedded into the surface at higher normal stresses. This increases the contact radius (amount of particle in contact with the surface) which in turn is reflected in an increase in the dominant wavelength.

5.3.2.2. Post-Shearing Profiles: Particle Mixtures

The surface profile changes as a result of shearing against binary particle mixtures will now be presented. Figure 5.18, Figure 5.19 and Figure 5.20 below show how the surface profiles obtained after shearing at 500 kPa change as a function of the mixture proportions. Mixtures with 20%, 40% and 70% of finer particles were tested. The other normal stress values were also tested but only the profiles for 500 kPa will be presented. The complete set of roughness data is subsequently presented in summary format.

Figure 5.21, Figure 5.22 and Figure 5.23 show how the average roughness varies with applied normal stress for the three different particle size ratio cases for the different mixture proportions tested.

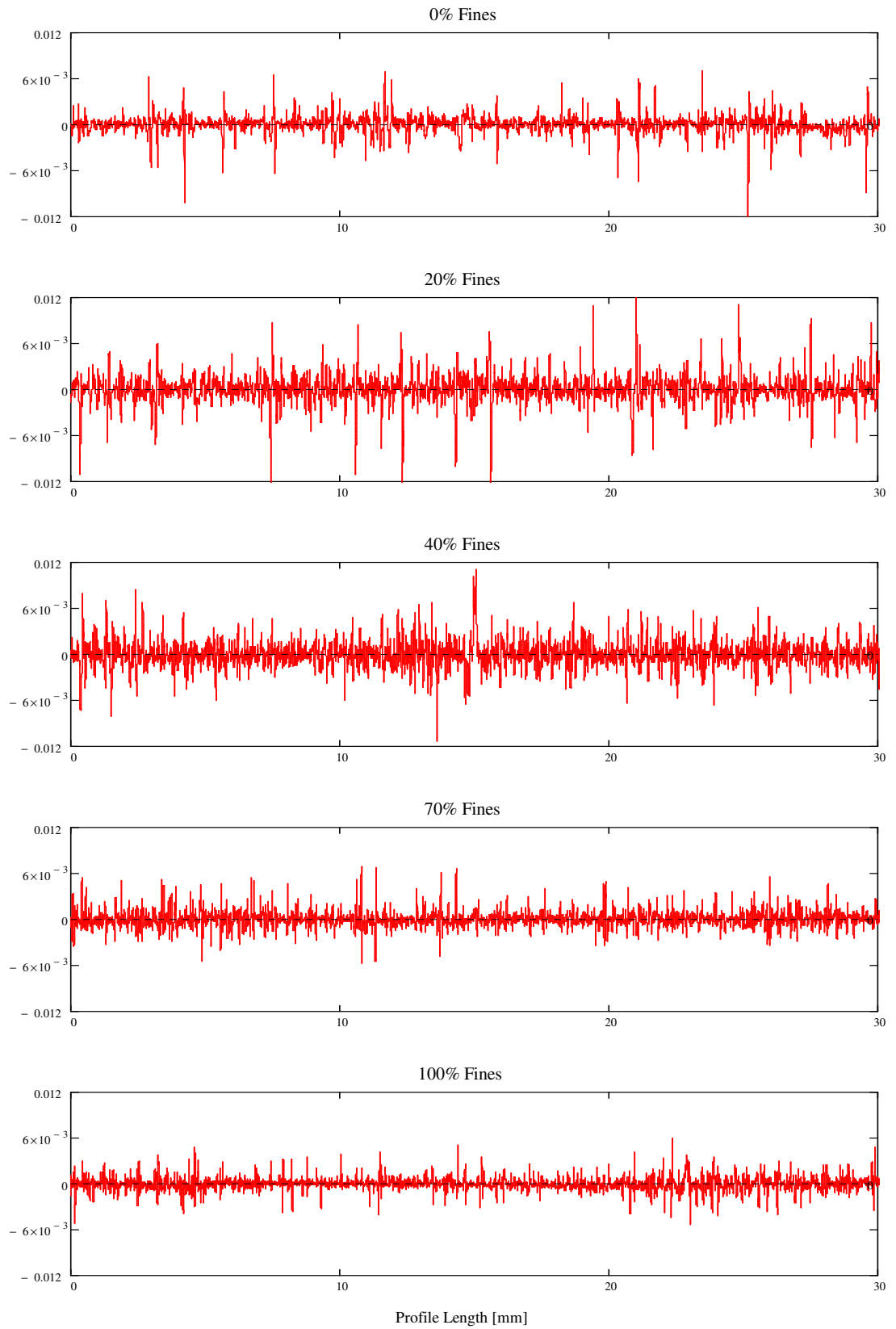


Figure 5.18 Post-Shear Surface Profiles for P.S.R. 2.1 at 500kPa

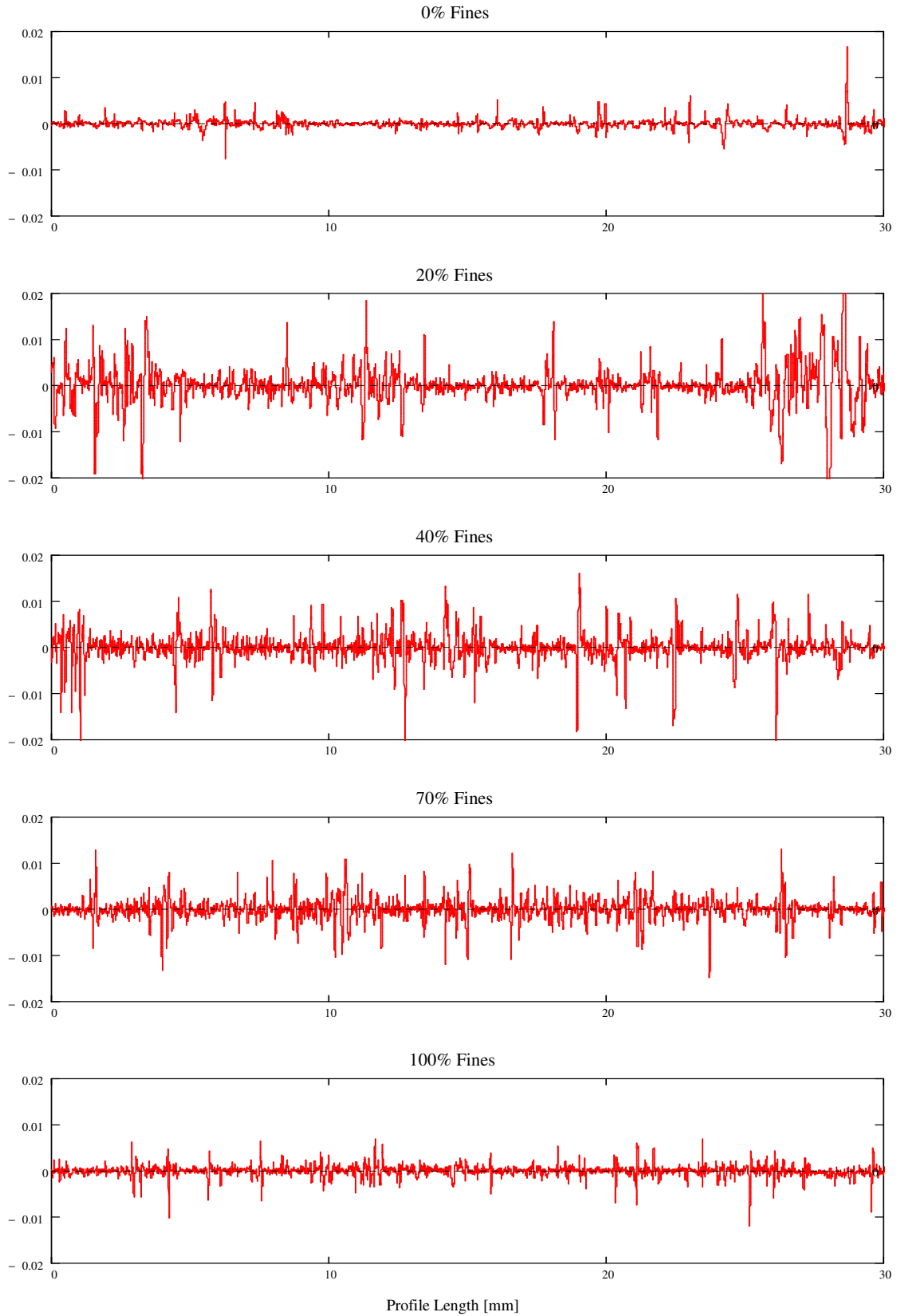


Figure 5.19 Post-Shear Surface Profiles for P.S.R. 2.8 at 500kPa

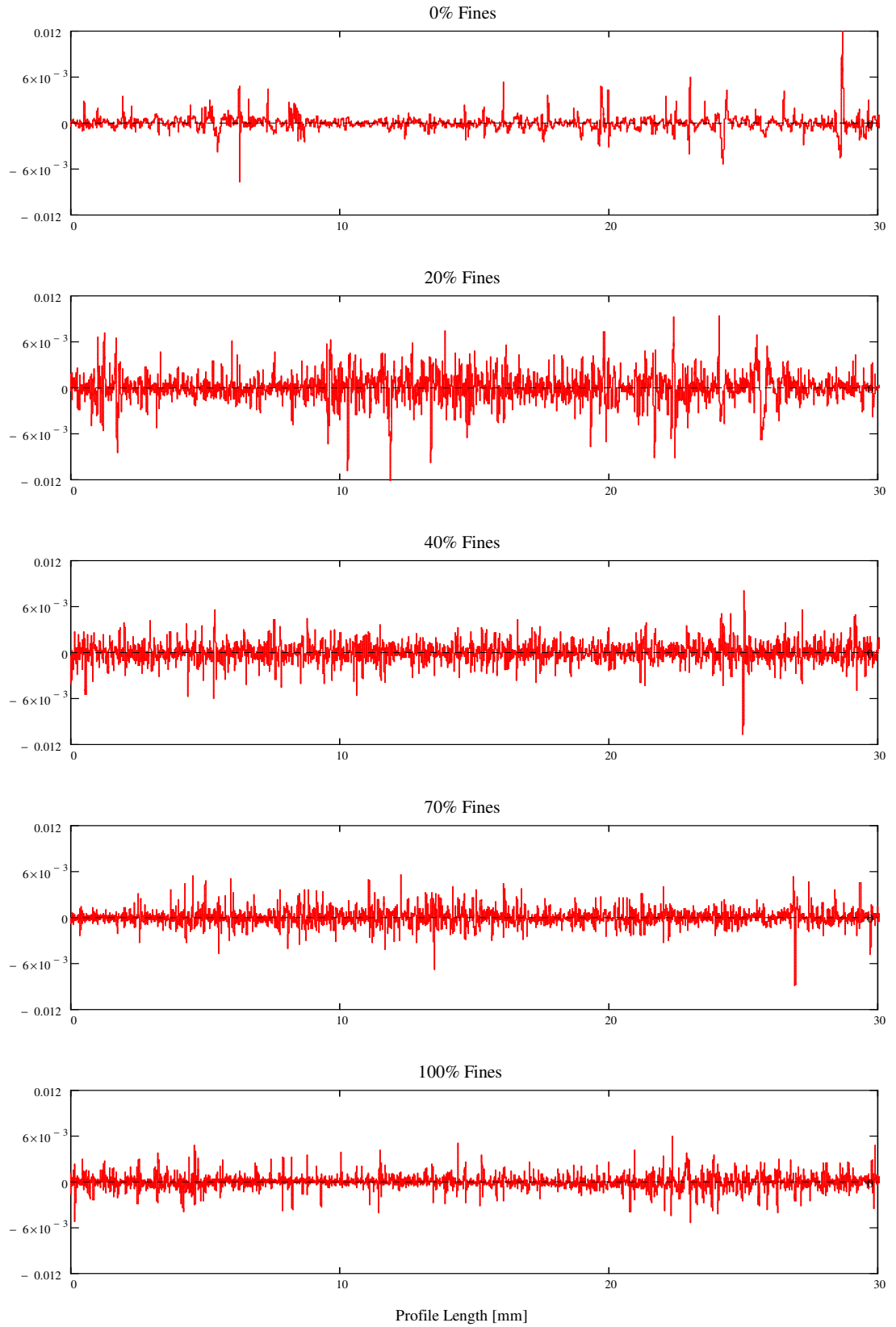


Figure 5.20 Post-Shear Surface Profiles for P.S.R. 6.1 at 500kPa

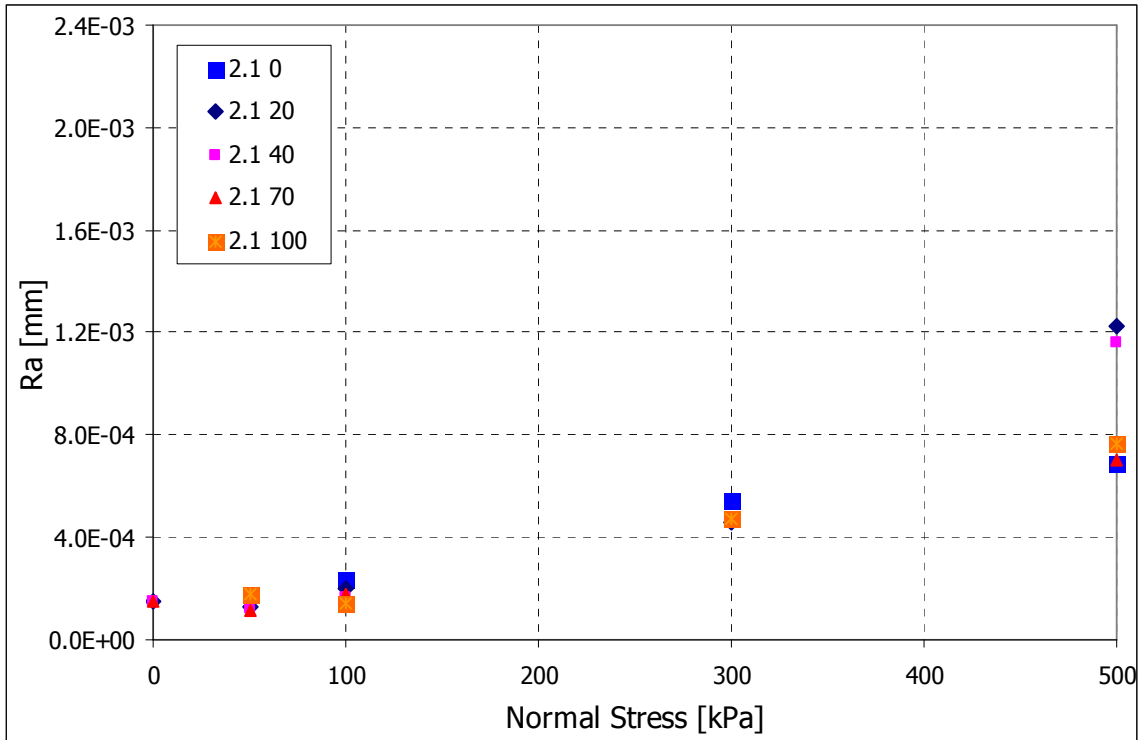


Figure 5.21 Average Roughness after Shearing for P.S.R. 2.1 Mixture

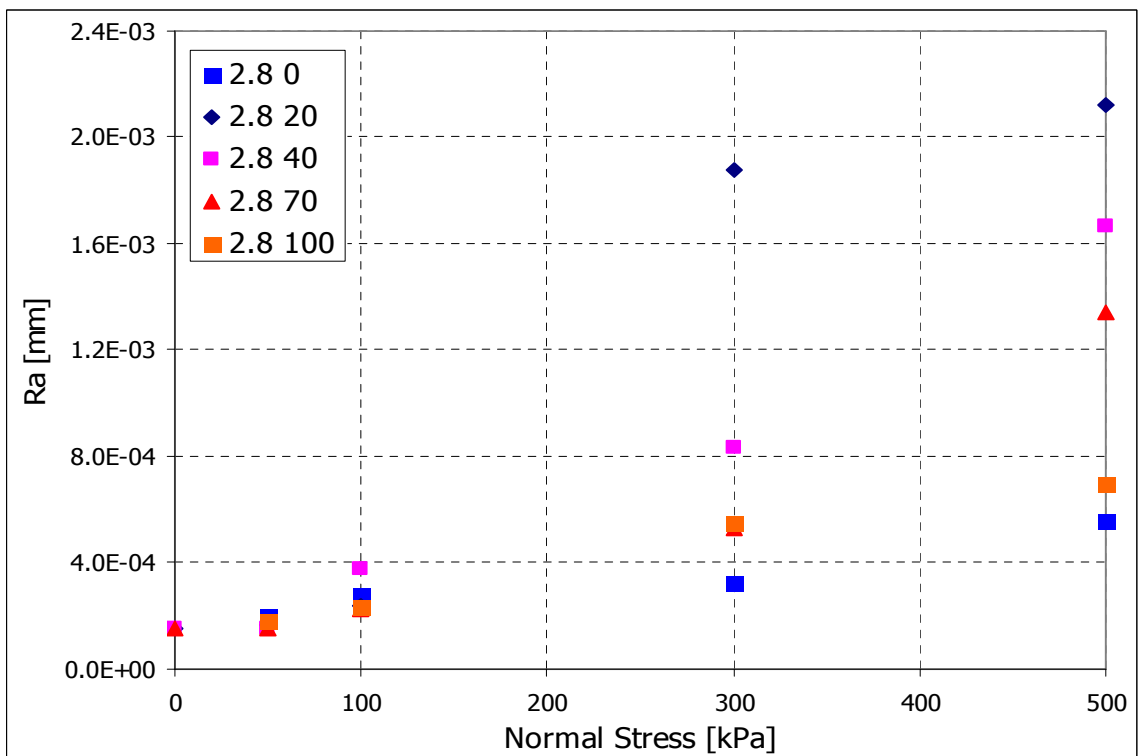


Figure 5.22 Average Roughness after Shearing for P.S.R. 2.8 Mixture

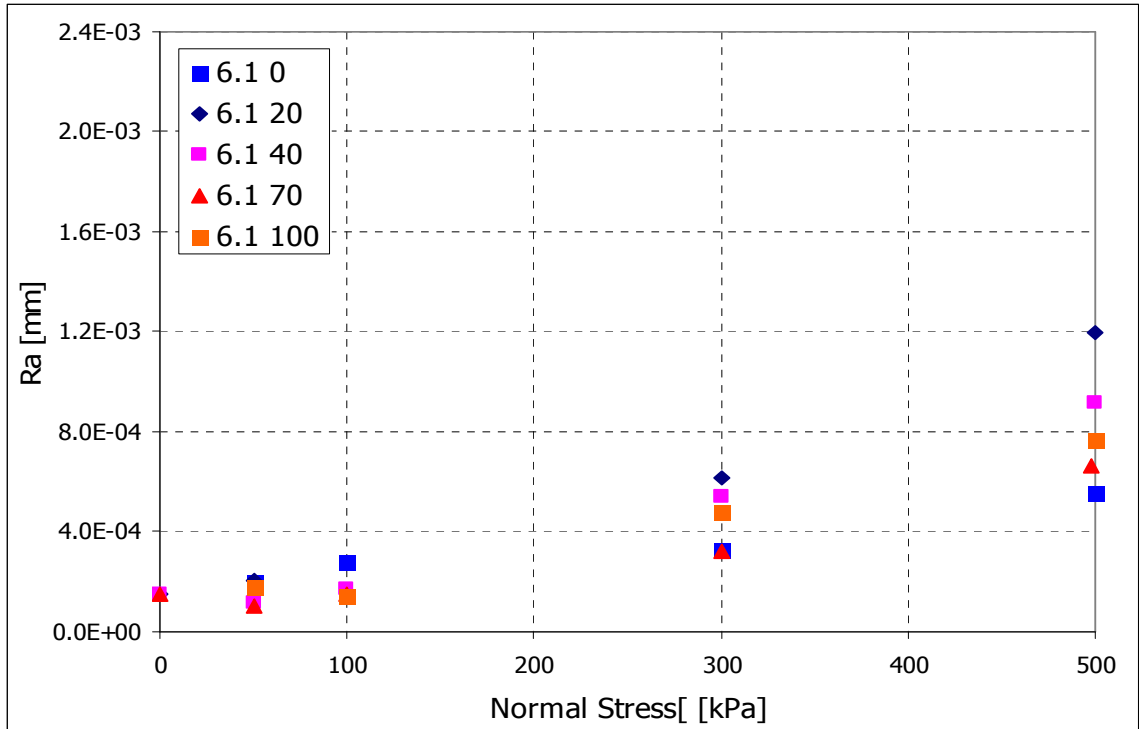


Figure 5.23 Average Roughness after Shearing for P.S.R. 6.1 Mixture

In Figure 5.18, for a P.S.R. of 2.1, it is clear that the surface is most affected by shearing when the mixture contains 20% and 40% finer particles. At a mixture ratio of 70% finer particles the induced roughness is marginally more than that at 100% finer material, but significantly less than that at 40% finer material.

Figure 5.19 shows the surface profiles for the P.S.R. of 2.8. This is the mixture with the two largest particle sizes mixed together. Comparing the 0% and 100% finer particle cases it is interesting to note that the 100% case shows a greater degree of surface texture than for the 0% case. The surface texture in both of these cases is, however, visually less pronounced than the other three cases. In contrast to the P.S.R. 2.1 case, the roughness for the 70% mixture for P.S.R. 2.8 is noticeably greater than the uniform cases for a P.S.R. of 2.8. It must be noted that the absolute level of texturing induced by the P.S.R. 2.8 mixture is the greatest out of all those tested. This is despite that fact that the

two component particles making up the P.S.R. 2.8 mixture are the most rounded of the three components tested.

The final figure in this series, Figure 5.20, shows the case of a mixture with a P.S.R. of 6.1. The behavior is generally very similar to the P.S.R. 2.8 case, with the 20% mixture showing the greatest amount of texturing, followed by the 40% mixture. In this case, however, the 70% mixture shows less induced texturing than the 100% case, which had not been observed in any of the other mixtures.

Figure 5.21, Figure 5.22 and Figure 5.23 all show a similar trend of increasing roughness with an increase in the normal stress. For the binary mixture however there is a clear size effect: the mixture comprised of the largest absolute particle sizes exhibits the largest increase in roughness. This is most apparent for the 20% and 40% mixtures.

For the P.S.R. 2.8 case the 0% mixture shows an induced roughness of approximately 4 times the virgin roughness when sheared at 500 kPa. When just 20% of the finer material is added the induced roughness increases by a further 3.5 times, to approximately 14 times greater than the virgin roughness. This is a very substantial increase in induced roughness for a relatively small change in the particle size distribution. The other mixtures (P.S.R. 2.1 and 6.1) do not show such dramatic increases, but in all cases the 20% mixture shows the greatest capacity to induce roughness at all stress levels.

5.4. Contact Mechanics and Friction

In typical geotechnical scenarios, both in the field and in the laboratory, the boundary forces and the global properties of the materials are known. The mechanics of what is happening right at the contact interface between the soil particles and the surface

is however not usually observed or measured directly due to the difficulty in making such measurements.

It is possible, however, to relate measurements made at the boundaries (macro-scale, on the order of centimeters or larger) to the behavior at the interface (micro-scale, on the order of microns) by using analytical models. In this section a brief review of fundamental aspects of friction and contact mechanics will be presented, followed by the development of a model to predict the friction coefficient for sliding between a binary particle mixture and a smooth surface. In this study only dry surface friction will be considered. Friction with hydrodynamic lubrication, where a lubricating fluid prevents direct contact between the solid surfaces, will not be considered.

5.4.1. Single Particle Contact Behavior (Hertzian Contact)

Hertz provided the first satisfactory analysis of contact stresses between two elastic solids in 1882 (Johnson, 1985). Consider two smooth spheres brought into contact under an external force, the radius of the area of contact, a , is given in terms of the applied load and material properties as:

$$a^3 = \frac{3}{4}(k_1 + k_2)RW$$

where

$$k_1 = \frac{1-\nu_1^2}{E_1}$$

$$k_2 = \frac{1-\nu_2^2}{E_2}$$

$$\frac{1}{R} = \frac{1}{R_1} + \frac{1}{R_2}$$

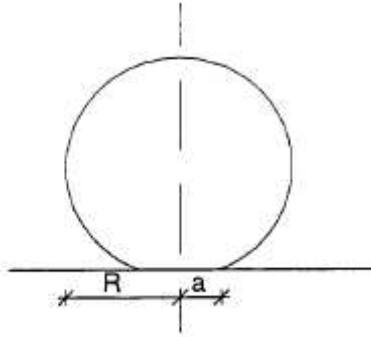


Figure 5.24 Illustration of particle radius, R , and contact radius, a

The external applied force is W , ν and E are the Poisson ratio and Young's modulus respectively where the subscripts denote the different surfaces in contact. R is the effective radius of curvature. This theory is valid under a number of assumptions:

- The surfaces are continuous and non-conforming
- The strains are small
- Each solid can be described as an elastic half-space

For elastic contact between a single particle and a smooth flat surface, the value of R_2 can be taken as infinite, hence R will be equal to R_1 , the radius of the contacting particle. The area of contact per particle, δA_c , can be expressed as:

$$\delta A_c = \pi(D^* R \delta W)^{\frac{2}{3}}$$

where

$$D^* = \frac{3}{4} \left(\frac{1-\nu_1^2}{E_1} + \frac{1-\nu_2^2}{E_2} \right)$$

δW = Normal force per particle

The variation of contact area with normal force can thus be expressed in a more general form as:

$$\delta A_c = k \delta W^{\frac{2}{3}}$$

where

$$k = \pi(D^* R)^{\frac{2}{3}}$$

This indicates that the contact area for a single point elastic contact is proportional to the $2/3$ power of the normal force. However, multi-asperity and plastic conditions can also occur, both of which will result in the contact area being directly proportional to the normal force. Multi-asperity contact is an elastic process that results in an increasing number of contacts between contacting surfaces as the normal force is increased. A more generalized relationship is given by Archard (1957) as:

$$\delta A_c = k \delta W^n$$

Where k is the friction factor and n is the load index. The friction factor contains information about the material properties and size of the particle while the load index describes contact conditions, which could be elastic ($n=2/3$), fully plastic or multi-asperity ($n=1$) or some value in between these limits. A load index of $2/3$ implies a decreasing friction coefficient with increasing normal load since the contact area increases at a slower rate than the normal force. A load index of 1 implies a constant friction coefficient.

Ludema (1996) reports that polymeric materials, such as the one used in this study, typically show elastic behavior. Dove (1996) shows that for HDPE geomembranes in contact with Ottawa 20/30 sand, the assumption of single point contact (as opposed to multi-asperity contact) is appropriate at the scale of measurement and observation employed.

For the remainder of this study it will be assumed that single point elastic conditions occur at the contacts between particles and surfaces. While this is known to be an approximation of the real contact conditions, these assumptions have a basis in observations made by tribological researchers and will allow for the development of a model to predict the coefficient of friction for a binary mixture in contact with an HDPE surface.

The frictional force, F , acting to retard relative lateral displacement between a particle and its contacting surface is governed by two main components. The first component is an adhesion component and the second is a plowing component. This is illustrated in Figure 5.25.

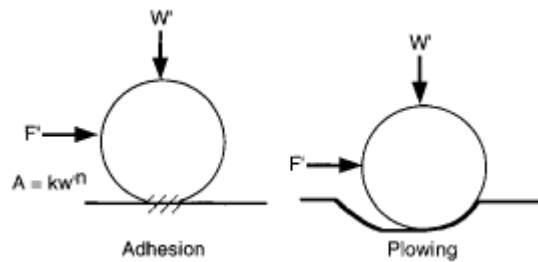


Figure 5.25 Components of Friction: Adhesion and Plowing (Dove, 1999)

The total frictional resistance can thus be written as a sum of these two components:

$$F = F_{adhesion} + F_{plowing}$$

Each of these two components will be examined separately in the following sections.

5.4.1.1. Adhesion Component of Friction

The adhesion component arises as a result of a microscale process occurring at the junctions formed by pressing two surfaces together into contact at localized points. The

shear resistance offered by these junctions, which have become “bonded” together provides the resistance to shearing which is manifest as adhesion. There is some debate as to whether this is actually the true mechanism or not, but for the purposes of this study the exact mechanism of adhesion is not important as it occurs on a scale smaller than the scales used in this investigation.

The model that will be used in this study to describe the adhesion component is presented by Briscoe and Tabor (1978) and is expressed as:

$$\delta F_{adhesion} = \tau_0 \delta A_c + \alpha \delta W$$

Where τ_0 is the intrinsic interfacial shear strength and α is the normal pressure coefficient. These are material properties that can be derived from experimental data. This relationship can also be expressed as a coefficient of friction as:

$$\mu_{adhesion} = \frac{\tau_0}{\delta \sigma_c} + \alpha$$

Where $\delta \sigma_c$ is the normal stress acting across the contact area. At high levels of normal force (higher levels of contact stress) the friction coefficient tends to the value of α .

This can be rewritten as;

$$\mu_{adhesion} = \tau_0 \pi \left[\frac{D^{*2} R^2}{\delta W} \right]^{\frac{1}{3}} + \alpha$$

by using the prior relationship between contact area and normal force. This expression relates the friction coefficient due to adhesion to measurable properties of the surface and the particle. The friction coefficient is made up of two parts, one part is

dependant on the material properties, particle size and applied normal force while the other, α , is a constant term regardless of what other parameters change.

The normal pressure coefficient can be found by calculating the slope of a plot of the frictional force, F , against W , the normal load. Dove (1999) presents data from single particle interface friction tests that can be used to determine α . These tests sheared a single steel particle, that was prevented from rotating, across an HDPE geomembrane. Both smooth and roughened spheres were used to investigate a possible range of values. It was also shown through back-analysis that the real particles exhibited behavior that was essentially an average of the rough and smooth particles. A similar approach is adopted here in that the estimate for α for real particles will be an average of the α values for roughened and smooth particles. Figure 5.26 shows the calculation of α .

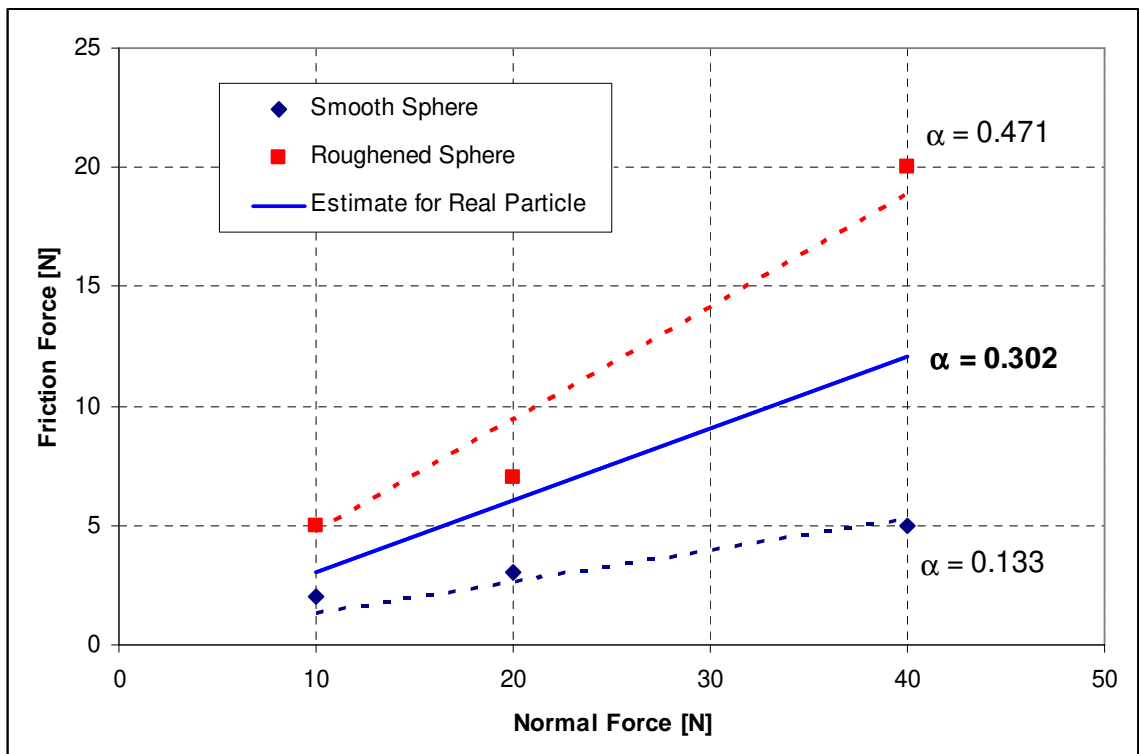


Figure 5.26 Calculation of pressure coefficient, α

In order to determine the value of τ_0 , a plot of interface shear stress against the normal force to power 1/3 is used. The intercept of the best-fit line and the vertical axis yields the value of τ_0 as shown in Figure 5.27 below.

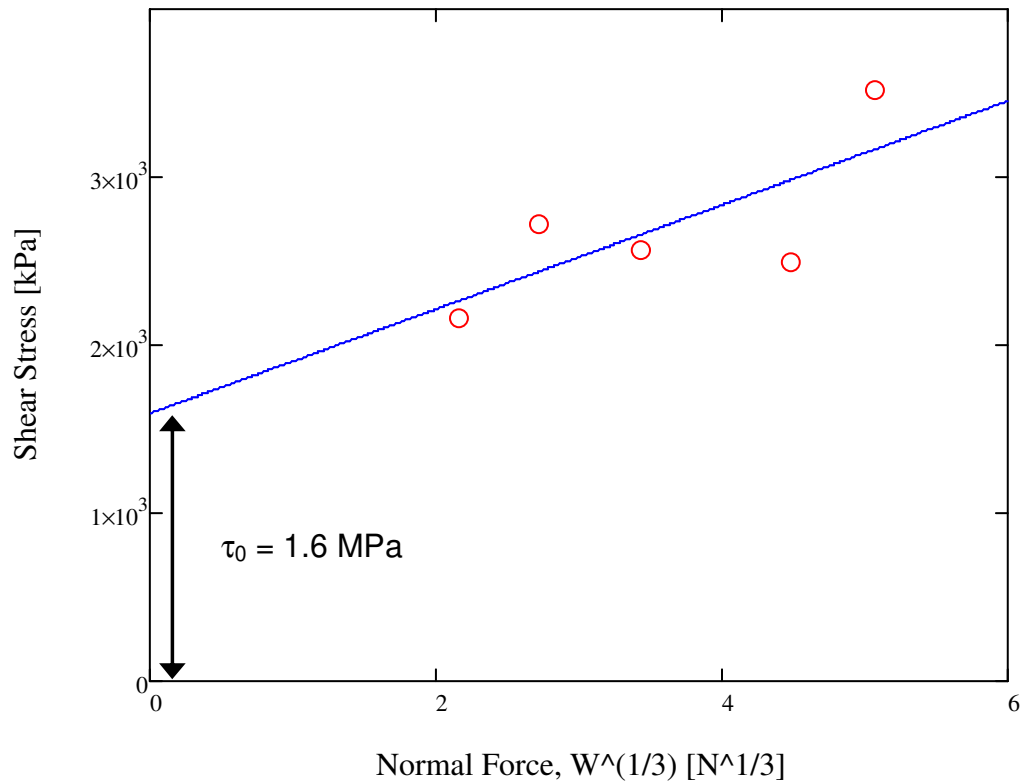


Figure 5.27 Calculation of τ_0

These values of α and τ_0 will be used in the remainder of this study. These values compare suitably to the values obtained by Abou-Chakra (1998) for glass ballotini in contact with a Perspex surface ($\alpha = 0.18$ and $\tau_0 = 4$ MPa).

5.4.1.2. *Plowing Component of Friction*

The plowing component of friction is significant when a hard particle slides across a relatively soft surface. This results in grooves or tracks being formed in the surface which is a permanent deformation. Shooter and Tabor (1952) showed that

plowing results in a higher friction coefficient than adhesion acting by itself. Estimates of the friction coefficient due to the plowing component have been made, with those estimates by Czichos (1985), Sin et al. (1979) and Bhushan (1999) presented below and illustrated (for the first two references) in Figure 5.28.

$$\mu_{plowing} = \frac{2}{\pi} \tan(\theta) \quad (\text{Czichos, 1985})$$

$$\mu_{plowing} = \frac{2}{\pi} \left\{ \left(\frac{2r}{w} \right)^2 \sin^{-1} \left(\frac{w}{2r} \right) - \left[\left(\frac{2r}{w} \right)^2 - 1 \right]^{\frac{1}{2}} \right\} \quad (\text{Sin et al., 1979})$$

$$\mu_{plowing} = \frac{4}{3\pi} \left(\frac{r_{contact}}{R_{particle}} \right) \quad (\text{Bhushan, 1999})$$

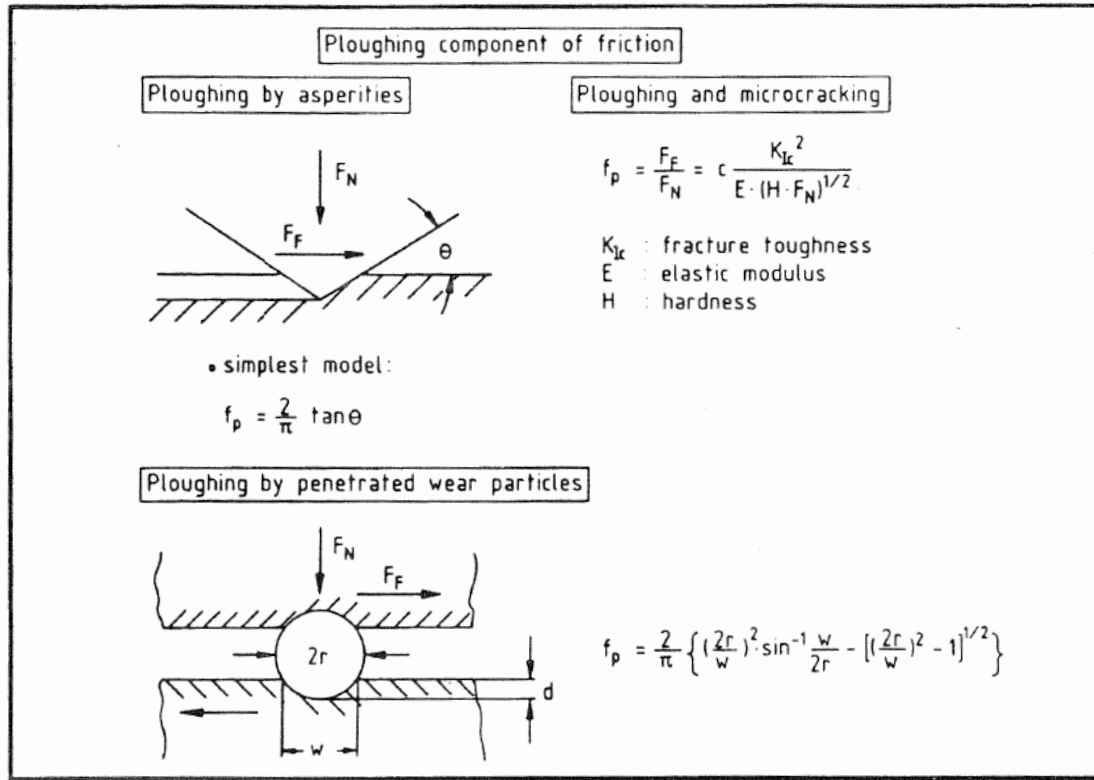


Figure 5.28 Plowing Component of Friction

The method proposed by Czichos (1985) results in a constant value for the friction coefficient. Based on an approximate shape analysis of the 20/25 sands used in this study (see elsewhere in Chapter 5) the angle, θ , is approximately 4 to 5 degrees. This results in a friction coefficient due to plowing of approximately 0.045 to 0.056. These values are considered to be a lower bound as the method does not take into account the presence of material that is mounded up in front of the particle due to plowing. This may have a significant effect on the friction coefficient as the particle will have to plow through a cross-sectional area of material.

The methods proposed by Sin et al (1979) and Bhushan (1999) are operationally very similar over the range of stresses and particle sizes tested. The Bhushan (1999) relationship was chosen as it is simpler to implement. An important feature of both of

these relationships is the inclusion of a ratio between the particle size and size of the contact area. Since the contact area varies with load according to equations previously presented, a new relationship could be developed that explicitly included the normal stress. The relationship between particle size, applied normal force and friction coefficient is presented below and shown in Figure 5.29 (using Bhushan, 1999).

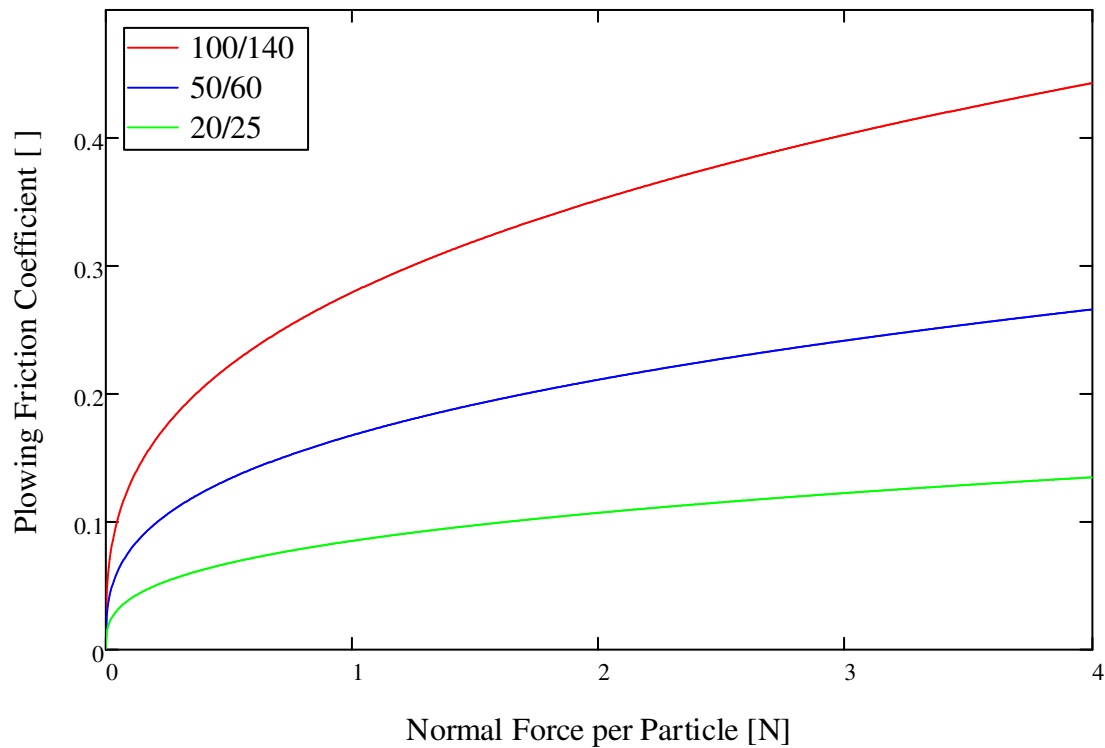


Figure 5.29 Friction Coefficient due to Plowing

Figure 5.29 shows that for a given normal force the smaller the particle the greater the contribution to shearing resistance due to plowing effects. As normal force increases it is clear that the effect reduces as the normal force increases. The maximum gain in sliding resistance occurs at very low normal forces, when one might typically not expect to see any effect of plowing at all.

Figure 5.30 also shows the plowing component of the overall friction coefficient and how it varies as a function of the Young's modulus of the surface material. As expected, the plowing component increases as the material becomes softer. The modulus of the particle has a much lesser effect as it is a much larger number.

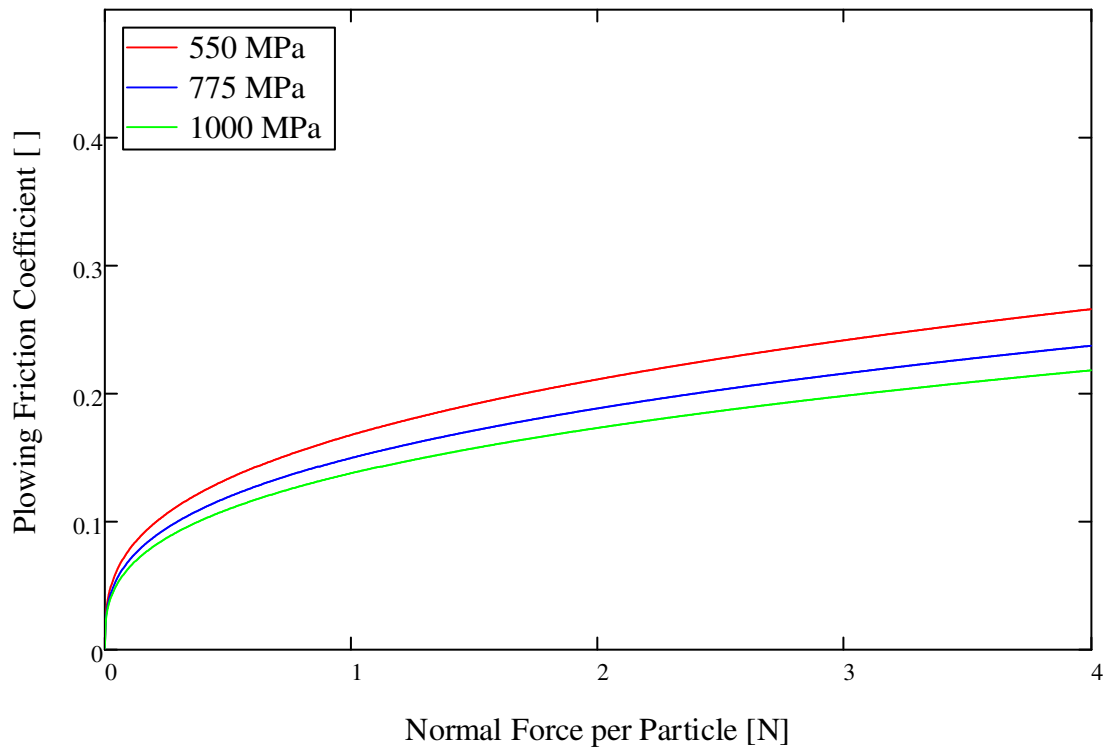


Figure 5.30 Friction Coefficient due to Plowing

It is also important to note that the aforementioned models do not consider the rotation of particles. The particles are assumed to remain in an essentially locked mode as they traverse across the surface. In an actual physical experiment or field setting it is very unlikely that such conditions would occur, so it is important to address how much of an affect this simplification may have.

Based on observations of the tracks left in the geomembrane surface after shearing, it appears unlikely that significant particle rotations are occurring at the

interface. Pit or pock marks are not seen, which would have indicated particles rolling and the edges of particles creating repeatable indentations or marks in the soft geomembrane. Even at low normal stresses the only marks on the geomembrane are micro-striations, evidence of particle sliding.

5.4.2. Multiple Uniform Particles in Contact

The relationships developed in the previous section all dealt with individual particles. This will now be extended to the case of a bed of uniform particles in contact with a surface. It will be assumed that all of the particles are of the same size and that each particle is subject to an equal normal force. This is equivalent to assuming a uniform stress distribution across the bed of particles.

The load per particle, δW , can be calculated based on the number of particles in contact with the surface. This depends on both the particle size and how the particles are packed together. Since it has been assumed that all the particles are of the same size and are spherical the problem can be treated as packing circles in two dimensions.

The packing limit states for stable arrangements are known. The loosest stable arrangement is the square packing arrangement and the densest arrangement is the hexagonal packing arrangement. These two arrangements are shown below in Figure 5.31 along with their corresponding porosity values.

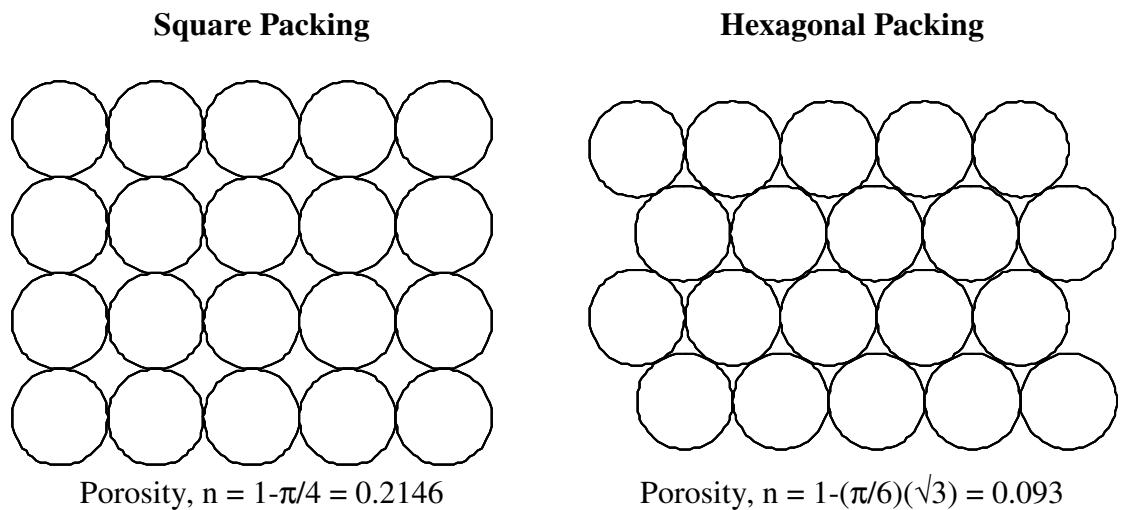


Figure 5.31 Limiting Stable Packing Arrangements

The load per particle, δW , can be expressed as:

$$\delta W = \frac{\sigma_n A_{total}}{no. particles} = \frac{\sigma_n A_{total} \pi r^2}{A_{solids}} = \frac{\sigma_n \pi r^2}{(1-n)}$$

Introduce the variable β , such that:

$$\beta = \frac{4(1-n)}{\pi}$$

And so:

$$\delta W = \frac{\sigma_n \pi r^2}{(1-n)} = \frac{\sigma_n d^2}{\beta} \quad \text{where } d = \text{particle diameter}$$

$$\text{For a square packing (loosest possible):} \quad n = 1 - \frac{\pi}{4} \quad \beta = 1$$

$$\text{For a hexagonal packing (densest possible):} \quad n = 1 - \frac{\pi}{6} \sqrt{3} \quad \beta = \frac{2}{\sqrt{3}}$$

By varying the β parameter between these two values, the entire range of possible stable arrangements will be included. The load per particle can now be incorporated into previous expressions where the term δW is present.

5.4.2.1. Adhesion Component of Friction for Multiple Uniform Particles

Recall that for a single particle:

$$\delta F_{adhesion} = \tau_0 \delta A_c + \alpha \delta W$$

Since

$$\delta A_c = \pi (D^* R \delta W)^{\frac{2}{3}}$$

This gives rise to

$$\delta F_{adhesion} = \tau_0 \pi (D^* R)^{\frac{2}{3}} (\delta W)^{\frac{2}{3}} + \alpha \delta W$$

We can now modify this expression for a single particle to be valid for multiple particles by multiplying by the number of particles. Where N is the number of particles in contact with the surface and F and W are the total shear and normal forces respectively:

$$F = (N)(\delta F)$$

$$W = (N)(\delta W)$$

We can thus express:

$$F_{adhesion} = \tau_0 \pi (D^* R)^{\frac{2}{3}} N (\delta W)^{\frac{2}{3}} + \alpha W$$

Expressing the friction coefficient by dividing by W :

$$\mu_{adhesion} = \tau_0 \pi (D^* R)^{\frac{2}{3}} \left(\frac{N}{W}\right)^{\frac{1}{3}} + \alpha$$

The projected area of all particles can be written as $A_p = N\pi R^2$ and the total normal force, $W = A_t \sigma_n$. Hence we can write:

$$\mu_{adhesion} = \tau_0 (\pi D^*)^{\frac{2}{3}} \left(\frac{A_p}{A_t}\right)^{\frac{1}{3}} \left(\frac{1}{\sigma_n}\right)^{\frac{1}{3}} + \alpha$$

This is a general expression that allows for the coefficient of friction to be calculated for a monosized assembly of particles subject to a compressive normal stress.

Since $(A_p/A_t) = (1-n) = (\beta\pi/4)$ one could also write it as:

$$\mu_{adhesion} = \tau_0 \pi (D^*)^{\frac{2}{3}} \left(\frac{\beta}{4\sigma_n}\right)^{\frac{1}{3}} + \alpha$$

It is interesting to note that this expression is independent of the particle size, fairly weakly dependent on the normal stress and packing geometry, and somewhat dependant on the elastic material properties and intrinsic shear strength. The parameter

that has the largest influence is the pressure coefficient, α . It is clear that as the applied normal stress increases the value of μ_{adhesion} tends to a value of α .

A similar development for the plowing component of friction will now be presented, followed by an investigation of the predictive utility of these expressions.

5.4.2.2. *Plowing Component of Friction for Multiple Uniform Particles*

Utilizing the Bhushan model for the plowing component of friction and combining it with Hertzian contact theory which gives a relationship between the applied normal force and the contact area one can derive an expression for the plowing component as a function of the normal force.

Give that:

$$\mu_{\text{plowing}} = \frac{4}{3\pi} \left(\frac{a}{R} \right)$$

$$\delta A_c = \pi a^2 = \pi (D^* R \delta W)^{\frac{2}{3}}$$

Hence,

$$a = (D^* R \delta W)^{\frac{1}{3}}$$

Substitute into Bhushan's relationship, to give:

$$\mu_{\text{plowing}} = \frac{4}{3\pi} \left(D^* \delta W \right)^{\frac{1}{3}} R^{-\frac{2}{3}}$$

For uniform particles we know the following:

$$\delta W = \frac{\sigma_n \pi r^2}{(1-n)} = \frac{4\sigma_n R^2}{\beta}$$

Hence,

$$\mu_{plowing} = \frac{4}{3\pi} (D^*)^{\frac{1}{3}} \left(\frac{4\sigma_n}{\beta} \right)^{\frac{1}{3}}$$

The total coefficient of friction for uniform particles in contact with a surface is given as:

$$\mu_{uniform} = \tau_0 \pi (D^*)^{\frac{2}{3}} \left(\frac{\beta}{4\sigma_n} \right)^{\frac{1}{3}} + \alpha + \frac{4}{3\pi} (D^*)^{\frac{1}{3}} \left(\frac{4\sigma_n}{\beta} \right)^{\frac{1}{3}}$$

where

$$D^* = \frac{3}{4} \left(\frac{1-\nu_1^2}{E_1} + \frac{1-\nu_2^2}{E_2} \right)$$

It is important to note that the model is independent of particle size and thus also independent of the number of contacting particles. The model parameters are summarized below in Table 5.4.

Table 5.4 Model Parameters

Parameter	Values	Source
τ_0	1.6 MPa	Empirically derived
E_1	76 GPa	Santamarina (2001)
E_2	550 MPa	Manufacturer supplied
ν_1	0.31	Santamarina (2001)
ν_2	0.30	Dove (1996)
β	1.0 to $2/\sqrt{3}$ (1.15)	Theoretically derived
α	0.302	Empirically derived

Note: Subscript 1 indicates particle, 2 indicates surface

The effect of packing density is shown in Figure 5.32 below. The figure shows how the coefficient of friction varies as a function of the global normal stress. The two lines in the figure show the behavior for the loosest and densest stable packing arrangements for uniform particles. It is clear from the figure that the packing density has virtually no influence on the friction coefficient in this case.

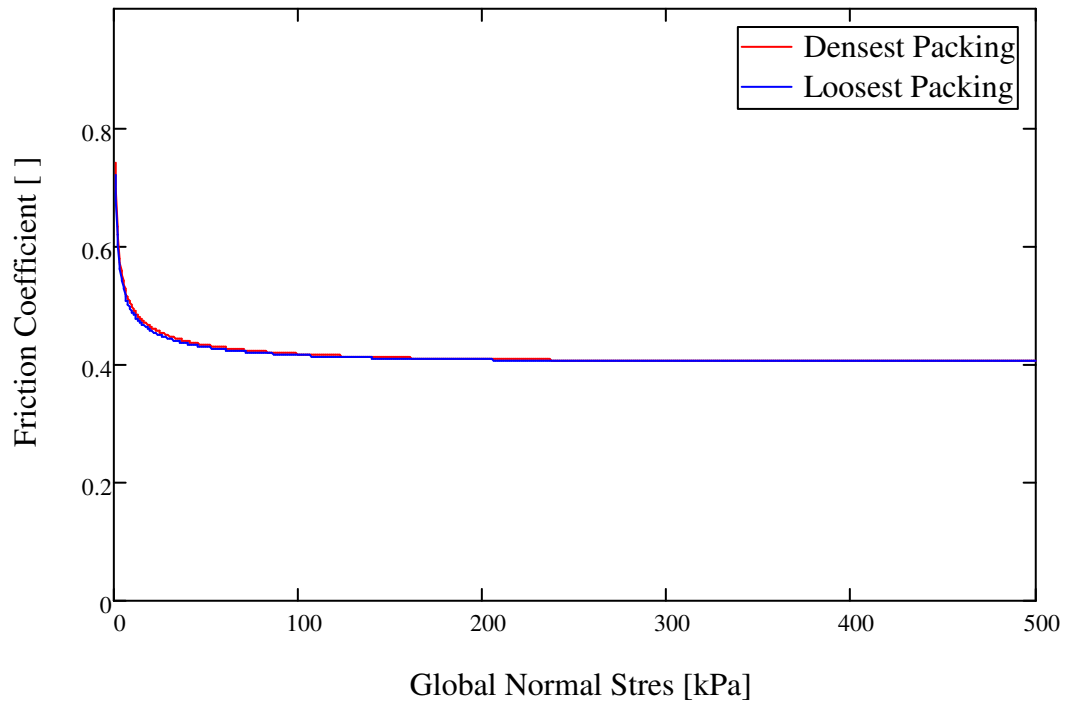


Figure 5.32 Effect of Packing Density, β

This is somewhat unexpected behavior since the packing density (void ratio) is generally considered in soil mechanics to be a useful correlator to behavior. This observation has, however, been made by previous experimentalists. Dove (1999) indicates that the friction coefficient behavior relative to normal stress appears to not be affected by either particle size or density (packing) and in that case the relative densities varied from approximately 50% to 85%. The model presented provides insight into why this behavior is observed.

Since the packing density has virtually no effect, the value of β will be taken as 1 for all future comparisons.

Figure 5.33 shows how changing the Young's Modulus of the surface affects the friction coefficient. The modulus was varied by 200 MPa in each direction from the value applicable to the actual material used. This was done for illustrative purposes.

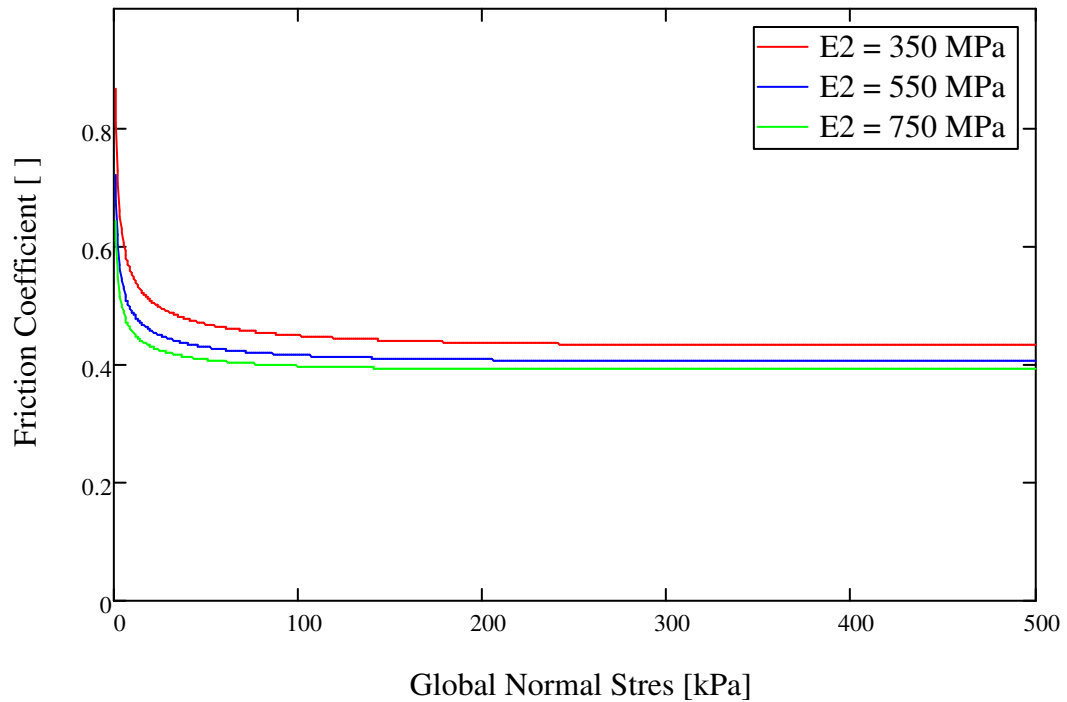


Figure 5.33 Effect of Young's Modulus of the Surface, E_2

As can be seen in the figure the lower the modulus of the surface material the greater the friction coefficient. As the modulus increases the coefficient decreases, although the effect does diminish with an increasing modulus. The difference in the friction coefficient at 500 kPa is approximately 0.025 between the 350 MPa and 550 MPa cases. This is equivalent to a change in friction angle of less than 1.5 degrees, a relatively minor change. A changing elastic modulus also changes the relative contributions of adhesion and plowing to the total friction coefficient. This is illustrated in Figure 5.34 which shows the percentage that plowing contributes towards the total friction coefficient as a function of normal stress.

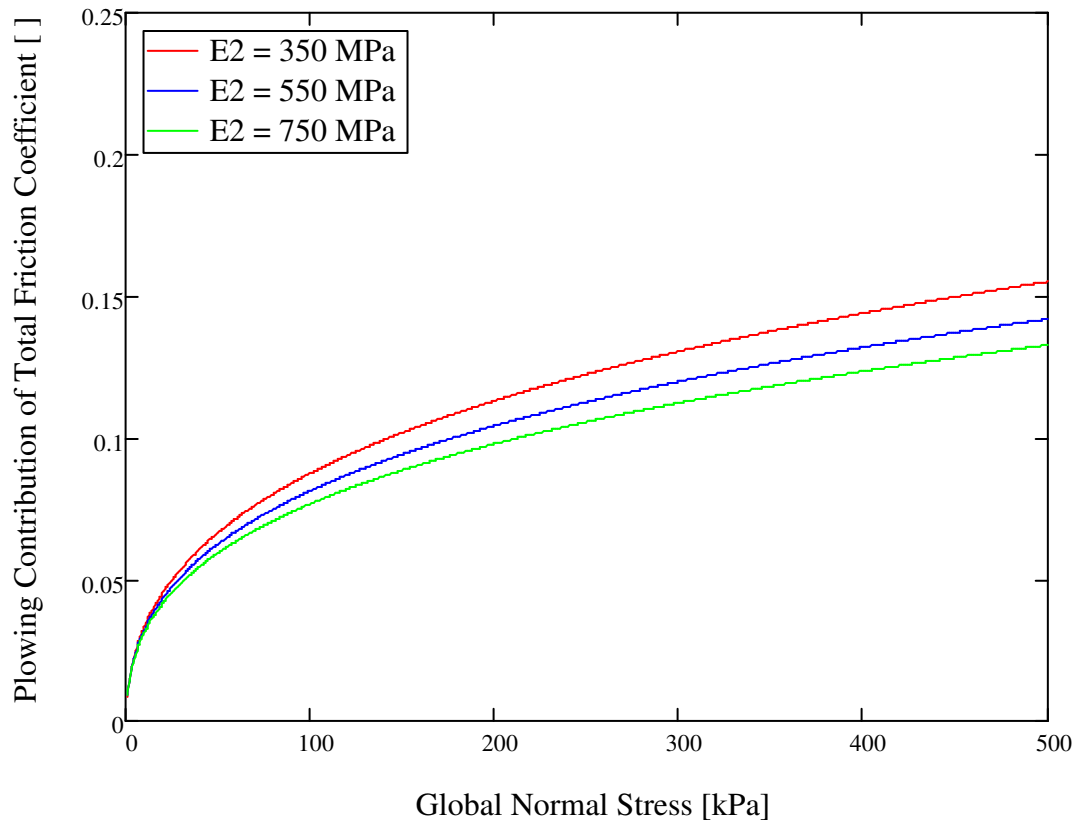


Figure 5.34 Effect of Young's Modulus of the Surface, E_2

It is evident that as the modulus of the surface is decreased the plowing component takes on a larger relative role. The observations related to the previous two figures have relevance to other current research (Karademir, 2010). Studies are being undertaken to investigate the interface friction between geomembranes and other engineering materials as a function of temperature. In general, an increase in the temperature of the geomembrane results in an increased interface friction. If the increase in temperature is analogous to a decrease in the modulus, then the model developed here may be used as a framework to predict changes in interface behavior as a result of changes in temperature.

Figure 5.35 shows that the Young's modulus of the particle has almost no influence on the friction coefficient. Plots are shown for quartz material (sand particles) and for steel. Even though the modulus varies by a factor of 2.5, the friction coefficient barely changes at any stress level.

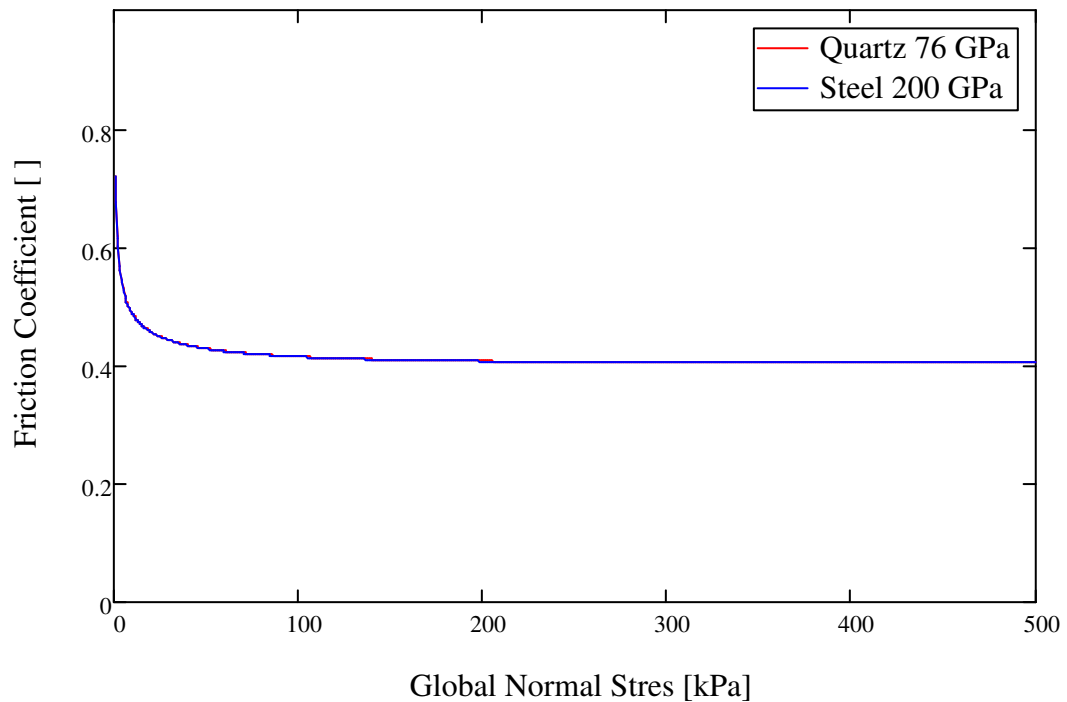


Figure 5.35 Effect of Young's Modulus of Particle, E_1

This is an important observations as it allows test results to be compared even if the indenting particles have been comprised of materials of different elastic modulus. Care should be taken, however, as the elastic modulus is not the only change between steel and quartz materials (for example). The surface roughness of the contacting particles as well as the elemental composition also play roles in determining the friction coefficient. These issues are outside the scope of the current work.

Figure 5.36 shows a comparison between the experimental data obtained and the model developed. The two lines representing the plowing and no-plowing cases both

provide reasonably good estimates of the actual friction coefficient, with the default model (inclusive of the plowing term) arguably providing the better fit to the data.

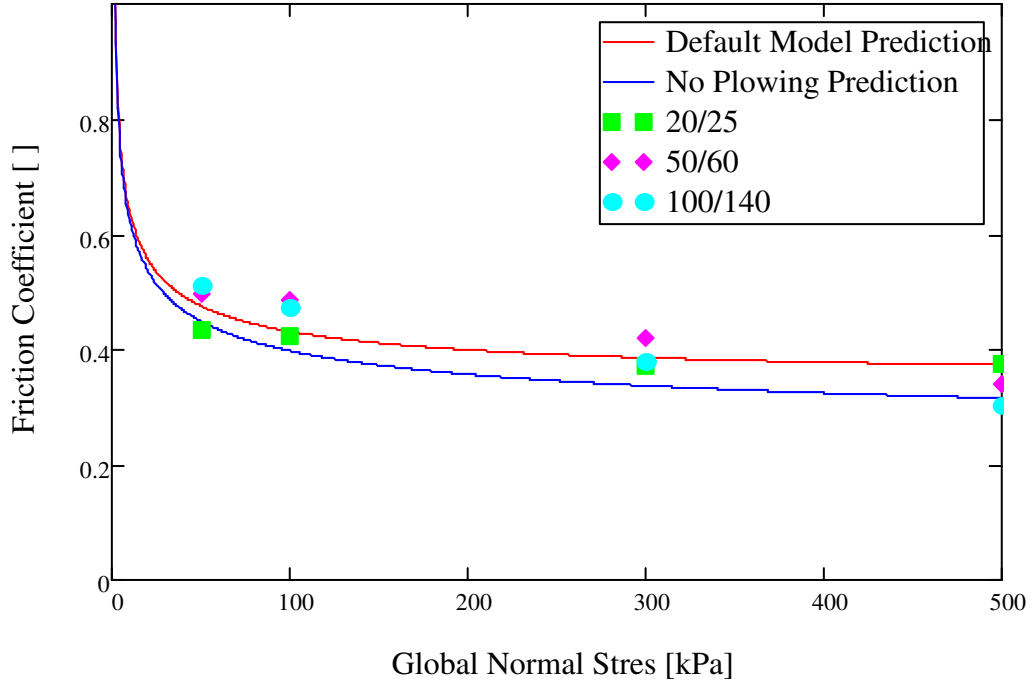


Figure 5.36 Comparison with Experimental Data

5.4.3. Binary Mixtures in Contact

In a similar fashion to that employed above, a model will be presented below that relates the friction coefficient to particle characteristics and surface material properties. In this case, however, the assumption of uniform particle size is rescinded and instead it is assumed that a binary mixture is present with two distinct particle sizes.

The total normal and shear forces acting on the surface are thus:

$$F = N_f \delta F_f + N_c \delta F_c$$

$$W = N_f \delta W_f + N_c \delta W_c$$

Where: N_f = number of contacting fine grains

N_c = number of contacting coarse grains

By combining and manipulating the expression above, along with expressions already given, one can express the adhesion component of the friction coefficient for binary mixtures in contact with a surface as:

$$\mu_{a-binary} = \tau_o \pi (D^*)^{\frac{2}{3}} \left(\frac{N_f (R_f \delta W_f)^{\frac{2}{3}} + N_c (R_c \delta W_c)^{\frac{2}{3}}}{W} \right) + \alpha$$

This expression should allow for the coefficient of friction due to adhesion to be calculated, however, there are two primary concerns when using this equations directly.

The first concern is knowing the number of fine and coarse grains in contact with the surface. It is not possible to measure these directly in a test of the kind that was performed as part of this study. The second concern is knowing how the normal forces are transmitted between the two phases and the surface. Do the larger or smaller particles take a disproportionate amount of the load? Does this change with particle size ratio and/or the proportion of finer materials?

The question of load distribution between particles in a binary particle mixture against a surface was studied by Abou-Chakra (1998) using finite element simulations. In that study mixtures with particle size ratios of 2.4 and 3.9 were studied. The large particles were arranged in a square packing arrangement ($\beta = 1$ in the terminology employed herein) and the smaller particles were packed in between the larger ones without disturbing their positions. The resulting bed of particles was thus packed in a dense configuration. The particle bed was then subjected to a uniform load on a loading plane located at the top of the large particles. It was found that the force acting on the

base from the large particles was almost the same as that acting on the base from the small particles. In the terminology used in this chapter, $\delta W_c = \delta W_f$.

This study was limited to only two particle size ratios but it is expected that the result could be extended down to a particle size ratio of 1.0. It is natural to assume (as was done for the uniform case above) that the load per particle will be equal. The result cannot, however, be extended to particle size ratios greater than that studied (i.e. greater than a particle size ratio of 3.9). A further limitation of the study was that the effect of shear forces acting on the particles was not considered.

The primary result of the study, that $\delta W_c = \delta W_f$, will be used to further the development of the friction coefficient model. It is important, however, to remain cognizant of the limits now built into the applicable scope of the model.

Given that $\delta W_c = \delta W_f = \delta W$:

$$W = (N_f + N_c)\delta W$$

Substituting into the previous equation and manipulating gives:

$$\mu_{a-binary} = \tau_o \pi (D^*)^{\frac{2}{3}} \left(\frac{N_f (R_f)^{\frac{2}{3}} + N_c (R_c)^{\frac{2}{3}}}{(N_f + N_c)^{\frac{2}{3}} W^{\frac{1}{3}}} \right) + \alpha$$

Since $W = A_t \sigma_w$

$$\mu_{a-binary} = \tau_o \pi \frac{(D^*)^{\frac{2}{3}}}{(A_t)^{\frac{1}{3}}} \left(\frac{N_f (R_f)^{\frac{2}{3}} + N_c (R_c)^{\frac{2}{3}}}{(N_f + N_c)^{\frac{2}{3}}} \right) \left(\frac{1}{\sigma_n^{\frac{1}{3}}} \right) + \alpha$$

The plowing component of the friction coefficient will be presented. In this development it will be assumed that $\delta W_c = \delta W_f = \delta W$.

Since,

$$\mu_{plowing} = \frac{4}{3\pi} (D^*)^{\frac{1}{3}} \left(\frac{4\sigma_n}{\beta} \right)^{\frac{1}{3}}$$

$$W = (N_f + N_c) \delta W$$

$$F_{plowing} = \delta F_f N_f + \delta F_c N_c$$

The expression for the plowing component of the friction coefficient is:

$$\mu_{p-binary} = \frac{4}{3\pi} (D^*)^{\frac{2}{3}} \left(\frac{N_f}{N_f + N_c} \right) \left(\frac{\sigma_n A_t}{N_f + N_c} \right)^{\frac{1}{3}} \left(\frac{1}{R_f^{\frac{2}{3}}} + \frac{N_c}{N_f} \frac{1}{R_c^{\frac{2}{3}}} \right)$$

Combining the expression for the adhesion and plowing components of friction yields an expression for the total friction coefficient for a binary particle mixture.

Given the geometrical constraints of being able to determine how many fine and course particles are in contact at the interface, the above expression will be compared to a subset of the experimental data. The case of a P.S.R. 2.1 mixture with 20% finer particles will be examined since the number of particles at the interface can be estimated with a greater degree of certainty than other size ratio and mixture proportions. Figure 5.37 shows an estimation of the friction coefficient for the aforementioned sand mixture. As was discussed previously, the plowing component tends to underestimate the true plowing contribution. To compensate for this, an additional stress-level dependent factor was introduced, and multiplied into the plowing component only. A factor of $\sigma_n/200$ was used to plot the blue line shown below.

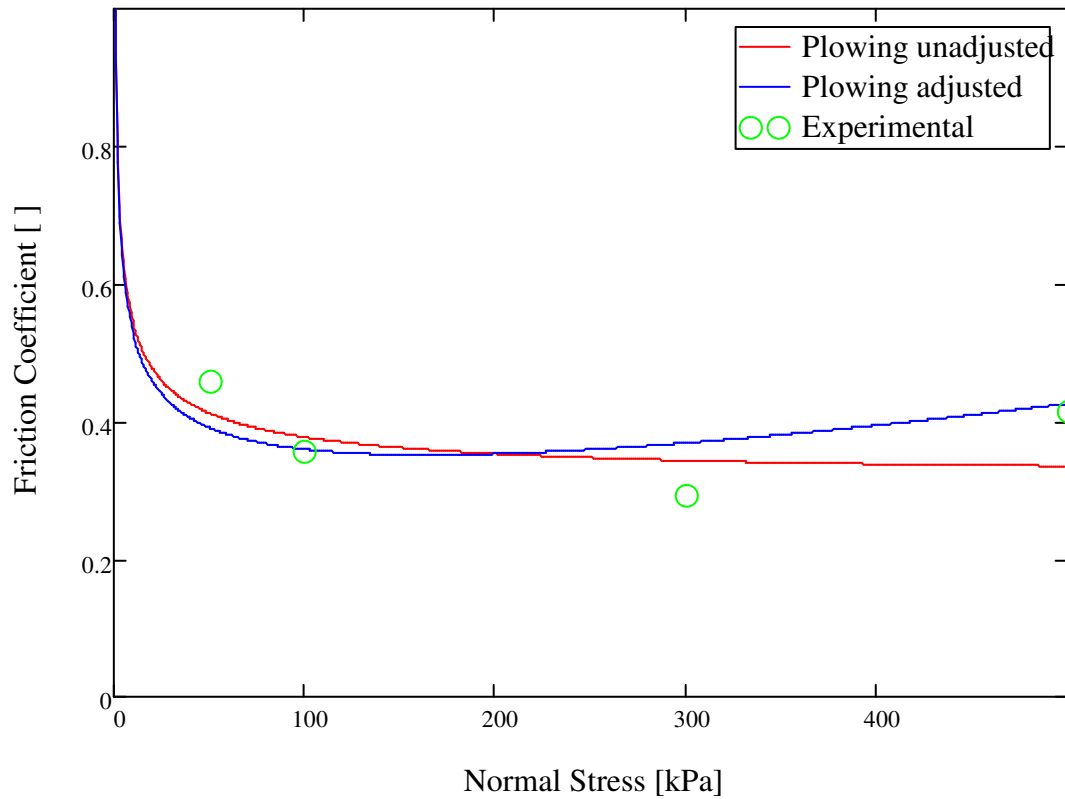


Figure 5.37 Estimation of friction coefficient for binary particle mixture

The unadjusted model provides a reasonable fit to the experimental data at lower stress levels but underestimates the friction coefficient at 500 kPa. The adjustment provided ensures that the data is well fit at 500 kPa but at the expense of the data point at 300 kPa. The adjusted model is however able to capture the increase in friction coefficient beyond a certain stress level.

6. INTERFACE SHEAR BEHAVIOR OF BINARY PARTICLE MIXTURES WITH ROUGH COUNTERFACES

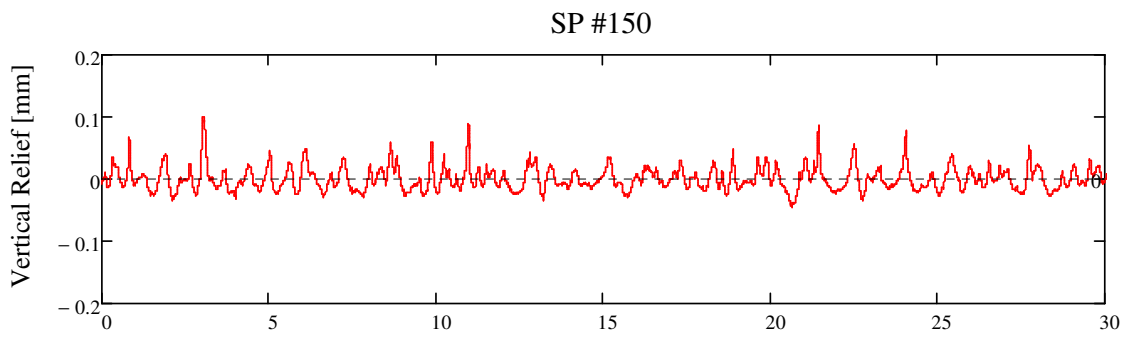
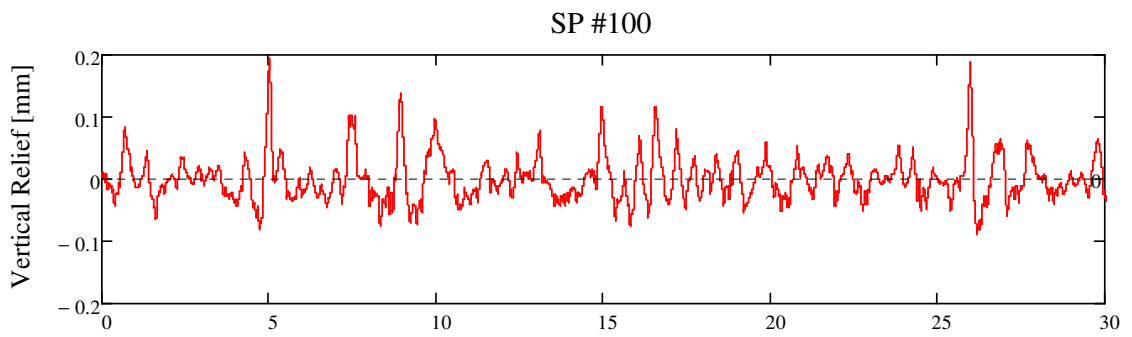
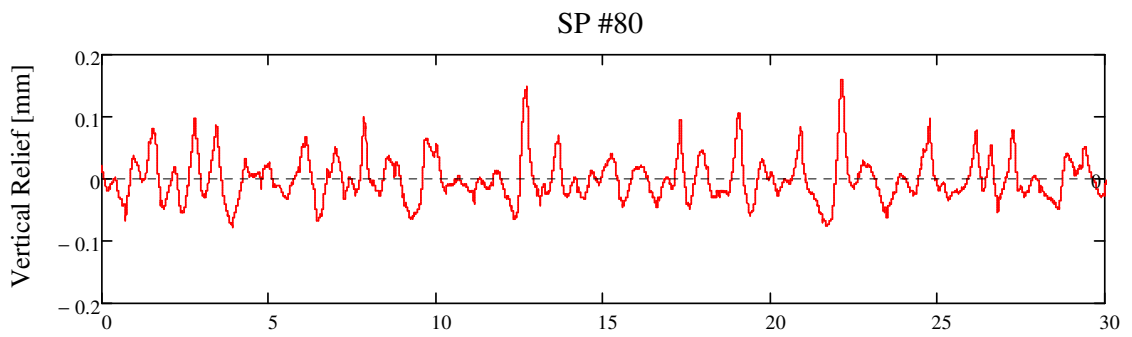
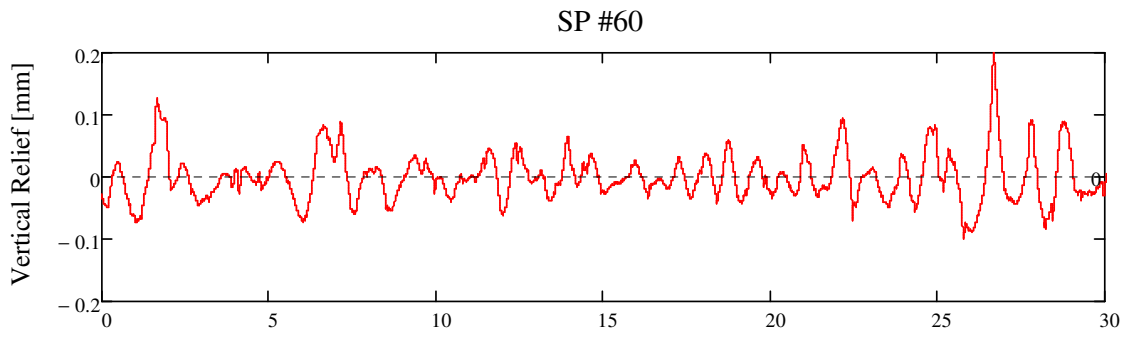
This chapter examines the interface shear behavior of binary particle mixtures in contact with hard, textured surfaces. The test procedures and equipment were outlined in Chapter 3. One of the key questions to be considered in this chapter is what the most appropriate descriptor of particle size is when a binary particle mixture is in contact with a rough surface. A series of interface shear tests, along with an examination of relative roughness, were completed in order to explore these topics.

6.1. Relative Roughness

A number of measures for relative roughness exist, most importantly the parameter called “normalized roughness” developed by Uesugi and Kishida (1986). This parameter was proposed to improve the correlation between the coefficient of friction and surface roughness values that were being measured. Normalized roughness, R_n , is defined as the ratio of maximum roughness (R_{max}) measured over a distance equal to the mean grain size to the mean grain size (d_{50}).

In order to calculate this parameter one calculates R_{max} (peak to valley height) over a length of the profile equal to d_{50} . This calculation is then repeated for every section of the profile. Measuring local R_{max} over a distance equal to d_{50} prevents a peak from one side of the profile being twinned with a valley on the other side of the profile resulting in a potentially very large R_{max} value but one that was irrelevant since a single particle would not experience such a roughness.

Relative roughness will be investigated using the materials used in the interface shear testing phase of this study. Typical surface profiles for the sandpaper surfaces tested are shown below in Figure 6.1.



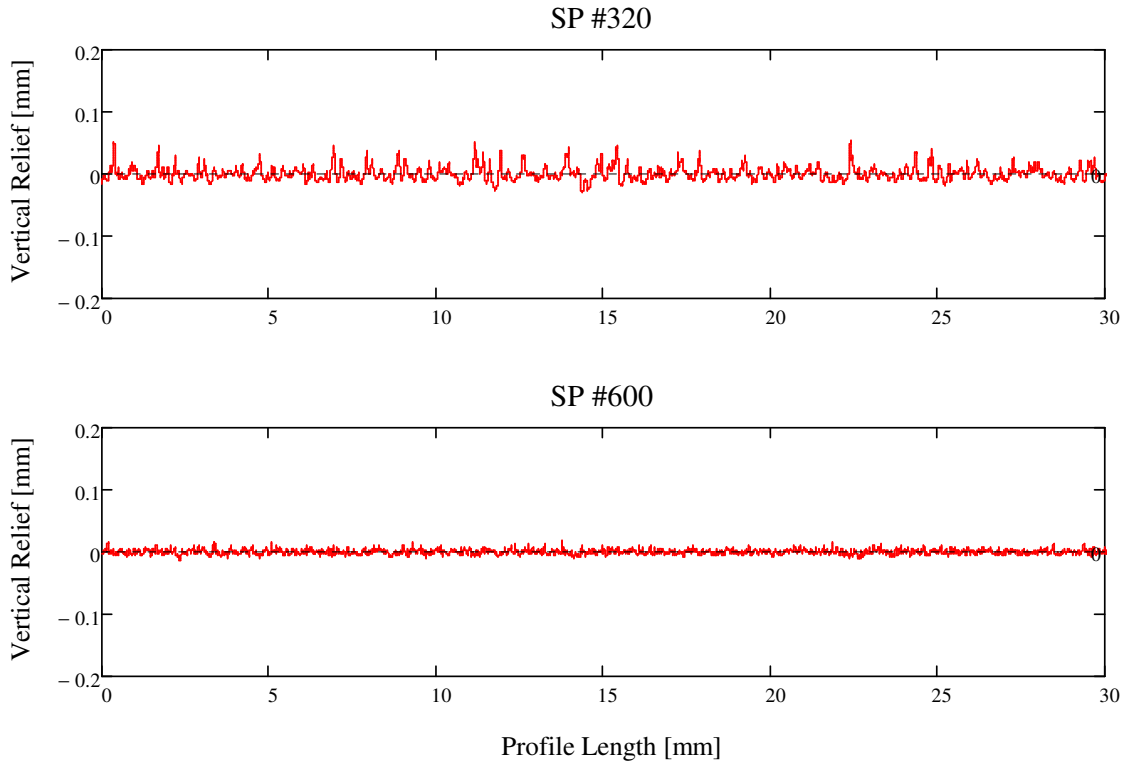


Figure 6.1 Typical Sandpaper Surface Profiles

As the grit size of the sandpaper decreases (increasing number) one can observe a corresponding decrease in the texturing of the surface.

Histograms showing the distribution of local R_{\max} values for a given surface and D_{50} are shown in Figure 6.2 below. This histograms show the frequency with which specific intervals of localized R_{\max} values occur over the entire profile length. A scaled lognormal probability density function has been overlaid. The scaling factor scales the probability density function by the bin width of the histogram. This keeps the same shape as the original probability density function but allows for a direct comparison on the same vertical scale as the histogram, which maintains the significance of indicating the frequency. Nine histograms have been plotted, for sandpaper surfaces #60, #150 and #320, and for the three d_{50} values of the uniform sands (0.13mm, 0.28mm and 0.78mm).

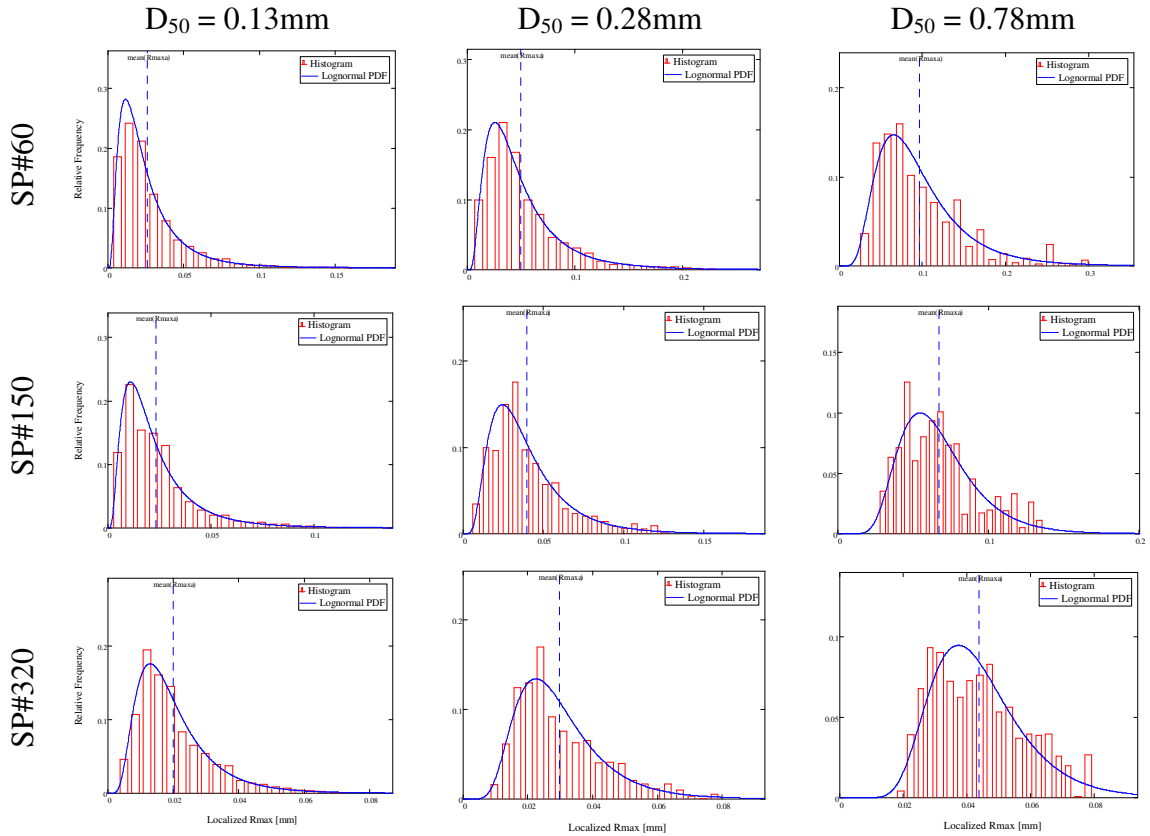


Figure 6.2 Local R_{\max} Histograms

From Figure 6.2 it can be seen that the lognormal distribution fits the distribution of local R_{\max} values very well.

The original method of calculating R_n was to use the mean value of local R_{\max} , as indicated by the vertical dashed line in the above plots. Examination of the distributions indicates that a more representative value to describe the R_{\max} value may be the modal value. An evaluation of using the mode rather than the mean value to calculate R_n is presented next. This new normalized roughness parameter will be designated mR_n , where the “m” stands for “modal”.

Figure 6.3 shows the two normalized roughness parameters plotted as a function of particle size for the same sandpaper surfaces as were presented previously.

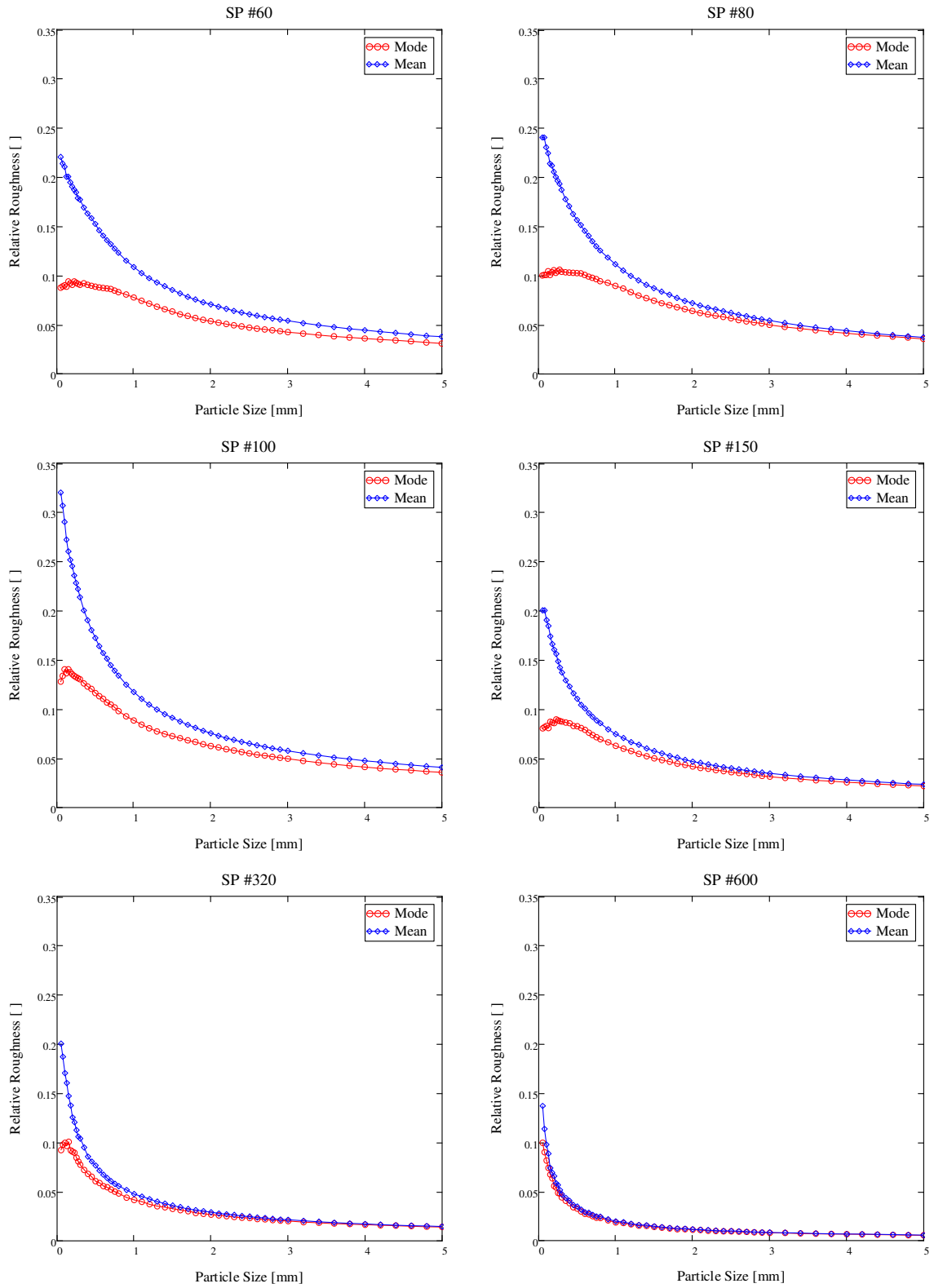


Figure 6.3 Comparison of modal and mean normalized roughness parameters - sandpaper

It is evident from Figure 6.3 that by changing the calculation from the mean to the mode the resulting normalized roughness parameter is changed. R_n shows a strong increase as the particle size (or the measurement length) decreases in size. This is due to the decreasing denominator (D_{50}) which thus increases R_n dramatically as D_{50} approaches zero. In all cases, mR_n plots beneath R_n . Probably the most striking aspect of Figure 6.3 is that mR_n is seen to increase as the particle size increases, this is especially evident in the case of the sand papers #100 and #150. The roughness parameter increases to a peak and then decreases again, indicating a potential “resonant” wavelength at which the particle size and interface features may interact the most fully.

Similar plots are shown below in Figure 6.4 for pipe sections commonly used in the pipe-jacking industry. Again, there is a clear difference between the two measures of normalized roughness.

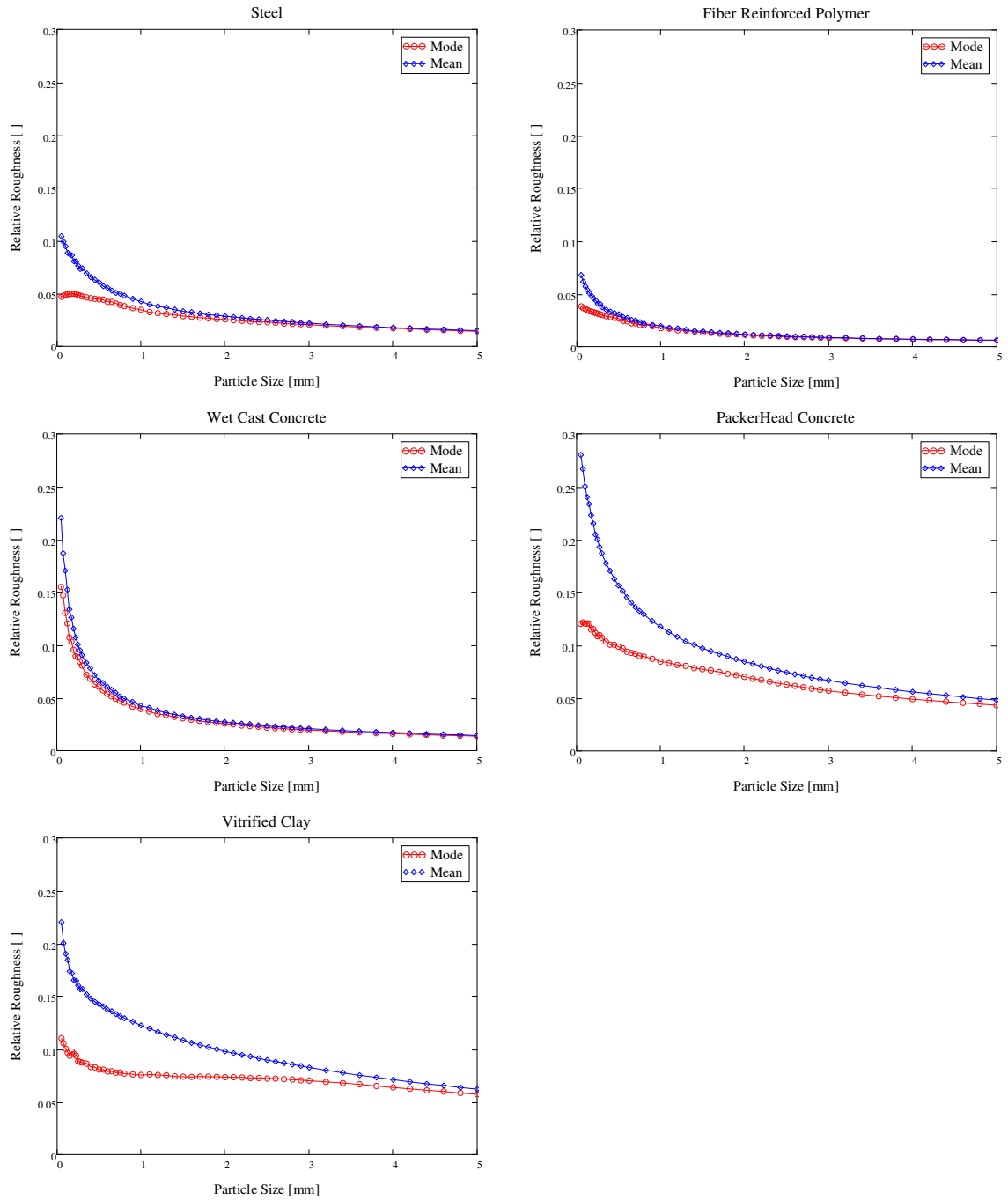


Figure 6.4 Comparison of modal and mean normalized roughness parameters - pipes

A comparison between the sandpapers is shown below in Figure 6.5 and Figure

6.6.

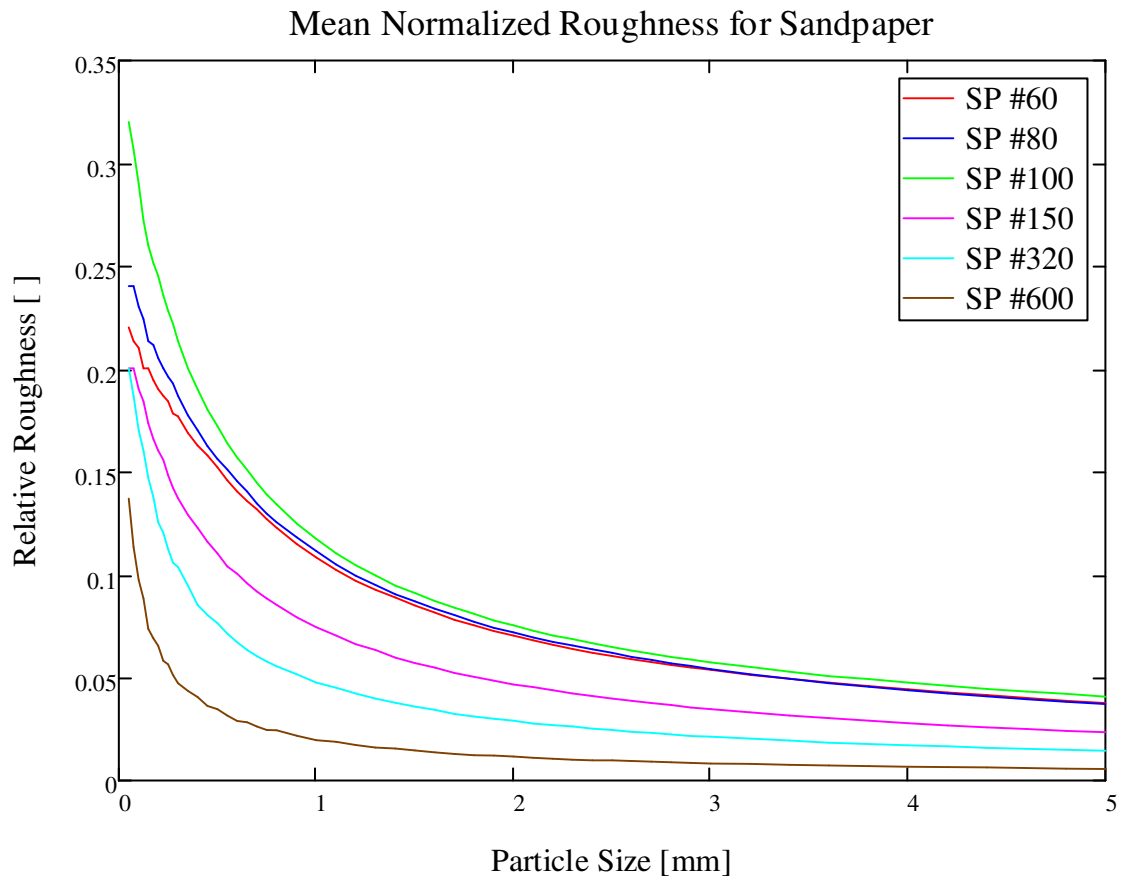


Figure 6.5 Mean Normalized Roughness - Sandpaper

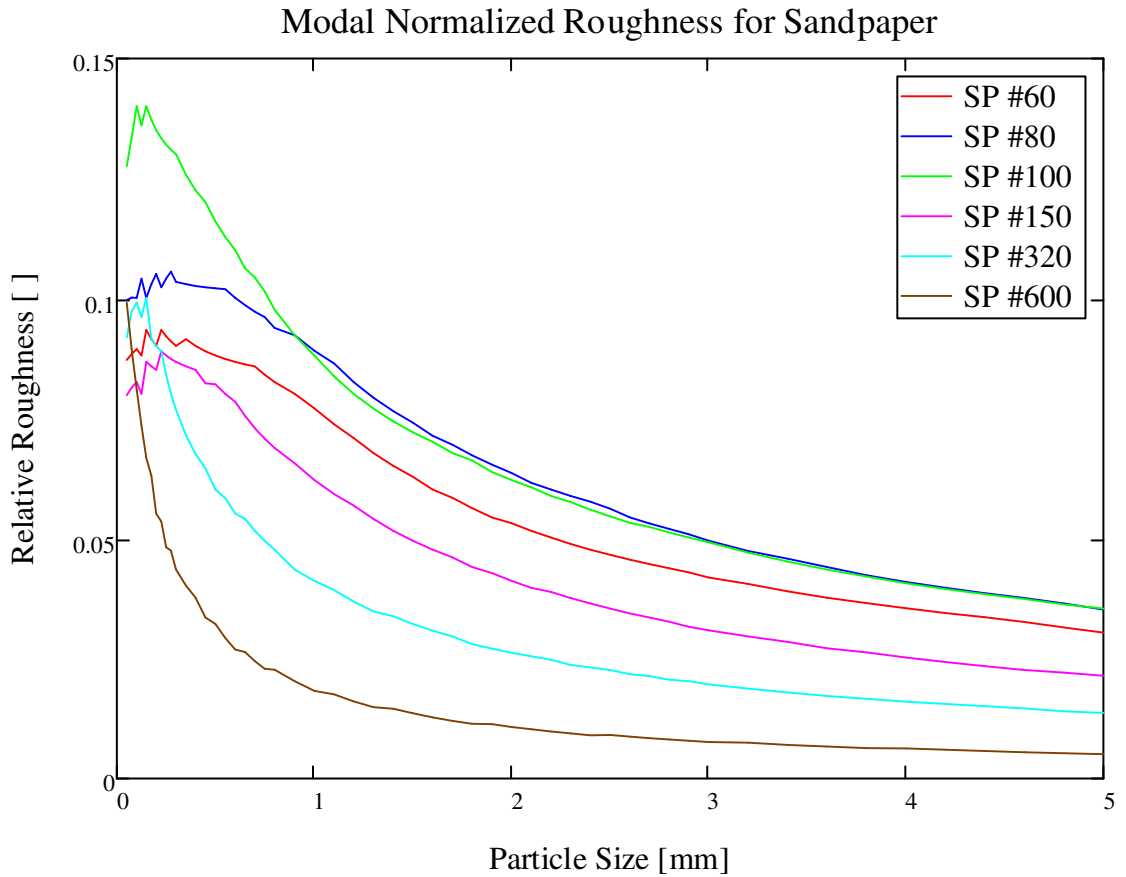


Figure 6.6 Modal Normalized Roughness - Sandpaper

These figures highlight an important, yet often overlooked, aspect of surface roughness – that one surface may be rougher than another at one particle size, but smoother at a different particle size. To the best of the authors knowledge this observation has not previously been explicitly noted.

It is thus not strictly correct to term one surface as “rougher” than another without reference to a particle size. With most soils exhibiting a range of particle sizes the concept of relative roughness becomes even more ambiguous. The same phenomenon is seen to occur with the pipe sections, with the vitrified clay pipe being alternately smoother and rougher than the PackerHead concrete pipe, depending on the particle size considered.

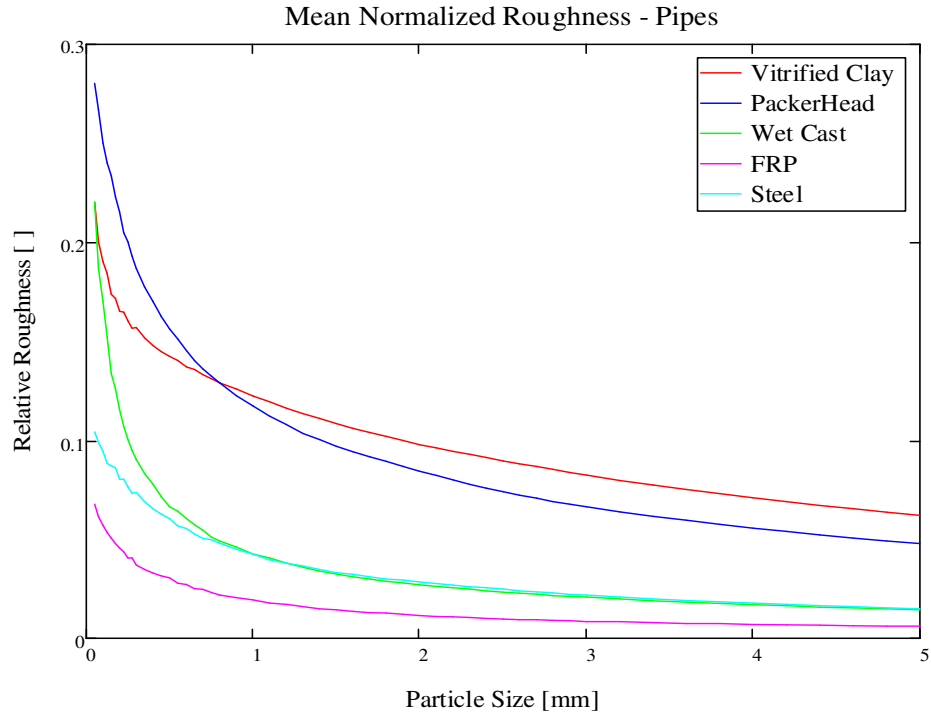


Figure 6.7 Mean Normalized Roughness - Pipes

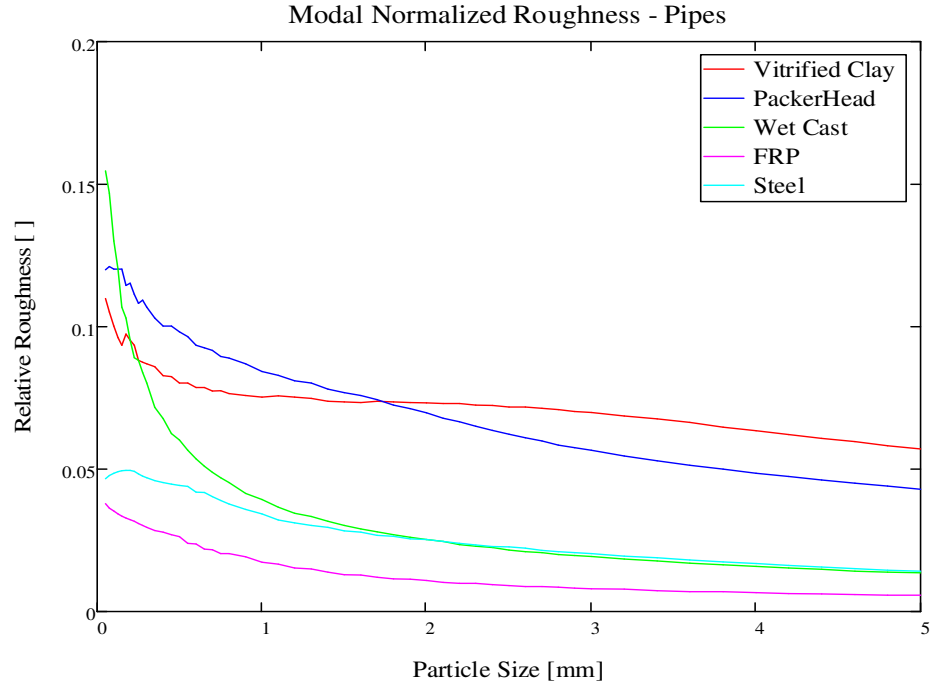


Figure 6.8 Modal Normalized Roughness - Pipes

In order to further evaluate the suitability of both R_n and mR_n , each method were was employed in this study. Analyzing the results using both methods will lead to clarity on which one is more suited for describing the relative roughness of these surfaces.

Knowledge of the particle size distribution is most helpful if the size of the governing particles for a particular process is known. For example, Hazen identified that the d_{10} of a soil corresponds well to the hydraulic conductivity of that soil. For many processes there may well not be such a clear relationship with particle size, but for other processes, the link with particle size may have been obscured by poorly chosen particle size descriptors and/or a poor choice of the governing particle size.

The most relevant example of this is the continued use of D_{50} as a measure of the particle size in interface shear studies. Since the development of the concept that particle size and surface profile (or roughness) are fundamentally related in this particular process, scant attention has been paid to choosing the most appropriate measure of particle size.

6.2. Choosing a representative particle size for binary mixtures

When an “average” size for a given particle mass is offered it is usually implied that that particle size is the most relevant to the topic or process under consideration. It is usually assumed that d_{50} is an appropriate measure of size to use when considering interface shear. For example, the pioneering work by Uesugi (1986) uses d_{50} to calculate normalized roughness. Their research highlighted the relative nature of interface roughness, that is, that the surface profile and particle size need to be assessed together to establish roughness. In other applications different measures of size are more appropriate, reflecting an understanding of the true nature of the processes. A good example of this is

the use of d_{10} in Hazen's permeability equation, reflecting the fact that smaller particles in a distribution control the permeability. Another example is Hardin's use of d_5 in studying the importance of the smaller particles in determining G_{\max} .

In the case of binary particle mixtures undergoing interface shear the question remains – what is the most appropriate particle size descriptor to use? This chapter will address this question.

6.2.1. Weighted-Average Approach

One can use a weighted-average approach to determine the d_{50} for a binary particle mixture in a relatively straightforward manner. Each of the base sands used in this study was sieved to be within a very narrow size range (see Chapter 3 for more details) so the mean size of the particles captured between the two sieves gives a good representation of the particle size for each base sand. These base sands were then combined in different proportions and so a weighted-average approach can be used to determine the D_{50} . This does result in D_{50} values between the largest and smallest particle sizes (which makes sense), but without any particles actually being close to the reported D_{50} value (which may seem correct mathematically, but perhaps not physically). All of the studied combinations and the resulting weighted average D_{50} values are shown in the table below.

Table 6.1 Weighted Average Particle Size for Binary Particle Mixtures

P.S.R. 6.1			P.S.R. 2.8			P.S.R. 2.1		
% Fine	% Coarse	D ₅₀ [mm]	% Fine	% Coarse	D ₅₀ [mm]	% Fine	% Coarse	D ₅₀ [mm]
0	100	0.780	0	100	0.780	0	100	0.280
10	90	0.715	10	90	0.730	10	90	0.265
20	80	0.650	20	80	0.680	20	80	0.250
30	70	0.585	30	70	0.630	30	70	0.235
40	60	0.520	40	60	0.580	40	60	0.220
50	50	0.455	50	50	0.530	50	50	0.205
60	40	0.390	60	40	0.480	60	40	0.190
70	30	0.325	70	30	0.430	70	30	0.175
80	20	0.260	80	20	0.380	80	20	0.160
90	10	0.195	90	10	0.330	90	10	0.145
100	0	0.130	100	0	0.280	100	0	0.130

Based on this table it is evident that a number of different combinations of particles have very similar weighted average particle size. Notably, this indicates that the weighted-average D₅₀ is far from being a unique property of a soil. The combinations that show very similar weighted-average D₅₀ values are shown in the table below.

Table 6.2 Different Combinations of Particles with the same Weighted Average Particle Size

First Combination			Second Combination		
Fine	Coarse	Size [mm]	Size [mm]	Fine	Coarse
30% 100/140	70% 20/25	0.585	0.580	40% 50/60	60% 20/25
60% 100/140	40% 20/25	0.390	0.380	80% 50/60	20% 20/25
70% 100/140	30% 20/25	0.325	0.330	90% 50/60	10% 20/25
80% 100/140	20% 20/25	0.260	0.265	10% 100/140	90% 50/60
90% 100/140	10% 20/25	0.195	0.190	60% 100/140	40% 50/60

Examining the table above one can see that the two mixtures that both have a D_{50} close to 0.260mm are made up very differently. One is a mixture of 80% 100/140 with 20% 20/25 while the other is comprised of just 10% 100/140 with 90% 50/60. These two different mixtures, while sharing a weighted-average D_{50} , would most likely be expected to behave very differently under a given set of circumstances. The difference in their interface shear response is shown in Figure 6.13.

6.2.2. Sectional Approach

An alternative approach to determining a representative particle size builds on observations made in Chapter 4. In that chapter, it was observed that at a percentage of finer particles of approximately 40% there was a transition from a coarse dominated fabric to a fabric dominated by the finer particles. The transition is not abrupt, but a transition exists nonetheless.

The sectional approach thus divides a mixture into two or three sections, with each section being dominated by a different particle size. The dominant particle size thus changes in a step wise fashion as the mixture proportion changes.

In the two section approach, the dividing line between the regime dominated by finer particles and the coarse dominated regime would be the minimum point on a plot of

the VRR (volume reduction ratio, as discussed in Chapter 4). This is approximately 35% of finer particles. For any mixture with a percentage of finer particles less than 35%, the representative particle size would be taken as the size of the coarse particle. At a percentage of finer particles greater than 35%, the representative particle size would be taken as the size of the finer particle.

In a three section approach, a central transition zone is identified from approximately 25% to 55% of finer particles. At percentage of finer particles greater than 55%, the representative size would be that of the fine particles. At percentages less than 25%, the representative grain would be that of the coarse particles. At intermediate values from 25% to 55%, the representative grain size would be an average of the fine and coarse particle sizes.

This sectional approach is illustrated in Figure 6.9 and Figure 6.10 below for a P.S.R. of 2.8.

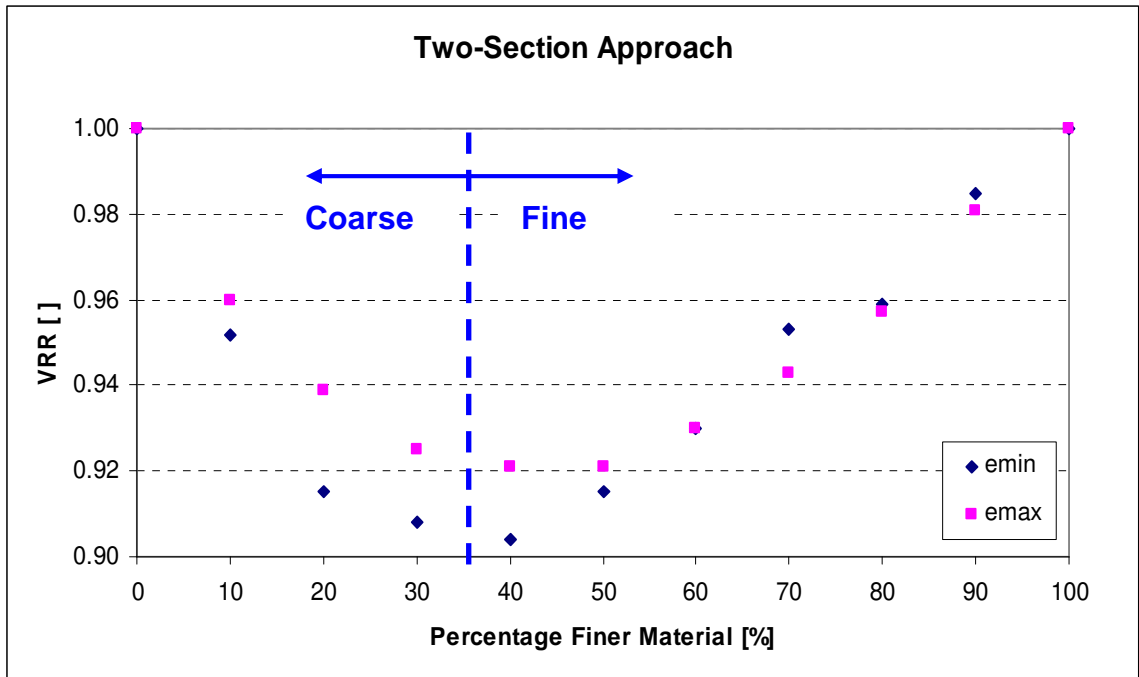


Figure 6.9 Two Section Approach

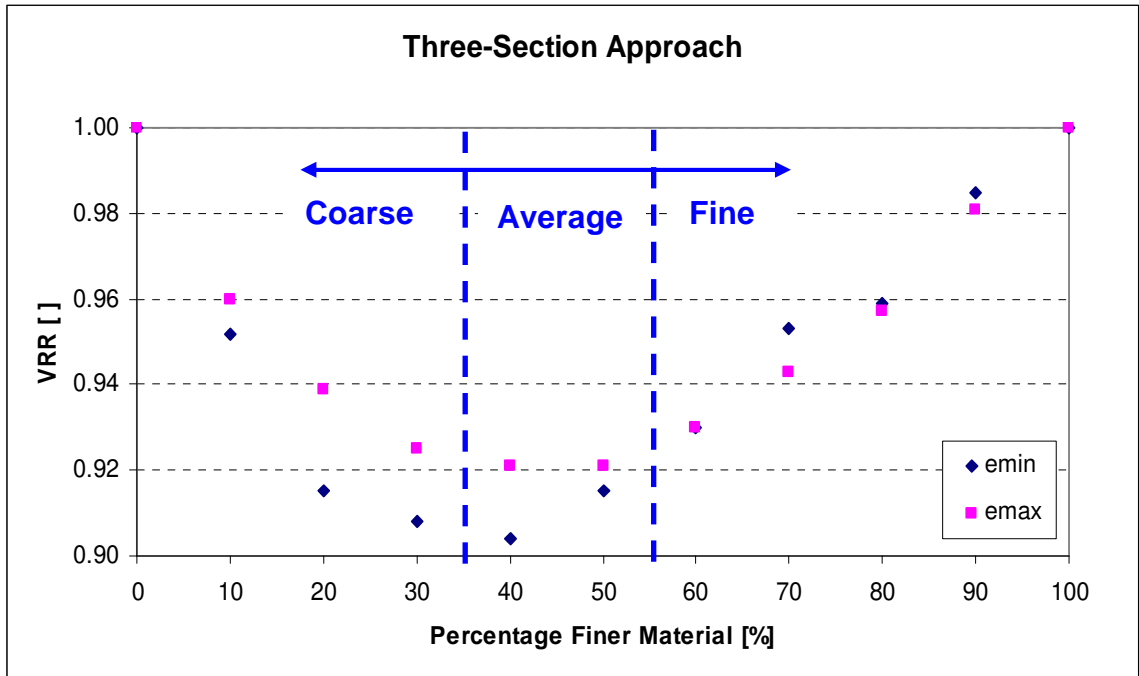


Figure 6.10 Three Section Approach

The tables below list the representative particle sizes for both two and three section approaches for the materials used in this study.

Table 6.3 Representative Particle Size using Two Section Approach

P.S.R.	Large Component		Small Component		Representative Size
	Proportion	Diameter [mm]	Diameter [mm]	Proportion	
2.1	100	0.28	0.13	0	0.28
2.1	90	0.28	0.13	10	0.28
2.1	80	0.28	0.13	20	0.28
2.1	70	0.28	0.13	30	0.28
2.1	60	0.28	0.13	40	0.28
2.1	50	0.28	0.13	50	0.13
2.1	40	0.28	0.13	60	0.13
2.1	30	0.28	0.13	70	0.13
2.1	20	0.28	0.13	80	0.13
2.1	10	0.28	0.13	90	0.13
2.1	0	0.28	0.13	100	0.13
2.8	100	0.78	0.28	0	0.78
2.8	90	0.78	0.28	10	0.78
2.8	80	0.78	0.28	20	0.78
2.8	70	0.78	0.28	30	0.78
2.8	60	0.78	0.28	40	0.78
2.8	50	0.78	0.28	50	0.28
2.8	40	0.78	0.28	60	0.28
2.8	30	0.78	0.28	70	0.28
2.8	20	0.78	0.28	80	0.28
2.8	10	0.78	0.28	90	0.28
2.8	0	0.78	0.28	100	0.28
6.1	100	0.78	0.13	0	0.78
6.1	90	0.78	0.13	10	0.78
6.1	80	0.78	0.13	20	0.78
6.1	70	0.78	0.13	30	0.78
6.1	60	0.78	0.13	40	0.78
6.1	50	0.78	0.13	50	0.13
6.1	40	0.78	0.13	60	0.13
6.1	30	0.78	0.13	70	0.13
6.1	20	0.78	0.13	80	0.13
6.1	10	0.78	0.13	90	0.13
6.1	0	0.78	0.13	100	0.13

Table 6.4 Representative Particle Size using Three Section Approach

P.S.R.	Large Component		Small Component		Representative Size
	Proportion	Diameter [mm]	Diameter [mm]	Proportion	
2.1	100	0.28	0.13	0	0.28
2.1	90	0.28	0.13	10	0.28
2.1	80	0.28	0.13	20	0.28
2.1	70	0.28	0.13	30	0.19
2.1	60	0.28	0.13	40	0.19
2.1	50	0.28	0.13	50	0.19
2.1	40	0.28	0.13	60	0.13
2.1	30	0.28	0.13	70	0.13
2.1	20	0.28	0.13	80	0.13
2.1	10	0.28	0.13	90	0.13
2.1	0	0.28	0.13	100	0.13
2.8	100	0.78	0.28	0	0.78
2.8	90	0.78	0.28	10	0.78
2.8	80	0.78	0.28	20	0.78
2.8	70	0.78	0.28	30	0.53
2.8	60	0.78	0.28	40	0.53
2.8	50	0.78	0.28	50	0.53
2.8	40	0.78	0.28	60	0.28
2.8	30	0.78	0.28	70	0.28
2.8	20	0.78	0.28	80	0.28
2.8	10	0.78	0.28	90	0.28
2.8	0	0.78	0.28	100	0.28
6.1	100	0.78	0.13	0	0.78
6.1	90	0.78	0.13	10	0.78
6.1	80	0.78	0.13	20	0.78
6.1	70	0.78	0.13	30	0.46
6.1	60	0.78	0.13	40	0.46
6.1	50	0.78	0.13	50	0.46
6.1	40	0.78	0.13	60	0.13
6.1	30	0.78	0.13	70	0.13
6.1	20	0.78	0.13	80	0.13
6.1	10	0.78	0.13	90	0.13
6.1	0	0.78	0.13	100	0.13

These representative particle sizes can be used in the calculation of the normalized roughness. The traditional bilinear plots presenting the interface friction

coefficient and normalized roughness are presented later in this chapter using these representative values.

6.3. Interface Shear Results

Due to the fact that many variables could be altered, the combination of possible tests to perform was very large. A comprehensive exploration of this entire experimental matrix was not feasible, so a targeted approach was used instead to highlight select aspects.

6.3.1. Changing surface roughness – uniform sands

Figure 6.11 shows the effect of changing the roughness of the counterface surface, from a very smooth steel to a very rough sandpaper. Table 6.5 presents the data from the interface shear tests with uniform sands and rough, hard counterfaces.

Table 6.5 Interface Shear Test Data for Rough Counterfaces with Uniform Particles

Sand	Counterface	Test Reference	Normal Stress [kPa]	Peak Friction Coeff.	Large Disp. Friction Coeff.
20/25	SP #60	IS_20/25_60	100	0.701	0.613
	SP #80	IS_20/25_80	100	0.690	0.593
	SP #100	IS_20/25_100	100	0.681	0.564
	SP #150	IS_20/25_150	100	0.633	0.509
	SP #320	IS_20/25_320	100	0.561	0.472
	SP #600	IS_20/25_600	100	0.523	0.488
	Steel	IS_20/25_ST	100	0.345	0.276
50/60	SP #80	IS_50/60_80	100	0.700	0.575
	SP #150	IS_50/60_150	100	0.714	0.570
	SP #320	IS_50/60_320	100	0.698	0.553
	SP #600	IS_50/60_600	100	0.570	0.511
	Steel	IS_50/50_ST	100	0.327	0.305
100/140	SP #100	IS_100/140_100	100	0.740	0.544
	SP #150	IS_100/140_150	100	0.721	0.567
	SP #320	IS_100/140_320	100	0.740	0.538
	SP #600	IS_100/140_600	100	0.679	0.542
	Steel	IS_100/140_ST	100	0.292	0.266

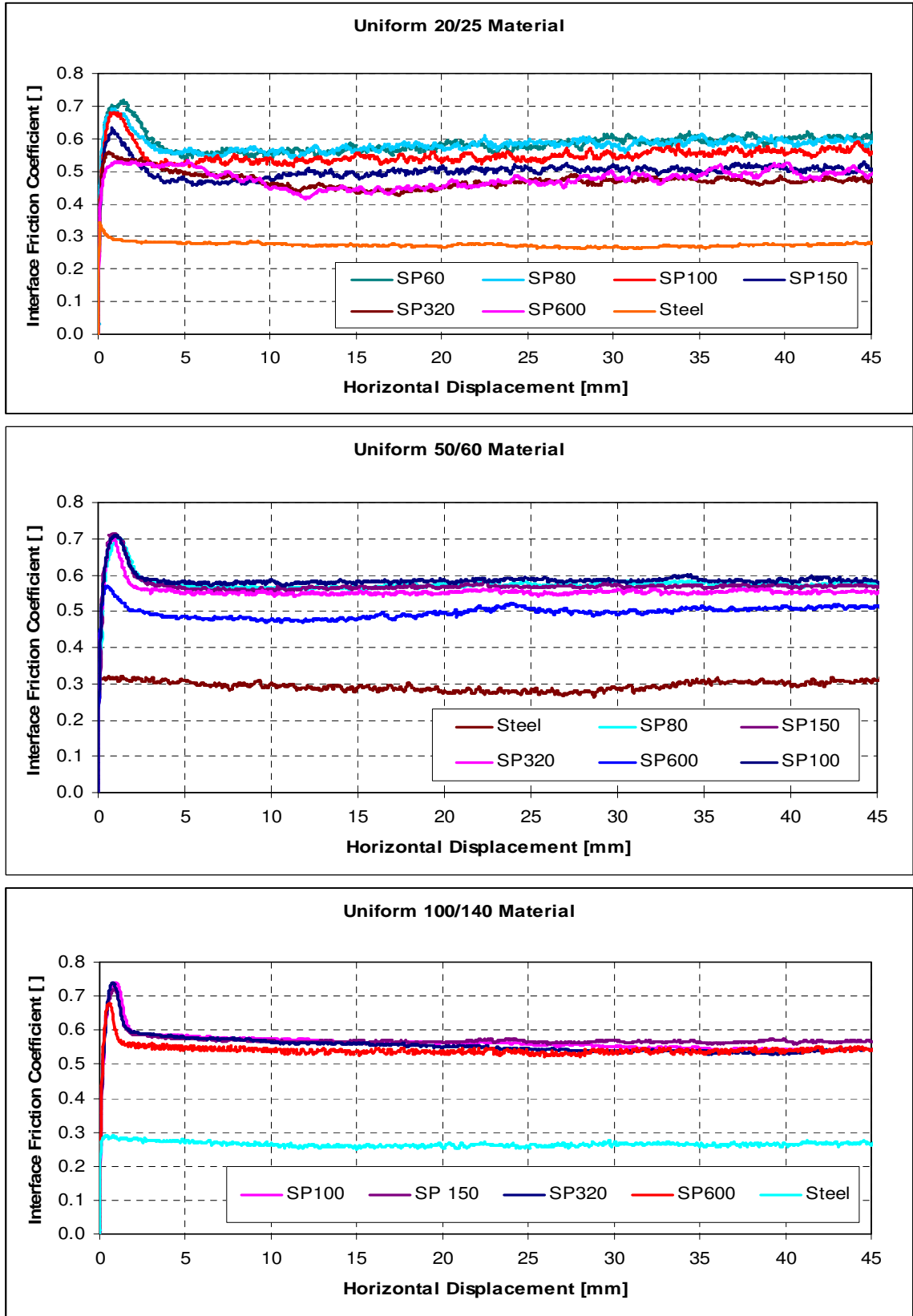


Figure 6.11 Effect of Surface Roughness on Interface Shear

The following observations are made:

- For the above particles any sandpaper coarser than SP100 will result in a fully mobilized shear zone
- For surfaces rougher than the critical roughness the peak strength is very similar
- For surfaces less rough than the critical roughness, the rougher the surface the greater the peak interface strength
- Very little surface texturing is required in order to significantly alter the interface strength
- There is a slight increase in post-peak strength with increasing displacement for all the roughened surfaces

6.3.2. Changing the mixture proportions

In the following section the effects of changing the mixture percentage will be highlighted. Figure 6.12 shows how the interface shear response for a PSR 6.1 mixture changes as the relative proportions of fine to coarse particles re changed, through the ratios from 0, 10, 30, 60, 80 and 100% finer particles. These interface shear tests were all performed at a normal stress of 100 kPa and with sandpaper #100 as the counterface.

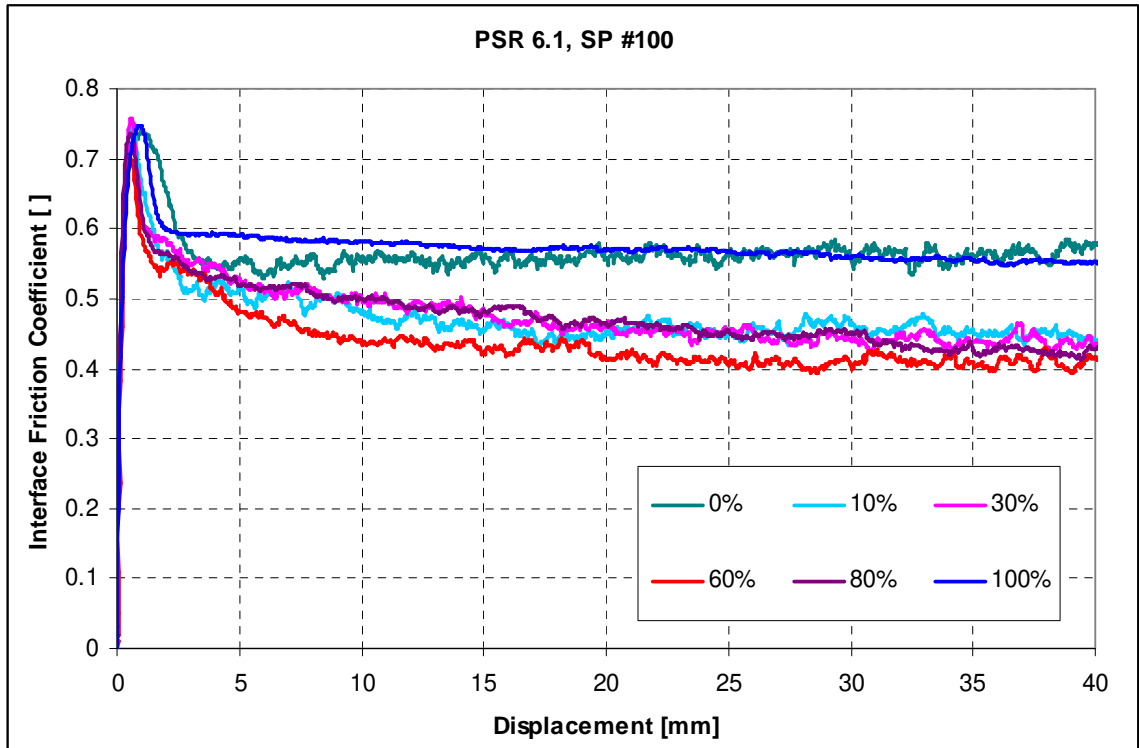


Figure 6.12 Effect of changing mix percentage (P.S.R 6.1, SP #100)

The following observations are made:

- The base sands have higher residual strength than all of the mixtures.
- The uniform sands show a reduced post-peak drop off in strength.
- All of the mixtures show relatively similar residual strengths, with the general trend of a decreasing strength with an increase in percentage of finer particles (note that the residual strength for each of the base sands is very similar and therefore the difference is attributable to the mix percentages and not the particle characteristics themselves).
- A small amount of finer particles (in this case just 10%) is all that is needed to significantly alter the strength-strain curve.
- A small amount of coarse material (in this case just 20%) is all that is needed to significantly alter the strength-strain curve.

- The 30% mixture exhibits the greatest peak strength, corresponding approximately with the percentage of finer particles required to reach the maximum density.

6.3.3. Changing mixture proportions while maintaining the same weighted-average D_{50}

Figure 6.13, Figure 6.14 and Figure 6.15, presented below, all show the clear difference in interface shear behavior despite the samples having the same weighted average d_{50} in each case. All tests were performed at a normal stress of 100 kPa, relative density of 80% and used sandpaper #100 as the counterface material.

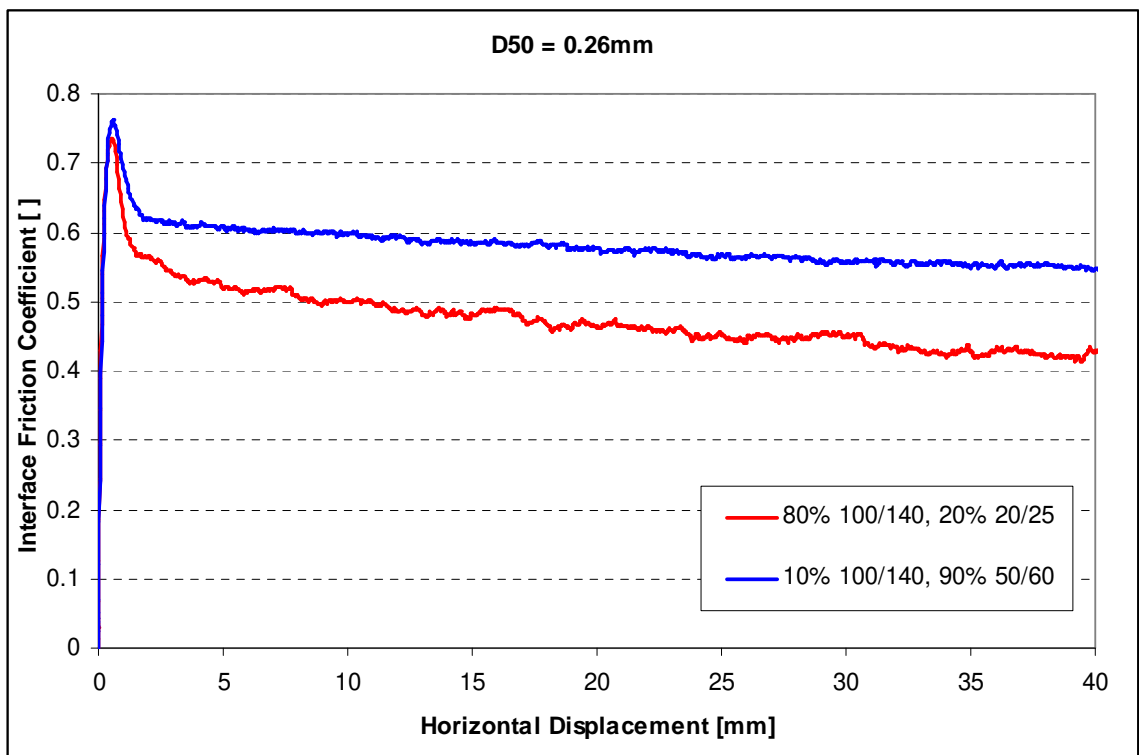


Figure 6.13 Different Mixtures with d_{50} of 0.26mm

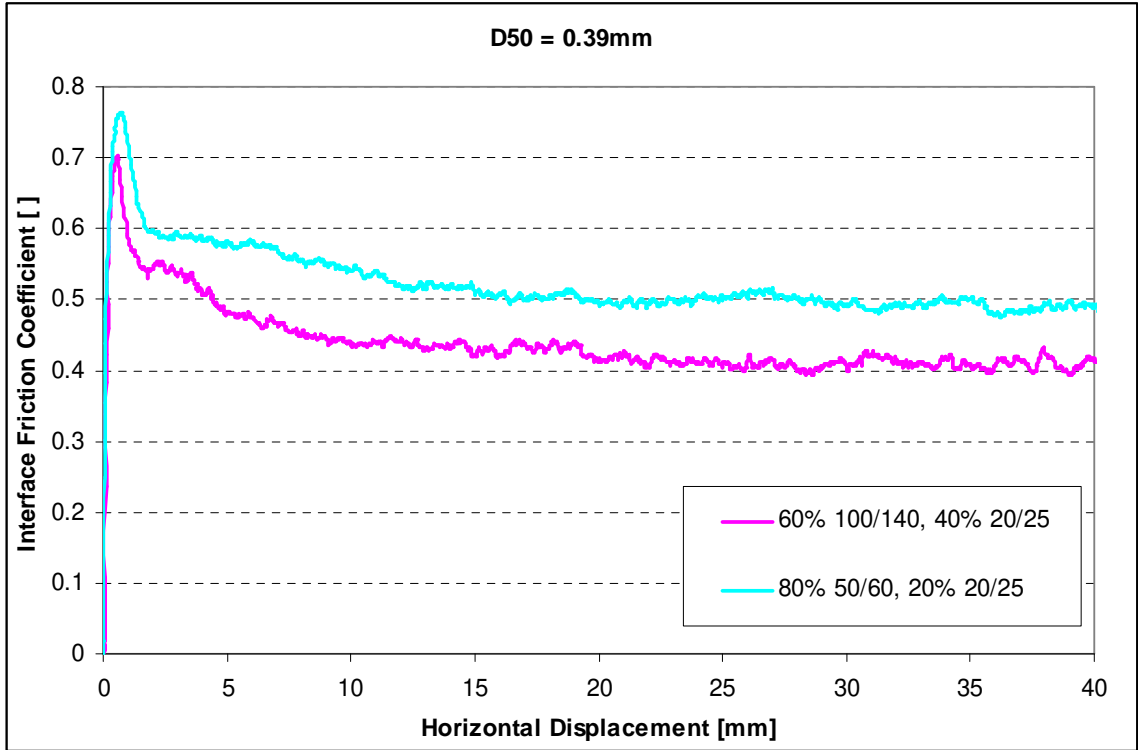


Figure 6.14 Different Mixtures with d_{50} of 0.39mm

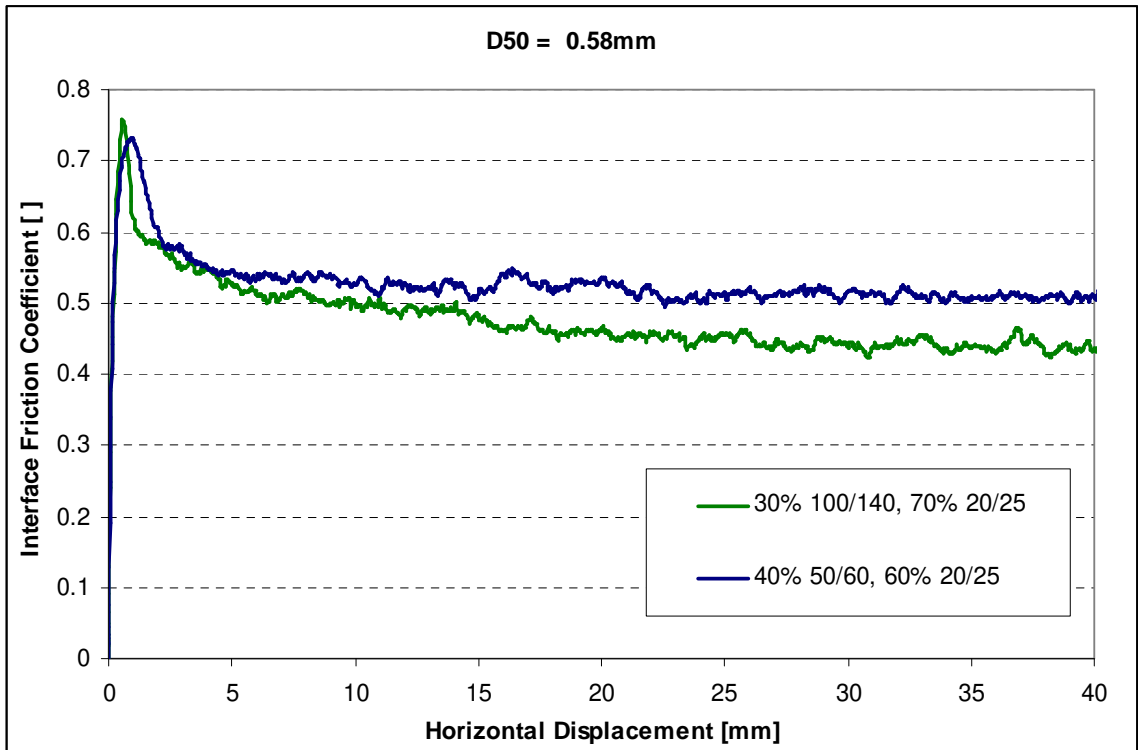


Figure 6.15 Different Mixtures with d_{50} of 0.58mm

A number of observations can be made:

- In each case there is a clear distinction between the two different mixtures
- Differences are observed both at the peak friction coefficient as well as in the post-peak (large-strain) region, with more pronounced differences occurring in the post-peak region.
- In Figure 6.3 it can be seen how the mixture with a percentage of finer particles of 40% (the most stable mixture) shows greater strength than the less stable mixture with 30% finer particles.

Further quantitative assessments cannot be made with confidence since the mixtures are all comprised of different particles in different proportions. In order to assess the effect that the binary nature of the mixtures has on the interface shear behavior the different aspects (mix percentage, size ratio, surface roughness) all need to be considered in isolation.

6.4. Aggregate Analysis of Results

The stress-strain curves shown in the previous section were analyzed further and the strength data combined with the roughness data. The resulting plots show the typical bilinear nature of the relationship. Up to a certain critical roughness the strength increases as the roughness increases. Past this critical roughness the strength is constant, despite increasing the roughness. This indicates that the interface strength is now solely controlled by the particles, and that the surface has no further influence.

6.4.1. Peak Interface Shear Strength – Uniform Sands

Figure 6.16 and Figure 6.17 both show how the peak friction coefficient varies with normalized roughness. Figure 6.16 shows R_n (calculated using the mean value) and

the expected bilinear nature of the plot is evident. The figure confirms what was observed in the stress-strain plots; that the peak shear strength is well correlated with surface roughness up to a certain critical roughness.

Figure 6.17 shows the same shear test data but this time with the normalized roughness expressed by mR_n . The same bilinear nature of the plot is observed, although the horizontal scaling is different.

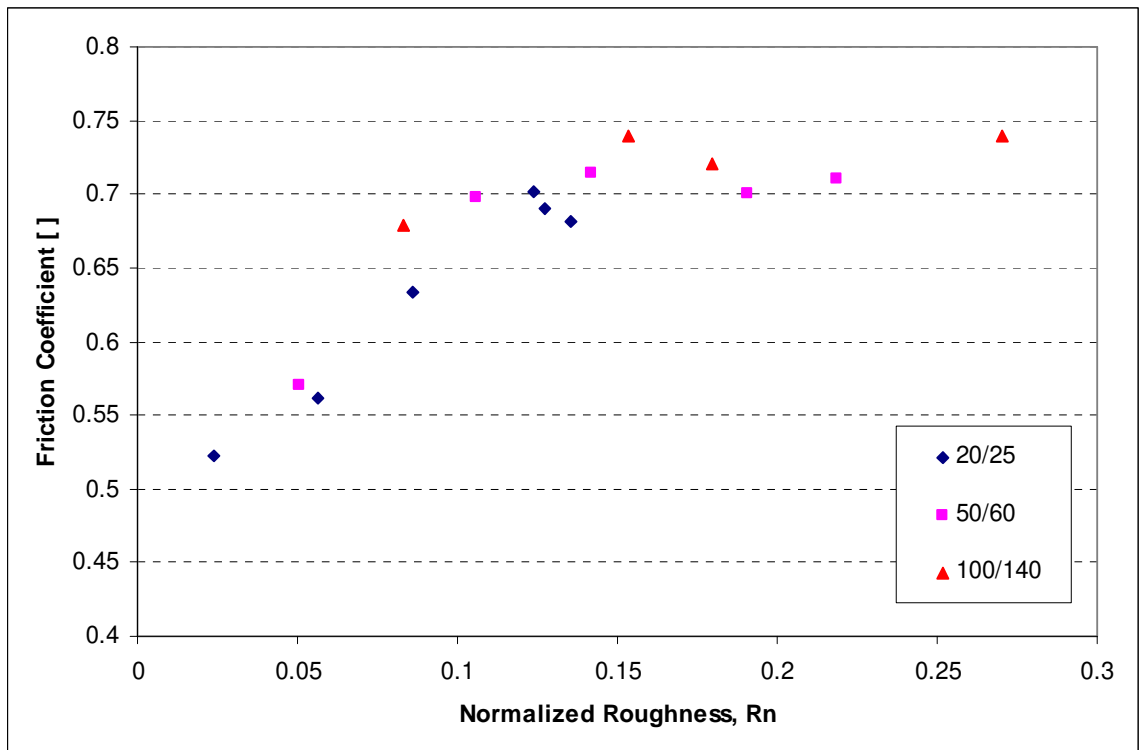


Figure 6.16 Normalized Roughness, R_n (using the mean)

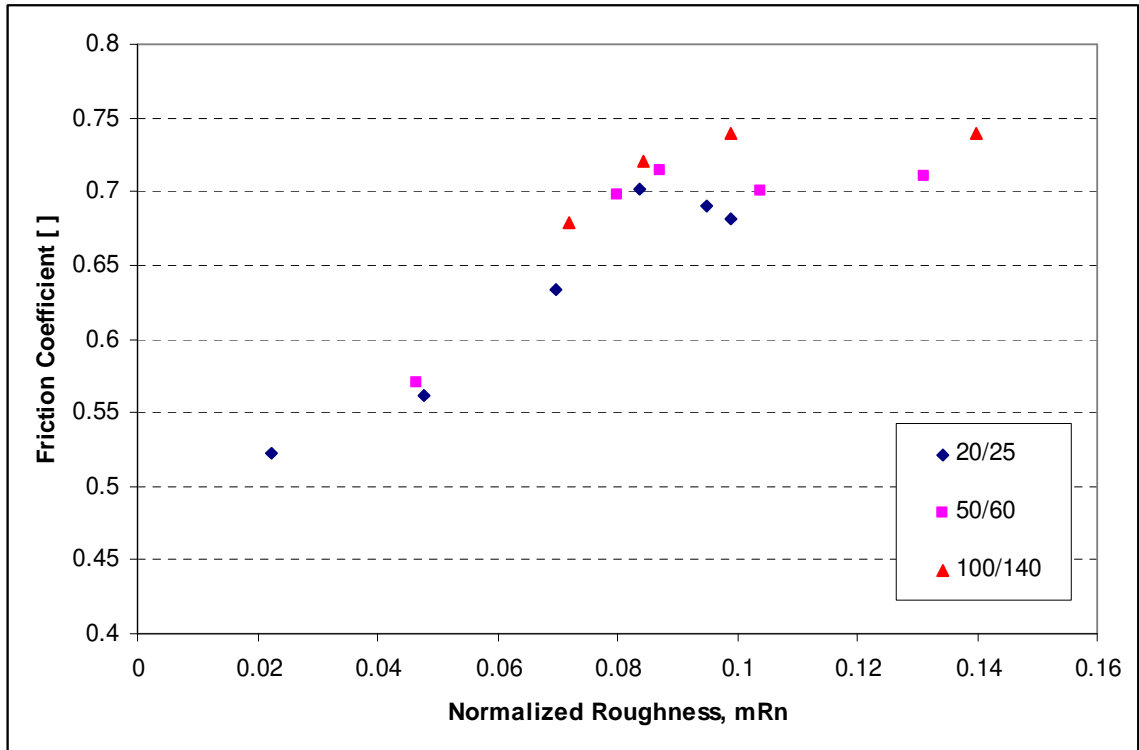


Figure 6.17 Normalized Roughness, mRn (using the mode)

Despite the modal value being expected to perform better as a normalizing value, the two figures above do not display any advantage to one method or another.

It is interesting to note that for the 100/140 sand, mRn displays the data almost as points on a smooth curve. The upper limit of the interface friction coefficient for these uniform sands is approximately 0.74, corresponding to a friction angle of 36.5 degrees. This is very close to the experimentally obtained value from the direct shear tests carried out and presented in Chapter 4. The peak internal friction angle of the soils used in this study was found to be approximately 37 degrees at a normal stress of 100 kPa (refer to Table 4.2).

6.4.2. Post Peak Interface Shear Strength – Uniform Sands

The post-peak interface shear strength can be plotted in a manner similar to the plots above. Figure 6.18 and Figure 6.19 show the post-peak interface friction coefficient plotted against normalized roughness. . Figure 6.18 is plotted using the mean R_n parameter while Figure 6.19 is plotted using the modal R_n parameter mR_n .

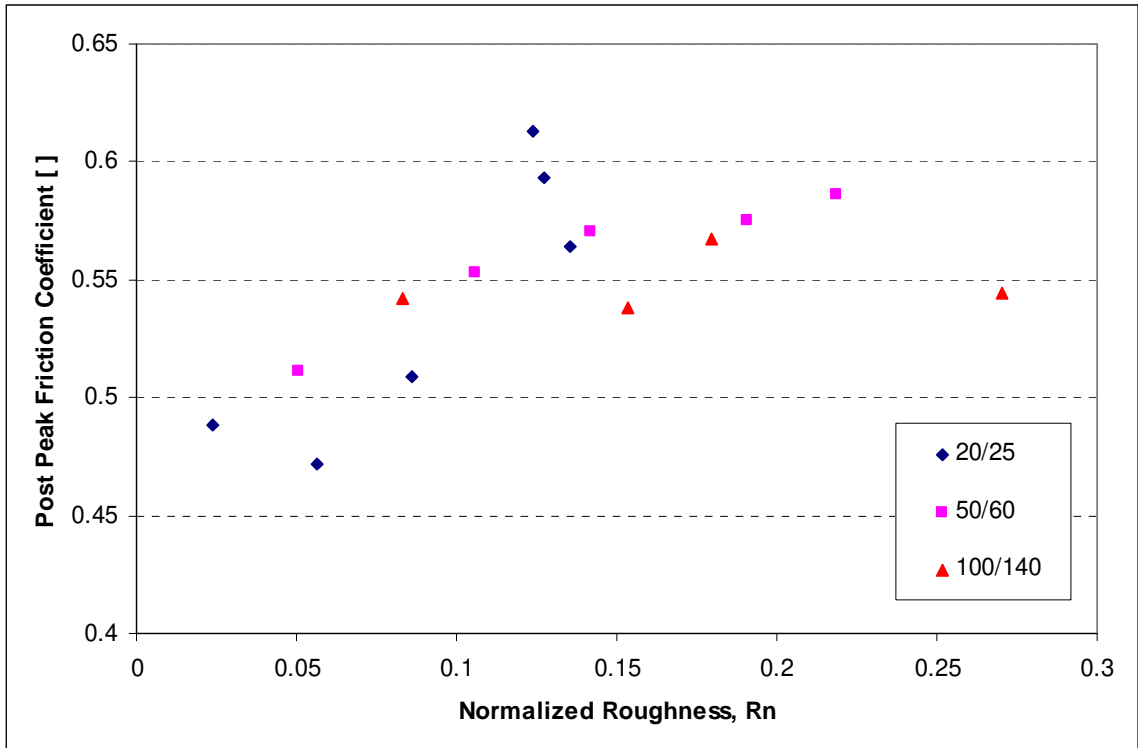


Figure 6.18 Post-Peak, Normalized Roughness, R_n (using the mean)

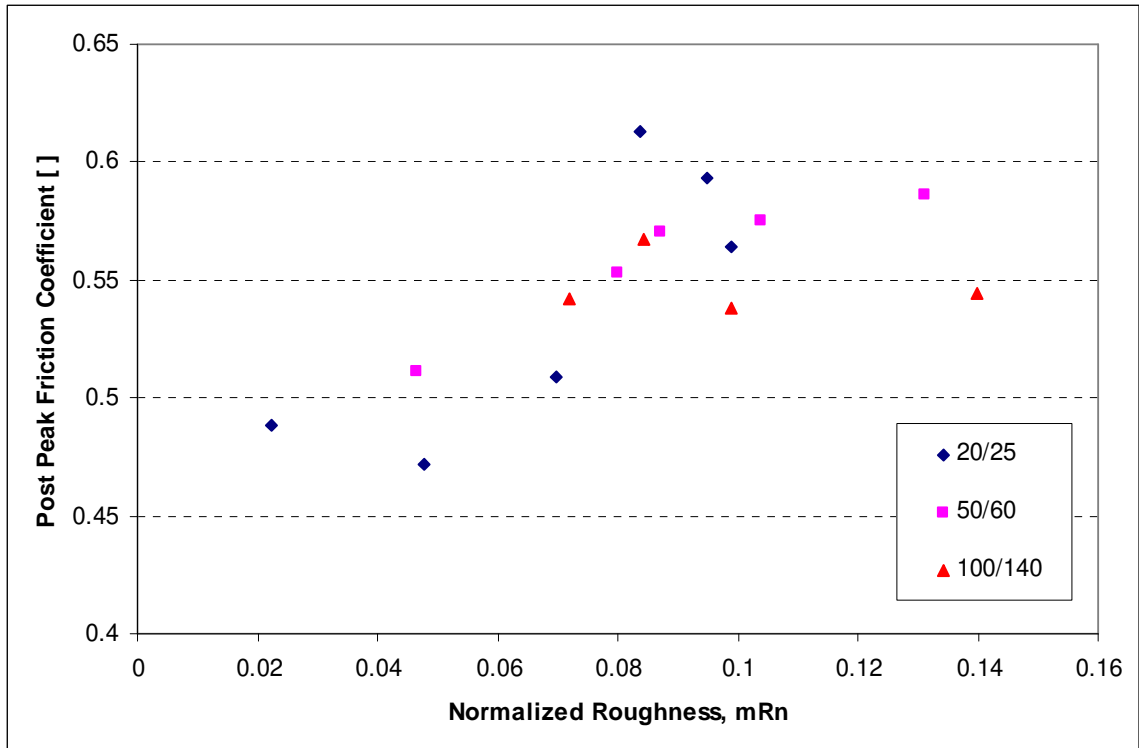


Figure 6.19 Post-Peak, Normalized Roughness, mRn (using the mode)

The plots for the post-peak interface friction coefficient are again similar to each other, with just minor horizontal scaling being the main difference, indicating that the choice of normalized roughness parameter does not significantly alter the relationship between friction coefficient and roughness.

In the case of post-peak friction coefficient, however, the trends appear to be dependant on the particle size. The largest particles, as indicate by the dark blue dots on the figures, show a trend where an increasing normalize roughness leads to an increasing post-peak friction coefficient, although with some scatter at the largest normalized roughness values. The intermediate particle size, as indicated by the pink dots, indicates a bilinear type of relationship, as was observed in all cases for the peak friction coefficient. The smallest particle size tested, indicated by the red dots, presents as a constant value, but with some scatter in the data.

6.4.3. Peak Interface Shear Strength – Mixed Sands

Figure 6.20 and Figure 6.21 provide a summary of 17 interface shear tests carried out on various combinations of particle mixtures and counterface surfaces. All tests were conducted at 100 kPa normal stress with the samples prepared to a relative density between 80 and 85%. Further details are provided in Table 6.6 below. For each test, three different representative particle sizes were determined: the weighted average, two section and three section representations of the most applicable particle size. These sizes were then used to calculate the R_n and mR_n parameters for each combination of particle size and sandpaper.

Table 6.6 Interface Shear Test Data for Rough Counterfaces

P.S.R.	% finer	Sand-paper	Peak Fric. Coeff.	W.A.		Two Section		Three Section	
				Size [mm]	Rn	Size [mm]	Rn	Size [mm]	Rn
2.1	10	100	0.774	0.265	0.222	0.28	0.218	0.28	0.218
2.8	10	80	0.694	0.73	0.131	0.78	0.127	0.78	0.127
2.8	10	100	0.763	0.73	0.140	0.78	0.135	0.78	0.135
2.8	10	150	0.667	0.73	0.089	0.78	0.086	0.78	0.086
2.8	10	600	0.505	0.73	0.024	0.78	0.023	0.78	0.023
2.8	40	80	0.731	0.58	0.146	0.78	0.127	0.53	0.152
2.8	40	100	0.732	0.58	0.159	0.78	0.135	0.53	0.166
2.8	40	150	0.75	0.58	0.101	0.78	0.086	0.53	0.106
2.8	40	600	0.53	0.58	0.031	0.78	0.023	0.53	0.031
2.8	60	80	0.696	0.48	0.159	0.28	0.190	0.28	0.190
2.8	60	150	0.729	0.48	0.111	0.28	0.141	0.28	0.141
2.8	60	600	0.536	0.48	0.034	0.28	0.050	0.28	0.050
2.8	80	100	0.764	0.38	0.194	0.28	0.218	0.28	0.218
6.1	10	100	0.752	0.715	0.142	0.78	0.135	0.78	0.135
6.1	30	100	0.759	0.585	0.158	0.78	0.135	0.78	0.135
6.1	60	100	0.702	0.39	0.192	0.13	0.270	0.13	0.270
6.1	80	100	0.736	0.26	0.224	0.13	0.270	0.13	0.270

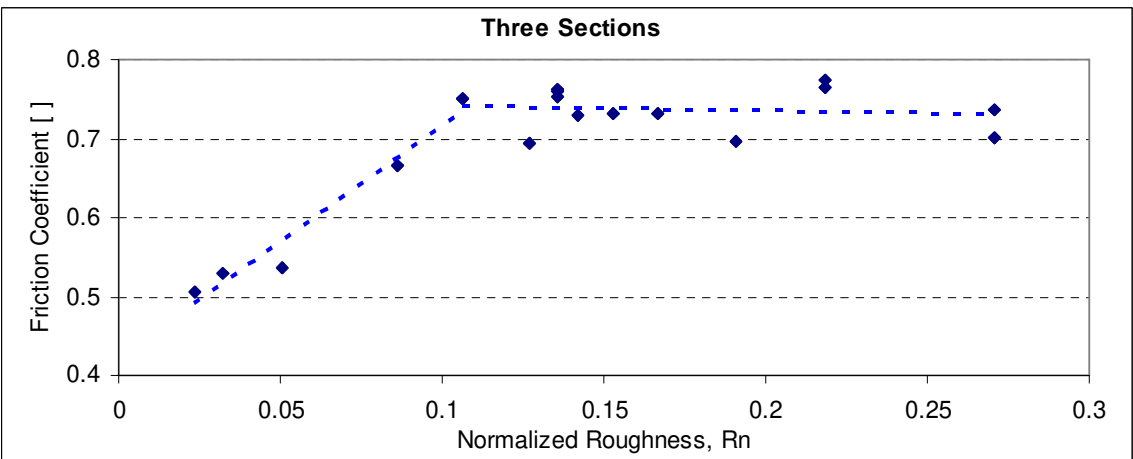
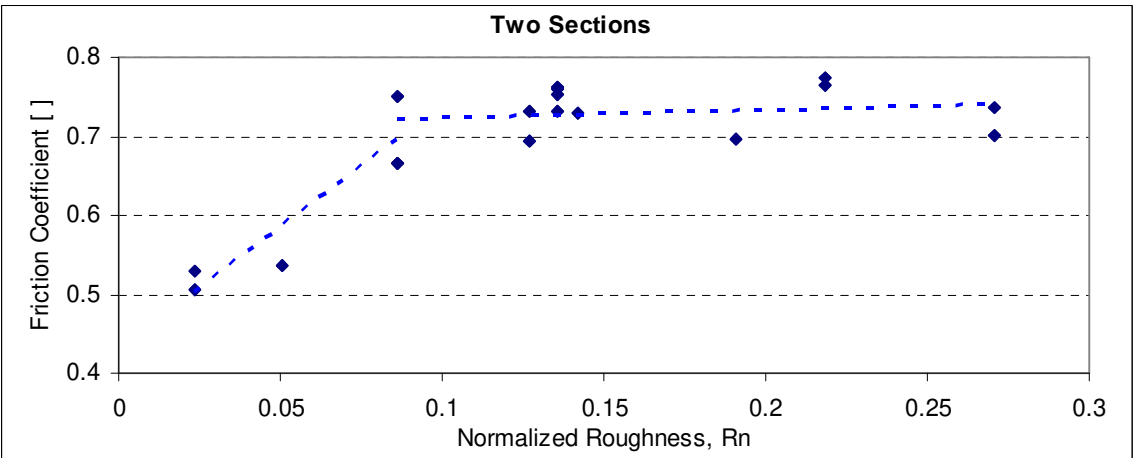
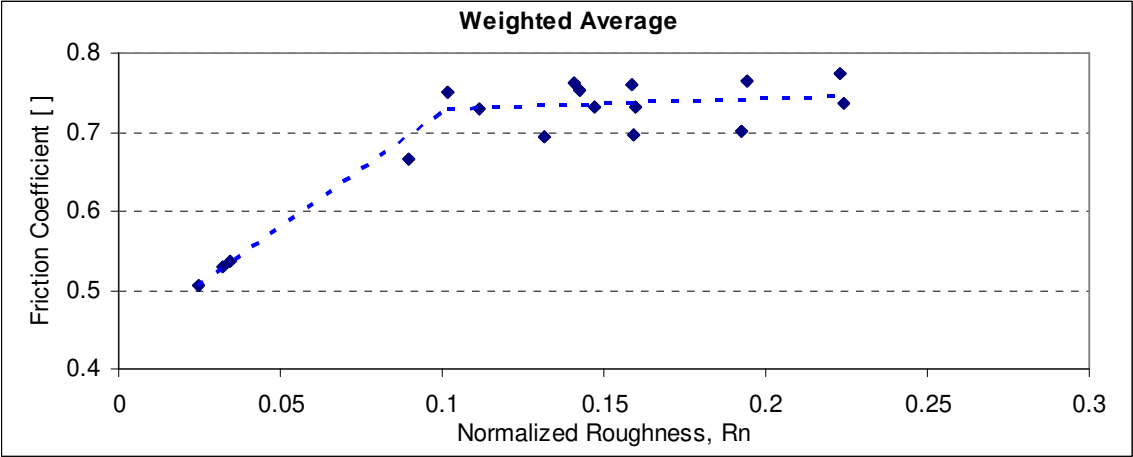


Figure 6.20 Normalized Roughness, Rn, for mixed sands

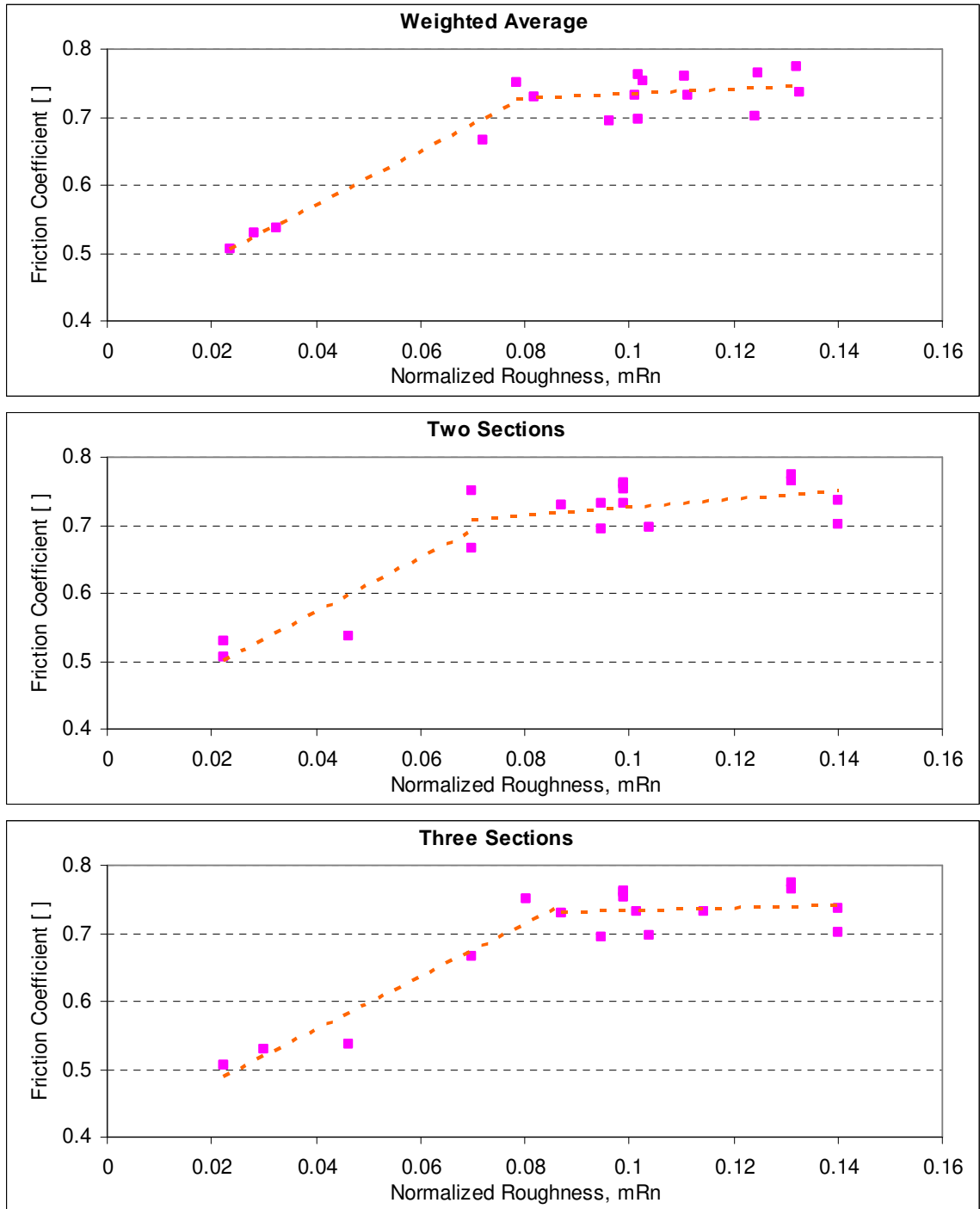


Figure 6.21 Normalized Roughness, mRn, for mixed sands

As can be see in the figure, the bilinear nature of the behavior is preserved regardless of which particle size measure or which measure of roughness is used. The three section approach does reduce the scatter in the data more than the other two

approaches do. Given that the range of mixture proportions and difference in particle sizes is large, some scatter in the data is inevitable. The maximum friction coefficient reached is, again, very similar to that obtained from the uniform sands and from the direct shear tests conducted on the same materials.

6.4.4. Post Peak Interface Shear Strength – Mixed Sands

Aggregate data for the post-peak interface friction coefficient is presented in Figure 6.22 and Figure 6.23 below. Regardless of the normalized roughness parameter chosen, the data shows that the interface friction coefficient is largely independent of the normalized roughness. There is however a range of values for the interface friction coefficient, with a minimum of approximately 0.40 and a maximum of approximately 0.56. This range of values corresponds to interface friction coefficients of 21.8 to 29.2 degrees, a relatively wide band. The range of values must be considered in light of the significant differences in particle size, mixture ratios and surface roughness, all reflected in the data.

A value of approximately 20 degrees would be a conservative estimate for the post-peak interface friction angle for binary mixtures in contact with rough surfaces.

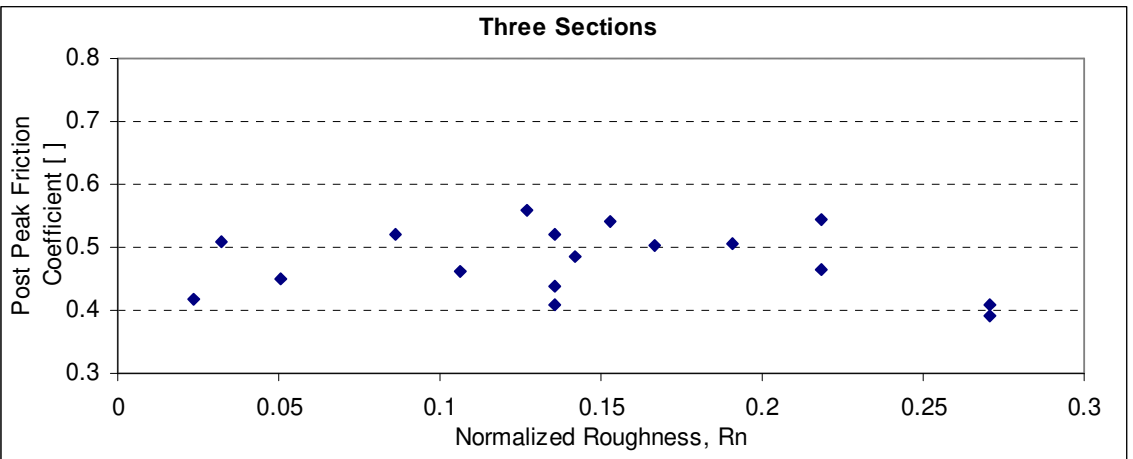
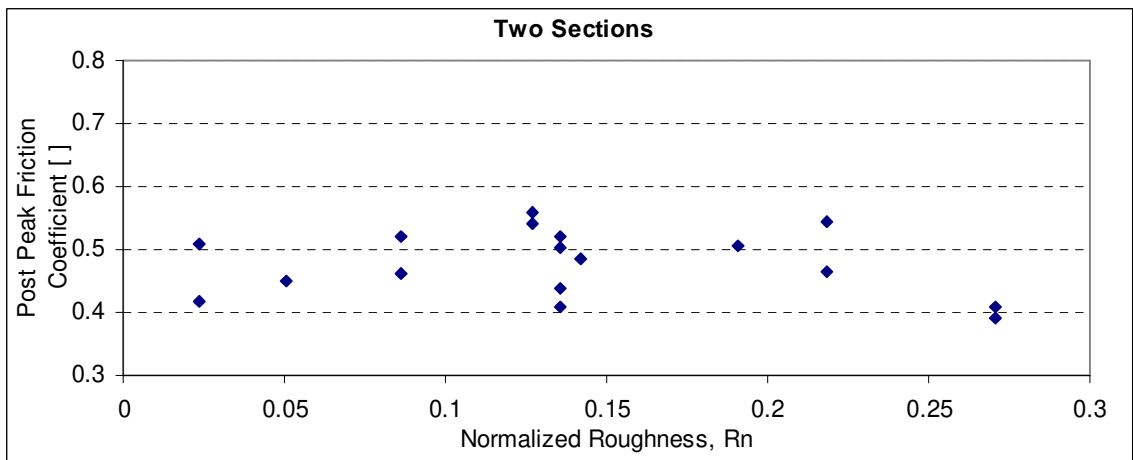
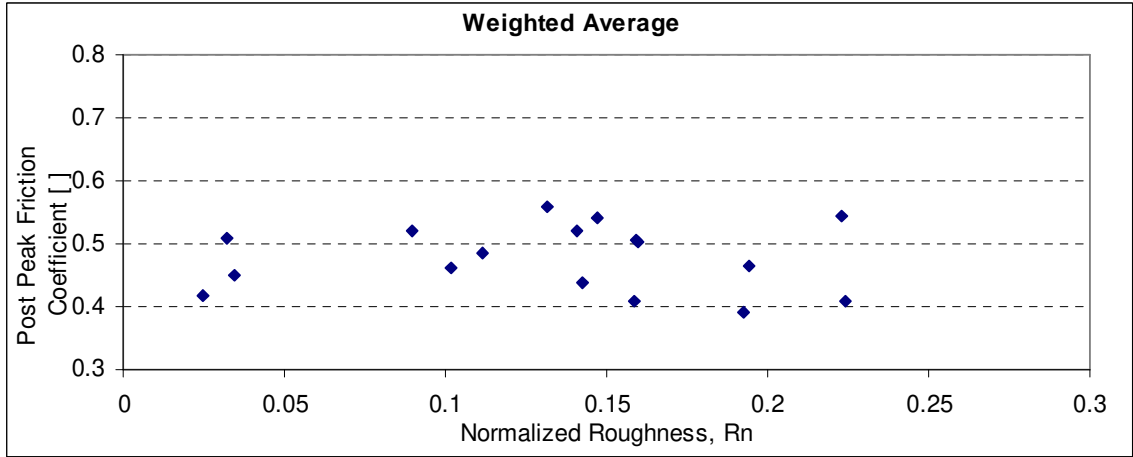


Figure 6.22 Post Peak, Normalized Roughness, Rn, for mixed sands

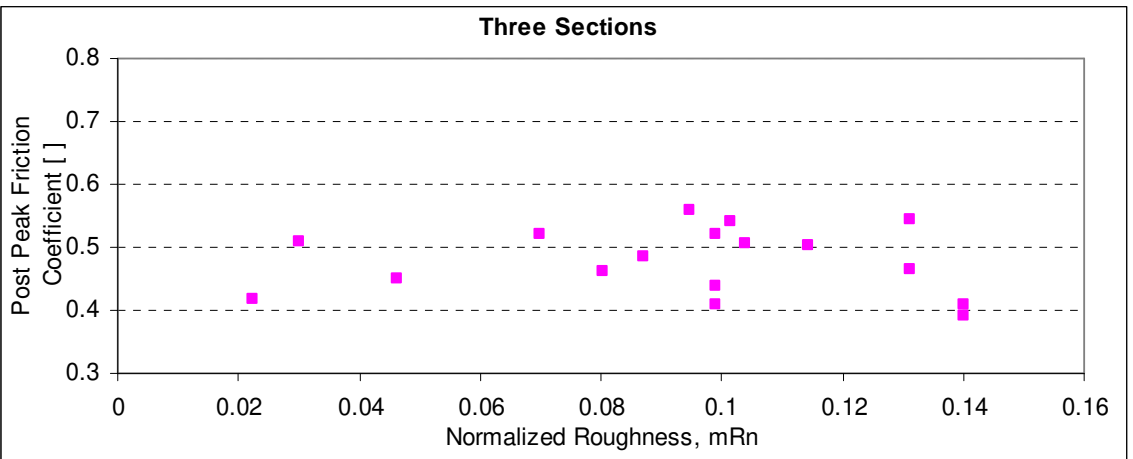
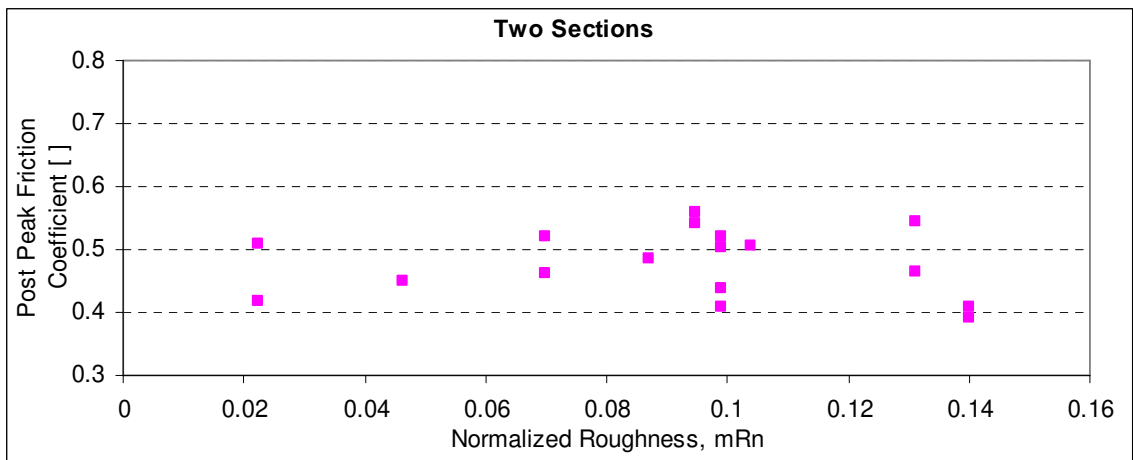
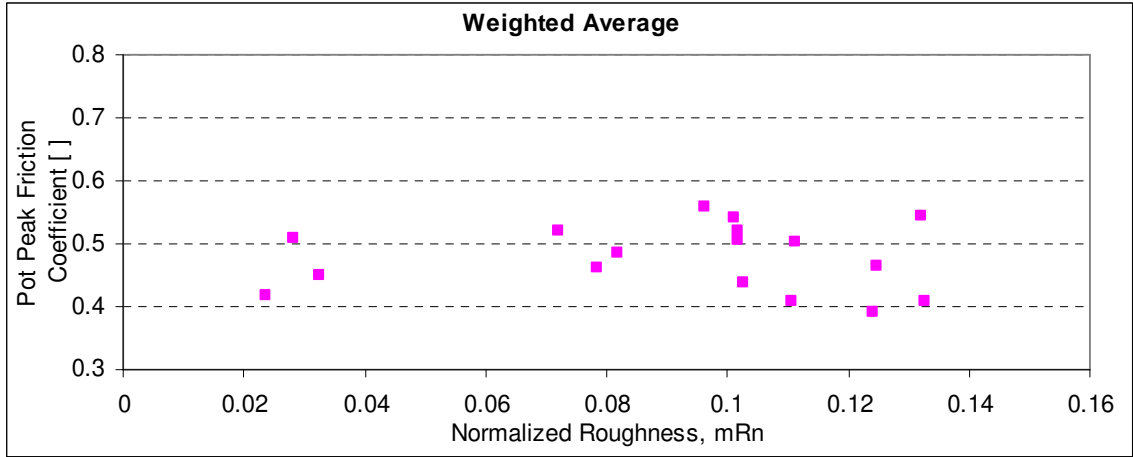


Figure 6.23 Post Peak, Normalized Roughness, mRn, for mixed sands

Table 6.7 Interface Shear Test Data for Rough Counterfaces

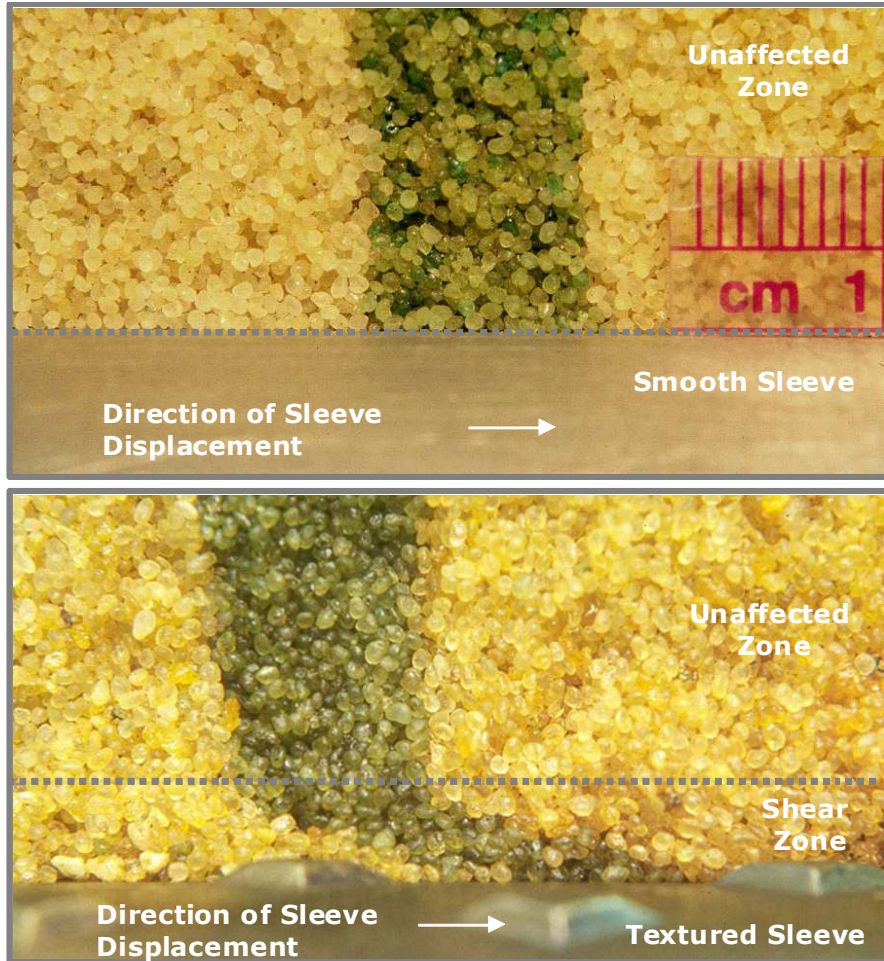
P.S.R.	% finer	Sand-paper	Post Peak Fric. Coeff.	W.A.		Two Section		Three Section	
				Size [mm]	Rn	Size [mm]	Rn	Size [mm]	Rn
2.1	10	100	0.545	0.265	0.222	0.28	0.218	0.28	0.218
2.8	10	80	0.559	0.73	0.131	0.78	0.127	0.78	0.127
2.8	10	100	0.520	0.73	0.140	0.78	0.135	0.78	0.135
2.8	10	150	0.522	0.73	0.089	0.78	0.086	0.78	0.086
2.8	10	600	0.417	0.73	0.024	0.78	0.023	0.78	0.023
2.8	40	80	0.541	0.58	0.146	0.78	0.127	0.53	0.152
2.8	40	100	0.503	0.58	0.159	0.78	0.135	0.53	0.166
2.8	40	150	0.463	0.58	0.101	0.78	0.086	0.53	0.106
2.8	40	600	0.510	0.58	0.031	0.78	0.023	0.53	0.031
2.8	60	80	0.506	0.48	0.159	0.28	0.190	0.28	0.190
2.8	60	150	0.484	0.48	0.111	0.28	0.141	0.28	0.141
2.8	60	600	0.451	0.48	0.034	0.28	0.050	0.28	0.050
2.8	80	100	0.464	0.38	0.194	0.28	0.218	0.28	0.218
6.1	10	100	0.437	0.715	0.142	0.78	0.135	0.78	0.135
6.1	30	100	0.409	0.585	0.158	0.78	0.135	0.78	0.135
6.1	60	100	0.392	0.39	0.192	0.13	0.270	0.13	0.270
6.1	80	100	0.408	0.26	0.224	0.13	0.270	0.13	0.270

6.5. Shear Zone Thickness

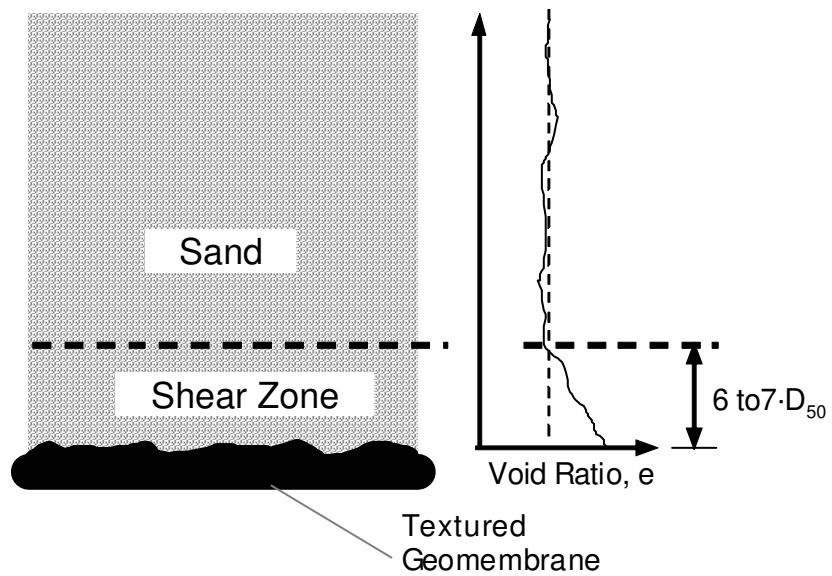
The primary purpose for designing a new shear box with a transparent window was to enable the direct observation of the interface during shear. While only the particles

in direct contact with the window can be seen, these observations still allow for some general observations regarding the thickness of the shear zone.

Previous research indicates that there exists a heavily sheared and rearranged zone of particles that extends upwards into the soil mass away from the interface. This has been observed both experimentally and in numerical simulations. This shear zone, which can be thought of as one-half of a shear band, can be directly observed or inferred from local void ratio measurements. Both of these are shown below in Figure 6.24.



(a) Frost et al., 2004



(b) Lee (2011), personal communication

Figure 6.24 Evidence of Shear Zone adjacent to Interface

Figure 6.24 (a) shows the end condition of two tests performed with Ottawa 20/30 sand at a normal stress of 50 kPa. For the smooth sleeve, no shear zone is evident, indicating that only sliding at the interface is occurring. For the textured sleeve, a shear zone is clearly evident, showing a horizontal deformation of the dyed sand column of approximately 11mm, with a total shear displacement of 63.5 mm. The thickness of this shear zone is approximately 5 to 7 particle diameters.

Figure 6.24 (b) shows how the local void ratio changes as a function of distance away from an interface, in this case for an interface that is a textured geomembrane. The void ratio increases in the shear zone due to localized dilation, occurring to allow for particle rearrangement which, in turn, facilitates continuing shearing. The thickness of the shear zone is indicated to be approximately 6 to 7 particle diameters.

The shear zone thickness was measured in this study by placing a light cotton thread inside the shear box against the transparent window. The thickness of the shear zone could thus be measured directly with a ruler placed against the window. This is illustrated in Figure 6.25 below, for a sample of P.S.R. 6.1 with 30% finer particles in contact with sand paper #100.

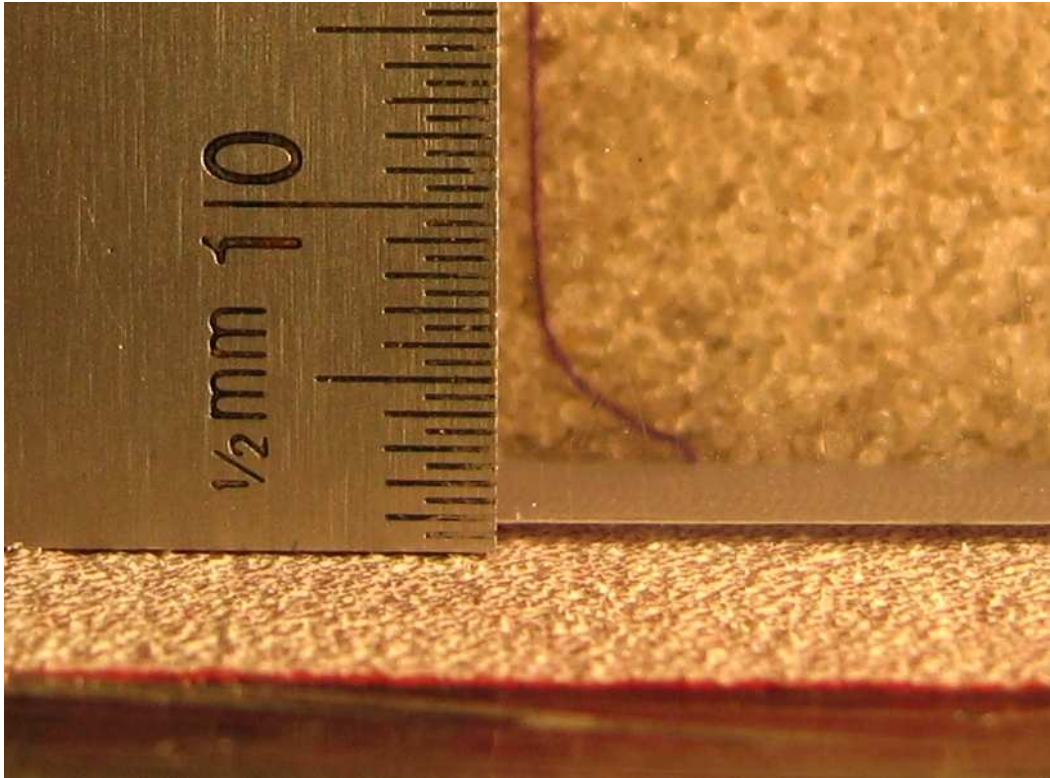
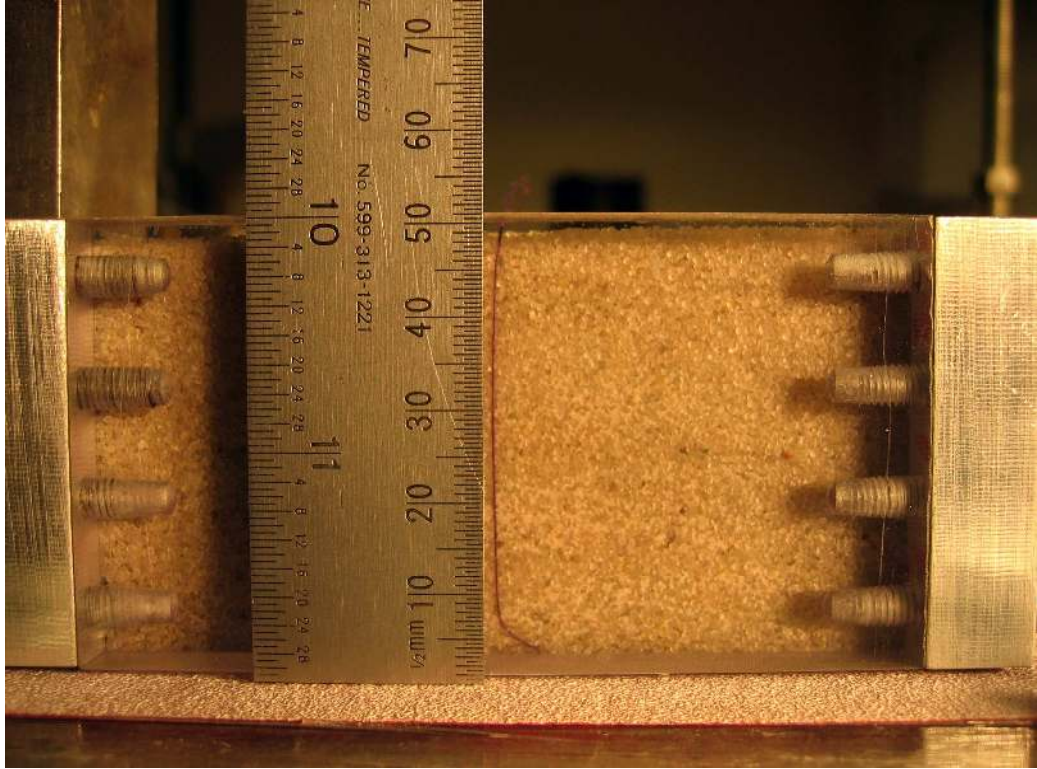


Figure 6.25 Measurement of Shear Zone Thickness

6.5.1. Shear Zone Thickness of Uniform Sands

For uniform sands, the results are shown in Table 6.8 below.

Table 6.8 Shear Zone Thickness for Uniform Sands

Counterface Material	Shear Zone Thickness (mm)		
	20/25	50/60	100/140
Steel	0	1.0	0.5
SP #60	5.0	--	--
SP #80	5.0	2.5	--
SP #100	5.0	--	1.5
SP #150	4.0	2.5	1.5
SP #320	5.0	2.5	1.0
SP #600	5.0	2.5	1.5
Average	6.2 d₅₀	8.9 d₅₀	10.6 d₅₀

These results compare well with other published data as is shown in Figure 6.26 below. The red circles are the data points from this study, and it is clear how they follow the same general trend indicated in the plot. This general trend shows a decreasing shear zone thickness (in terms of d_{50}) as the particle size increases. Analysis of Table 6.8 shows that the absolute thickness of the shear zone increases with particle size. Another noteworthy aspect of the data in Table 6.8 is that the shear zone thickness is independent of the surface roughness, once the surface roughness is greater than some critical level. In all of these cases, however, that critical level has been exceeded for even the combination of the largest particles and finest sandpaper grit (#600).

The development of a shear zone is thus very sensitive to some small level of surface roughness, but the thickness of the shear zone is not sensitive to the degree of texturing.

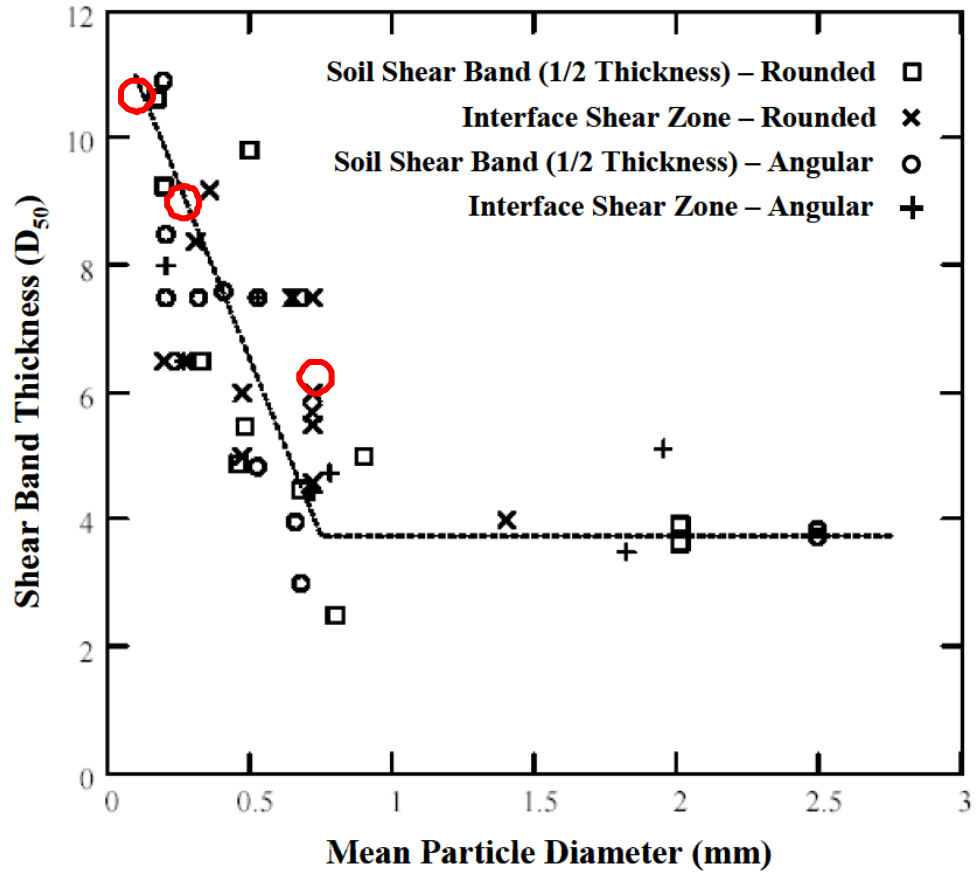


Figure 6.26 Shear Zone Thickness for Uniform Sands

6.5.2. Shear Zone thickness of Binary Mixtures

The shear zone thickness of binary mixtures was also investigated, the results are shown in Table 6.9 Shear Zone Thickness for Binary Mixtures Table 6.9 and Figure 6.27 below.

Table 6.9 Shear Zone Thickness for Binary Mixtures

P.S.R.	% Finer Particles	Sandpaper	Shear Zone Thickness (mm)
2.8	10	80	5.0
2.8	10	100	5.0
2.8	10	150	5.0
2.8	10	600	4.5
2.8	40	80	3.0
2.8	40	100	2.5
2.8	40	150	2.5
2.8	40	600	2.5
2.8	60	80	3.0
2.8	60	150	3.0
2.8	60	600	3.0
6.1	10	10	5.0
6.1	30	30	5.0
6.1	60	60	3.0
6.1	80	80	2.5

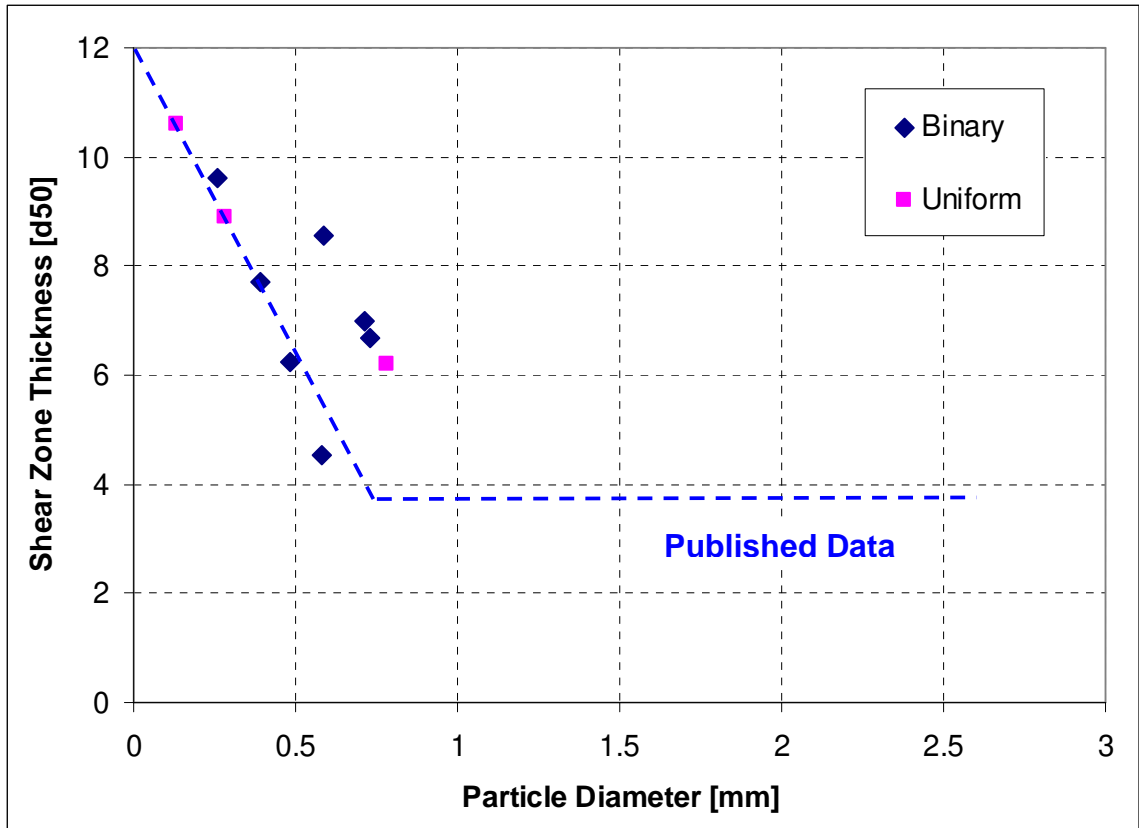


Figure 6.27 Shear Zone Thickness for Binary Mixtures

Based on the data presented for binary mixtures it is clear that for a given binary mixture, the degree of surface roughness does not play a role in determining the thickness of the shear zone. This finding is the same as was found for uniform sands.

The trend of a decreasing shear zone thickness (in terms of d_{50}) was also found to hold for binary mixtures, in the same way as for uniform sands.

The thickness of the shear zone (in terms of absolute thickness) is shown, in general, to decrease as the average particle size decreases.

7. CONCLUSIONS AND RECOMMENDATIONS

7.1. Introduction

This dissertation has presented the results of an experimental study focused on the behavior of binary particle mixtures in contact with continuum surfaces. A variety of particle mixtures and counterface surfaces were studied. This particulate-continuum interface is present in many geotechnical engineering applications, including deep foundations, geosynthetic liners, trenchless technologies, and many earth retaining systems. The behavior of many of these systems is controlled by the particulate-continuum interface and thus an understanding of the mechanisms governing interface behavior is essential for the improvement of geotechnical engineering design. This in turn results in improved safety and cost-efficiencies which benefit society at large.

The behavior of binary particle mixtures was investigated and new insights into the relationship between size ratio, mixture percentage and void ratio was observed. The behavior of particle mixtures in contact with smooth surfaces was also shown to be noticeably different from uniform particles. The investigations carried out have shown the importance of the relationship between the length scales of the particles and the surface features. In addition, the particle size distribution and the distribution of surface feature sizes also play a role. A new method for quantifying these relationships was proposed.

The findings of this experimental study provide a basis for future numerical simulations to extend the findings to different materials and interface systems.

This chapter summarizes the conclusions based on the research conducted and presents recommendations for further study in this area.

7.2. Conclusions

7.2.1. Binary Particle Mixtures

7.2.1.1. *Packing of Mixtures*

- The minimum void ratio for a particle mixture occurs at a mixture ratio of between 25% and 35% finer particles by mass.
- The lowest value for the maximum void ratio occurs at a mixture ratio of approximately 35% to 40%.
- The greater the particle size ratio the lower the amount of finer material is required to obtain the minimum void ratio.
- A new parameter, VRR, was developed to isolate the effect of mixing on the packing of particle mixtures.
- Using VRR it is clear that for the minimum void ratio case the largest reduction in void ratio due to mixing occurs for ratios of finer material between 30% and 40%. The data shows that for larger particle size ratios the amount of finer material to have an equivalent effect is lower.
- For the maximum void ratio case, the amount of finer material required to exhibit the largest decrease in void ratio due to mixing is independent of particle size ratio and occurs at approximately 40% of finer material by mass.
- Divergence in the VRR between the minimum and maximum void ratio cases occurs for all particle size ratios at approximately 60% finer particles by mass, this indicates the transition from a matrix dominated by finer particles (greater than 60% finer particles) to a transitional matrix,

where both fine and coarse particles have influence on the mixture properties.

- Mixing two particles together in ratios of greater than approximately 60% finer particles does not alter the way in which the particles pack together. At any ratio greater than 60% the packing structure remains essentially the same. Note that coordination number and void ratio do change, but the presence of the larger particles does not alter the way in which the smaller particles are arranged.
- The relationship between e_{\min} and e_{\max} is not constant, but varies as a function of both the particle size ratio and mixture ratio. This e_{\min}/e_{\max} relationship is particularly sensitive at low concentrations of finer particles and higher particle size ratios.
- The e_{\min}/e_{\max} ratio becomes substantially less influenced by particle size ratio when the amount of finer material reaches 50%.
- Segregation between the two different components during limiting void ratio tests was minimal. Some minor segregation occurred in the lowest layers of particles as a result of the manner in which the particles were initially placed inside the pipe. The minor degree of segregation is not expected to influence the results in a meaningful way.

7.2.1.2. Mixture Shear Strength

- The large displacement strength of mixtures is bounded by the large displacement strength of the uniform soils.

- Peak strengths of mixtures are not similarly bounded by uniform soils. In this case the strengths of uniform soils form an upper bound at low normal stresses while at higher normal stresses they tend towards the bottom of the peak strength envelope.
- The dilatancy angle is significantly affected by the mixture ratio. A change from 20% to 100% finer particles exhibits a change in the dilatancy angle twice that of a change in applied normal stress of 50 kPa to 500 kPa.

7.2.2. Interface Shear with Smooth HDPE Counterface

7.2.2.1. Uniform Sands

- Peak friction coefficient decreases with increasing normal stress for all particles tested.
- Post-peak friction coefficient decreases with increasing normal stress for all particles tested.
- Absolute particle size, for the range of sizes tested, does not play a role in determining the friction coefficient

7.2.2.2. Particle Mixtures

- Mixture proportion (percentage of finer particles) has a far greater effect on the friction coefficient than the particle size ratio.
- The 20% and 40% mixtures all show an “elbow” after which the peak friction coefficient increases within creasing normal stress.

- The 70% mixtures show the same trend as the uniform sands, most likely since these mixtures are dominated by the finer particles (greater than 60% finer particles).

7.2.2.3. Induced Roughness

- Induced roughness, as measured by Ra, shows a consistent linear increase with increasing normal stress for uniform mixtures.
- For uniform particles the dominant wavelength is seen to increase as the particle size is increased, corresponding to larger induced features from the larger particles
- For particle mixtures sheared under a normal stress of 500 kPa the 20% and 40% mixtures show the greatest induced roughness

7.2.2.4. Contact Mechanics Based Interface Friction Model

- A model to estimate the interface friction coefficient was developed based on Hertzian contact theory and Bhushan plowing equation. This is believed to be the first time that plowing was directly incorporated into a model estimating the friction coefficient for an assembly of particles in contact with a surface.
- The model can reasonably accurately predict values for the friction coefficient provided that the values of α and τ_0 are known with some certainty.
- The model shows that the friction coefficient is not sensitive to the packing density of the particles.

- The increase in friction coefficient due to plowing can be modeled by incorporating a factor to increase the plowing component.

7.2.3. Interface Shear with Rough Counterface

7.2.3.1. Relative Roughness

- An alternative measure of relative roughness was proposed, using the modal value of local R_{max} instead of the mean value. This was based on the insights gained from fitting a log-normal distribution to the local R_{max} histograms. The log-normal distribution was shown to be valid for a range of surface profiles and particle sizes.
- The proposed measure of relative roughness, mR_n , can exhibit a peak, indicating that surface roughness does not necessarily decrease as particle size increases, as was previously thought.

7.2.3.2. Interface Shear Strength

- D_{50} is not necessarily an appropriate descriptor for particle size when interface shear behavior is concerned
- D_{50} is far from being a unique property of a soil. The continued use of d_{50} is detrimental to this field of research as it obscures potentially relevant findings related to particle size and particle size distribution.
- Peak shear strength is dominated by having at least one component in the fully rough zone, particles need to engage to create that strength although a high percentage is not required
- For a given surface:

- a mixture of two components will exhibit a weaker residual strength than a uniform material
- The greatest peak interface shear strength is exhibited by the mixture that has a ratio closest to that ratio with which the minimum void ratio is obtained
- In general, an increase in percentage of finer particles leads to a decrease in post-peak strength
- Very minor amounts of surface texturing is required to significantly effect the interface shear behavior
- Surface roughness is well correlated to peak interface strength up to the point of critical roughness, thereafter becoming a non-factor
- Post-peak strength is correlated to surface roughness, even beyond the critical roughness
- Various methods of calculating an average particle size for a binary mixture were presented. The three-sectional approach was shown to be most suitable for describing the interface friction coefficient for binary particle mixtures.

7.2.3.3. Shear Zone Thickness

- For both uniform sands and binary mixtures the shear zone thickness was found to decrease (in terms of d_{50}) with increasing particle size, and data presented agrees well with published data sets.

- The thickness of the shear zone was found to be independent of the degree of surface roughness, provided that some minimum amount of surface texturing was present.

7.3. Recommendations for future research

As a result of this research a number of additional questions and areas needing further refinement and/or clarification arose. This indicates the potential for further profitable study in this area. A number of recommendations for future research are presented below.

- Three dimensional numerical simulations using a discrete element methods would be beneficial to further understand the stress distribution at the interface. This would aid in modeling the plowing behavior of mixtures in contact with smooth counterfaces.
- Three dimensional numerical simulations using a discrete element methods would also be beneficial in the study of hard, rough counterfaces. The particle level behavior could then be observed and the understanding of the interplay between surface features and particle size and size distribution could be further developed.
- Temperature effects on the interface shear behavior of binary mixtures in contact with smooth HDPE surfaces could also be examined.
- Counterface surfaces with varying degrees of hardness could be studied. The effects on plowing, wear, the interface shear coefficient and induced roughness could be examined.

- Additional study of statistical measures of particle size distribution for binary mixtures and different distribution types for measures of local R_{\max} values could also be implemented.

APPENDIX A

	20/25	50/60	100/140	e_{max}											e_{min}			
				1	2	3	4	5	6	7	8	9	10	Final	1	2	3	Final
P.S.R. 2.1	0	100	0	0.857	0.857	0.856	0.857	0.855	0.855	0.854	0.857	0.857	0.857	0.857	0.604	0.617	0.606	0.604
	0	90	10	0.819	0.820	0.818	0.818	0.820	0.817	0.818	0.819	0.821	0.819	0.821	0.549	0.545	0.551	0.545
	0	80	20	0.798	0.797	0.798	0.798	0.772	0.800	0.801	0.800	0.799	0.797	0.801	0.507	0.509	0.509	0.507
	0	70	30	0.778	0.777	0.776	0.779	0.781	0.780	0.781	0.778	0.779	0.780	0.781	0.513	0.507	0.501	0.501
	0	60	40	0.768	0.767	0.764	0.762	0.735	0.764	0.767	0.765	0.764	0.766	0.768	0.515	0.508	0.498	0.498
	0	50	50	0.772	0.767	0.771	0.773	0.772	0.773	0.764	0.770	0.771	0.768	0.773	0.521	0.515	0.517	0.515
	0	40	60	0.776	0.777	0.779	0.778	0.778	0.771	0.777	0.778	0.777	0.776	0.779	0.538	0.542	0.542	0.538
	0	30	70	0.810	0.811	0.810	0.810	0.809	0.807	0.811	0.806	0.809	0.809	0.811	0.566	0.569	0.573	0.566
	0	20	80	0.827	0.825	0.831	0.827	0.839	0.836	0.836	0.835	0.834	0.829	0.839	0.594	0.585	0.590	0.585
	0	10	90	0.867	0.866	0.866	0.866	0.865	0.867	0.864	0.866	0.865	0.867	0.867	0.623	0.613	0.616	0.613
	0	0	100	0.895	0.888	0.881	0.898	0.898	0.908	0.896	0.899	0.897	0.898	0.899	0.636	0.648	0.637	0.636
P.S.R. 2.8	100	0	0	0.767	0.763	0.765	0.767	0.767	0.767	0.765	0.764	0.763	0.767	0.767	0.529	0.529	0.534	0.529
	90	10	0	0.702	0.700	0.704	0.704	0.705	0.704	0.700	0.676	0.701	0.704	0.705	0.472	0.469	0.463	0.463
	80	20	0	0.672	0.675	0.676	0.664	0.668	0.672	0.673	0.676	0.668	0.671	0.676	0.421	0.423	0.413	0.413
	70	30	0	0.658	0.651	0.656	0.655	0.659	0.650	0.648	0.658	0.651	0.648	0.659	0.415	0.409	0.418	0.409
	60	40	0	0.654	0.651	0.659	0.656	0.661	0.658	0.652	0.655	0.654	0.651	0.661	0.423	0.410	0.410	0.410
	50	50	0	0.669	0.663	0.668	0.669	0.661	0.667	0.663	0.665	0.665	0.662	0.669	0.444	0.433	0.435	0.433
	40	60	0	0.689	0.682	0.693	0.693	0.691	0.693	0.692	0.687	0.688	0.690	0.693	0.465	0.469	0.464	0.464
	30	70	0	0.723	0.724	0.726	0.725	0.725	0.722	0.719	0.724	0.723	0.721	0.726	0.521	0.507	0.510	0.507
	20	80	0	0.758	0.759	0.759	0.753	0.575	0.758	0.759	0.760	0.760	0.754	0.760	0.524	0.535	0.545	0.524
	10	90	0	0.795	0.806	0.791	0.810	0.811	0.813	0.812	0.808	0.805	0.799	0.813	0.578	0.572	0.572	0.572
	0	100	0	0.857	0.857	0.856	0.857	0.855	0.855	0.854	0.857	0.857	0.857	0.857	0.604	0.617	0.606	0.604
P.S.R. 6.1	100	0	0	0.767	0.763	0.765	0.767	0.767	0.767	0.765	0.764	0.763	0.767	0.767	0.529	0.529	0.534	0.529
	90	0	10	0.662	0.664	0.665	0.663	0.664	0.662	0.665	0.663	0.664	0.666	0.666	0.405	0.393	0.401	0.393
	80	0	20	0.586	0.601	0.605	0.578	0.579	0.602	0.613	0.612	0.604	0.598	0.613	0.281	0.285	0.291	0.281
	70	0	30	0.579	0.578	0.570	0.571	0.575	0.580	0.579	0.578	0.575	0.573	0.580	0.287	0.285	0.287	0.285
	60	0	40	0.551	0.550	0.568	0.563	0.571	0.580	0.570	0.568	0.559	0.563	0.571	0.320	0.319	0.317	0.317
	50	0	50	0.599	0.594	0.596	0.590	0.594	0.589	0.587	0.594	0.597	0.592	0.599	0.387	0.387	0.389	0.387
	40	0	60	0.624	0.633	0.618	0.632	0.611	0.627	0.627	0.616	0.630	0.625	0.633	0.422	0.425	0.417	0.417
	30	0	70	0.691	0.686	0.694	0.693	0.692	0.693	0.692	0.690	0.691	0.688	0.694	0.469	0.475	0.474	0.469
	20	0	80	0.746	0.747	0.749	0.752	0.749	0.740	0.748	0.736	0.747	0.749	0.752	0.536	0.529	0.530	0.529
	10	0	90	0.832	0.832	0.834	0.833	0.830	0.829	0.835	0.834	0.835	0.832	0.835	0.584	0.591	0.583	0.583
	0	0	100	0.895	0.888	0.881	0.898	0.898	0.908	0.896	0.899	0.897	0.898	0.899	0.636	0.648	0.637	0.636

REFERENCES

- Abou-Chakra, H. and U. Tuzun (1999). "Coefficient of friction of binary granular mixtures in contact with a smooth wall - PART I: Direct shear box measurements of the effects of particle size ratio and particle surface roughness." Chemical Engineering Science 54: 5901-5912.
- Abou-Chakra, H. and U. Tuzun (1999). "Coefficient of friction of binary granular mixtures in contact with a smooth wall. Part B. Micro-structural model describing the effects of packing fraction and load distribution on the wall friction of smooth, elastic spheres." Chemical Engineering Science 54: 5913-5925.
- Archard, J. F. (1957). "Elastic Deformation and the Laws of Friction." Proceedings of the Royal Society of London. Series A, Mathematical and Physical Sciences (1934-1990) 243(1233): 190-205.
- Been, K. and M. G. Jefferies (1985). "State parameter for sands." Geotechnique 35(2): 99-112.
- Bhushan, B. (1999). Principles and applications of tribology, John Wiley and Sons Inc.
- Bierwagen, G. P. and T. E. Saunders (1974). "Studies of the effects of particle size distribution on the packing efficiency of particles." Powder Technology 10(3): 111-119.
- Bolton, M. D. (1986). "Strength and dilatancy of sands." Geotechnique 36(1): 65-78.
- Bowden, F. P. and D. Tabor (1956). Friction and Lubrication. London, Methuen and Company Ltd.
- Briscoe, B. J. and D. Tabor (1978). Friction and wear of polymers in polymer surfaces. D. T. Clark and W. J. Feast, John Wiley and Sons Inc.
- Brown, R. L. and J. C. Richards (1970). Principles of Powder Mechanics, Pergamon Press.
- Brumund, W. F. and G. A. Leonards (1973). "Experimental Study of Static and Dynamic Friction Between Sand and Typical Construction Materials." Journal of Testing and Evaluation 1(2): 162-165.
- Chik, Z. and L. E. Vallejo (2005). "Characterization of the angle of repose of binary granular materials." Canadian Geotechnical Journal 42(2): 683-692.
- Consiglio, R., D. R. Baker, et al. (2003). "Continuum percolation thresholds for mixtures of spheres of different sizes." Physica A: Statistical Mechanics and its Applications 319: 49-55.

- Czichos, H. (1985). Importance of Properties of Solids to Friction and Wear Behavior. New Directions in Lubrication, Materials, Wear, and Surface Interactions - Tribology in the 80's. Cleveland: 68-103.
- DeJong, J. T., J. D. Frost, et al. (2001). "Effect of surface texturing on CPT friction sleeve measurements." Journal of Geotechnical and Geoenvironmental Engineering 127(2): 158-168.
- Deresiewicz, H. (1958). Mechanics of Granular Matter. Advances in Applied Mechanics, Academic Press, Inc. 5: 233-306.
- Doddiah, D., H. S. Bhat, et al. (1969). "Shear characteristics of soil-gravel mixtures." Journal of the Indian National Society of Soil Mechanics and Foundations Engineering 8(1): 57-66.
- Dodds, J. A. (1980). "The porosity and contact points in multicomponent random sphere packings calculated by a simple statistical geometric model." Journal of Colloid and Interface Science 77(2): 317-327.
- Dove, J. E. (1996). Particle-Geomembrane Interface Strength Behavior as Influenced by Surface Topography, Georgia Institute of Technology.
- Dove, J. E. and J. D. Frost (1999). "Peak friction behavior of smooth geomembrane-particle interfaces." Journal of Geotechnical and Geoenvironmental Engineering 125(7): 544-555.
- Duran, J. (2000). Sands, powders and grains: An introduction to the physics of granular materials. New York, Springer-Verlag.
- Fang, L., X. L. Kong, et al. (1993). "Movement patterns of abrasive particles in three body abrasion." Wear 163-164: 782-789.
- Finkers, H. J. and A. C. Hoffmann (1998). "Structural ratio for predicting the voidage of binary particle mixtures." AIChE Journal 44(2): 495-498.
- Fragaszy, R. J., J. Su, et al. (1992). "Modeling strength of sandy gravel." Journal of Geotechnical Engineering 118(6): 920-935.
- Frost, J. D., Ed. (2010). Characterization and Behavior of Interfaces, IOS Press BV.
- Furnas, C. C. (1931). "Grading Aggregates I - Mathematical Relations for Beds of Broken Solids of Maximum Density." Industrial and Engineering Chemistry 23(9): 1052-1058.

- Graton, L. C. and H. J. Fraser (1935). "Systematic packing of spheres - with particular relation to porosity and permeability." Journal of Geology 43: 785-909.
- Gutierrez, M. (2003). Mixture Theory Characterization and Modeling of Soil Mixtures. Geomechanics 2003, Boston, Massachusetts, USA, ASCE.
- Holtz, W. G. and H. S. Gibbs (1956). "Triaxial shear tests on pervious gravelly soils." J. Soil Mechanics Foundations Division 82(SM1): 1-22.
- Iscimen, M. (2004). Shearing Behavior of Curved Interfaces, Georgia Institute of Technology.
- Jewell, R. A. (1989). "Direct shear tests on sand." Geotechnique 39(2): 309-322.
- Johnson, K. L. (1985). Contact Mechanics, Cambridge University Press.
- Karademir, T. (2010). Personal Communication.
- Lambe, T. W. (1951). Soil Testing for Engineers, John Wiley and Sons Inc.
- Lee, S.W. (2011). Personal Communication.
- Lings, M. L. and M. S. Dietz (2004). "An improved direct shear apparatus for sand." Geotechnique 54(4): 245-256.
- Lings, M. L. and M. S. Dietz (2005). "The peak strength of sand-steel interfaces and the role of dilation." Soils and Foundations 45(6): 1-14.
- Lu, Y. (2010). Reconstruction, Characterization, Modeling and Visualization of Inherent and Induced Digital Sand Microstructures, Georgia Institute of Technology.
- Ludema, K. C. (1996). Friction, Wear, Lubrication: A Textbook in Tribology, CRC Press.
- Marsal, R. J. and A. Fuentes de la Rosa (1976). "Mechanical properties of rockfill-soil mixtures." Transactions of the 12th International Congress on Large Dams, Mexico City 1: 179-209.
- McGeary, R. K. (1961). "Mechanical Packing of Spherical Particles." Journal of the American Ceramic Society 44(10): 513-522.
- Narsilio, G. A. and J. C. Santamarina (2008). "Terminal Densities." Geotechnique 58(8): 669-674.
- O'Rourke, T. D., S. J. Druschel, et al. (1990). "Shear strength characteristics of sand-polymer interfaces." Journal of Geotechnical Engineering 116(3): 451-469.

- Ouchiyama, N. and T. Tanaka (1989). "Predicting the densest packings of ternary and quaternary mixtures of solid particles." Industrial & Engineering Chemistry Research 28: 1530-1536.
- Paikowsky, S. G., C. M. Player, et al. (1995). "A dual interface apparatus for testing unrestricted friction of soil along solid surfaces." Geotechnical Testing Journal 18(2): 168-193.
- Peters, J. F. and E. S. Berney (2010). "Percolation Threshold of Sand-Clay Binary Mixtures." Journal of Geotechnical and Geoenvironmental Engineering 136(2): 310-318.
- Potyondy, J. G. (1961). "Skin friction between various soils and construction materials." Geotechnique 11(4): 339-353.
- Poulos, S. J. (1981). "The Steady State of Deformation." Journal of the Geotechnical Engineering Division 107(5): 553-562.
- Rahman, M. M. and S. R. Lo (2008). "The prediction of equivalent granular steady state line of loose sand with fines." Geomechanics and Geoengineering 3(3): 179-190.
- Rocoe, K. H., A. N. Schofield, et al. (1958). "On the Yielding of Soils." Geotechnique 8(1): 22-53.
- Rowe, P. W. (1962). "The Stress-Dilatancy Relation for Static Equilibrium of an Assembly of Particles in Contact." Proceedings of the Royal Society of London, Series A, Mathematical and Physical Sciences (1934-1990) 269(1339): 500-527.
- Santamarina, J. C. (2001). Soils and Waves, John Wiley & Sons, Inc.
- Selig, E. T. and R. S. Ladd, Eds. (1973). Evaluation of Relative Density and its role in Geotechnical projects involving cohesionless soils. ASTM Special Publication 523, ASTM.
- Shooter, K. V. and D. Tabor (1952). "The Frictional Properties of Plastics." Proceedings of the Physical Society, B: 661-671.
- Simoni, A. and G. T. Houlsby (2006). "The direct shear strength and dilatancy of sand-gravel mixtures." Geotechnical and Geological Engineering 24: 523-549.
- Sin, H., N. Saka, et al. (1979). "Abrasive Wear Mechanisms and the Grit Size Effect." Wear 55(1): 163-190.

- Skinner, A. E. (1969). "A note on the influence of interparticle friction on the shearing strength of a random assembly of spherical particles." Geotechnique 19(1): 150-157.
- Slichter, C. S. (1899). "Theoretical investigations of the motion of ground waters." U.S. Geological Survey 19th Annual Report, Part 2: 301-384.
- Sozer, B. (2005). Two Dimensional Characterization of Topographies of Geomaterial Particles and Surfaces, Georgia Institute of Technology.
- Stovall, T., F. De Larrard, et al. (1986). "Linear packing density model of grain mixtures." Powder Technology 48: 1-12.
- Suzuki, M. and T. Oshima (1985). "Co-ordination number of a multi-component randomly packed bed of spheres with size distribution." Powder Technology 44(3): 213-218.
- Taylor, D. W. (1948). Fundamentals of Soil Mechanics, John Wiley and Sons Inc.
- Thevanayagam, S. (1998). "Effect of fines and confining stress on undrained shear strength of silty sands." Journal of Geotechnical and Geoenvironmental Engineering 124(6): 479-490.
- Thevanayagam, S., T. Shenthan, et al. (2002). "Undrained fragility of clean sands, silty sands, and sandy silts." Journal of Geotechnical and Geoenvironmental Engineering 128(10): 849-859.
- Thomas, J. (1997). Morphology, Ageing and Engineering Behavior of Sands, Indian Institute of Technology - Kanpur.
- Uesugi, M. and H. Kishida (1986). "Influential Factors of Friction Between Steel and Dry Sands." Soils and Foundations 26(2): 33-46.
- Vaid, Y. P. and N. Rinne (1995). "Geomembrane Coefficients of Interface Friction." Geosynthetics International 2(1): 309-325.
- Vallejo, L. E. (2001). "Interpretation of the limits in shear strength in binary granular mixtures." Canadian Geotechnical Journal 38(5): 1097-1104.
- Vallejo, L. E. and R. Mawby (2000). "Porosity influence on the shear strength of granular material-clay mixtures." Engineering Geology 58: 125-136.
- Vasileva, A. A., V. V. Mikheev, et al. (1971). "How the strength of gravelly soils depend on the type of state of the sand filling the pores." Soil Mechanics and Foundation Engineering 8(3): 167-171.

- Viggiani, G., M. K□ntz, et al. (2001). An experimental investigation of the relationships between grain size distribution and shear banding in sand. Continuous and Discontinuous Modelling of Cohesive-Frictional Materials: 111-127.
- Westman, A. E. R. and H. R. Hugill (1930). "The Packing of Particles." Journal of the American Ceramic Society 13(10): 767-779.
- Williams, N. D. and M. F. Houlihan (1987). Evaluation of Interface Friction Properties Between Geosynthetics and Soils. Proceedings of Geosynthetics '87: 616-627.
- Yang, S., S. Lacasse, et al. (2006). "Determination of the transitional fines content of mixtures of sand and non-plastic fines." Geotechnical Testing Journal 29(2): 102-107.
- Yoshimi, Y. and T. Kishida (1981). "Friction between sand and metal surfaces." Proceedings of the 10th International Conference on Soil Mechanics and Foundation Engineering 1: 831-834.
- Youd, T. L. (1973). "Factors Controlling Maximum and Minimum Densities of Sands." Evaluation of Relative Density and Its Role in Geotechnical Projects Involving Cohesionless Soils, ASTM STP 523: 98-112.
- Yu, A. B. and N. Standish (1988). "An analytical-parametric theory of the random packing of particles." Powder Technology 55: 171-186.
- Yu, A. B. and N. Standish (1991). "Estimation of the porosity of particle mixtures by a linear-mixture packing model." Industrial & Engineering Chemistry Research 30(6): 1372-1385.
- Zettler, T. E. (1999). Operational induced changes in Geomembrane surface topography, Georgia Institute of Technology.
- Zettler, T. E., J. D. Frost, et al. (2000). "Shear Induced Changes in Geomembrane Surface Topogrphay." Geosynthetics International 7(3): 243-267.